MIXED MATRIX DUAL LAYER HOLLOW FIBER MEMBRANES

FOR NATURAL GAS SEPARATION

A Thesis
Presented to
The Academic Faculty

by

Shabbir Husain

In Partial Fulfillment
of the Requirements for the Degree
Doctor of Philosophy in the
School of Chemical & Biomolecular Engineering

Georgia Institute of Technology
August 2006

MIXED MATRIX DUAL LAYER HOLLOW FIBER MEMBRANES

FOR NATURAL GAS SEPARATION

Approved by:

Dr. William J. Koros, Advisor
School of Chemical & Biomolecular
Engineering
Georgia Institute of Technology

Dr. Christopher W. Jones
School of Chemical & Biomolecular
Engineering
Georgia Institute of Technology

Dr. Amyn Teja
School of Chemical & Biomolecular
Engineering
Georgia Institute of Technology

Dr. Sudhir S. Kulkarni
Senior Scientist,
Medal L.P, *Air Liquide*

Dr. Victor Breedveld
School of Chemical & Biomolecular
Engineering
Georgia Institute of Technology

Dr. Karl Jacobs
School of Polymer and Textile
Engineering
Georgia Institute of Technology

Date Approved: June 06, 2006

To Mom, Dad and my sisters,
Zaineb, Lamia and Fatema

ACKNOWLEDGEMENTS

There are many people who have been instrumental in helping me reach this stage. First, I would like to thank my parents for always being there and supporting me in my endeavors. Second, but not far behind, I would like to thank Dr. Koros for all his support through some rough times. His enthusiasm and drive kept me motivated to keep striving forward towards completion of the degree.

I would like to thank my committee members, Dr. Sudhir Kulkarni, Dr. Christopher Jones, Dr. Victor Breedveld, Dr. Amyn Teja and Dr. Karl Jacobs for providing thoughtful input and helping to mold my ideas. Their comments were greatly appreciated.

I have been influenced by my teachers and mentors in my high school and undergraduate studies. It would be remiss of me not to mention Mr. Errol Fernando, Dr. Lever, Fred Gregory, Dr. Grant C. Willson, Dr. Keith Johnston and Dr. Barlow, all of whom have great ability to teach and convey their enthusiasm for the love of knowledge.

Ted Moore and David Wallace are thanked for teaching me the ropes in mixed matrix membrane formation and fiber spinning. Both Ted and David also provided excellent critique of my research ideas allowing me to refine them. Ted's excellent thesis provided great help as a reference on mixed matrix work.

I would also like to thank Shu Shu, Alexis Hillock and Ryan Collins for providing data for this dissertation. Preeti Chandra and Madhava Kosuri were kind enough to proof read the dissertation and provided many helpful comments. They have also been good friends who were always willing to discuss research ideas.

TABLE OF CONTENTS

LIST OF TABLES

LIST OF FIGURES

SUMMARY

Mixed matrix membranes offer an attractive route to the development of high performance and efficiency membranes required for demanding gas separations. Such membranes combine the advantageous processing characteristics of polymers with the excellent separation productivity and efficiency of molecular sieving materials. This research explores the development of mixed matrix membranes, namely in the form of asymmetric hollow fiber membranes using zeolites as the molecular sieving phase and commercially available high performance polymers as the continuous matrix.

Lack of adhesion between the typically hydrophobic polymer and the hydrophilic native zeolite surface is a major hurdle impeding the development of mixed matrix membranes. Silane coupling agents have been used successfully to graft polymer chains to the surface of the zeolite to increase compatibility with the bulk polymer in dense films. However, transitioning from a dense film to an asymmetric structure typically involves significant processing changes, the most important among them being the use of phase separation to form the asymmetric porous structure. During the phase separation, it is believed that hydrophilic sieves can act as nucleating agents for the hydrophilic polymer lean phase. Such nucleation tendencies are believed to lead to the formation of gaps between the polymer and sieve resulting in poor mixed matrix performance.

This research focuses on defining procedures and parameters to form successful mixed matrix hollow fiber membranes. The first part of this dissertation describes dope mixing procedures and unsuccessful results obtained using a silane coupling agent to enhance polymer-zeolite adhesion. The next section follows the development of a highly successful surface modification technique, discovered by the author, employing the use of a Grignard reagent. As a test case, two zeolites of different silicon-to-aluminum ratios

are successfully modified and used to develop mixed matrix membranes with greatly increased gas separation efficiencies. The broad applicability of the surface treatment is also demonstrated by the successful incorporation of the modified zeolites in a second polymer matrix. The final section of the work describes the novel occurrence of large defects (macrovoids) caused by the presence of large zeolite particles proposing a particle size effect in the formation of such defects.

The research successfully develops a modification procedure using a Grignard reagent to modify the surface of two different types of zeolites allowing for their successful incorporation in multiple polymer matrices. Further, the work presented in this dissertation has identified considerable areas of research that can be probed further in detail in future work.

CHAPTER 1

INTRODUCTION

A functional definition of a membrane is a semi-permeable barrier that allows the transport of one component selectively over others in a multicomponent mixture. Although micromolecularly selective membranes have existed for the past hundred years, it is only the last fifty years that the use of membranes for separation processes has been applied. This application stems from advancement in membrane formation technology and increased research based on the identification of membrane based separations as low energy separation processes [1, 2].

Membranes can be composed of solid and liquid components, depending on the nature of their application [1]. These materials range from polymers, to metals, to carbon and inorganic molecular sieves (silicates, aluminosilicates, silicoaluminophosphates, and others), to organic or inorganic liquids. The diversity of membrane formation, materials and applications precludes an in-depth discussion of the different types of membranes in this work. The reader is directed to excellent works by Baker [1] and Mulder [3] for further reference. This thesis will concentrate on the development of polymer-inorganic composite hollow fiber membranes for challenging gas separations.

1.1. POLYMERIC MEMBRANES

Polymeric membranes perform their separation functions through a variety of mechanisms based on their structural morphology and material properties. Such membranes range from porous membranes used in filtration and ultrafiltration, to dense nonporous membranes used in gas separations and reverse osmosis.

The transport mechanism though micro and nano porous membranes used in liquid filtration takes place via a size exclusion principle. For gas separations, transport in microporous membranes depends on the pore size and/or the relative condensability of the gases/vapors as in the case of surface diffusion. In surface diffusion, the more condensable gas "A" preferentially adsorbs on to the surface of the pore and restricts transport of gas "B" [4].

When the size of the pore is smaller or equivalent to the mean free path of the gas molecules, transport through the pores takes place via Knudsen flow. In this flow regime, the separation efficiency for a gas mixture is determined by the square root of the molecular weight ratio of the gases [5]. Such porous membranes provide little or no selectivity for gas separations and find very limited use; an exception is the large scale use of ceramic microporous membranes during the Manhattan Project [1].

Generally, non-porous membranes are used for gas separations. Transport through these membranes is described by the solution-diffusion mechanism, where the gas molecule dissolves at the upstream face of the membrane, diffuses across the membrane thickness and desorbs at the downstream face of the membrane. This mechanism is described in more detail in Section 2.1. Figure 1.1 presents a schematic of the above transport mechanisms based on the multiple membrane morphologies.

Polymeric membranes have typically been used for gas separations because of their robustness and capability to withstand mechanical abuse. Based on the chemical composition and structural flexibility of the polymer chains, dense polymers membranes can distinguish between different gas species in a mixture. The driving force for this separation is a chemical potential difference across the membrane, or in process terms, a pressure differential across the membrane. The utility of polymeric membranes lies in their relative ease in processing, formation and manufacturing cost when compared to

inorganic membranes. However, currently this processibility comes with disadvantages of lower productivity and efficiency of separation resulting in economic viability only in small to medium scale processes or in specialized applications. This tradeoff between the efficiency and the productivity for a large number of polymers was tabulated by Robeson for multiple gas separation targets [6]. The performance of polymers versus inorganic molecular sieving materials along with the economically viable region is shown for carbon dioxide/methane separation in Figure 1.2.
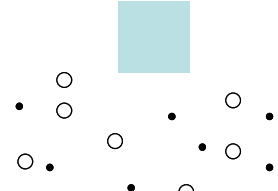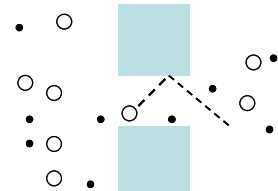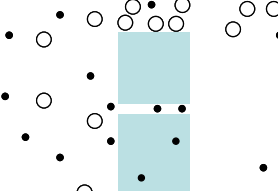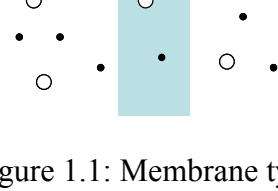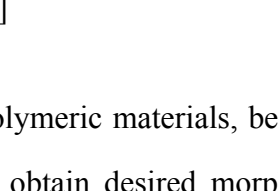
	Separation Mechanism	Pore Size (nm)	Application
	Viscous flow	$>10^2$	Microfiltration
	Knudsen Diffusion	10^2-10^0	Ultrafiltration
	Surface Diffusion (reverse selective)	10^1 - $<10^0$	Purification of condensable gases, separation organics
	Molecular Sieving	$<10^0$	Nanofiltration
	Solution-Diffusion	N/A	Separation of gases, pervaporation, reverse osmosis

Figure 1.1: Membrane types and separation mechanisms for a gas mixture. Adapted from [7]

Polymeric materials, because of their excellent processibility, can thus be easily tailored to obtain desired morphologies and increasingly are being used in diverse membrane

applications. Newer application for membranes are being developed; examples for which can be found in membrane reactors and membranes for biomedical applications [1].
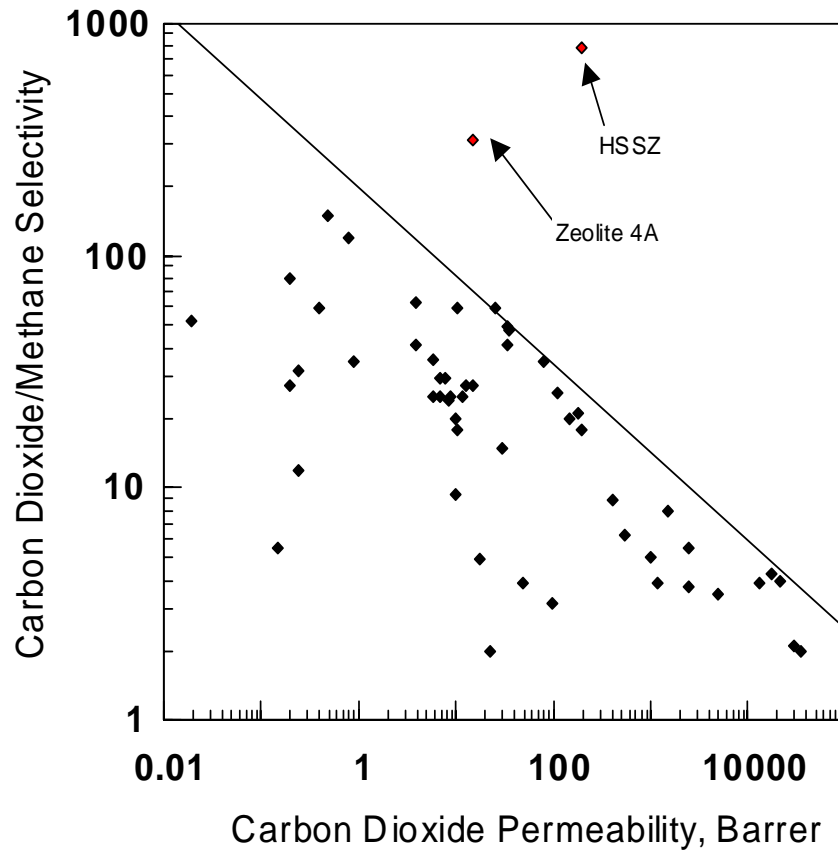
Figure 1.2: Upper-bound trade-off curve (1991) for carbon dioxide – methane gas pair along with the transport properties of zeolites used in this work. Adapted from [6]. Figure generated by Moore [8].

On the other hand, zeolites with extremely high separation efficiencies are difficult to process and currently prohibitively expensive to fashion into large scale membrane modules. Thus polymers and zeolites offer complementary strengths for use in membrane formation.

The recognition of the selectivity/permeability trade-off has directed research in gas separation membranes along multiple routes. Traditional routes concentrate on

producing increasingly selective polymers for polymer-only membranes or defect-free membranes using molecular sieving materials. A second intriguing option relies on forming workable membranes from existing polymer and inorganic components by taking advantage of the strengths of the individual materials to fashion a composite or mixed matrix membrane. These mixed matrix membranes are defined as multiphase structures, where one phase mainly provides the retaining/support structure, and the dispersed phase performs the primary separation function. Using a combination of solid/polymer, liquid/polymer and solid/liquid/polymer material combinations, superior membranes for individual application requirements can be developed.

The vastness of the possible combinations of mixed matrix materials precludes a detailed analysis in this research work. A brief overview on existing research directions is presented in Chapter 2 under other mixed matrix materials. However, this thesis will primarily focus on addressing challenges and developing solutions in the formation of zeolite/polymer hollow fiber membranes for natural gas separation.

1.2. COMMERCIAL APPLICATION OF GAS SEPARATION MEMBRANES

Significant advancement was achieved in membrane research with the formation of asymmetric membranes by Loeb and Sourirajan [9], which allowed high productivities to be realized and paved the path for membranes to be used commercially.

Major use of asymmetric membranes so far, has been for ultrafiltration and reverse osmosis applications for water purification. However, gas separation membranes currently represent the fastest growing membrane-based separation market [10]. Membranes are increasing being used for the recovery of hydrogen in ammonia synthesis and petroleum cracking plants, for the production of low purity (95-99.5%) nitrogen for blanketing and for remote site generation, and natural gas purification [1, 10]. This growth has the potential to expand exponentially if increasingly selective and productive

membranes and membrane materials can be developed, thereby improving the economics of membrane processes.

1.2.1. Hollow Fiber Membranes for Gas Separations

Hollow fiber technology represents the optimized geometry for high production rates and ease of module formation. Other membrane module geometries employing flat sheets and spirally wound flat sheets require much larger investment in materials to obtain the same separating surface area obtained with the use of hollow fiber membranes. Figure 1.3 compares the surface area to volume ratio for plate type, spirally wound and hollow fiber membrane module configurations [11].
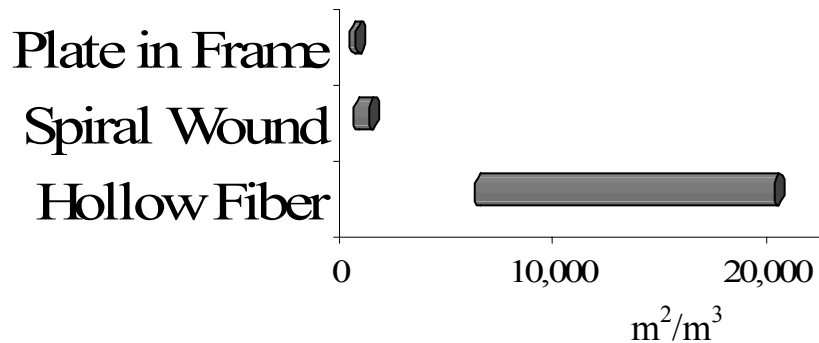
Figure 1.3: Comparison of surface area per unit volume between plate-in-frame, spirally wound and hollow fiber modules [11]

One of the reasons that the formation of hollow fibers has been deemed to be as much of an art form as a science, is the complexity and interactions of a large number of variables involved in hollow fiber spinning. A large number of possible membrane morphologies can be generated by changing either the polymer solution (dope) composition or spinning parameters or a combination of both. Thus it is possible, in hollow fiber form, for a polymer material to have application in wide ranging separation processes, which include reverse osmosis, ultrafiltration, gas separations, pervaporation and ion exchange.

1.2.2. Driving Force for High Performance Gas Separating Membranes

Currently the largest market for gas separation membranes is in the generation of nitrogen enriched air [1, 12, 13]. The benefits of using membranes for this application are limited to lower purity nitrogen (~99.5%) and on-site generation capability where transportation costs are high. However, this market does not represent one of the strong drivers for high selectivity mixed matrix membranes as the corresponding decrease in compressor costs (the major cost factor) shows decreasing marginal returns for O_2/N_2 selectivities higher than 8 [10]. This selectivity is currently available with polymer-only membranes.

This is not the case for membrane-based gas separations in the petroleum industry where significant benefits can be obtained with the use of higher selectivity membranes. Increased energy consumption and the high cost of fossil fuels has focused attention on enhanced production of oil and natural gas. As a "clean burning" fuel, natural gas has considerable appeal and is being increasingly used for power generation in the United States [14]. Currently, increasing demand for natural gas is being met via increased exploration, more efficient processing of existing gas streams and processing gas streams with high levels of impurities where increasing gas prices have made processing costs viable.

Generally, natural gas fields contain appreciable quantities of components/impurities that must be removed from the gas stream before being piped or transported for sale. Using conventional polymer-only membranes or an amine absorption tower for gas processing involves wastage in terms of processing loss, and operating costs (the operating costs include depreciation of capital investments). The processing loss is the loss of product that cannot be economically recovered and is either flared or re-injected into the well head to maintain reservoir pressure. It is estimated that more than 110 billion cubic

meters of natural gas is flared each year due to the lack of economical separation processes [15].

Amine based adsorption systems are generally capital intensive, however, they have low processing losses. In membrane operations, in natural gas processing, losses are caused by the passage of methane to the permeate stream consisting mainly of carbon dioxide. The loss of methane in the permeate stream can be reduced either by using increased number of stages (membrane module units) or by using a more selective membrane for carbon dioxide. As the costs for the separation scale with membrane surface area, higher selectivity membranes are preferred.

Likewise, discovered natural gas fields containing high concentrations of carbon dioxide, 30% and above, are less cost effective to process with amine based separation processes because of high plant and operational costs [16]. Table 1.1 provides a breakdown of the chemical composition of sub-quality non-associated natural gas fields in the lower-48 states of United States of America. Selection of a membrane system versus an amine based system hinge on the gas processing flow rates, carbon dioxide content, natural gas prices and site specific criteria (e.g. space premium on offshore gas rigs). Membrane units based on existing separation efficiencies are favored at low to medium processing feed rates of 5-40 million standard cubic feet per day (MMSCFD) and high carbon dioxide content (≥ 20 %) [10, 17].

Table 1.1. Chemical Composition of Raw, Lower-48, Non-associated Natural Gas [18]

	Proven reserves	Production	Undiscovered resources	Discovered, non-producing
High quality gas	**91,232**	**10,607**	**724,775**	0
Subquality gas	**52,976**	**4,875**	**307,588**	**135,000**
High N_2	16,488	1,230	44,091	
High CO_2	15,766	1,590	122,430	
High H_2S	4,966	597	24,782	
High N_2 and CO_2	1,158	67	17,221	
High N_2 and H_2S	2,354	271	3,555	
High CO_2 and H_2S	9,753	815	81,560	1,000
High N_2, CO_2 and H_2S	2,671	305	12,949	134,000
Lower-48 total	**144,208**	**15,482**	**1,032,363**	**135,000+**

Units are in billion cubic feet (bcf), based on 1991 reserve data published by the US Department of Energy.

The growth of markets for gas separation based membranes as estimated by Baker [19] is shown in Table 1.2. The market is predicted to increase from a value of US$ 155 million per year in 2000 to US$ 760 million per year by the year 2020 based on incremental advancement in membrane technology. Although this represents a healthy growth rate, the predictions underestimate the effect of disruptive technologies such as the mixed matrix membranes when used in large volume and energy intensive separations such as acid gas removal from natural gas and olefin/paraffin separations, respectively.

Table 1.2: Estimated market for gas separation membranes [19]

Separation	Membrane Market (US$ million)		
	2000	**2010**	**2020**
Nitrogen from air	75	100	125
Oxygen from air	<1	10	30
Hydrogen	25	60	150
Natural gas			
CO_2	30	60	100
Natural gas liquids	<1	20	50
N_2/H_2O	0	10	25
Vapor/nitrogen	10	30	60
Vapor/vapor	0	20	100
Air dehydration/other	15	30	100
Total	155	340	760

1.3. MIXED MATRIX MEMBRANES

At the current stage, successful mixed matrix hollow fiber membranes have been reported in the patent literature [20, 21].   However, successful mixed matrix hollow fiber membranes have been difficult to consistently reproduce, a requirement necessary for commercial production. Challenges are faced in understanding the interaction between the inorganic molecular sieve and the polymer, including many different types of defective morphologies in dense films. Recently, considerable effort has been expended in trying to understand defective morphologies in mixed matrix dense films [22, 23], however, such an analysis of defective morphologies is absent in the asymmetric hollow fiber geometry, where the membrane is formed via a phase separation process. This forms the major objective of this thesis work.

1.4. RESEARCH OBJECTIVES

The research objectives are structured towards a strong push into mixed matrix hollow fiber spinning. The goals are characterized as follows:

1. To identify challenges in mixed matrix hollow fiber spinning

The spinning of polymer-molecular sieve suspensions for gas separation membranes is an emerging research field. This research aims to explore suspension spinning and identify important factors necessary for the spinning of successful mixed matrix hollow fibers.

2. Explain defective morphologies in mixed matrix hollow fiber membranes that decrease their gas separation potential

This goal considers the effect of transitioning from a dense film morphology to that of an asymmetric hollow fiber structure formed via a phase separation process. Included in such defective morphologies, are so-called "sieve-in-a-cage" formation and macrovoids.

3. Define a framework to practically form mixed matrix membranes with different combinations of inorganic molecular sieve and polymers

The observations from defective morphologies and the results of successful mixed matrix membranes will be applied to another polymer system to demonstrate the applicability of the discovered procedure across both multiple zeolite types and polymers.

1.5. THESIS OVERVIEW

Chapter 2 presents background and theory of gas transport in gas membranes and spinning of hollow fiber membranes. Additionally, an overview of the Maxwell model for estimating mixed matrix membrane performance is presented. Methods and materials used in the research of both polymer-only and mixed matrix membranes are covered in Chapter 3. Chapter 4 describes the spinning of mixed matrix hollow fiber membranes using Ultem® polyetherimide and Ultem® "sized" inorganic zeolites and presents a

hypothesis for the defective morphologies observed. Chapter 5 presents the results of successful mixed matrix hollow fiber membranes made using a novel modification of the zeolite surface using 2 different zeolites and a second polymer system. The zeolite surface modification described in Chapter 5 is characterized and a hypothesis for the increased polymer-zeolite adhesion presented in Chapter 6. Chapter 7 describes the observation of particle induced defects in hollow fiber membranes. Conclusions and recommendations for future work are provided in Chapter 8.

1.6. REFERENCES

1.   Baker, R.W., *Membrane Technology and Applications*. 2nd ed. 2004: John Wiley & Sons, Ltd. 538 pp.

2.   Koros, W.J., *Evolving beyond the thermal age of separation processes: Membranes can lead the way*. AIChE Journal, 2004. **50**(10): p. 2326-2334.

3.   Mulder, M. and Editor, *Basic Principles of Membrane Technology, Second Edition*. 1996. 564 pp.

4.   Rao, M.B. and S. Sircar, *Nanoporous carbon membranes for separation of gas mixtures by selective surface flow*. J. Membr. Sci., 1993. **85**(3): p. 253-64.

5.   Knudsen, M., *The Law of the Molecular Flow and Viscosity of Gases Moving through Tubes*. Annalen der Physik (Weinheim, Germany), 1909. **28**: p. 75-130.

6.   Robeson, L.M., *Correlation of separation factor versus permeability for polymeric membranes*. J. Membr. Sci., 1991. **62**(2): p. 165-85.

7.   Carruthers, S.B., *Integral-skin formation in hollow fiber membranes for gas separations*. 2001. p. 233 pp.

8.   Moore, T.T., *Effects of materials, processing, and operating conditions on the morphology and gas transport properties of mixed matrix membranes*. 2004. p. 311 pp.

9.   Loeb, S. and S. Sourirajan, *Sea water demineralization by means of an osmotic membrane*. Advances in Chemistry Series, 1963. **38**: p. 117-32.

10.   Baker, R.W., *Future Directions of Membrane Gas Separation Technology*. Industrial & Engineering Chemistry Research, 2002. **41**(6): p. 1393-1411.

11.   Kesting, R. and A. Fritzsche, *Polymeric Gas Separation Membranes*. 1993, New York: John Wiley & Sons.

12.   Koros, W.J. and R. Mahajan, *Pushing the limits on possibilities for large scale gas separation: which strategies?* J. Membr. Sci., 2000. **175**(2): p. 181-196.

13.   Strathmann, H., *Membrane separation processes: current relevance and future opportunities*. AIChE Journal, 2001. **47**(5): p. 1077-1087.

14.   http://www.energy.gov/energysources/naturalgas.htm, Date accessed, May 9, 2006.

15.   Gerner, F., B. Svensson, and S. Djumena, *Gas Flaring and Venting: A Regulatory Framework and Incentives for Gas Utilization*, in *Public Policy Journal Note No. 279*. 2004, World Bank: Washington, D.C.

16.   Chinn, D., *Personal communication*. 2004: Chevron Corp.

17.   Spillman, R.W., *Economics of gas separation membranes*. Chem. Eng. Prog., 1989. **85**(1): p. 41-62.

18.   Meyer, H.S. and D. Leppin, *Research targets lower gas-processing operating costs*. Oil & Gas Journal. **95**(52): p. 83.

19.   Baker, R., *Future directions of membrane gas-separation technology*. Membrane Technology, (138): p. 5-10.

20.   Ekiner, O.M. and S.S. Kulkarni, *Process for making hollow fiber mixed matrix membranes*. 2003, L' Air Liquide Societe Anonyme a Directoire et Conseil de Surveillance pour l'Etude et l'Exploitation des Procedes Georges Claude: United States.

21.   Kulkarni, S.S. and D.J. Hasse, *Molecular sieve-containing polyimide mixed matrix membranes*. 2005, (USA). Application: US. p. 13 pp.

22.   Moore, T.T., R. Mahajan, D.Q. Vu, and W.J. Koros, *Hybrid membrane materials comprising organic polymers with rigid dispersed phases*. AIChE Journal, 2004. **50**(2): p. 311-321.

23.   Moore, T.T. and W.J. Koros, *Non-ideal effects in organic-inorganic materials for gas separation membranes*. Journal of Molecular Structure, 2005. **739**(1-3): p. 87-98.

CHAPTER 2

BACKGROUND AND THEORY

2.1. TRANSPORT IN POLYMERIC MEMBRANES

Membrane materials research is carried out mostly using dense films, which are formed by slowly evaporating the solvent from a polymer solution. The evaporation of the solvent from the solution typically causes the amorphous polymer to vitrify and form a dense layer. The permeation of a gas through the dense polymer can be described using the solution-diffusion theory. In terms of this model, the productivity of a membrane is defined by the permeability of the gas through the membrane. The permeability of a gas, i, is given by:

$$P_i = \overline{D}_i \cdot \overline{S}_i \qquad (2.1)$$

where D and S represent the diffusion and solubility coefficient, respectively. Permeability can also be expressed as flux normalized by film thickness, ℓ, and pressure difference Δp across the membrane as follows:

$$P_i = \frac{Flux_i \cdot \ell}{\Delta p_i} \qquad (2.2)$$

However, when the thickness is difficult to define, pressure normalized flux, or permeance (P_i/ℓ) is used instead. The ratio of the permeabilities can be used to signify the selectivity of separation of the desired component within the mixture The ideal selectivity of the membrane, thus, is the ratio of the permeability or permeance of the individual gases. For mixture of gas A and B the selectivity is described by:

$$\alpha_{A/B} = \frac{P_A}{P_B} \qquad\qquad (2.3)$$

2.2. ASYMMETRIC MEMBRANES

A variant of the dense film is an asymmetric film which in simple terms can be described as a thin dense film on a porous support. The support provides the mechanical strength to the membrane, while the dense (skin) layer performs the separation function. An immediate effect of this morphology is that skin thicknesses can be greatly reduced as the skin no longer has to be self-supporting. This decrease in skin thickness increases the productivity of the membrane as the flux is inversely proportional to the thickness.

Asymmetric films can be formed in a variety of ways including through phase separation, interfacial polymerization on a porous support, dip or spin coating on a porous support, and plasma deposition [1]. Alternatives also include multi-layered membranes which are formed by packing a dense layer on a porous support to form a layered composite.

However, it is advantageous to form membranes with reduced processing steps. The Loeb-Sourajan type membrane solves this requirement by contacting the polymer solution with a non-solvent [2] and forming the membrane in a one step process. On contact with the non-solvent, mass transfer takes place between the non-solvent from the coagulation bath and the solvent in the nascent membrane resulting in micro-phase separation within the membrane. Depending on the pathway of phase separation, a dense layer, also called the skin layer, can form on the surface of the membrane. The skin formation occurs when solvent outflow from the membrane exceeds the non-solvent inflow resulting in delayed demixing. This process increases the concentration of the polymer at the membrane – coagulant interface and forms the skin [3, 4]. An evaporative step can be included prior to the phase separation step to enhance skin formation by the evaporation of the volatile solvent from the nascent membrane.

The phase separation of a polymer solution occurs via the following two mechanisms; (1) nucleation and growth, and/or (2) spinodal decomposition. The phase separation mechanisms of the polymer solution can be described with the aid of a ternary phase diagram shown in Figure 2.1. In the figure, the binodal separates the one and two phase regions of the polymer/solvent/nonsolvent system. The two phase region can be further subdivided into the metastable and the spinodal regions. In the meta-stable state (see Figure 2.1), if the associated energy barrier to nucleation is overcome, a polymer lean phase is nucleated. This energy is required to form new surfaces and if the nucleus is larger than the critical size needed for stability, it grows with the advent of the non-solvent until the non-solvent activity within the nucleus causes the vitrification of the cell structure, thereby producing a closed-cell morphology. Alternatively, before the cell walls vitrify, stresses may enable their rupture and formation of a bi-continuous morphology which ultimately vitrifies by losing residual solvent [5].
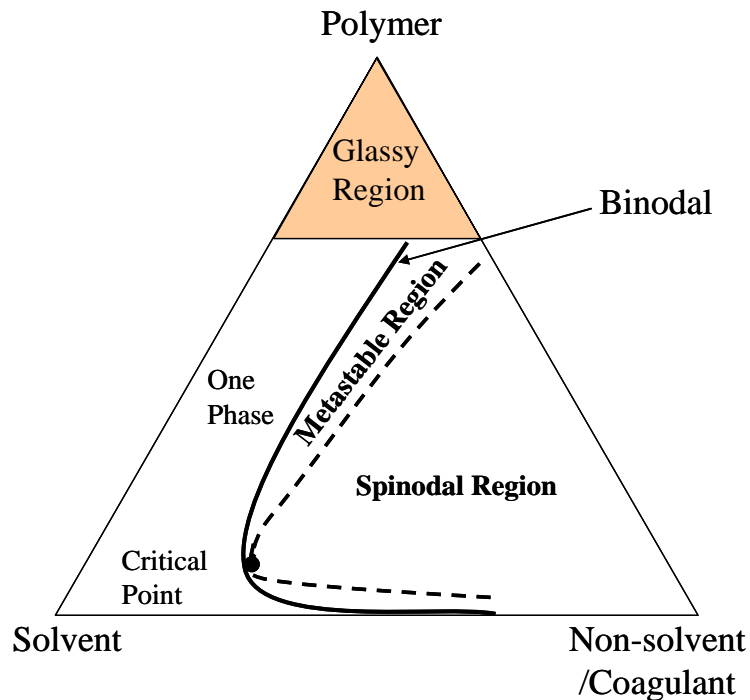
Figure 2.1: Ternary phase diagram of polymer, solvent, and non-solvent [6].

A second phase separation mechanism can occur if the solution can be driven into the spinodal region prior to nucleation and growth in the metastable region. In this case, phase separation occurs instantaneously and a bi-continuous network of polymer rich and polymer lean phase is formed which provides little resistance to gas flow [7]. A truly bi-continuous network formed via either mechanism results in the formation of a low resistance membrane support but one with no molecular selectivity (in viscous flow) or with Knudsen selectivity.

2.2.1. Hollow Fiber Membranes

Asymmetric membranes can be formed via multiple phase separation techniques. These include immersion precipitation (Loeb-Sourajan type), evaporation of a volatile solvent, absorption of a nonsolvent, and thermally induced phase separation (TIPS) [1].

The asymmetrical film can be taken a step further and developed into an asymmetrical hollow fiber, which aside from being self-supporting, permits the use of higher feed pressures- translating into higher productivity. Figure 2.2 shows the asymmetric nature of a hollow fiber membrane.
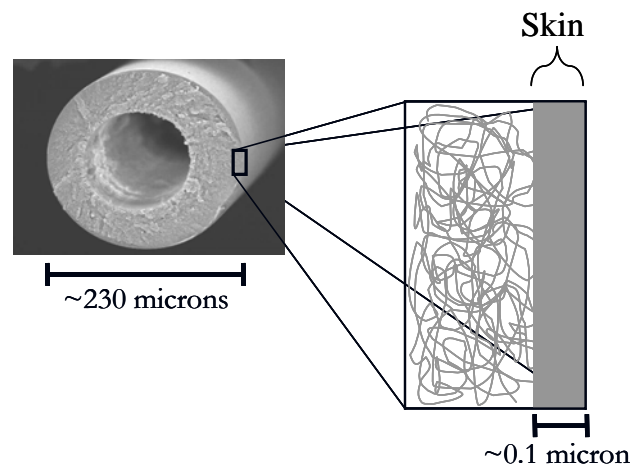
Figure 2.2: Asymmetric hollow fiber membrane [8]

18

Such skinned asymmetrical fibers are produced by a combined solution wet spinning and dry spinning process. Wet spinning involves extrusion of the nascent hollow fiber directly into a coagulation bath of a strong non-solvent. A solvent having high interaction with the non-solvent is chosen to accelerate phase separation. On the other hand, in dry spinning, a volatile solvent is evaporated leading to phase separation in the polymer solution, which forms the asymmetric fiber morphology. The combination of the two processes, "dry-wet", takes place when the dope consisting of polymer, volatile and non-volatile solvents is spun with an air gap into a coagulation bath. The evaporation of the volatile solvent in the air gap forms a stable skin layer of the membrane while the phase separation in the coagulation bath forms the underlying porous support layer of the membrane. Alternatively, the skin can also be formed by a delayed demixing process as described earlier.

During the formation of the skin in the air gap it is preferred that the fiber does not phase separate as this may cause defects in the fiber surface as it is drawn [9]. The skinned structure provides high productivity and selectivity characteristic of a defect-free film, since any phase separated regions do not "percolate" to form a non-selective flow path. It is preferable in asymmetric membranes, but perhaps even essential in the case of mixed matrix membranes, that phase separation not take place in the selective skin region. The suppression of phase separation at the polymer-sieve interface is hypothesized to be critical in achieving a mixed matrix effect in asymmetric membranes as will be discussed later in Chapter 4.

The ideal hollow fiber consists of a very thin separating skin layer and a porous support layer that does not offer any resistance to gas flow. The resistance, defined as sub-structure resistance, if present, is non-selective and affects the fast moving gas more than the slow gas, resulting in a decrease in selectivity between the high and low permeability gas pair [10, 11]. For example, an intrinsic (dense film) selectivity for oxygen/nitrogen

gas pair along with a depressed (less than intrinsic) selectivity of helium/nitrogen (He/N_2) gas pair is indicative of sub-structure resistance as the fast gas (He) is slowed more than the slower gas (N_2) resulting in a lower He/N_2 selectivity.

In recent years, the development of complex spinnerets [12] has allowed dual layer fibers to be spun using two co-extruded polymer solutions, where the outer sheath layer of the dual layer hollow fiber acts as the separating layer. In this research, both monolithic (single polymer layer) and dual layer fibers are spun, with the monolithic fiber used to first confirm proof-of-concept. A schematic of the spinning setup and a dual layer spinneret is depicted in Figure 2.3.
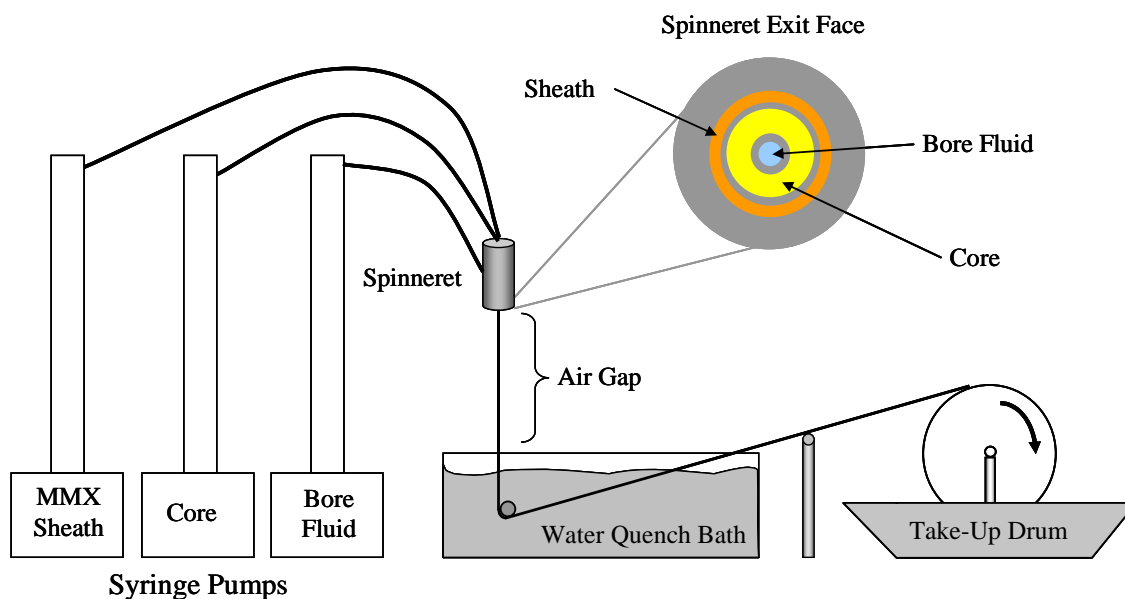
Figure 2.3: Schematic for hollow fiber spinning set-up

As described earlier, the separating layer of the hollow fiber at most consists of the outer few microns. By using a less expensive polymer to form the support layer, significant cost advantages can be achieved. Additionally, in the case of mixed matrix fibers as the porous support provides no separation function, the use of dual layer membranes with

expensive, high performance sieve particles only in the sheath layer appears very attractive.

Dual layer membranes have been made by dip coating [13], reactive polymerization, and through the simultaneous spinning of two polymer solutions. Recently, the latter process has received considerable attention [14-16], where different polymer shrinking rates [15] and low time for diffusion between the layers of the nascent membrane [16] are cited as causes of delamination between the layers of the fiber.

To prevent the sheath from bursting or collapsing under a high pressure gas feeds, strong adhesion between the two layers of the dual layer membrane is essential. In a dual layer membrane made with a common polymer but with different dope compositions, the issue of phase compatibility does not arise. However, interpenetration between the layers for good adhesion [17] is limited by rate of mass transfer between the nascent layers in the spinneret and air gap. This interpenetration is believed to be enhanced by the use of solvent gradients between the two layers [18], where it is hypothesized that the highly mobile solvent molecules promote the movement of polymer chains via convective flow.

2.2.1.1. *Dope Development*

Polymer solutions used in fiber spinning consist of three or more components comprising polymer, solvents, non-solvent and additives. A pseudo-ternary phase diagram of more than three components can be devised by dividing the components into categories of polymer, solvent and non-solvent. Within each category, the components can be fixed in ratio to each other to restrict solvency and/or non-solvency power. This approach based on fixed ratios enables holding solvency parameters constant for the solvents and non-solvents that can be explored in the system.

Ternary phase diagrams can be developed by the, (1) titration of the polymer solution with non-solvent, (2) though the use of the three-phase Flory-Huggins theory for polymer

solutions [19] and (3) by inspection of polymer solutions of various compositions of polymer/solvent/nonsolvent. In our group, we have selected to use the latter method, as titration is difficult to work with concentrated viscous solutions and theoretical results via Flory-Huggins would have to be confirmed by experimental results. Depending on the polymer viscosity in solution, the dope compositions are made to cover the region of interest for fiber spinning (usually 26 – 35 wt % polymer for a polymer with Mw ~ 50,000 – 100,000). The binodal curve is generated by making small samples (10 – 15 gram) of various compositions and visually inspecting them for phase separation.

Once the binodal has been identified, two factors have to be considered when determining the dope formulation as follows: (1) proximity of the dope composition to the binodal, and (2) dope viscosity. The proximity of the dope composition to the binodal determines the kinetics of membrane formation and the morphology of the membrane. As shown in the ternary phase diagram, the position of the dope composition influences the phase separation pathway. If the dope composition is close to the binodal, then only a small amount of non-solvent is required to phase separate the nascent membrane by penetration into the metastable, preferably spinodal region.

A minimum dope viscosity is required to avoid capillary instability in the air gap [20]. This minimum viscosity depends on the cohesive strength of the polymer solution under elongation that takes place after the fiber exits the spinneret. Based on the air gap and draw ratio, this minimum viscosity must be defined for each polymeric-solvent-nonsolvent system. A higher viscosity can be achieved by increasing the polymer concentration in the dope or by adding viscosity enhancers, like lithium nitrate ($LiNO_3$) and carboxylic acids which complex with the solvent. Although a high polymer concentration is required to promote skin growth and increase viscosity for spinning, too high a concentration would reduce porosity in the support layer and form a support layer with substantial resistance to gas flow.

Solvents and non-solvents are selected, in part, for their miscibility with the aqueous coagulant. Another factor to consider in the selection of the dope solvent is the generation of osmotic pressure during phase separation. The osmotic pressure is a function of the activities of the solvent and coagulant non-solvent, and is believed to be instrumental in the formation of macrovoids [6, 21]. Macrovoids and their presence in polymer-only and mixed matrix fibers are discussed in Chapter 7.

2.2.1.2. *Spinning Parameters*

The spinning parameters influence the phase separation kinetics and thus strongly determine the final morphology of the membrane. Although equilibrium thermodynamics direct the phase separation pathway in the nascent fiber, the rapid phase separation traps polymer chains in non-equilibrium states. The spinning parameters, discussed below, control the rate of phase separation and can thus be used to fine tune the final membrane morphology and obtain a wide range of morphologies.

2.2.1.2.1. *Bore Fluid*

The bore fluid provides support to the nascent hollow fiber membrane as it is extruded from the spinneret. Bore fluid composition have varied from gas and pure liquids, to liquid mixtures and salt solutions [22-24]. Earlier approaches have used bore fluids to coagulate the hollow fiber from the bore side, however, in the Koros group, we have chosen to formulate bore fluids that result in minimum interaction with the dope. These "thermodynamically neutral" bore fluids are envisioned to neither dissolve polymer from the dope, nor cause phase separation [8]. Wallace suggests a method for determining the "neutral" bore fluid composition for a solvent/nonsolvent bore fluid composition by drawing a tangent at the dope polymer concentration on the polymer/solvent/nonsolvent ternary phase diagram and extrapolating to the solvent/nonsolvent axis [8]. As such, bore fluid compositions varying between 5-10 wt% deionized water in N-methyl-2-

pyrrolidine (NMP) were used as the bore fluid in this work to obtain a "neutral" bore fluid.

2.2.1.2.2. *Spinning Temperature*

For polymer solutions displaying an upper critical solution temperature (UCST), dope compositions are more stable at higher temperatures. Spinning temperature is an extremely important parameter when thermally induced phase separation (TIPS) is used to form the membrane. In this work, immersion precipitation was exclusively used to form the asymmetric membranes and as such a constant and convenient spinning temperature of 50 ℃ was used throughout the work. This temperature was selected based on the lowest boiling point of the lowest boiling component of the dope (upper bound) and extrusion pressure drop based on solution viscosity (lower bound).

2.2.1.2.3. *Air Gap*

The air gap has been used as a parameter to encourage skin formation. Based on the presence of volatile solvents within the dope, evaporation of the solvents/nonsolvents within the air gap can be used to increase the concentration of the polymer in the outer circumference of the fiber. The use of air gap for skin formation has been extensively studied by Carruthers [9, 25]. The air gap was primarily used in this work to enhance the formation of the skin via the evaporation of volatile solvents/nonsolvents. Air gaps between 0.5 cm and 20 cm were explored in this work with an air gap of 10 cm used as the base case.

2.2.1.2.4. *Draw Ratio*

Draw ratio in this work is defined as the ratio of the fiber take-up rate to the average dope extrusion velocity. This definition discounts the effect of possible die swell of the polymer solution after extrusion from the spinneret. Including the effect of die swell

would result in higher draw ratios than reported here. However, as the estimation of die swell was not performed in this work, the nominal draw ratio, as defined above, is used. Drawing of the nascent membrane in the air gap can be used to increase the orientation of the polymer chains in the skin region of the hollow fiber. Additionally, higher draw ratios have been found to suppress macrovoid growth in polymer-only fibers [26, 27]. Draw ratios (nominal) varying between 2.7 and 6.2 were used in this work primarily to probe the effect of macrovoid suppression in hollow fibers.

2.2.1.2.5. *Quench Bath Composition*

The quench medium strongly influences the phase separation kinetics of the membrane. Use of poor nonsolvents results in denser, low porosity membranes with large skin thicknesses. Addition of solvents and salts to the generally strong non-solvent in the quench bath has also been performed to lower non-solvent activity, thus also leading to denser membranes [28, 29]. As the objective in this work was to produce fibers with industrially relevant productivities, a strong nonsolvent, water, as the coagulant, was used to produce high porosity in the membrane support structure. A constant quench bath temperature of 25 ºC, based on prior work by Carruthers [9], was used in this work.

2.3. MIXED MATRIX MEMBRANES

2.3.1. Mixed Matrix Dense Films

Combinations of solid/polymer mixed matrix membranes include nonporous inorganic/polymer, microporous and mesoporous inorganic molecular sieve/polymer, carbon/polymer, layered materials/clays/polymer and microporous organic host/polymer. Considerable differences exist between formulations for dense films versus asymmetric membranes with dense film formulations typically consisting of fewer components. Dense films are made via the gradual removal of the solvent while asymmetric films are made through a phase separation mechanism. The difference in formation mechanisms is the primary reason for the difference in formulations for the two types of membranes.

While in dense films, homogeneous mixing of solids and stresses at the film-support interface are the major concerns, asymmetric membrane formation includes more complications induced by phase separation, especially at the solid/polymer interface.

Initial research work on characterization and measuring transport properties is generally carried out with dense films. However, with introduction of solids, the earlier simplicity in forming dense films is lost, leading to increased complications in processing of mixed matrix dense films. Early researchers have coped with devising mixing procedures to homogeneously disperse solids in polymer solutions followed by casting of membranes at high temperatures [30], under controlled evaporation regimes and using various annealing procedures [31, 32]. Initial mixing procedures have varied from the addition of powdered dispersed phase (DP) into the polymer solution and processed through an extruder, use of high speed mixers and sonicators [33, 34] to mix the DP dispersion with the polymer solution and multi step mixing procedures where a small quantity of polymer is sonicated in a dispersion solvent and DP dispersion (a so called "priming" step) followed by the addition of additional polymer to increase viscosity for casting and to produce the desired polymer-to-inorganic or carbon solid ratio in the final sample [35, 36]. The tradeoff between excessive mixture viscosity (casting difficulty) and inadequate viscosity (sedimentation of the denser DP) is especially important in the formulation concentrations. The experience gained from dense film work has been used as a first step in processing mixed matrix dopes for asymmetric membranes, since the selection of such structures must also allow the dense selective skin layer to function properly.

Dense mixed matrix film formulation typically includes the polymer, solvent and the DP. For an enhancement in the selectivity (mixed matrix effect) it is necessary that the sieve have good contact with the polymer to prevent non-selective bypass of the gas molecules. Although the objective is to study as simple a system as possible, additives are typically included in the formulation to improve polymer and DP adhesion. Foremost among

26

them, plasticizers have been used to increase the flexibility of the matrix polymer, however, the presence of the plasticizer though improving the adhesion between the polymer and zeolite, usually results in poor transport properties of the membrane [37]. Further silane coupling agents have been used with varying success to improve the adhesion between the polymer and the DP [31, 38-40] and using polymers with reactive functionality that could interact with the DP [41].

Casting procedures generally include using a doctor knife to spread the mixture on a support, Teflon or glass among others, from which the film can be easily removed after drying. The initial solvent evaporation is generally done under controlled conditions and temperatures, followed by a drying step at higher temperatures to remove any remaining solvent [42].

2.3.2. Asymmetric Mixed Matrix Membranes

Practical membranes used in film or hollow fiber geometry for separations consist of an asymmetric structure, where a thin skin layer performs the actual separation and the porous layer underneath acts as a support to the skin. This structure sharply increases the productivity of the membrane, since the productivity is inversely proportional to the separating layer thickness, with the support layer ideally providing little or no resistance to gas flow. As the skin layer performs the separation function, the highly selective DP need only be dispersed in the skin region of the asymmetric membrane. Dual layer membranes, where the DP is included only in the outer layer with the inner layer forming the porous support, lower the use of expensive DP in mixed matrix membranes.

The dope formulation for dense mixed matrix films must be revisited for making asymmetric membranes as the asymmetric structure of the membrane is controlled by phase separation kinetics. Solvents used in dense film formulation may be replaced in asymmetric formulations to control the phase separation rate of the membrane within the

nonsolvent (quench) bath and obtain membranes of varying porosities [43]. Further, non-solvents and additives can be added to fine tune the morphology of the membrane to control pore sizes and suppress the formation of large voids within the membrane [23, 44-48]. Asymmetric skinned membranes can also contain a second more volatile solvent which can evaporate and form a high solids concentration layer (skin) on the exposed surface of the membrane [49]. A final difference between films and fibers can include a higher viscosity dope for fiber spinning to prevent capillary instability during the spinning process [50].

Once the formulation is established, asymmetric membrane can be cast or spun (extruded through a spinneret) into fiber form, followed either by an evaporation step, or directly submerged into the quench bath. In this process, the nonsolvent penetrates the membrane and the solvent diffuses out into the quench bath. The entering nonsolvent causes the phase separation of the membrane with the porosity being formed by the domains of polymer lean phase which are washed out of the final membrane structure. For mixed matrix membranes, it is believed that defects (sieve-in-cage) can form due to the nucleation of nonsolvent/polymer lean phase around the DP during the phase separation [51]. One successful approach to combat this problem describes the modification of the DP to decrease the interaction of the surface with the solvents and nonsolvents within the dope mixture leading to a hypothesized suppression of the nucleation of the hydrophilic polymer lean phase. This approach is described in Chapter 5.

Successful spinning of mixed matrix hollow fiber membranes for gas separation has so far been only demonstrated in a patent by Ekiner et al.[52]. Ekiner et al. grafted polymer to the surface of the molecular sieve using a silane coupling agent. In this process, the surface modification of the sieve along with a dope additive (tetramethylenesulfone), which presumably adsorbs onto the surface of the zeolite, were cited as the cause of the enhanced adhesion between the polymer and the sieve. However, as discussed in Chapter

4, in the absence of tetramethylesulfone, poor bonding between the polymer and sieve is observed.

A major hurdle to the commercial implementation of mixed matrix membranes has been the lack of reproducibility in forming successful mixed matrix membranes. Increasing challenges with poor polymer-sieve interaction, variability in molecular sieve transport and surface characteristics and effect of contaminants on molecular sieve performance have been identified in dense mixed matrix fields which are also highly relevant to asymmetric membranes [53].

A recent publication raises the issue of possible particle migration within the mixed matrix hollow fiber membranes [54]. Comparing with earlier evidence of particle migration in sheared viscoelastic suspensions [55-57], such a development seems possible in mixed matrix hollow fiber spinning, however, only if the particle concentration in the spinning dope is high (generally greater than 10% by volume) or the elasticity of the dope is very large [56, 58]. Additionally, the authors report using Energy Dispersive Spectroscopy (EDS) line-scans across membrane morphology filled with voids to determine particle distribution data. Such methods, depending on the electron beam voltage and void size, analyze extensive regions below the visible surface of the sample and can easily lead to erroneous results brought about by embedded particle agglomerates. These issues must be understood in a general framework across multiple molecular sieve and polymer combinations before the technology of mixed matrix hollow fibers can be applied successfully in the field.

While porous defects between the solid and polymer are undesirable in microporous solid/polymer membranes gas separation membranes, the opposite is true for ultrafiltration [59] and ion exchange mixed matrix membranes [60]. The presence of such voids enhances membrane performance as the solid acts only in the adsorbent

capacity and not as a molecular sieve as required in the case of the membranes for gas separations.

Mesoporous solid/polymer membranes can be easily formed in asymmetric form using carbons and mesoporous ion exchange resins embedded in a polymer matrix. Although, carbons and activated carbons have traditionally been used for their adsorbent properties, increasing attention is being paid to their use in gas separation [61, 62]. The research on carbon/polymer and carbon/zeolite mixed matrix membranes is still in its infancy and challenges of membrane brittleness seen in carbon/polymer membranes with relevant carbon loadings must be overcome before their general application.

2.4. MAXWELL MODEL FOR PERMEATION IN MIXED MATRIX MEMBRANES

The constitutive equations governing electric potential and the flux through membranes are analogues, permitting the application of Maxwell's equation to transport in mixed matrix membranes [63-65]. This model provides a simple, quantitative framework to predict the transport properties of mixed matrix materials when the transport properties of the constituent phases are known, especially at relatively low dispersed phase volume fractions. Studies on the validity of the model for particle loadings of 28 volume % have been reported by Petropoulos [65].

Since other models such as the Landauer model (Effective Medium Theory) [66], Bruggemann model [67] and Higuchi model [68, 69] usually give similar predictions, without providing an intuitive physical framework of the transport process, the Maxwell model was used in this work to predict mixed matrix performance. The Maxwell model for the permeability of a dilute suspension of spherical particles is as follows:

$$P_{mm} = P_c \left[\frac{P_d + 2P_c - 2\phi_d \left(P_c - P_d \right)}{P_d + 2P_c + \phi_d \left(P_c - P_d \right)} \right] \qquad (2.4)$$

where, P_c and P_d refer to the continuous and dispersed phases, respectively. The volume fraction of the dispersed phase is Φ_d.

2.5. REFERENCES

1. Baker, R.W., *Membrane Technology and Applications*. 2nd ed. 2004: John Wiley & Sons, Ltd. 538 pp.

2. Loeb, S. and S. Sourirajan, *Sea water demineralization by means of an osmotic membrane.* Advances in Chemistry Series, 1963. **38**: p. 117-32.

3. Reuvers, A.J., J.W.A. Van den Berg, and C.A. Smolders, *Formation of membranes by means of immersion precipitation. Part I. A model to describe mass transfer during immersion precipitation.* Journal of Membrane Science, 1987. **34**(1): p. 45-65.

4. Li, S.G., G.H. Koops, M.H.V. Mulder, T. van den Boomgaard, and C.A. Smolders, *Wet spinning of integrally skinned hollow fiber membranes by a modified dual-bath coagulation method using a triple orifice spinneret.* Journal of Membrane Science, 1994. **94**(1-3): p. 329-40.

5. Koros, W.J. and G.K. Fleming, *Membrane-based gas separation.* J. Membr. Sci., 1993. **83**(1): p. 1-80.

6. McKelvey, S.A., *Formation and characterization of hollow fiber membranes for gas separation (fiber breaks, macrovoids).* 1997. p. 227 pp.

7. Barrer, R.M., *Diffusion and permeation in heterogeneous media*, in *Diffusion in polymers*, J. Crank and G.S. Park, Editors. 1968, Academic Press: New York. p. 165-217.

8. Wallace, D.W., *Crosslinked hollow fiber membranes for natural gas purification and their manufacture from novel polymers*, in *Chemical Engineering*. 2004, University of Texas--Austin. p. 221 pp.

9. Carruthers, S.B., *Integral-skin formation in hollow fiber membranes for gas separations*, in *Chemical Engineering*. 2001, University of Texas--Austin. p. 233 pp.

10. Pinnau, I. and W.J. Koros, *Relationship between substructure resistance and gas separation properties of defect-free integrally skinned asymmetric membranes.* Industrial & Engineering Chemistry Research, 1991. **30**(8): p. 1837-40.

11. Clausi, D.T., S.A. McKelvey, and W.J. Koros, *Characterization of substructure resistance in asymmetric gas separation membranes.* Journal of Membrane Science, 1999. **160**(1): p. 51-64.

12. Moore, S., E., *Apparatus for spining of multicomponent hollow fibers*. 1994, E.I. du Pont de Nemours and Company: US 5,320,512.

13.   Shieh, J.J., T.S. Chung, R. Wang, M.P. Srinivasan, and D.R. Paul, *Gas separation performance of poly(4-vinylpyridine)/polyetherimide composite hollow fibers.* Journal of Membrane Science, 2001. **182**(1-2): p. 111-123.

14.   Li, D.F., T.-S. Chung, R. Wang, and Y. Liu, *Fabrication of fluoropolyimide/polyethersulfone (PES) dual-layer asymmetric hollow fiber membranes for gas separation.* Journal of Membrane Science, 2002. **198**(2): p. 211-223.

15.   Liu, Y., T.-S. Chung, R. Wang, D.F. Li, and M.L. Chng, *Chemical Cross-Linking Modification of Polyimide/Poly(ether sulfone) Dual-Layer Hollow-Fiber Membranes for Gas Separation.* Industrial & Engineering Chemistry Research, 2003. **42**(6): p. 1190-1195.

16.   He, T., M.H.V. Mulder, H. Strathmann, and M. Wessling, *Preparation of composite hollow fiber membranes: co-extrusion of hydrophilic coatings onto porous hydrophobic support structures.* Journal of Membrane Science, 2002. **207**(2): p. 143-156.

17.   Myers, D., *Surfaces, Interfaces, and Colloids: Principles and Applications.* 1991. p. 433 pp.

18.   Pereira, C.C., R. Nobrega, K.V. Peinemann, and C.P. Borges, *Hollow fiber membranes obtained by simultaneous spinning of two polymer solutions: a morphological study.* Journal of Membrane Science, 2003. **226**(1-2): p. 35-50.

19.   Altena, F.W. and C.A. Smolders, *Calculation of liquid-liquid phase separation in a ternary system of a polymer in a mixture of a solvent and a nonsolvent.* Macromolecules, 1982. **15**(6): p. 1491-7.

20.   Ziabicki, A., *Fundamentals of fibre formation.* 1976, London: John Wiley & Sons. 488.

21.   McKelvey, S.A. and W.J. Koros, *Phase separation, vitrification, and the manifestation of macrovoids in polymeric asymmetric membranes.* Journal of Membrane Science, 1996. **112**(1): p. 29-39.

22.   Cabasso, I., E. Klein, and J.K. Smith, *Polysulfone hollow fibers. I. Spinning and properties.* Journal of Applied Polymer Science, 1976. **20**(9): p. 2377-94.

23.   Cabasso, I., E. Klein, and J.K. Smith, *Polysulfone hollow fibers. II. Morphology.* Journal of Applied Polymer Science, 1977. **21**(1): p. 165-80.

24.   Pesek, S.C. and W.J. Koros, *Aqueous quenched asymmetric polysulfone hollow fibers prepared by dry/wet phase separation.* Journal of Membrane Science, 1994. **88**(1): p. 1-19.

25.   Carruthers, S.B., G.L. Ramos, and W.J. Koros, *Morphology of integral-skin layers in hollow-fiber gas-separation membranes.* Journal of Applied Polymer Science, 2003. **90**(2): p. 399-411.

26.   Ekiner, O.M. and G. Vassilatos, *Polyaramide hollow fiber membranes for gas separation-spinning and properties.* Polymeric Materials Science and Engineering, 2002. **86**: p. 120.

27.   Wang, K.Y., D.F. Li, T.-S. Chung, and S.B. Chen, *The observation of elongation dependent macrovoid evolution in single- and dual-layer asymmetric hollow fiber membranes.* Chemical Engineering Science, 2004. **59**(21): p. 4657-4660.

28.   Frommer, M.A., R. Matz, and U. Rosenthal, *Mechanism of formation of reverse osmosis membranes. Precipitation of cellulose acetate membranes in aqueous solutions.* Industrial & Engineering Chemistry Product Research and Development, 1971. **10**(2): p. 193-6.

29.   Boom, R.M., I.M. Wienk, T. Van den Boomgaard, and C.A. Smolders, *Microstructures in phase inversion membranes. Part 2. The role of a polymeric additive.* Journal of Membrane Science, 1992. **73**(2-3): p. 277-92.

30.   Mahajan, R., R. Burns, M. Schaeffer, and W.J. Koros, *Challenges in forming successful mixed matrix membranes with rigid polymeric materials.* J. Appl. Polym. Sci., 2002. **86**(4): p. 881-890.

31.   Duval, J.M., A.J.B. Kemperman, B. Folkers, M.H.V. Mulder, G. Desgrandchamps, and C.A. Smolders, *Preparation of zeolite filled glassy polymer membranes.* Journal of Applied Polymer Science, 1994. **54**(4): p. 409-18.

32.   Cornelius, C., C. Hibshman, and E. Marand, *Hybrid organic-inorganic membranes.* Separation and Purification Technology, 2001. **25**(1-3): p. 181-193.

33.   Kulprathipanja, S., R.W. Neuzil, and N.N. Li, *Separation of fluids by means of mixed matrix membranes.* 1988, (Allied-Signal, Inc., USA): U.S. p. 7 pp.

34.   Rojey, A., A. Deschamps, A. Grehier, and E. Robert, *Process for separation of the constituents of a mixture in the gas phase using a composite membrane.* 1990, (Institut Francais Du Petrole): US. p. 10 pp.

35.   Mahajan, R. and W.J. Koros, *Factors Controlling Successful Formation of Mixed-Matrix Gas Separation Materials.* Ind. Eng. Chem. Res., 2000. **39**(8): p. 2692-2696.

36.   Vu, D.Q., W.J. Koros, and S.J. Miller, *Mixed matrix membranes using carbon molecular sieves. I. Preparation and experimental results.* Journal of Membrane Science, 2003. **211**(2): p. 311-334.

37.   Mahajan, R., R. Burns, M. Schaefer, and W. Koros, *Challenges in forming successful mixed matrix membranes with rigid polymeric materials.* Journal of Applied Polymer Science, 2002. **86**: p. 881-90.

38.   Vankelecom, I.F.J., S. Van den Broeck, E. Merckx, H. Geerts, P. Grobet, and J.B. Uytterhoeven, *Silylation To Improve Incorporation of Zeolites in Polyimide Films.* J. Phys. Chem., 1996. **100**(9): p. 3753-8.

39.   Mahajan, R. and W.J. Koros, *Mixed matrix membrane materials with glassy polymers. Part 1.* Polymer Engineering and Science, 2002. **42**(7): p. 1420-1431.

40.   Kulkarni, S.S., D.J. Hasse, D.R. Corbin, and A.N. Patel, *Gas separation membrane with organosilicon-treated molecular sieve.* 2003, (L'Air Liquide - Societe Anonyme a Directoire et Conseil de Surveillance pour l'Etude et l'Exploitation des Procedes Georges Claude, Fr.). Application: US. p. 12 pp.

41.   Mahajan, R. and W.J. Koros, *Mixed matrix membrane materials with glassy polymers. Part 2.* Polymer Engineering and Science, 2002. **42**(7): p. 1432-1441.

42.   Moore, T.T., *Effects of materials, processing, and operating conditions on the morphology and gas transport properties of mixed matrix membranes.* 2004, Univ. of Texas, Austin, TX, USA. p. 311 pp.

43.   Frommer, M.A., I. Feiner, O. Kedem, and R. Bloch, *The mechanism for formation of "skinned" membranes : II. Equilibrium properties and osmotic flows determining membrane structure.* Desalination, 1970. **7**(3): p. 393-402.

44.   Pinnau, I. and W.J. Koros, *Structures and gas separation properties of asymmetric polysulfone membranes made by dry, wet, and dry/wet phase inversion.* Journal of Applied Polymer Science, 1991. **43**(8): p. 1491-1502.

45.   Fritzsche, A.K., C.A. Cruse, R.E. Kesting, and M.K. Murphy, *Polysulfone hollow-fiber membranes spun from Lewis acid:base complexes. II. The effect of Lewis acid-to-base ratio on membrane structure.* Journal of Applied Polymer Science, 1990. **39**(9): p. 1949-56.

46.   Kesting, R.E., A.K. Fritzsche, C.A. Cruse, and M.D. Moore, *The second-generation polysulfone gas-separation membrane. II. The relationship between sol properties, gel macrovoids, and fiber selectivity.* Journal of Applied Polymer Science, 1990. **40**(9-10): p. 1575-82.

47.   Ekiner, O.M. and G. Vassilatos, *Polyaramide hollow fibers for hydrogen/methane separation - spinning and properties.* J. Membr. Sci., 1990. **53**(3): p. 259-73.

48.   Pesek, S.C. and W.J. Koros, *Aqueous quenched asymmetric polysulfone membranes prepared by dry/wet phase separation.* Journal of Membrane Science, 1993. **81**(1/2): p. 71-88.

49.   Pinnau, I., *Skin Formation of Integral-Asymmetric Gas Separation Membranes Made By Dry/Wet Phase Inversion (Gas Separation)*, in *Department of Chemical Engineering*. 1991, Univ. of Texas, Austin, TX, USA. p. 342.

50.   Wallace, D.W., *Crosslinked hollow fiber membranes for natural gas purification and their manufacture from novel polymers*. 2004, Univ. of Texas, Austin, TX, USA. p. 202 pp.

51.   Husain, S. and W.J. Koros. *Mixed matrix hollow fibers for gas separation*. in *North American Membrane Society*. 2005. Providence, RI.

52.   Ekiner, O.M. and S.S. Kulkarni, *Process for making mixed matrix hollow fiber membranes for gas separation*. 2003, (L'Air Liquide Societe Anonyme A Directoire Et Conseil De Surveillance Pour L'etude Et L'exploitation Des Procedes Georges Claude, Fr.). US 6,663,805.

53.   Moore, T.T. and W.J. Koros, *Non-ideal effects in organic-inorganic materials for gas separation membranes*. Journal of Molecular Structure, 2005. **739**(1-3): p. 87-98.

54.   Jiang, L.Y., T.S. Chung, C. Cao, Z. Huang, and S. Kulprathipanja, *Fundamental understanding of nano-sized zeolite distribution in the formation of the mixed matrix single- and dual-layer asymmetric hollow fiber membranes*. Journal of Membrane Science, 2005. **252**(1-2): p. 89-100.

55.   Karnis, A. and S.G. Mason, *Particle motions in sheared suspensions. XIX. Viscoelastics media*. Transactions of the Society of Rheology, 1966. **10**(2): p. 571-92.

56.   Tehrani, M.A., *An experimental study of particle migration in pipe flow of viscoelastic fluids*. Journal of Rheology (New York), 1996. **40**(6): p. 1057-1077.

57.   Gauthier, F., H.L. Goldsmith, and S.G. Mason, *Particle Motions in Non-Newtonian Media. II. Poiseuille Flow*. Trans. Soc. Rheology, 1971. **15**(2): p. 297-330.

58.   Leighton, D. and A. Acrivos, *The shear-induced migration of particles in concentrated suspensions*. Journal of Fluid Mechanics, 1987. **181**: p. 415-39.

59.   Polotskaya, G., Y. Biryulin, and V. Rozanov, *Asymmetric Membranes Based on Fullerene-Containing Polyphenylene Oxide*. Fullerenes, Nanotubes, and Carbon Nanostructures, 2004. **12**(1 & 2): p. 371-376.

60.   Kiyono, R., G.H. Koops, M. Wessling, and H. Strathmann, *Mixed matrix microporous hollow fibers with ion-exchange functionality*. Journal of Membrane Science, 2004. **231**(1-2): p. 109-115.

61. Zimmerman, C.M., A. Singh, and W.J. Koros, *Tailoring mixed matrix composite membranes for gas separations.* Journal of Membrane Science, 1997. **137**(1-2): p. 145-154.

62. Vu, D.Q., *Formation and characterization of asymmetric carbon molecular sieve and mixed matrix membranes for natural gas purification*, in *Department of Chemical Engineering*. 2001, Univ. of Texas, Austin, TX, USA.

63. Maxwell, J.C., *A treatise on electricity and magnetism.* Vol. 1. 1873, Oxford: Clarendon press.

64. Robeson, L.M., A. Noshay, M. Matzner, and C.N. Merriam, *Physical property characteristics of polysulfone/poly(dimethylsiloxane)block copolymers.* Angew. Makromol. Chem., 1973. **29-30**: p. 47-62.

65. Petropoulos, J.H., *A comparative study of approaches applied to the permeability of binary composite polymeric materials.* J. Polym. Sci., Polym. Phys. Ed., 1985. **23**(7): p. 1309-24.

66. Landauer, R., *The electrical resistance of binary metallic mixtures.* J. Appl. Phys., 1952. **23**: p. 779-84.

67. Bruggemann, D.A.G., *Berechnung verschiedener physikalischer Konstanten von heterogenen Substanzen. I. Dielektrizitatskonstanten und Leitfahigkeiten der Mischkorper aus isotropen Substanzen (The calculation of various physical constants of hetereogeneous substances. I. The dielectric constants and conductivities of mixtures composed of isotropic substances.* Annalen der Physik V, 1935. **24**: p. 636.

68. Higuchi, W.I., *A new relation for the dielectric properties of two-phase mixtures.* J. Phys. Chem., 1958. **62**: p. 649-53.

69. Higuchi, W.I. and T. Higuchi, *Theoretical analysis of diffusional movement through heterogeneous barriers.* J. Am. Pharm. Assoc., Sci. Ed., 1960. **49**: p. 598-606.

CHAPTER 3

MATERIALS AND METHODS

3.1. MATERIALS

Most materials used in this research were used as-received without any further purification. The hollow fiber spinning setup used in this research was designed to provide easy scale-up for manufacturing as such, conditions generally employed in the industry with regard to material purity and processing were used. Whenever possible, commercial sources for materials of particular batch identification were used for consistency in product quality.

3.1.1. Polymers

Extending the work of Mahajan [1] from the dense film morphology to asymmetric hollow fiber geometry, Ultem® 1000 polyetherimide (GE Plastics, Pittsfield, MA)) was selected as the polymer of choice for exploratory spinning of mixed matrix materials. Ultem® is an engineering polymer with high selectivities for oxygen/nitrogen (O_2/N_2) with considerable flexibility provided by the ether linkage in the polymer backbone. It is thought that the flexibility of the polymer, as observed by positive mixed matrix results with polyvinylacetate (glass transition temperature (T_g) = 35 ºC), allows the polymer chains to form durable attachments that are more resistant to stresses and thermal cycling. Unfortunately, polymers with desirable properties of high temperature stability and spinnability are generally high T_g polymers with T_g's exceeding 200 ºC. A second polymer, popular as a membrane material for O_2/N_2 and carbon dioxide/methane (CO_2/CH_4) separations, Matrimid® 5218 (Vantico; Brewster, NY), was also used in this work. Matrimid® has a higher gas permeability than Ultem® and as a result of higher glass transition temperature (315 ºC) is less flexible than Ultem® and poses greater

challenges as a mixed matrix material [2]. The material and permeation (dense film) properties of Ultem® and Matrimid® are shown in Table 3.1 and Table 3.2. The structures of the polymers are displayed in Figure 3.1.

Table3.1: Selected physical properties of Ultem® and Matrimid®

	Density (g/cm^3)	Tg (ºC)	Young's modulus, MPa (tensile)	Mw
Ultem®	1.28 [3]	215 [4]	3309 [3]	62,161 [5]
Matrimid®	1.2 [6]	305 [7]	2689 [6]	71,870

Table 3.2: Pure gas permeation properties of Ultem® and Matrimid® at 35 ºC.

	Permeability (Barrer)			Selectivity			
	O_2	CO_2	He	O_2/N_2	CO_2/CH_4	CO_2/N_2	He/N_2
Ultem® [8]	0.4	1.4	9.4	7.6	37.4	24.7	178.6
Matrimid® [7]	2.0	10.0	20.8 [†]	6.9	35.3	34.5	95.4 [†]

[†] [9]
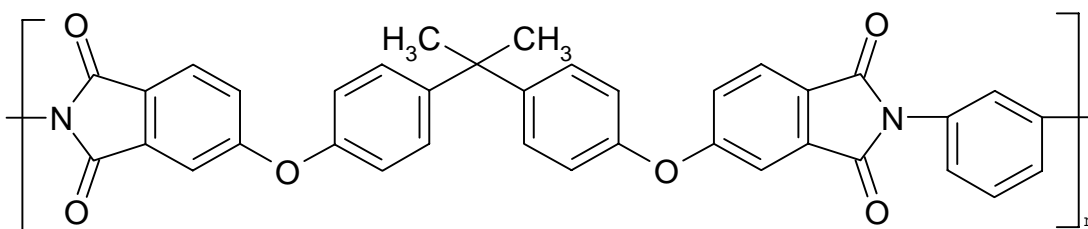
BPADA-mPDA (Ultem®) 2,2-bis[4-(3,4-dicarboxyphenoxy)phenyl] propane dianhydride - 1,3-phenylenediamine
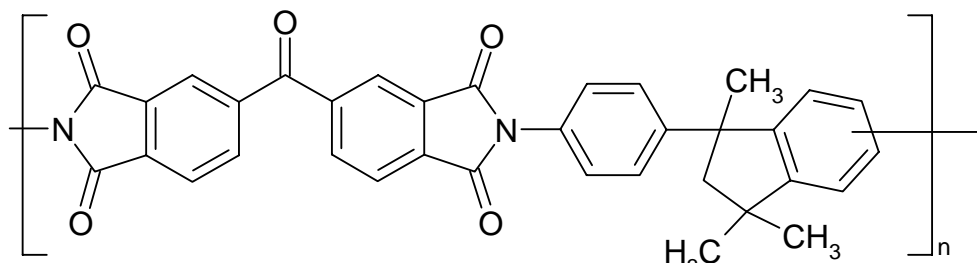
BTDA-DAPI (Matrimid®); 3,3',4,4'-benzophenonetetracarboxylic acid dianydride - 5(6)-amino-1-(4' aminophenyl)-1,3,3-trimethylindane

Figure 3.1: Structural repeat units of Ultem ® polyetherimide and Matrimid® polyimide

3.1.2. Molecular Sieves/Inserts

3.1.2.1. *Zeolites*

This research concentrated on the separation of carbon dioxide from methane and nitrogen production from air, and as such, zeolite molecular sieves, with high selectivities for these separations were used. Two zeolite types, HSSZ-13 (CHA) and Zeolite 4A (Linde Type A), providing two different silicon to aluminum ratios were selected for this work. The zeolite framework structures are shown in Figure 3.2 and Figure 3.3. Selected properties for the two zeolites are given in Table 3.3.
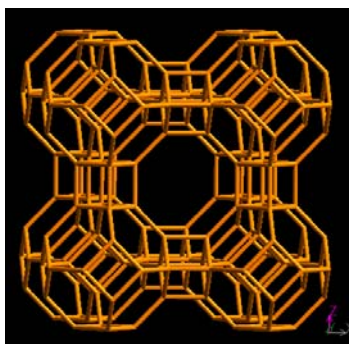
Figure 3.2: Framework structure for the zeolite 4A (LTA). Each vertex represents the center of a silica or alumina tetrahedron. Structures from International Zeolite Association; http://www.iza-structure.org.
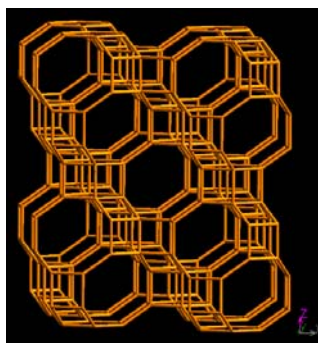
Figure 3.3: Framework structure for the SSZ-13 (CHA) zeolite. Each vertex represents the center of a silica or alumina tetrahedron. Structures from International Zeolite Association; http://www.iza-structure.org.

Table 3.3: Selected properties of zeolite 4A and SSZ-13 [7]

| | Permeability (Barrer) | | Selectivity | | Density (g/cm^3) | Pore Size Å |
	O_2	CO_2	O_2/N_2	CO_2/CH_4		
Zeolite 4A	0.77	15	37	340	1.52	3.8
SSZ-13	10	200	40	800	1.51	3.8

Zeolites from a specific batch were used throughout this work to eliminate variation in the Si:Al ratio typically seen from batch to batch. The Si:Al ratio for SSZ-13 is about 25 while that of the zeolite 4A is typically about 1. These molecular sieves were synthesized and provided by Chevron Research and Technology Company (Richmond, CA). SEM microphotographs of the as-received zeolites are shown in Figure 3.4 and Figure 3.5.
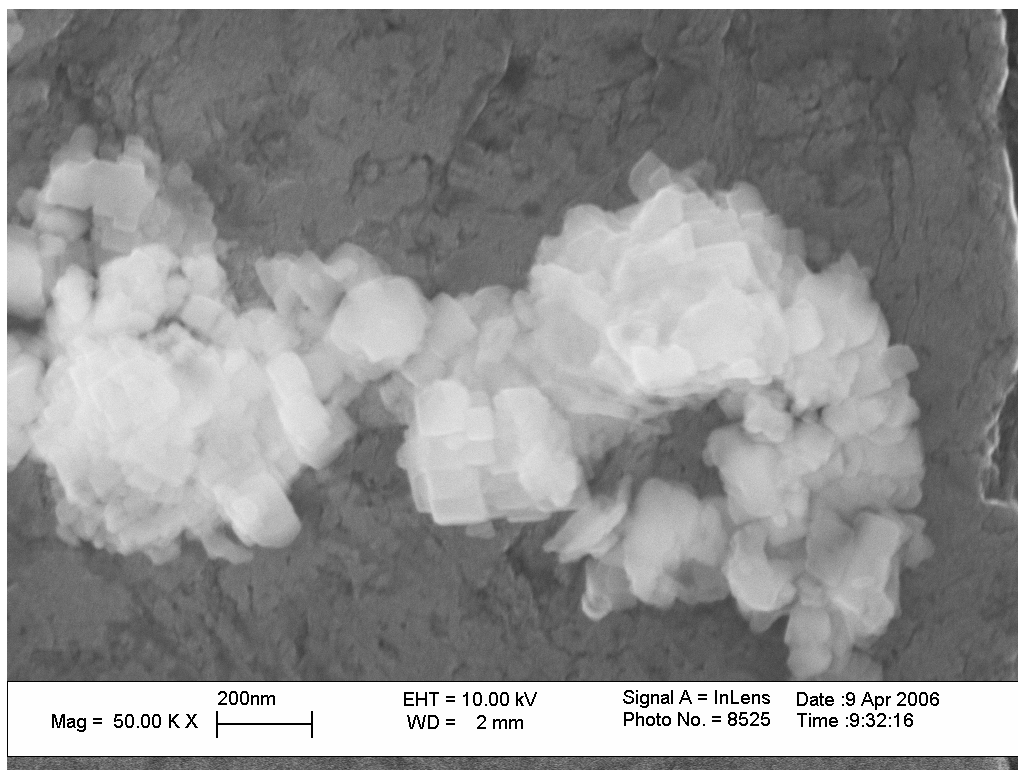
Figure 3.4: SEM micrograph of as-received zeolite SSZ-13

41
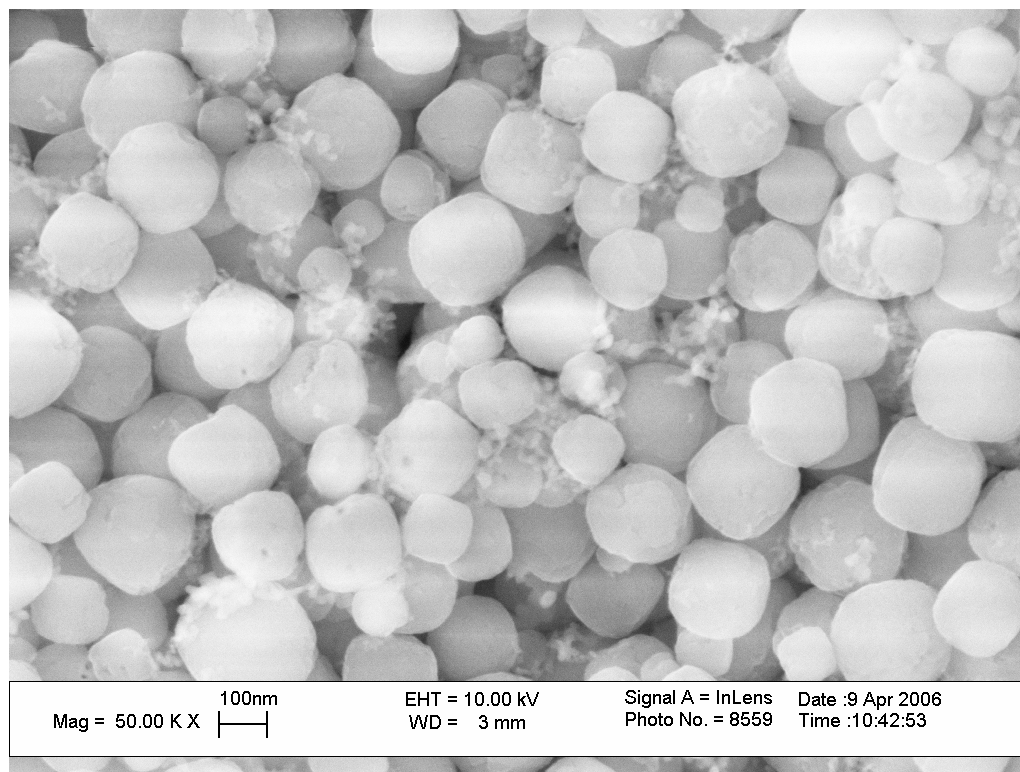
Figure 3.5: SEM micrograph of as-received zeolite 4A

3.1.2.2. Non-porous Silica

Non-porous 110 nm spherical silica particles (MP-1040) were graciously provided by Nissan Chemicals (Houston, TX). The particles were received as a 40 wt% dispersion in water. The dispersion was dialyzed with de-ionized water, thrice, followed by dialysis with methanol (three repeats). The methanol was allowed to evaporate at room temperature followed by drying of the particles at 150 ℃ under vacuum before use. A SEM micrograph of the particles is shown in Figure 3.6.
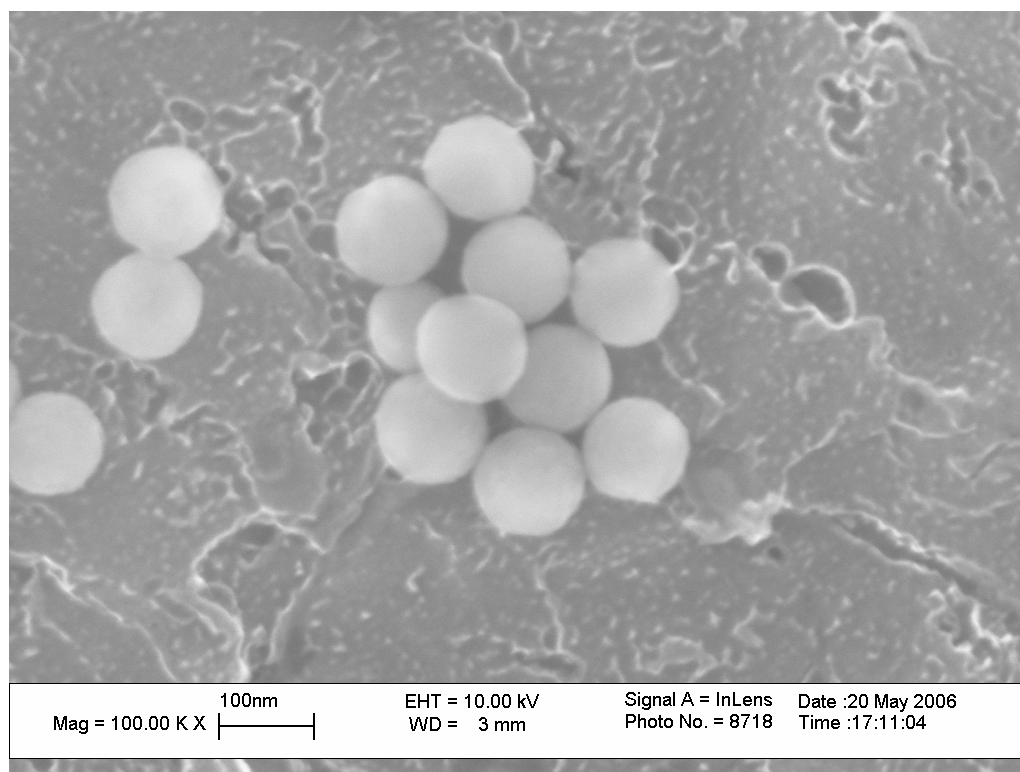
Figure 3.6: SEM micrograph of 110nm silica particles

3.1.3. Solvents and Nonsolvents

N-methyl-2-pyrrolidione (NMP) (*ReagentPlus*™ 99 % or anhydrous 99.5 %, Aldrich, Milwaukee, WI) was used as the primary solvent for dissolving the polymers and dispersing the sieves. NMP is a strong solvent for both Ultem® and Matrimid® and is completely miscible in water. Tetrahydrofuran (THF) (Anhydrous 99.9 %, Aldrich) was used as the "evaporative solvent" to promote skin formation. THF is a good solvent for Matrimid® but a weak swelling agent for Ultem®.

Methanol (99.8 %, ACS reagent, Aldrich) was used during the solvent exchange step to exchange out water from the hollow fibers. Hexanes (ACS reagent > 98.5 %, Baker) was used to exchange out methanol from the fibers. The objective of the solvent exchange was to replace a higher surface tension fluid with a lower surface tension fluid prior to drying, to prevent collapse of the delicate membrane morphology due to capillary forces.

2-propanol (IPA) (Anhydrous 99.5 %, Aldrich) was used during the silanation of the zeolites (described in Section 4.3.1) and also as a quenching agent for the excess Grignard reagent during the Grignard treatment of zeolites (described in Section 5.3). Toluene (Anhydrous 99.8 %, Aldrich) was used as the solvent for the Grignard surface modification of the zeolites used in this research.

3.1.4. Surface Modifying Agents

3.1.4.1. Silane Coupling Agent

Based on earlier work by Mahajan [10, 11], γ-aminopropyldimethylethoxy silane (APDMES) (Gelest ,Morrisville, PA) was used as the silane coupling agent of choice in this work. The grafting of the polymer on the surface of the zeolite imparts steric stability to the particles and allows the particles to be better dispersed in solvent.

3.1.4.2. Reactants for the Grignard Treatment

A treatment for enhancing the adhesion between sieve and polymer (Ultem®, Matrimid®) was developed in this research. Thionyl Chloride (*ReagentPlus™*, 99.5 %, low iron, Sigma-Aldrich) was used as the first step treatment followed by methylmagnesium bromide (3.0 M in diethyl ether, Aldrich).

3.1.4.3. Other Chemicals

Lithium Nitrate (Sigma-Aldrich) was used to enhance viscosity of the dopes to provide capillary stability for spinning. The use of lithium nitrate allows a lower concentration of polymer to be used in the spinning dope, resulting in more porous and higher flux asymmetric membranes. The lithium nitrate was dried at 120 ºC overnight under vacuum before use.

Trimesoyl Chloride (purum, ≥ 96.0 %, Fluka), Diethyltoluenediamine (Ethacure® 100, Albermarle Corporation, Baton Rouge, LA), Sylgard® 184 (Dow Chemicals, Midland, MI), iso-octane (Anhydrous 99.8 %, Aldrich) and n-heptane (99 %+, Acros Organics)

were used in this research for post-treatment/caulking of defective hollow fibers. The post-treatment procedure is described in section 3.2.6.

3.1.4.4. *Gases*

All gases used were provided by Air Products/Air Gas. Pure gases (O_2, N_2, CO_2 and CH_4) were of purity 99.999 % or greater. Mixed gas (80.0 mol % CH_4, balance CO_2) was used to confirm that the thin skin and/or post-treated layer were not being plasticized at testing CO_2 partial pressures.

3.2.   HOLLOW FIBER MEMBRANE FORMATION

3.2.1.   Core Dope Preparation

The polymer-only dopes were made by weighing out the requisite quantities of NMP and THF in a one liter glass jar sealed with a polytetrafluoroethylene (PTFE) lined cap. Dried lithium nitrate was then dissolved in the solvent mixture using sonication (Model: 1510R-MTH, *maximum* output 70 W, Branson Ultrasonics Corp., Danbury, CT). After the salt dissolved in the NMP/THF mixture, dried polymer powder was added and the mixture placed on a roll mill until complete dissolution occurred. The dissolution rate was accelerated by the use of heated air (50 °C) directed on the mixture jar while rotating on the roll mill.

3.2.2.   Mixed Matrix Sheath Dope Preparation

Mixed matrix dopes were made by dispersing the zeolites/inserts in NMP using sonication (1000 W max horn, Dukane, Leesburg, VA) in bursts of 30 seconds to form a 10 wt % zeolite dispersion. An ice bath was used to prevent heating of the solvent above 30 ºC during the sonication. Sonication was continued until a homogeneous dispersion was observed. An increase in dispersion viscosity was observed. The dispersion appeared gel-like at higher particle loadings (> 15 wt % zeolite in solvent). The dispersion was then added to a sealed glass reaction vessel using a plastic syringe and a 6

45

inch stainless steel needle. A high torque motor (TalBoys Laboratory Stirrers, Model: 409, Troemner LLC, Thorofare, NJ) with a PTFE impeller was used to stir the mixture. Polymer solution (23 − 30 wt % Ultem® or 20 wt % Matrimid) containing lithium nitrate (LiNO$_3$) in NMP and THF was added to the sieve dispersion and the mixture stirred for 15 − 30 minutes. The polymer solution is believed to stabilize the dispersion and prevents particle agglomeration that could be caused by the addition of large quantity of polymer powder [12]. When the dispersion appeared well blended, dried polymer powder was added to the mixture to achieve adequate polymer concentration for spinning. The mix was then stirred for 5.5 − 6 hours at 45 − 55 °C to completely dissolve the polymer. The prepared dope was then allowed to cool to room temperature and poured into a clean syringe pump (Model 100DM, Isco, Lincoln, NE). The dope was allowed to degas for 24 − 48 hrs within the sealed pump. A picture of the mixing setup for mixed matrix dopes is shown in Figure 3.7.

Figure 3.7: Mixed matrix dope mixing setup

3.2.3. Spinning

The bore, core, and sheath fluids were co-extruded using a dual layer spinneret graciously provided by Medal L.P. (Newport, DE) with various air gaps, extrusion rates and draw ratios in a quench bath of tap water maintained at 25 °C. Typical spinning parameters are given in Table 3.4.

Table 3.4: Typical spinning parameters for dual layer mixed matrix hollow fibers membranes

Spinning Parameter	Range
Core Flow Rate (ml/hr)	150 – 180
Sheath Flow Rate (ml/hr)	15 – 18
Bore Flow Rate (ml/hr)	50 – 60
Air Gap (cm)	1 – 20
Draw Ratio	2.8 – 6.2
Quench Bath Temperature (water) ºC	25

The Isco syringe pumps provide excellent flow stability, high pressure operation and are ideal for use in laboratory spinning of hollow fibers. The bore fluid consisted of a mixture of de-ionized (DI) water (18 MΩ; Model: D4521, Barnstead International, Dubuque, IA) in NMP. Bore fluid composition varied from 90:10 wt % to 95:5 wt % NMP:DI water. Filters (Swagelock, OH) were attached upstream of the spinneret to trap large particles which could potentially block the spinneret channels. A 60 micron sintered metal filter was used for the core solution and a 40 micron mesh filter was used for the sheath dope. The mesh type filter provides a lower pressure drop than the sintered metal filter element.

The spinning was carried out at 50 °C by heating the spinneret and filter blocks using multiple heating tapes (BriskHeat™, Barnstead International, Dubuque, IA) regulated by temperature controllers (Model: CN9111A, Omega Engineering Inc., Stamford, CT). The nascent membrane was extruded through an adjustable air gap into the quench bath, passed under a PTFE guide roll in the quench bath and collected on a rotating drum (diameter = 0.32 m) partially immersed in tap water.

3.2.4. Solvent Exchange

The fibers were removed from the drum by cutting cleanly using a sharp blade and placed in DI water for 3 days, with the water being changed everyday. At the end of three days, the fibers (approximately 50 – 100 g) were solvent exchanged by immersing for 20 minutes each in three successive aliquots (400 ml) of methanol, followed by 20 minutes each in three aliquots (400 ml) of hexane.   The fibers were removed from the last hexane bath and allowed to dry in the hood for 1 hour. The fibers were then dried in a vacuum oven at 75 °C for 2 hours.

3.2.5. Module Preparation

Modules of 30 – 50 fibers of 20 cm active lengths with total membrane surface areas between 50 – 75 cm^2 were typically made for permeation testing. Details on module preparation can be found in Appendix A.

3.2.6. Post-Treatment of Hollow Fiber Membranes

Fibers with pinholes defects were repaired by "caulking" the surface with a highly permeable polymer. The objective of the treatment was to plug pinholes from providing a nonselective flow pathway [13]. The high permeability of the "caulking" layer does not significantly decrease the overall membrane permeability, however, non-selective gas flow through the pinholes are considerably reduced. Two post-treatment methods were employed in this research. The first method involves the preparation of a 2 wt % high

molecular weight polydimethylsiloxane (PDMS, Sylgard 184, Dow Chemicals) solution in heptane. The solution was heated at 100 ºC for 4 – 6 hours until a slight increase in viscosity of the solution was observed [14]. This increase in viscosity represents partial crosslinks of PDMS chains, which are more effective in caulking larger size defects in the membranes. The defective fibers in a hollow fiber module were soaked (shell-side) for 30 minutes in this mixture, after which the solution was drained. The modules were dried in the hood for 6 – 24 hrs at room temperature followed by curing at 75 – 80 ºC for 2 hours under vacuum.

The second post-treatment (reactive post-treatment) was developed by Ekiner et al [15]. In this treatment, the fibers in a module were first contacted (on the shell-side) with a 0.2 wt % solution of diethyltoluenediamine in iso-octane for 30 minutes. The solution was drained and the fibers were then contacted with a 0.2 wt % trimesoyl chloride, 2 wt % Sylgard 184 mixture in iso-octane for 30 minutes. A milky solution was drained and the fibers were allowed to dry overnight at room temperature in the hood. The caulking layer was then cured at 75 – 80 ºC under vacuum for 2 hrs.

3.3. CHARACTERIZATION METHODS

3.3.1. Gas Permeation

Transport properties of the fibers were tested with pure (CH_4, N_2, O_2, He and CO_2) and mixed gas mixtures (CO_2/CH_4) at feed pressures varying between 8 – 100 psig. Gas compositions for mixed gas testing were determined by injecting equilibrated gas samples into a gas chromatograph (EG&G Chandler Engineering, Carle Series 100 AGC, model: 72000-00). Details on permeation testing are provided in Appendix B.

3.3.2. Scanning Electron Microscopy

Dried fibers were soaked in hexane for a couple of minutes, gently patted dry and placed in liquid nitrogen for at least 1 minute before they were shear fractured using two fine

point tweezers. The fractured fibers were sputter coated with a 10 – 20 nm thick coating of gold (Model P-S1, ISI, Mountain View, CA). Zeolite and silica particles were dispersed in a volatile solvent and a couple of drops of the dispersion allowed to evaporate on the sample mount. Images of gold coated fibers and uncoated zeolite/silica particles were captured using a high resolution Field Emission Scanning Electron Microscope, Leo 1530 (Leo Electron Microscopy, Cambridge, UK).

3.3.3. Nitrogen Adsorption

Nitrogen adsorption was used in this work to monitor change in surface areas of the zeolites after surface modification. The data was collected using a Micromeritics ASAP 2020 instrument (Micromeritics, Norcross, GA). The samples were degassed for 18 hrs at 300 ºC under vacuum (2 μm mercury) prior to being analyzed. The samples were probed for both micropore and mesopore volumes. Calculation for BET surface areas and pore volumes were performed by the software provided by Micromeritics.

The pore volume was determined using the Horvath-Kawazoe (H-K) method (cylindrical pore) – all pores less than 57 Å were included in the micropore volume. Similar pore volume was obtained by using Density Functional Theory (DFT) modeled with oxide surfaces and cylindrical pores.

The validity of the t-Plot external surface area was confirmed for non-porous materials by performing nitrogen adsorption on nonporous silica (t-Plot micropore volume = 0.00266 cm^3/g) of nominal 110 nm particle size. The t-Plot external surface area of 26.1 m^2/g (BET surface area = 32.7 m^2/g) was found to be comparable to surface area calculation based on particle diameter of 110 nm (36.4 m^2/g).

3.3.4. X-ray Photoelectron Spectroscopy

X-ray Photoelectron Spectroscopy (XPS) was used to obtain surface elemental composition of the zeolites used in this work. The surface of the zeolites is radiated with

monochromatic X-rays with sufficient energy, which results in the ejection of electrons from the atoms near the surface, typically within 2 – 5 nm [16]. The detection of these characteristic electrons permits the identification (via the binding energies) and quantification (via intensity) of the elements present in the sample. By integrating the peak areas of a plot of intensity versus electron binding energies, the atomic composition of the elements observed in the scan can be obtained. The data obtained have an approximate error of 10 – 20 percent which could be reduced by taking additional scans over multiple sample areas [17].

A SPEC 100 X-ray Photoelectron Spectroscopy (XPS) instrument was used to obtain the elemental analysis of the surface modification of the zeolite and silica particles used in the research work. 8 scans over a specified area of the powdered sample (zeolite or silica) were performed to reduce noise in the data.

3.3.5. Rheology

The rheology of the mixed matrix dopes was tested in a Paar Physica MCR 300 Rheometer (Anton Paar USA, Ashland, VA) using a 17 mm diameter Couette cell. The instrument's torque measurement capability limited shear rates up to 100 s^{-1} for the highly viscous dopes used in fiber spinning.

3.3.6. Infra-Red Spectroscopy

A Bruker Tensor 27 FTIR spectrometer outfitted with a Harrick MVP2™ ATR mini-sampler (Harrick Scientific Products, Inc, Pleasantville, NY) was used to obtain the infra-red spectrum of zeolites used in the research. The zeolite samples were dried at 150 ºC for 24 – 48 hours under vacuum before the IR scans. Typically 512 scans were obtained per sample at a resolution of 2 cm^{-1}.

3.4. REFERENCES

1. Mahajan, R., *Formation, characterization and modeling of mixed matrix membrane materials*, in *Department of Chemical Engineering*. 2000, University of Texas at Austin: Austin, TX. p. 230.

2. Mahajan, R., R. Burns, M. Schaeffer, and W.J. Koros, *Challenges in forming successful mixed matrix membranes with rigid polymeric materials.* J. Appl. Polym. Sci., 2002. **86**(4): p. 881-890.

3. *Ultem Product Data Sheet*. 1997, GE Plastics: Pittsfield, MA.

4. Kesting, R. and A. Fritzsche, *Polymeric Gas Separation Membranes*. 1993, New York: John Wiley & Sons.

5. Moore, T.T., *Personal communication*. 2004.

6. *Matrimid Product Data Sheet*. 2000, Vantico, Inc.: Brewster, NY.

7. Moore, T.T., *Effects of materials, processing, and operating conditions on the morphology and gas transport properties of mixed matrix membranes*. 2004. p. 311 pp.

8. Barbari, T.A., W.J. Koros, and D.R. Paul, *Polymeric membranes based on bisphenol A for gas separations.* Journal of Membrane Science, 1989. **42**(1-2): p. 69-86.

9. Yong, H.H., H.C. Park, Y.S. Kang, J. Won, and W.N. Kim, *Zeolite-filled polyimide membrane containing 2,4,6-triaminopyrimidine.* Journal of Membrane Science, 2001. **188**(2): p. 151-163.

10. Mahajan, R. and W.J. Koros, *Mixed matrix membrane materials with glassy polymers. Part 1.* Polym. Engr. and Sci., 2002. **42**(7): p. 1420-1431.

11. Mahajan, R. and W.J. Koros, *Mixed matrix membrane materials with glassy polymers. Part 2.* Polym. Engr. and Sci., 2002. **42**(7): p. 1432-1441.

12. Kulkarni, S.S., *Personal Communication, Medal L.P / Air Liquide*. 2003.

13. Henis, J.M.S. and M.K. Tripodi, *Composite hollow fiber membranes for gas separation: the resistance model approach.* J. Membr. Sci., 1981. **8**(3): p. 233-46.

14. Pesek, S.C., *Personal Communication*. 2003.

15. Ekiner, O.M., R.A. Hayes, and P. Manos, *Reactive posttreatment for gas separation membranes*. 1989, (du Pont de Nemours, E. I., and Co., USA). Application: US. p. 7 pp.

16.   Wachtman, J.B. and Z.H. Kalman, *Characterization of Materials*. 2003, Boston: Butterworth-Heinemann.

17.   Carter, W.B., *Personal Communication, Department of Material Science and Engineering, Georgia Institute of Technology*. 2006.

CHAPTER 4

MIXED MATRIX HOLLOW FIBERS BASED ON ULTEM® SIZED SSZ-13 AND ULTEM® POLYMER MATRIX

4.1. OVERVIEW

Asymmetric mixed matrix hollow fiber membranes were spun via a dry jet-wet quench procedure using surface modified inorganic small pore size zeolite (SSZ-13) incorporated in an Ultem® 1000 polyetherimide matrix. The zeolites were modified by treating the zeolites with a silane coupling agent to allow Ultem® polymer chains to be grafted to the surface. Poor adhesion was observed between the bulk polymer and most of the zeolite particles in the final membrane as gauged by SEM microscopy. The post-treated fibers did not display enhanced selectivity over neat polymer with either pure gas oxygen/nitrogen (O_2/N_2) testing or mixed gas carbon dioxide/methane (CO_2/CH_4) gas pair. The absence of the mixed matrix effect is hypothesized to be due to the nucleation of the solvent and non-solvent around the Ultem® "sized" zeolite particles during phase separation in the quench bath forming a so called sieve-in-a-cage defect. Although such defects have been reported in dense mixed matrix films [1, 2], they have not yet been investigated in hollow fibers format which are formed via a phase separation process and thus remain prone to the effects of the non-solvent quenching media**.**

4.2. ZEOLITES AND PHASE SEPARATION KINETICS IN ASYMMETRIC MEMBRANES

For high gas transport rates, the dense separating layer of the membrane must be as thin as possible, yet strong enough to withstand considerable transmembrane pressure differential driving forces. Such an arrangement is ideally achieved with asymmetric hollow fibers which consist of a thin dense (skin) layer and a porous support layer. Such

membranes are typically formed in a single step via a dry jet-wet quench spinning process where phase separation within the quenched membrane is initiated as rapidly as possible. The rapid phase separation traps in significant porosity for the support layer of the membrane, while a thin skin can be formed in the prior step via solvent evaporation in the air gap.

While dope additives are used to control the phase separation kinetics of the membrane, their presence could potentially obstruct the formation of successful mixed matrix membranes since zeolites are highly susceptible to contaminants which can block the molecular sieving function of the zeolite [3]. Addressing this factor is critical if any enhancement in selectivity is to be achieved in the membrane.

There are two aspects of selecting dope additives for mixed matrix dopes. As mentioned above, the first aspect is that the components of the dope must not interfere or block the molecular sieving attributes of the zeolite. The second aspect is that the additive must not negatively impact the adhesion between the zeolite and the polymer. While the first aspect can be dealt with using large components in the dope mixture with molecular diameters greater than the pore size of the zeolite, the effect on polymer-sieve adhesion is more difficult to predict especially when dealing with the considerable variation in functionality on the surface of the zeolite.

Initial research carried out in dense film format has identified many material issues leading to the optimization in the selection of molecular sieves and polymers for use in mixed matrix membranes [4]. These challenges include agglomeration of molecular sieves, defective sieve-polymer interfaces and surface pattern formation in the mixed matrix films [5-9]. Yet transitioning from a dense film to asymmetric hollow fiber morphology introduces considerably more components and parameters into the membrane formation process. These challenges are driven by the use of phase separation

to form asymmetric membranes, thereby necessitating reconsideration of material selection and process parameters used for dense mixed matrix films. This reconsideration derives from the influence of zeolites on phase separation kinetics, and subsequently on the final membrane morphology.

Although the effects of phase separation on membrane morphology have been widely studied for polymer-only membranes, the effect of zeolites on phase separation equilibrium and kinetics in mixed matrix fibers has not yet been explored. This remains a critical aspect, as the desired asymmetric morphology is formed via a control of the phase separation kinetics using a number of dope components including non-solvents, viscosity modifiers and inorganic salts and quenching media [10-12].

4.2.1. Zeolite Surface Characteristics

In the dope, the zeolites interact via their surface functionalities. The first approximation equates zeolites surfaces with the surface characteristics of silica and alumina materials. The zeolite surface, by comparison to silica, is believed to contain as many as $4 - 5$ hydroxyl groups per square nanometer of the surface attached to silicon and, if present, aluminum [3]. This estimate of the number of hydroxyl groups on the zeolite SSZ-13 surface has been validated by the reaction of surface hydroxyls with vanadium oxytrichloride ($VOCl_3$) followed by an elemental analysis of vanadium on the surface [3].

With these surface hydroxyl groups, zeolites added to the dope mixture cannot be considered inert filler. These zeolites affect long term dope stability and phase separation kinetics of the membrane. The stability of the dope refers to the characteristic of the zeolite particles to remain homogeneously suspended in the spinning dope. Such stability, firstly, depends on the rate of settling of the non-colloidal particles, and secondly, on the compatibility of the zeolite surface with the remaining components of the dope. When sub-micron particles are used, dope stability only remains a function of

the zeolite surface interactions with the dope components. This dictates whether zeolite aggregates are formed, which could settle out of the dispersion.

The zeolites can have favorable, unfavorable or neutral interaction with the dope components. These interactions involve zeolite-solvent/nonsolvent and zeolite-polymer interactions. Earlier work by Mahajan [2], employing Hildebrand solubility parameters to select solvents, though feasible for the limited production of dense films, is difficult to implement in large scale production of hollow fibers where safety concerns limit the choice of solvents and non-solvents. The industrial preference for the non-solvent for the quench bath is water due to safety concerns with the use of large quantities of organic solvents. Further, among the limited number of solvents for Ultem® 1000, N-methyl-2-pyrrolidine (NMP) is selected due to its relatively benign nature. These liquids have a high affinity for the zeolite surface through a variety of interactions, including, hydrogen bonding and acid-base type interactions. Mahajan [2] suggests the use of solvents that interact less or poorly with the molecular sieve compared to the polymer; thus preventing competition of the solvent molecules with the polymer for the sieve surface. Table 4.1 outlines the solubility parameters of selected solvents and non-solvents for Ultem® along with the estimated liquid-solid parameters for the same solvents with silica and alumina. Similar values of the solubility parameter indicate higher compatibility between any two components (neglecting polar and hydrogen bonding interactions), while a higher liquid-solid parameter indicates a more favorable interaction between the liquid and the solid.

As can be seen in Table 4.1, the liquid-solid interaction parameters indicate strong interaction between water and the silica and alumina surfaces suggesting that zeolite surfaces, by comparison to silica and alumina surfaces, may also have strong interaction with water. Further, even though NMP and tetrahydrofuran (THF) have very similar solubility parameters, NMP is a strong solvent for Ultem®, while THF is only a weak swelling agent for the polymer. Likewise, even though the solubility parameter for

dichloromethane (DCM) of 20.3 $(MJ/m^3)^{1/2}$ is considerably different from that calculated for Ultem® of 26.3 $(MJ/m^3)^{1/2}$ using group contributions [13], DCM is a strong solvent for Ultem®. These discrepancies highlight the significant contribution of polarity and acid/base type interactions prevalent in the components used in this research.

Table 4.1 Hildebrand solubility and liquid-solid interactions parameters for silica and alumina for selected solvents and non-solvents of Ultem® [13]

Solvent/Polymer	Hildebrand solubility parameter δ_t $(MJ/m^3)^{1/2}$	$\varepsilon°$ silica (liquid-solid interaction parameter for silica)	$\varepsilon°$ alumina (liquid-solid interaction parameter for alumina)	Solvent for Ultem®
N-methyl-2-pyrrolidione	22.93	0.467	0.615	Yes
Dimethyl sulfoxide	26.4	0.616	0.827	Yes
N,N-Dimethylformamide	24.8	0.547	0.729	Yes
Dichloromethane	20.3	0.354	0.454	Yes
Tetrahydrofuran	22.5	0.449	0.589	No
n-Hexane	14.8	0.117	0.118	No
Methanol	29.1	0.732	0.992	No
Water	47.9	1.541	2.141	No
Ultem® 1000 Polyetherimide	26.3	-	-	-

While comparisons to silica and alumina surfaces are made as first approximation for the zeolite surface, zeolites having multiple acid sites may be poorly modeled by silica and/or alumina surfaces. Additionally, the synthesis of sub-micron zeolite particles is still a relatively new field and zeolite surfaces and particle characteristics (including the formation of multi crystal particles) can vary from batch to batch during synthesis. Of

particular concern are multi-crystal particles which contain multiple grain boundaries. These grain boundaries are believed to have significantly higher reactivities because of the high free energy of the defects [14]. The estimation of surface chemistry is further complicated by differences in surface and bulk elemental compositions within a zeolite particle, which is again strongly dependent on the batch processing parameters used in the zeolite synthesis. These factors have made the estimation of the interactions between the zeolite and dope components difficult to quantify and only qualitative assessments can be made currently. This understanding has been one of the drivers for the modification of the zeolite to obtain a uniform characterizable surface.

4.2.2. Zeolite Surface Modification

Although predicting zeolite-solvent and zeolite-polymer interactions accurately can be difficult, by analogy to organic/inorganic composites, silanes can be used to modify the zeolite surface to improve compatibility with the polymer [1, 5]. Due to the reactivity with the silica surface, silanes could be attached to the surface of the zeolites via the surface hydroxyls. Further, silanes with a second reactive end group could be used to bond polymer chains to the zeolite thus promoting adhesion between the zeolite and the bulk polymer phase in the membrane. Often, γ-aminopropyldimethylethoxy silane (APDMES) has been used since it is believed to be large enough to be unable to enter into and block internal zeolite pores in small pore zeolites (pore size 3.8 - 4.2 Å), and yet able to form a tether between the zeolite and the polymer (Ultem®) that would not allow non-selective flow of gases between the zeolite and the attached polymer [6]. Earlier work with APDMES indicated that the silane reacted well with zeolite 4A and did not impede the molecular sieving function of the zeolite [6]. Figure 4.1 shows a schematic of the envisioned coupling reaction.
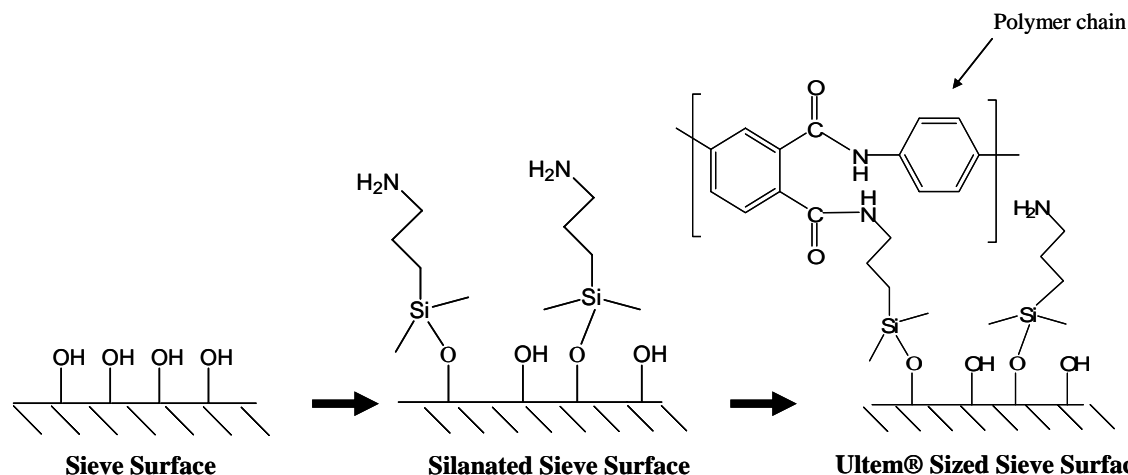
Figure 4.1: Schematic of envisioned Ultem® "sizing" of the zeolite surface using a silane coupling agent (APDMES)

4.3. EXPERIMENTAL

4.3.1. Silanation and Ultem® Sizing Treatment

10 g of SSZ-13 sieves were dried overnight in a vacuum oven at 120 °C. The drying was carried out based on results from dense film work which indicated that better membranes were obtained with the drying of the sieves before they were added to the aqueous alcohol solution for silanation [3]. The dried sieves were added to a 95:5 volume % solution of iso-propanol (IPA) and deionized (DI) water. The mixture was sonicated at high intensity using a 1000 W (*maximum* power output) sonication horn to disperse the zeolites. After adding 5.0 ml of fresh APDMES, the mixture was sonicated with the 1000 W sonication horn for a total of 30 minutes in 10 minute installments with 10 minute "rest" periods in between to prevent excess heating of the mixture. The maximum temperature of the mixture attained was 50 °C. The zeolite dispersion in IPA was then left undisturbed overnight to allow larger (greater than 1 – 2 micron) particles to settle out. Thereafter, the supernatant containing the dispersed zeolites was pipetted off. The zeolites were recovered using a high pressure filtration setup (#4280, Pall Gelman, East Hills, NY) and 0.2 micron polytetrafluoroethylene (PTFE) filters with 160 psig of

nitrogen back pressure to aid filtration. The zeolites were washed with a 150 ml aliquot of IPA with sonication used to disperse the zeolites in IPA followed by the above mentioned filtration. The washing, sonication and filtration was repeated twice more. The collected zeolites were dried in a vacuum oven at 140 °C for 12 hours.

In order to graft the polymer on to the surface of the zeolite, the dried zeolites were dispersed in NMP to form a 10 wt % dispersion using sonication (1000 W sonication horn). The dispersion was heated in an oil bath at 145 – 150 °C. Dried Ultem® 1000 polymer, enough to form a 0.5 wt % solution in NMP, was added to the dispersion. The mixture was stirred with a PTFE coated stir bar for 4 hours in the oil bath until a thick paste was formed due to the evaporation of the NMP. The mixture was then removed from heat and a further 25 ml of NMP added to dissolve the paste which dispersed rapidly in the added solvent. The Ultem® sized particles were used to form a mixed matrix dope as described in section 3.2.2. The core and sheath dope compositions are provided in Table 4.2.

Table 4.2: Core and sheath dope compositions for Ultem®-Ultem® hollow fiber membranes containing Ultem "sized" SSZ-13 zeolites

Component	Core Dope (wt %)	Sheath Dope (wt %)
Ultem® 1000	32.0	29.8
N-methyl-2-pyrrolidione	55.7	51.3
Tetrahydrofuran	10.1	13.2
Lithium Nitrate	2.2	1.2
Ultem "sized" zeolite	-	4.4

4.4. RESULTS AND DISCUSSION

Macroscopic views of the Ultem® core and Ultem® based sheath (Ultem®-Ultem®) hollow fibers made from Ultem® "sized" sieves show circular and concentric bores. No interface between the sheath and core layers is observable indicating good adhesion and intermixing between the layers. Figure 4.2 displays SEM micrographs of selected fibers.
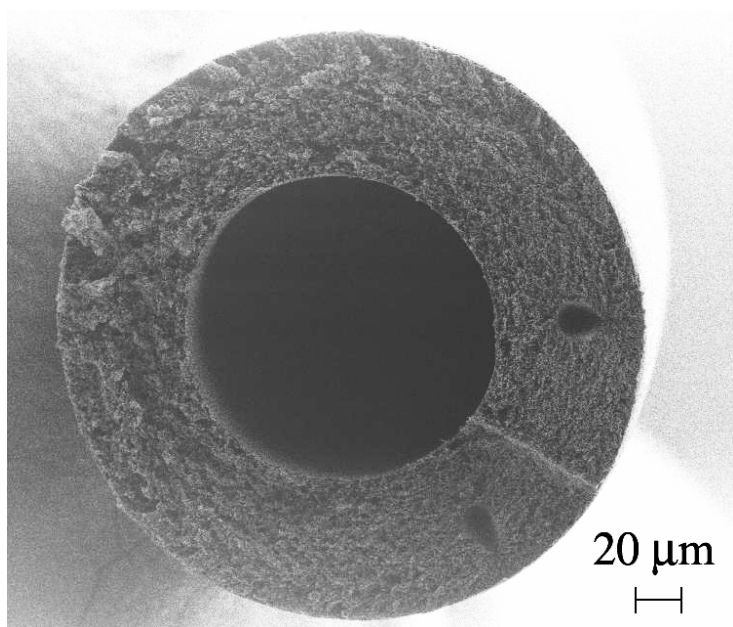
Figure 4.2: SEM microphotograph of Ultem®-Ultem® dual layer mixed matrix hollow fiber membranes incorporating 11.2 vol. % (12.9 wt %) Ultem® "sized" SSZ-13 zeolites

High permeability and low selectivity, though above Knudsen selectivity for the O_2/N_2 gas pair, obtained in the permeation data of unpost-treated fibers indicated that defects were present in the skin of the fiber through which non-selective gas flow could take place. As the selectivity was greater than that through Knudsen diffusion, very few such defects existed; however, these defects were enough to reduce selectivity significantly below intrinsic polymer levels. As a similar dope composition without zeolites was earlier spun with a defect-free skin, it is postulated that these defects most likely exist in

the region surrounding zeolite particles protruding through the skin region of the hollow fiber. The defects/gaps may be formed due to poor zeolite polymer contact. After post-treatment, the fibers attained only intrinsic polymer selectivity demonstrating that although, the skin defects were caulked, any enhancement in selectivity (mixed matrix effect) for both O_2/N_2 and CO_2/CH_4 gas pairs was absent. The data for fibers spun with a draw ratio (DR) of 3.5 and air gap (AG) of 20 cm are shown in Table 4.3; the mixed matrix fiber permeation results are compared to those of earlier spun Ultem® defect-free fibers (DR = 2.8; AG = 20 cm), dense neat polymer film values and Maxwell model predicted values. A film thickness of 100 nanometers (nm) was used to generate permeances for dense film and Maxwell model predictions. Experimental permeance values for fibers lower than predicted film values indicate the presence of a skin thickness greater than 100 nm.

Table 4.3: Comparison of data for silanated and Ultem® "sized" mixed matrix fibers with neat Ultem® fibers and Maxwell model predictions. Measurements made at 114.7 psia feed pressure and 35 ºC. Error represents the standard deviation in the measurements.

Membrane	Post Treatment (PT)	O_2/N_2 Selectivity Pure gas	$(P/\ell)_{O2}$ (GPU)	CO_2/CH_4 Selectivity Mixed gas (20:80)	$(P/\ell)_{CO2}$ (GPU)
SH31 Fibers (Ultem® sized sieves)	Reactive PT	7.7 ± 0.1	3.26 ± 0.02	35.9 ± 0.2	11.4 ± 0.1
SH21 Fibers (neat Ultem®)	No PT	7.26 ± 0.03	3.0 ± 0.01	39.6 ± 0.2	13.8 ± 0.3
Ultem® Dense Film †	N/A	7.6	3.6	-	-
Maxwell Model based on 11.2 vol % SSZ-13[†]	N/A	8.4	5.6	42	20

[†] Dense film and Maxwell model permeance (P/ℓ) calculation for a thickness of 100 nm

The absence of the mixed matrix effect is believed to be due the bypassing of the zeolite particle by the gas molecules via submicron spaces between the bulk polymer and zeolite. These defects were visually observed in SEM micrographs of hollow fiber membranes as poor bonding between the polymer and zeolites. The zeolites were observed sitting in a closed polymer cage, represented the so-called sieve-in-a-cage morphology. Figure 4.3 displays SEM micrographs of the skin region of these fibers. Although some particles appear close together, they do not appear to be agglomerates.
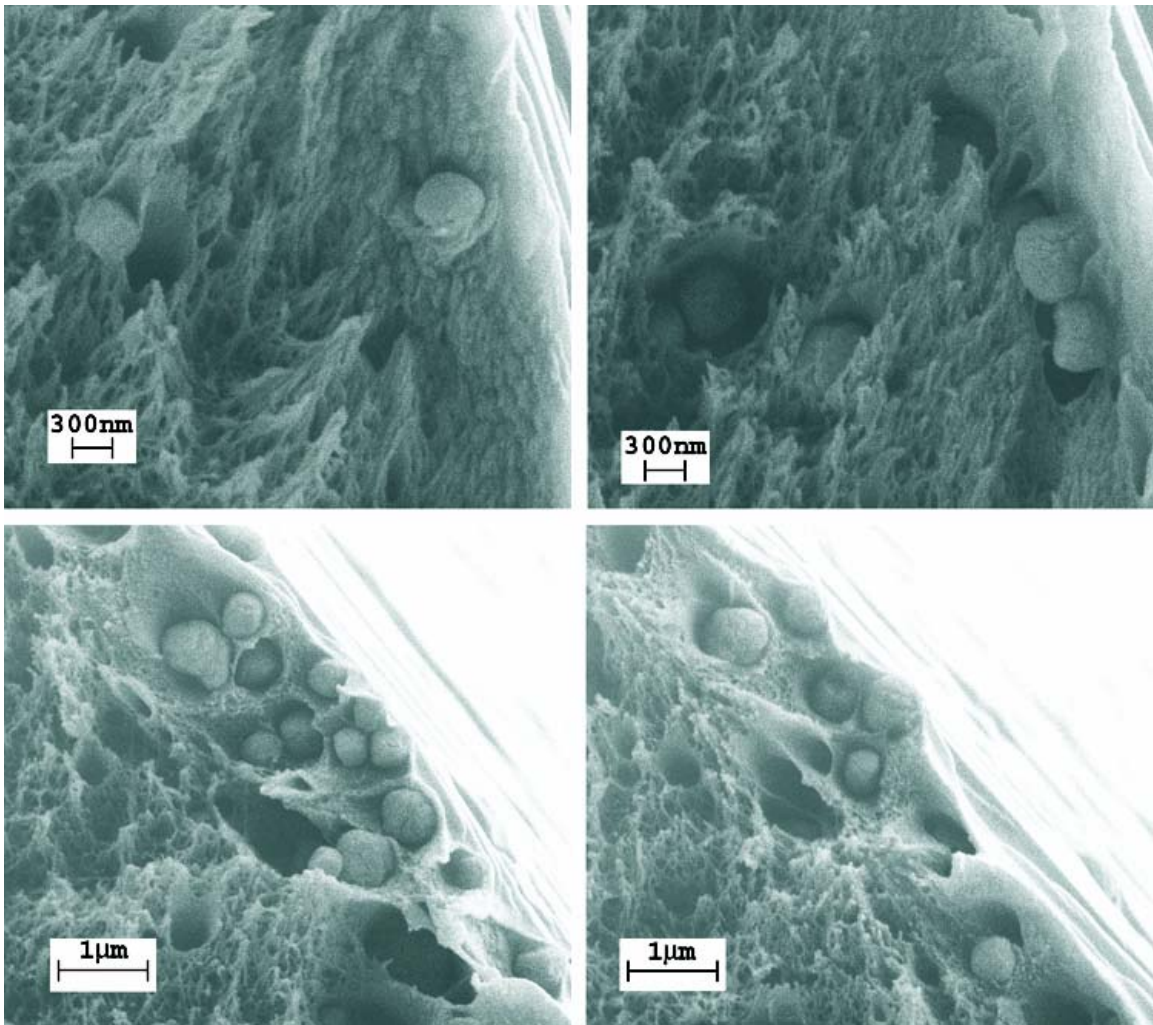
Figure 4.3: SEM microphotographs of the skin region showing sieve-in-a-cage morphology in mixed matrix hollow fiber membranes incorporating Ultem® "sized" SSZ-13 zeolites

4.5. FORMATION OF SIEVE-IN-A-CAGE DEFECTS

4.5.1. Background

A variety of explanations have been considered to explain sieve-in-a-cage morphology seen in mixed matrix dense films. Foremost theories among them suggest that these defects are formed as a result of polymer and sieve surface incompatibility. Although, an attempt was made by Mahajan [2] to estimate such incompatibilities using Hildebrand solubility parameters by approximating the zeolite surface as a combination of silica and alumina surfaces, they still remain theories that need to be tested in practice with each polymer, zeolite and solvent combination.

Recently a second hypothesis has been put forward to account for the formation of sieve-in-a-cage defects seen in mixed matrix dense films made using Ultem® "sized" sieves in Ultem® matrix [3]. This hypothesis claims that sieve-in-a-cage defects originate due to stresses that develop in a shrinking film on a constrained surface. Arguments are made that as the solvent evaporates the film tries to shrink in both the thickness and the plane of the film, however, due to the rigid substrate this shrinkage is constrained in the planar direction resulting in the development of large stresses. If the polymer is not flexible, the polymer chains are unable to dissipate stresses that are built up. For Ultem® polymer with 10 wt % residual solvent these stresses have been calculated to be as high as 170 MPa [3]. These stresses are significantly higher than the expected interfacial strength of the silanated zeolite and the bulk polymer and are believed to result in the debonding of the interface [3]. However, in asymmetric hollow fiber membranes, as the nascent membrane encounters a free surface in the air gap before coagulating in the quench bath, the presence of sieve-in-a-cage defects indicates a different mechanism for their formation.

4.5.2. Nucleation of Solvents and Nonsolvents on the Zeolite Surface

The binodal in the ternary phase diagram describes equilibrium states; however, systems can exist in the metastable region, which are not at equilibrium as a result of a thermodynamic barrier. This barrier is a function of the surface tension of the nucleating phase and corresponds to the change in free energy required to form a new interface. In heterogeneous nucleation, this free energy requirement is significantly reduced in the presence of an existing surface (particle) that interacts favorably with the nucleating phase. The level of interaction of the nucleating phase and the surface is described by the contact angle. As the contact angle of the nucleating phase with the surface decreases, the free energy of nucleation is reduced [15, 16]. This implies that as long as the contact angle of the nucleating phase on the particle surface is less than 180º for a given system, the energy barrier to nucleation will be lower for heterogeneous nucleation compared to homogeneous nucleation.

It is proposed that sieve-in-a-cage defects in asymmetric hollow fibers are a product of the phase separation phenomena and can be attributed to nucleation initiated around a particle. Even though the silanation procedure followed by the grafting of Ultem® onto the surface of the zeolite has been proven to occur, complete silane coverage of the surface is not observed [3]. Based on thermogravametric analysis (TGA) and $VOCl_3$ titration, Moore estimates a maximum of two silane molecules per square nanometer of the zeolite surface after the silanization reaction [17]. Thus, the silanated zeolite particles still retain a high number of hydroxyl groups which can act as excellent adsorption sites for polar hydrophilic molecules in the dope mixture, including traces of water. If comparisons drawn with adsorbed water layers on silica surfaces are applicable [18, 19], the adsorbed layer on the zeolite surface may be as thick as 10 nm. This favorable interaction with the solvents and nonsolvents of the dope over and above the polymer molecules can lead to the formation of a locally phase separated polymer lean phase or a

lower polymer concentration region around the zeolite particle. Such regions of local phase separation are believed to lead to agglomeration of the sieve particles which can be observed in poor-stability mixed matrix dopes a few days after preparation. Figure 4.4 shows the described storage instability of the mixed matrix dope.
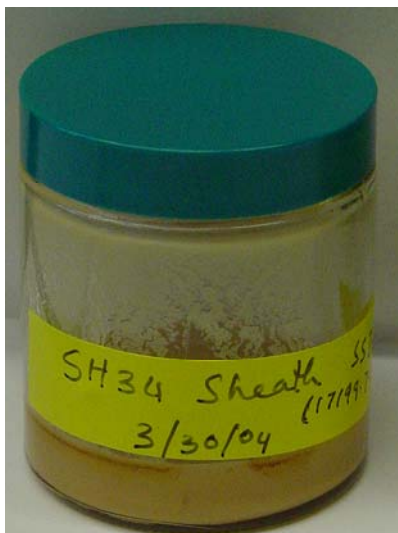
Figure 4.4: Phase separation of the zeolites in the dope mixture. Note phase separated particles on the wall of the container.

Although poor stability of the dope is visually observed within a week, an adsorbed layer of hydrophilic molecules around the particle can be envisioned to form or exist during the formation of the dope mixture as the liquid-solid interaction parameters (based on silica and alumina) in Table 4.1 suggest. When this dope is extruded into the quench bath, non-solvent, usually water, enters the membrane and initiates phase separation. The ingressing water molecules are attracted to the surface of the zeolite particle (high liquid-solid interaction parameter) where the particles with pre-absorbed layers of hydrophilic molecules can act as natural nuclei. Here, the decrease in free energy from phase separation does not have to contend with an increase in free energy from making new interfaces as the interface already exists. The ingressing water molecules can expand this

adsorbed layer thereby increasing the non-solvent concentration around the zeolite particle. When this non-solvent concentration reaches a critical value, phase separation can occur around the zeolite, with the polymer lean phase surrounding the zeolite and the polymer rich phase forming a cage around it. Figure 4.5 presents a cartoon depiction of the proposed hypothesis.
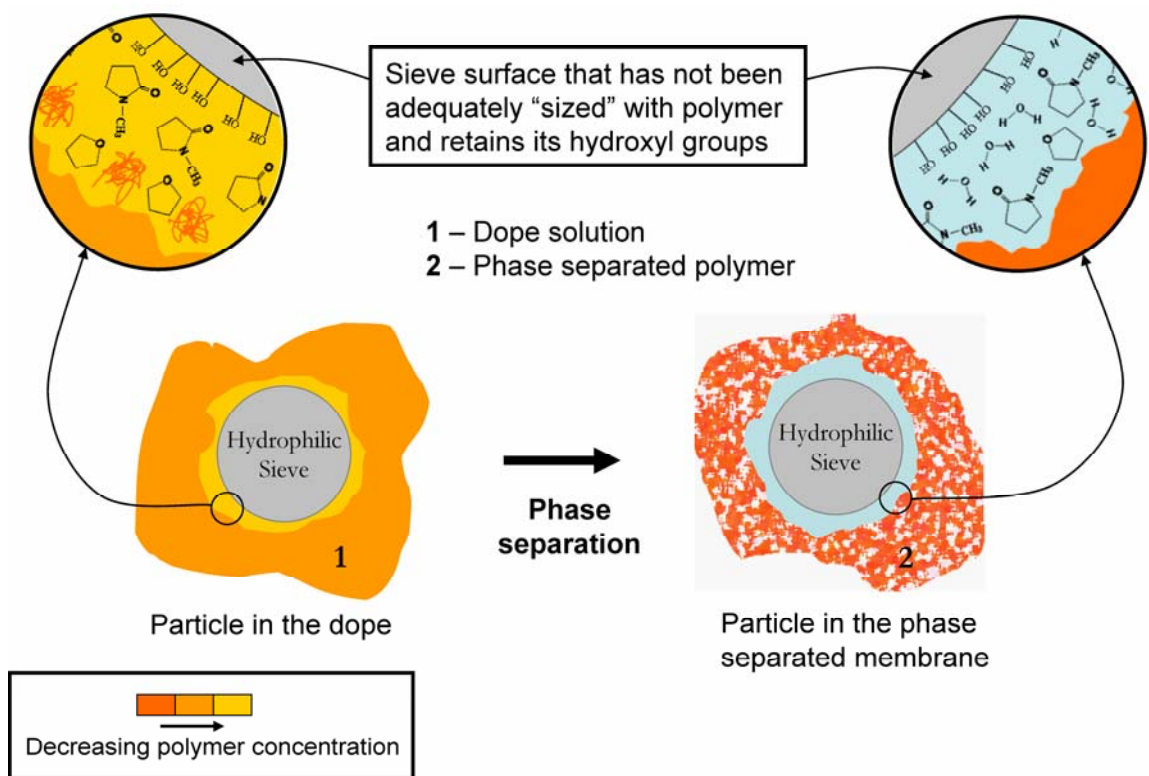
Figure 4.5: Cartoon depiction of nucleation around a sieve particle. Molecules shown in the insets are hydroxyls attached to the sieve surface, polymer molecules, N-methyl-2-pyrrolidione, tetrahydrofuran and water

In the case where the kinetics of the nonsolvent (coagulant) ingress within the nucleus is slowed, the nuclei can expand into macrovoids as the polymer cage does not vitrify around the zeolite particle. Such macrovoids and their formation is complex and will be described in Chapter 7.

If the particle initiated nucleation hypothesis in mixed matrix hollow fiber membranes is valid, successful mixed matrix membranes can only be achieved if nucleation at the sieve surface can be suppressed. One such method to test this suggestion could be via the use of zeolites with hydrophobic surfaces which would energetically not support the nucleation of the hydrophilic components of the dope.

4.6. CONCLUSIONS

Successful mixed matrix membranes are proposed to form only if good bonding of the zeolite particle can be achieved with the polymer matrix. Generally, zeolites with hydrophilic surfaces do not interact well with hydrophobic polymers used in fiber spinning. This requires that the surface of the zeolite particles be modified to change the level of interaction between polymer and the zeolite. The first method of increasing zeolite-polymer compatibility via the use of silane coupling agents and subsequent polymer "sizing" did not result in a mixed matrix enhancement of selectivity. Sieve-in-a-cage defects were observed in the fibers and identified as the cause for the absence of the mixed matrix effect. The defects are hypothesized to form as a result of nucleation of nonsolvent and/or polymer lean phase around the zeolite during the phase separation process. For successful mixed matrix asymmetric hollow fiber membranes it appears necessary that nucleation of solvents and non-solvents at the zeolite surface be restricted. One such approach could be implemented by increasing the hydrophobicity of the zeolite surface by capping surface hydroxyls with hydrophobic organic molecules. Such a surface modification of zeolites was attempted and is described in Chapter 5.

4.7. REFERENCES

1. Duval, J.M., A.J.B. Kemperman, B. Folkers, M.H.V. Mulder, G. Desgrandchamps, and C.A. Smolders, *Preparation of zeolite filled glassy polymer membranes.* Journal of Applied Polymer Science, 1994. **54**(4): p. 409-18.

2. Mahajan, R. and W.J. Koros, *Factors Controlling Successful Formation of Mixed-Matrix Gas Separation Materials.* Ind. Eng. Chem. Res., 2000. **39**(8): p. 2692-2696.

3. Moore, T.T., *Effects of materials, processing, and operating conditions on the morphology and gas transport properties of mixed matrix membranes*, in *Department of Chemical Engineering*. 2004, Univ. of Texas, Austin, TX, USA. p. 312.

4. Zimmerman, C.M., A. Singh, and W.J. Koros, *Tailoring mixed matrix composite membranes for gas separations.* Journal of Membrane Science, 1997. **137**(1-2): p. 145-154.

5. Mahajan, R. and W.J. Koros, *Mixed matrix membrane materials with glassy polymers. Part 1.* Polymer Engineering and Science, 2002. **42**(7): p. 1420-1431.

6. Mahajan, R. and W.J. Koros, *Mixed matrix membrane materials with glassy polymers. Part 2.* Polymer Engineering and Science, 2002. **42**(7): p. 1432-1441.

7. Mahajan, R., R. Burns, M. Schaefer, and W. Koros, *Challenges in forming successful mixed matrix membranes with rigid polymeric materials.* Journal of Applied Polymer Science, 2002. **86**: p. 881-90.

8. Zimmerman, C.M., R. Mahajan, and W.J. Koros, *Fundamental and practical aspects of mixed matrix gas separation membranes.* Polymer Material Science and Engineering, 1997. **77**: p. 328-329.

9. Moore, T.T., R. Mahajan, D.Q. Vu, and W.J. Koros, *Hybrid membrane materials comprising organic polymers with rigid dispersed phases.* AIChE Journal, 2004. **50**(2): p. 311-321.

10. Pesek, S.C., *Aqueous quenched asymmetric polysulfone flat sheet and hollow fiber membranes prepared by dry/wet phase separation*, in *Department of Chemical Engineering*. 1993, Univ. Texas, Austin, TX, USA. p. 260 pp.

11. Ekiner, O.M. and G. Vassilatos, *Polyaramide hollow fibers for hydrogen/methane separation - spinning and properties.* J. Membr. Sci., 1990. **53**(3): p. 259-73.

12. Boom, R.M., *Membrane formation by immersion precipitation: the role of the polymeric additive*. 1992, University of Twente, The Netherland.

13. Barton, A.F.M., *CRC Handbook of Solubility Parameters and Other Cohesion Parameters*. 1983, Boca Raton, FL: CRC Press Inc.

14. Callister, W.D., *Materials Science and Engineering: An Introduction,*. 4th ed. 1996: John Wiley & Sons. 864 pp.

15. Volmer, M., *Kinetik der Phasenbildung*. 1939: Steinkopff, Dresden and Leipzig.

16. Dunning, W.J., *Theory of crystal nucleation from vapor, liquid, and solid systems*, in *Chemistry of the Solid State*, W.E. Garner, Editor. 1955, Butterworths Publication Ltd: London. p. 159-83.

17. Moore, T.T., *Effects of materials, processing, and operating conditions on the morphology and gas transport properties of mixed matrix membranes*. 2004. p. 311 pp.

18. Nutting, P.G., *The adsorptive force of silica for water.* Journal of Physical Chemistry, 1927. **31**: p. 531-4.

19. Ershova, G.F., Z.M. Zorin, and N.V. Churaev, *Temperature dependence of the thickness of polymolecular adsorption films of water on quartz surfaces.* Kolloidnyi Zhurnal, 1975. **37**(1): p. 208-10.

CHAPTER 5

MIXED MATRIX HOLLOW FIBERS BASED ON GRIGNARD TREATED ZEOLITES

5.1. OVERVIEW

A new surface modification technique using a Grignard reagent is described which allows the formation of successful mixed matrix membranes via increased polymer-zeolite adhesion. The technique was discovered while pursuing the goal of suppressing the heterogeneous nucleation (phase separation) tendencies of zeolites in the asymmetric membrane formation process described in Chapter 4.

The technique was applied to two zeolites of significantly different silicon:aluminum ratios that were then successfully incorporated into asymmetric hollow fiber membranes based on an Ultem® matrix. These fibers, optimized for thin skin thicknesses, have slightly defective skins that can be repaired with post-treatment (caulking). The caulked fibers display increased selectivity for multiple gas pairs over the intrinsic polymer (Ultem®) values.

The general applicability of the modified zeolites was tested by incorporating the zeolites in a higher glass transition (T_g) polymer, Matrimid®, where excellent polymer-zeolite adhesion was observed. The successful incorporation of Grignard treated zeolites in asymmetric hollow fiber membranes contributes significantly to the development of successful mixed matrix materials with excellent interface properties.

5.2. INTRODUCTION

Silica surfaces for chromatographic media have routinely been treated with alkylsilanes and primary alcohols to obtain hydrophobic surfaces [1-8]. In these treatments the hydrophobic alkane is attached to the silica surface via a siloxy (using silanes) or alkoxy

(using alcohols) bond. Zeolites, with similar concentrations of hydroxyl groups on the surface could likewise be reacted with alkylsilanes and alcohols to develop a hydrophobic surface. However, the silane and Si-O-R (R= alkyl group) bonds are not highly stable over the long term and in the presence of water, hydrolysis of these bonds takes place easily [9, 10]. This issue is worrisome in the development of zeolite-polymer asymmetric membranes where water is used as the quench media.

Recently, methods have been developed to attach alkane groups directly to the silica surface via a silicon-carbon bond [11-15]. The procedure involves the reaction of the silica surface with a chlorinating agent (thionyl chloride, phosphorus pentachloride or tetrachlorosilane) followed by reaction with the appropriate Grignard reagent. The following surface chemistry is postulated using the thionyl chloride reagent [12],

$$\langle Si \rangle - OH + SOCl_2 \rightarrow \langle Si \rangle - Cl + SO_2 + HCl \qquad (5.1)$$
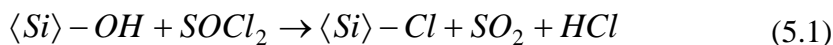
The chlorinated surface is reacted with a suitable Grignard reagent to directly bond the alkyl group to the silicon surface as follows:

$$\langle Si \rangle - Cl + RM \rightarrow \langle Si \rangle - R + MCl \qquad (5.2)$$

where RM is the organometallic (e.g. Grignard) reagent.

The silicon-carbon bond is resistant to hydrolysis, and with the capping of the hydroxyl groups, it is hypothesized that the nucleation of the hydrophilic polymer lean phase around the zeolite particle will tend to be suppressed during membrane phase separation. The schematic of the envisioned reaction on the zeolite surface is shown in Figure 5.1.
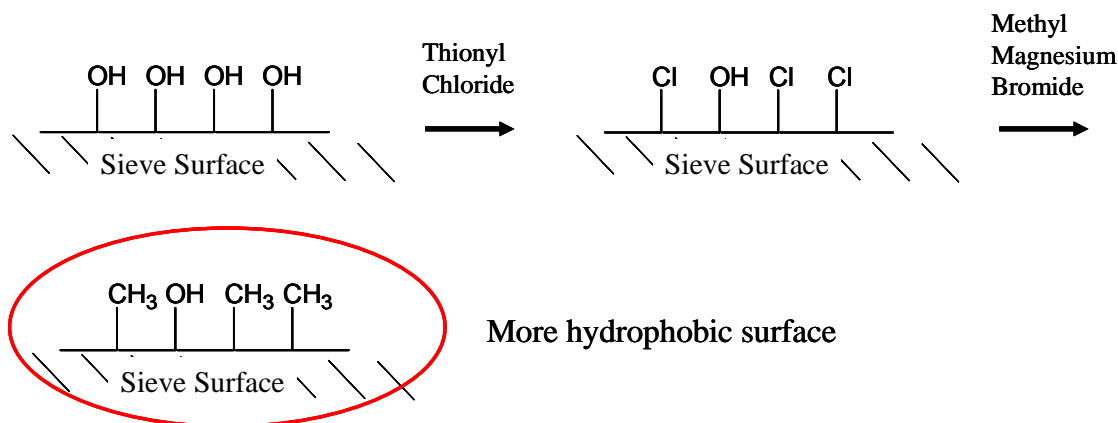
Figure 5.1: Schematic of envisioned hydrophobizing reaction on the zeolite surface [16]

5.3. EXPERIMENTAL

5.3.1. Step 1: Reaction with Thionyl Chloride

Molecular sieves used in the work were dried in a vacuum oven at 150 °C for 24 hours to remove adsorbed water. Under anhydrous conditions in a sealed flask, 8.0 grams of the sieves were sonicated at low intensity in 80 ml of anhydrous toluene and 10 ml of thionyl chloride ($SOCl_2$) for 4 hours in a sonication bath (Model: 1510R-MTH, *maximum* output 70 W, Branson Ultrasonics Corp., Danbury, CT). For each dispersion step, the lowest sonication energy sufficient to disperse the sieve particles was used. The dispersion was allowed to stir overnight with a dry nitrogen sweep at room temperature and then sonicated in the sonication bath for 4 hours. This step was followed by heating at temperatures varying between 90 – 110 °C with stirring until the sieves formed a dry cake. A vacuum was applied on the sieves to remove remaining solvent/reactant.

5.3.2. Step 2: Grignard Reaction

The sieves from the above step were re-dispersed in anhydrous toluene using a 130 W (*maximum* power output) sonication horn (Vibracell Model VC-130, Sonics & Materials Inc., Danbury, CT) for a total of 8 minutes.

To the above sieve dispersion, 20 ml of methyl magnesium bromide (MMB) (3.0 M solution in diethyl ether) was gradually added with stirring under anhydrous conditions. Thereafter the dispersion was sonicated in the sonication bath for 3 hours. A thin bore needle was used as a vent to prevent pressure build-up within the flask. After sonication, the flask was stirred overnight at room temperature. Sonication in the bath was repeated for 3 hrs. The excess MMB was quenched by slowly adding iso-propanol (IPA) while cooling in an ice bath. A vigorous reaction was observed and a gel-like mixture was formed. The sieves were collected and washed using a high pressure filtration setup with 0.2 micron polytetrafluoroethylene (PTFE) or polyvinylidene fluoride (PVDF) filters. The sieves were washed with three aliquots of 150 ml of IPA followed by 200 ml aliquots of DI water until the conductivity of the filtrate was reduced to about 50 – 75 microSiemens. The sieves were then dried at 150 °C for 24 hours under vacuum.

To test the effect of thionyl chloride on the dealumination tendencies, thionyl chloride only treated zeolites were obtained by omitting the Grignard reaction step[†]. The zeolites were rinsed with anhydrous toluene followed by washing with anhydrous IPA. The zeolites were then dispersed in DI water using sonication and the rinses continued until a low conductivity of the rinse water was obtained. The water washing step was included to remove any aluminum chloride that is believed to be generated during the dealumination step. This mechanism is discussed in more detail in Chapter 6. A final exchange with IPA was done with the sieves dispersed by a wrist-shaker and the zeolites were dried in the vacuum oven at 150 ºC for 12 – 24 hours. Figure 5.2 outlines the processing steps carried out during the Grignard treatment.

[†] As is discussed later, it was suggested by a colleague, Shu Shu, that dealumination may be occurring during exposure to thionyl chloride. Since this may alter the zeolite properties, an investigation of this effect was pursued.
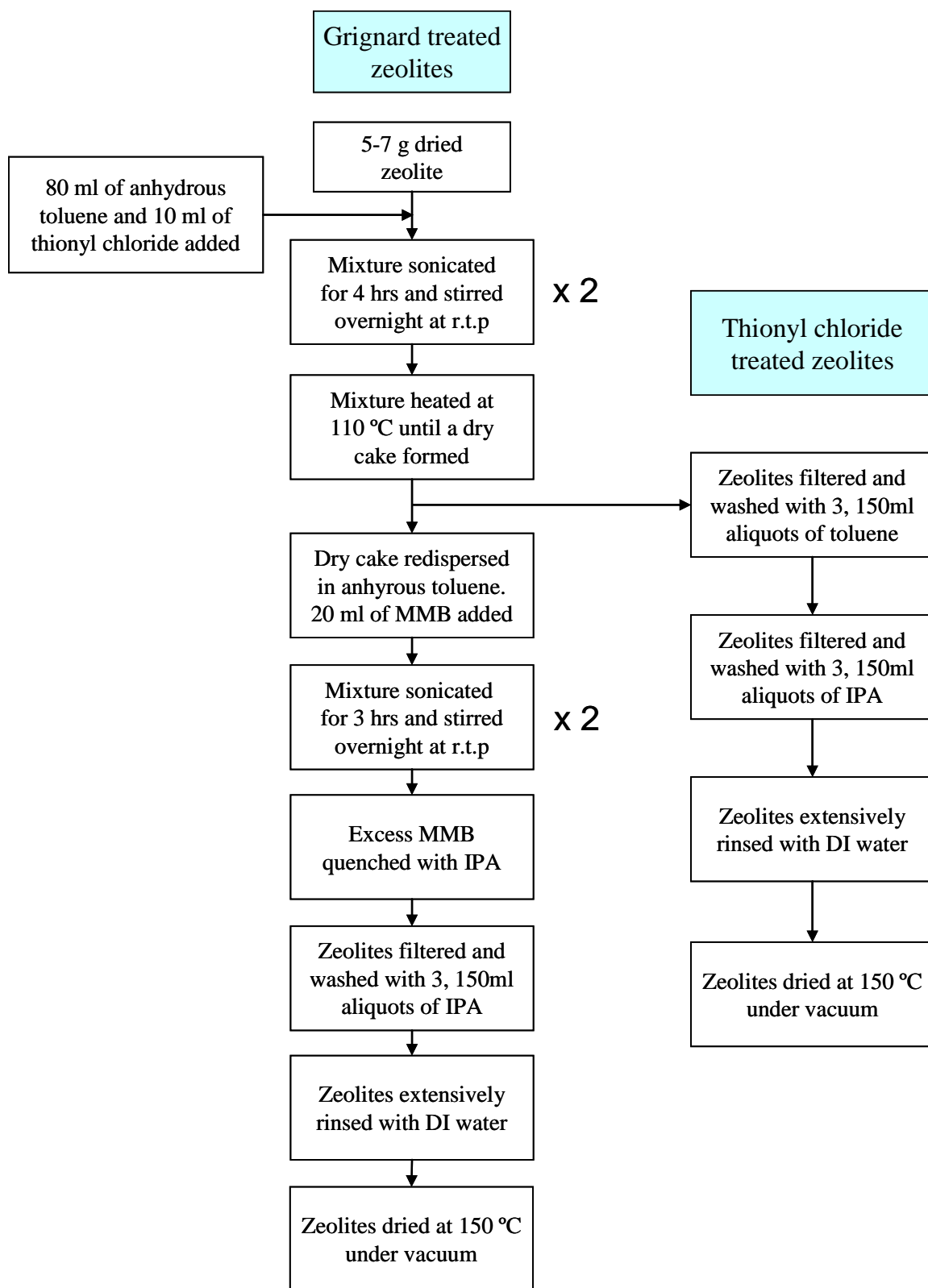
Figure 5.2: Reaction procedure for Grignard and thionyl chloride treated zeolites

5.4. MIXED MATRIX HOLLOW FIBER MEMBRANES

As hypothesized in Chapter 4, the formation of the sieve-in-a-cage defects around zeolites was believed to be promoted by the hydrophilic nature of the zeolite surface even after silanation and Ultem® "sizing". The Grignard treated (GT) zeolites were developed and tested with the hypothesis, that a methylated surface (Figure 5.1), being hydrophobic in nature, would suppress the zeolite particles from acting as nucleating agents for solvents and nonsolvents in the membrane formation process.

Reaction procedures for the Grignard modification were developed by the author after consulting work by Tao et al. [12], Sunseri et al. [15], and Bansal et al. [14]. The modified zeolites were successfully incorporated into Ultem® polyetherimide matrix and spun as dual layer asymmetric hollow fibers, which displayed significant enhancement in O_2/N_2 and CO_2/CH_4 gas pair selectivities [16]. Following the successful results of the Grignard treatment in producing asymmetric mixed matrix membranes, a parallel study was initiated in the area of mixed matrix dense film membranes based on Grignard treated zeolites by a colleague, Shu Shu, for her PhD investigation.

The following sections report the permeation results of incorporating the Grignard treated zeolites in Ultem® polyetherimide matrix and Matrimid® polyimide to form asymmetric hollow fiber membranes. The effect of the Grignard reagent on the sieve surface will be discussed in Chapter 6.

5.4.1. Dual Layer Ultem®-Ultem® Mixed Matrix Hollow Fiber Membranes Incorporating GT SSZ-13 Zeolites

Dual layer fibers incorporating 10.3 volume % (11.9 wt %) of GT SSZ-13 in an Ultem® matrix were spun. The inner core layer based on Ultem® was formulated for a highly porous support structure and was very similar to the core dope formulation in described in Chapter 4 for the hollow fibers based on Ultem® sized particles. The sheath dope was

mixed using the procedures outlined in section 3.2.2. The core and sheath dope compositions are provided in Table 5.1.

Table 5.1: Core and sheath dope compositions for Ultem®-Ultem® hollow fiber membranes containing Grignard treated SSZ-13 zeolite

Component	Core Dope (wt %)	Sheath Dope (wt %)
Ultem® 1000	32.0	28.0
N-methyl-2-pyrrolidione	57.7	49.6
Tetrahydrofuran	8.1	17.6
Lithium Nitrate	2.3	1.0
GT SSZ-13 zeolite	-	3.8

GT = Grignard treated

An SEM micrograph of a characteristic fiber cross-section is shown in Figure 5.3. Some incidence of macrovoids is apparent in the fibers and the source and suppression of these undesirable features is discussed in Chapter 7. Most importantly for the present discussion, the SEM micrographs of the skin region of the fibers suggest excellent adhesion between the zeolite and the polymer matrix as can be seen in Figure 5.4. The fibers initially display Knudsen selectivity when tested with pure gas oxygen (O_2) and nitrogen (N_2) gas pairs, indicating that defects exist in the skin region of the fibers. It is believed that these defects reflect a small fraction of trans-skin nanoscopic defects, rather than pervasive defects between the matrix and the sieve surface of the embedded particles. These "simple" trans-skin defects are typical even in thin skinned asymmetric fibers and can be repaired or "caulked" by conventional post-treatment [17]. As the porous support does not provide any resistance to gas flow, these trans-skin defects provide percolation pathways for the flow of gases. It is calculated that defects on the

order of 5Å comprising 0.001 percent of the surface area are enough to degrade membrane selectivity [18]. Fortunately, as noted above, these defects can be easily repaired by "caulking" the surface of the fiber which prevents Knudsen flow through these defects.
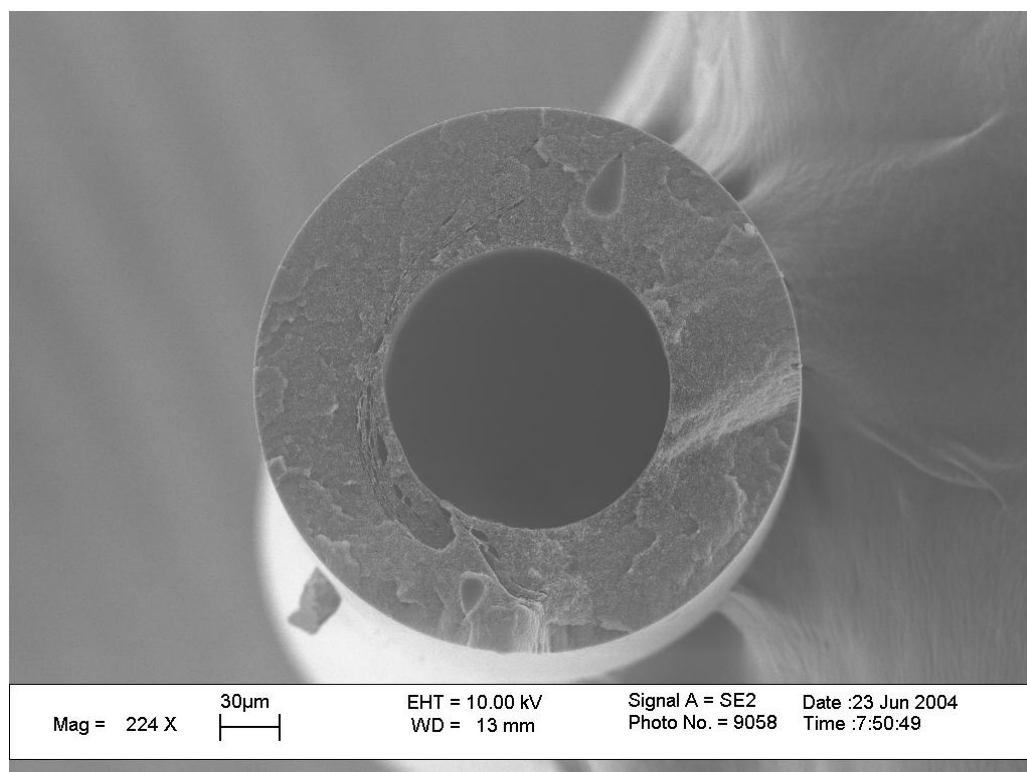
Figure 5.3: Dual layer Ultem®-Ultem® fibers containing 10.3 vol. % Grignard treated SSZ-13 zeolite in the sheath
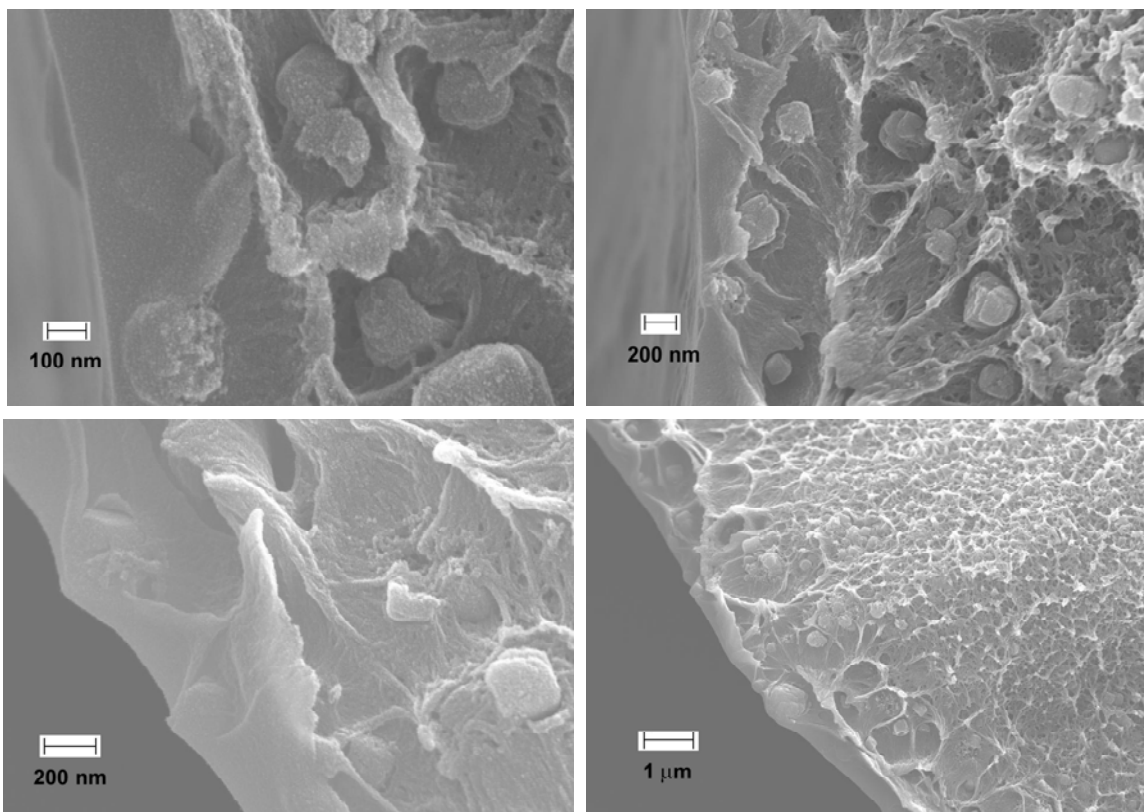
Figure 5.4: SEM micrographs of the skin region of fibers made with Grignard treated SSZ-13 zeolites

Correspondingly, a defect free polymer-zeolite composite membrane could be developed by increasing the skin thickness to prevent/minimize percolation pathways caused by a small number of defective polymer-zeolite interfaces. As the skin thickness is increased, a defective interface can be encapsulated in the skin region preventing Knudsen flow though the membrane. Figure 5.5 explains this analysis, so we anticipate that subsequent membranes may not require such "caulking" treatments.
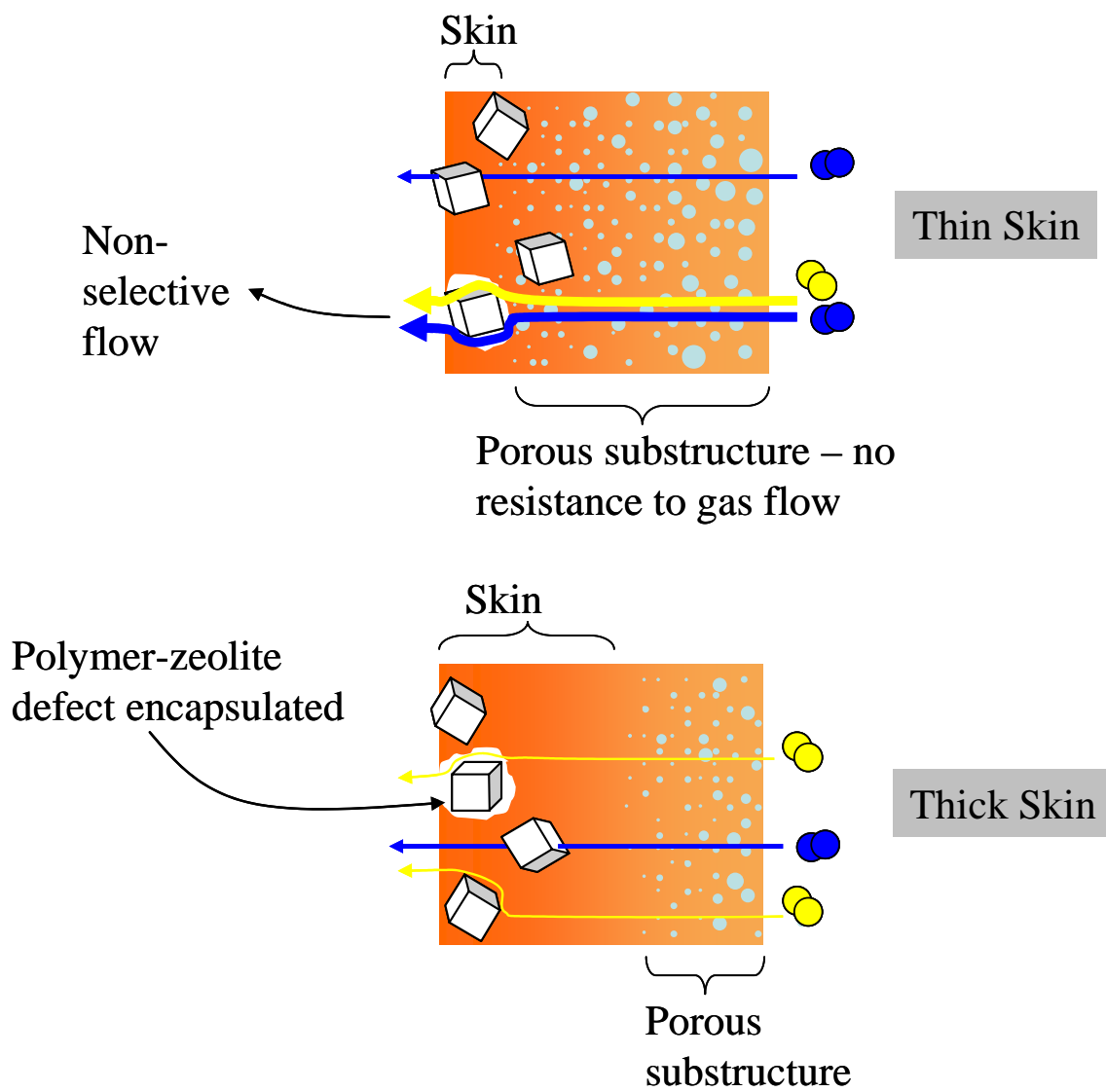
Figure 5.5: Depiction of gas pathway through thick versus thin skins in the presence of defects in the polymer-zeolite interface. Arrow thicknesses provide relative fluxes.

Unfortunately, increasing skin thicknesses results in a corresponding decrease in the gas flux/productivity of the membrane, which is undesired. As a result, the skin thicknesses of the hollow fibers were minimized in this work with the objective of attaining high gas fluxes.

After the application of the reactive post-treatment, described in section 3.2.5, the fibers display enhancement in selectivity for oxygen/nitrogen (O_2/N_2), helium/nitrogen (He/N_2)

and carbon dioxide/methane (CO_2/CH_4) gas pairs. The permeabilities and selectivities for mixed matrix fibers (SH38) spun with a draw ratio (DR) of 3.5 and air gap (AG) of 10 cm are shown in Table 5.2; the mixed matrix fiber permeation results are compared to those of earlier spun Ultem® defect-free fibers (DR = 2.8; AG = 20 cm), dense neat polymer film values and Maxwell model predicted values.

Table 5.2: Comparison of data for Grignard treated SSZ-13 zeolite based mixed matrix hollow fiber membranes with neat Ultem® fibers and Maxwell model predictions. Pure gas permeation measurements made at feed pressure of 114.7 psia and 35 °C. Error represents the standard deviation in the measurements.

Membrane	Post Treatment (PT)	O_2/N_2 Selectivity Pure gas	$(P/\ell)_{O2}$ (GPU)	He/N_2 Selectivity Pure gas	$(P/\ell)_{He}$ (GPU)
SH38 Fibers (Grignard treated SSZ-13)	Reactive PT	8.20 ± 0.09	1.70 ± 0.02	231 ± 4	48 ± 0.8
Neat Ultem® Fibers	No PT	7.26 ± 0.03	3.0 ± 0.01	158.9 ± 0.4	65.4 ± 0.2
Ultem® Dense Film [†]	No PT	7.6	4.0	178.6	94
Maxwell Model based on 10.3 vol. % sieve loading in Ultem® [†]	-	8.4	5.4	N/A[‡]	N/A[‡]

[†] Dense film and Maxwell model permeance (P/ℓ) calculation for a film thickness of 100 nm
[‡] Helium permeability data for SSZ-13 not currently available

An 8 – 10 % increase in O_2/N_2 selectivity over intrinsic values is seen for the post-treated fibers which match Maxwell model predictions. A corresponding 29 % increase in He/N_2 selectivity for the same fibers is also observed. Unfortunately, the prediction of He/N_2

selectivity based on the Maxwell model can not be currently obtained because of the lack of SSZ-13 helium permeability data. This data can be obtained by forming polyvinylacetate (PVAc) - GT SSZ-13 mixed matrix membranes and back-calculating the helium permeability for the modified zeolite using the Maxwell model. This is a time consuming dense-film procedure that is beyond the scope of the current study.

The results for CO_2/CH_4 mixed gas and pure gas for GT SSZ-13 mixed matrix hollow fiber membranes (shown in Table 5.3) exceed the enhancement in selectivity as predicted by the Maxwell model, displaying a 19 % increase in selectivity above neat Ultem® fiber selectivity for both mixed and pure gas results. The difference in mixed gas and pure gas selectivities may be explained by competition effects of the highly sorbing CO_2 molecule. This competition effect is believed to be a result of the CO_2 molecules filling the Langmuir sites (transient holes) within the membrane. The occupation of these sites excludes CH_4 from sorption and transport pathways available to it as a pure component; resulting in a higher overall selectivity [19].

It is possible that the higher selectivity obtained with both mixed and pure gas results than those predicted by the Maxwell model may be attributed to the change in the transport properties of the modified zeolite with respect to the properties of the as-received zeolite used in the model. Such changes will be considered in Chapter 6.

Table 5.3: Comparison of mixed gas and pure gas CO_2/CH_4 data for Ultem® based Grignard treated SSZ-13 zeolite mixed matrix fibers with neat Ultem® fibers and Maxwell model predictions. Permeation measurements using feed pressures: mixed gas (114.7 psia), pure gas CH_4 (114.7 psia) and pure gas CO_2 (23 psia). Measurements made at 35 ºC. Error represents the standard deviation in the measurements.

Membrane	Post Treatment (PT)	CO_2/CH_4 Selectivity Mixed gas (20:80)	CO_2/CH_4 Selectivity Pure gas
SH38 Fibers (Grignard treated SSZ-13)	Reactive PT	46.9 ± 0.1	43.9 ± 0.3
Neat Ultem Fibers	No PT	39.6 ± 0.2	36.0 ± 0.2
Maxwell Model based on 10.3 vol. % zeolite loading in Ultem®		42	42

5.4.2. Dual Layer Ultem®-Ultem® Mixed Matrix Hollow Fiber Membranes Incorporating GT Zeolite 4A

To determine the effect of framework aluminum on the success of the Grignard treatment, submicron size Zeolite 4A (Si:Al ratio typically around 1) were modified. Using procedures outlined in Chapter 3, mixed matrix dopes incorporating Grignard treated zeolite 4A in an Ultem®-Ultem® dual layer hollow fiber were spun. The core and sheath compositions of the polymer dopes are shown in Table 5.4.

The fibers had excellent concentricity and low incidence of macrovoids. A sample SEM microphotograph of the cross-section of a representative fiber is shown in Figure 5.6.

84

Table 5.4: Core and Sheath dope compositions for Ultem-Ultem® hollow fiber membranes containing Grignard treated zeolite 4A

Component	Core Dope (wt %)	Sheath Dope (wt %)
Ultem® 1000	32.0	29.0
N-methyl-2-pyrrolidione	57.4	48.9
Tetrahydrofuran	8.1	17.9
Lithium Nitrate	2.5	1.0
Grignard Treated Zeolite 4A - Batch 2[†]	-	3.2

[†] See section 6.2.3.2. for characterization of zeolite batch
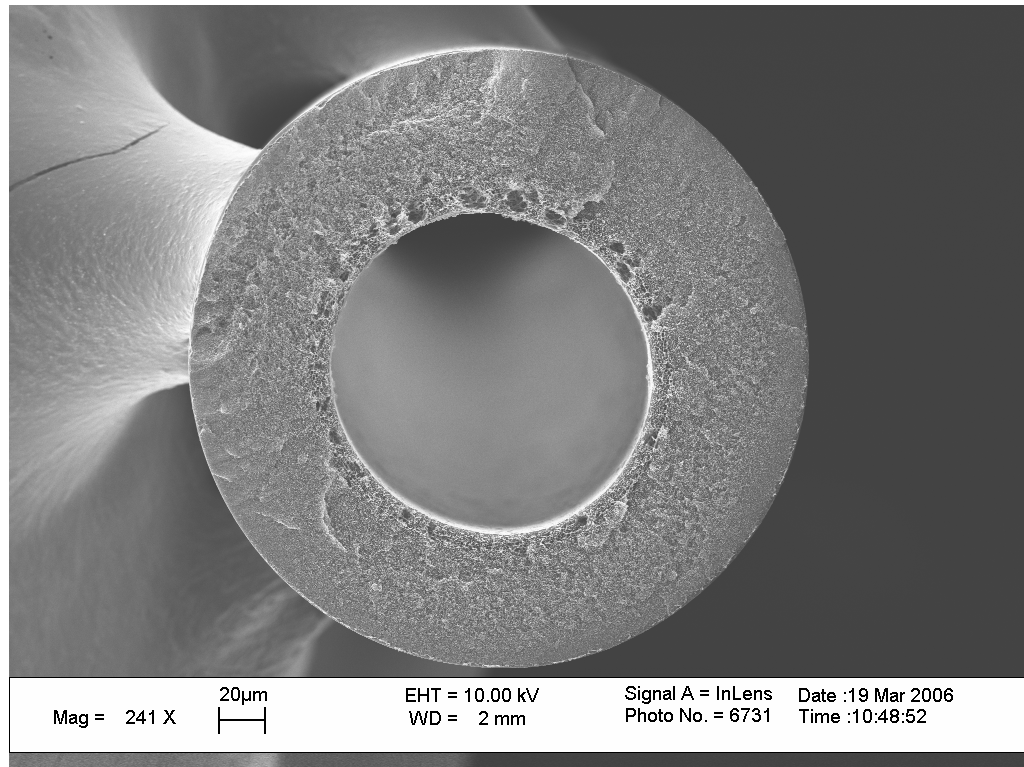
Figure 5.6: Dual layer Ultem®-Ultem® hollow fiber membrane incorporating 8.4 vol. % (9.8 wt %) Grignard treated submicron zeolite 4A in Ultem® sheath

A higher resolution SEM micrograph of the sheath and skin region of the fiber is shown in Figure 5.7, confirming the excellent bonding between Grignard treated zeolite 4A and Ultem®.
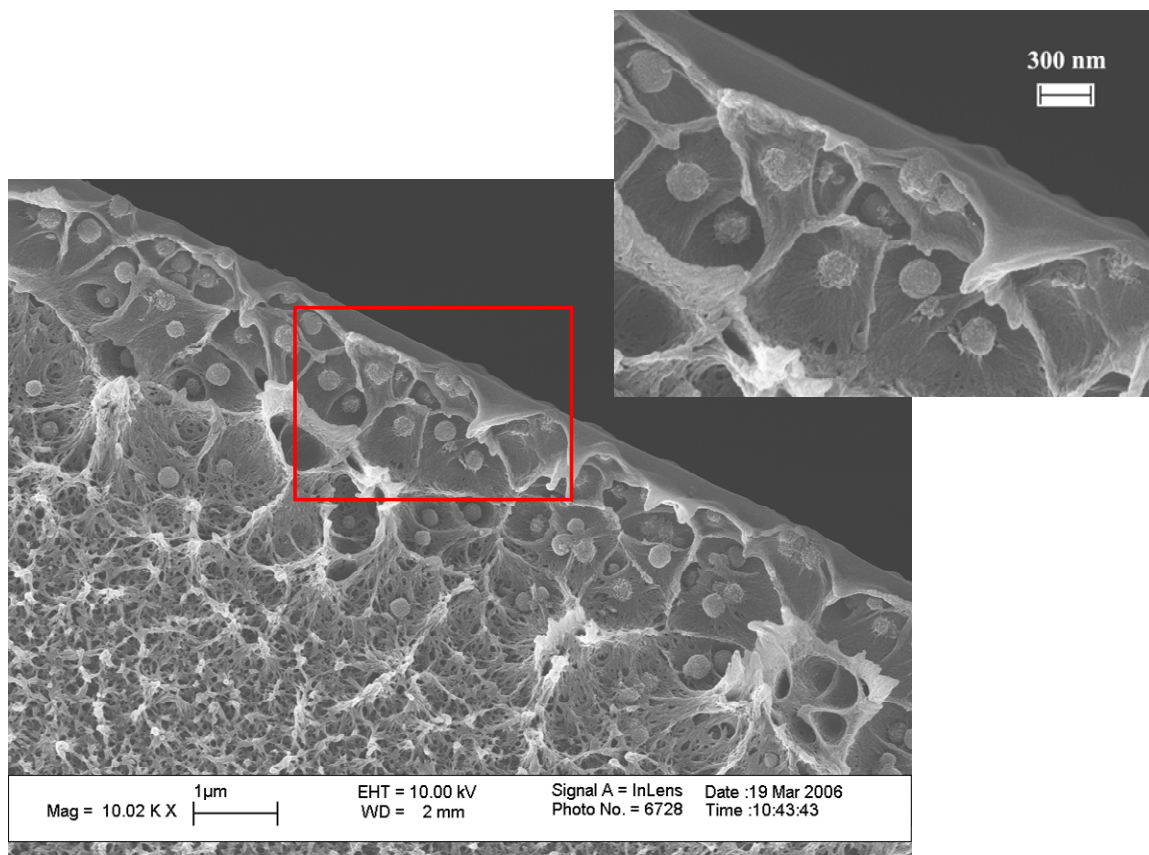
Figure 5.7: SEM image of sheath region of Ultem®-Ultem® dual layer fiber incorporating Grignard treated zeolite 4A. Inset shows the excellent sieve-polymer bonding in the skin region of the fiber

Permeation results of post-treated fibers (reactive post-treatment) support SEM analysis that good bonding exists between the polymer and the zeolite surface. Increased selectivity, above the polymer intrinsic selectivity, is seen for pure gas O_2/N_2 and He/N_2

gas pairs. The results of O_2/N_2 and He/N_2 selectivity versus draw ratio are shown in Figure 5.8.
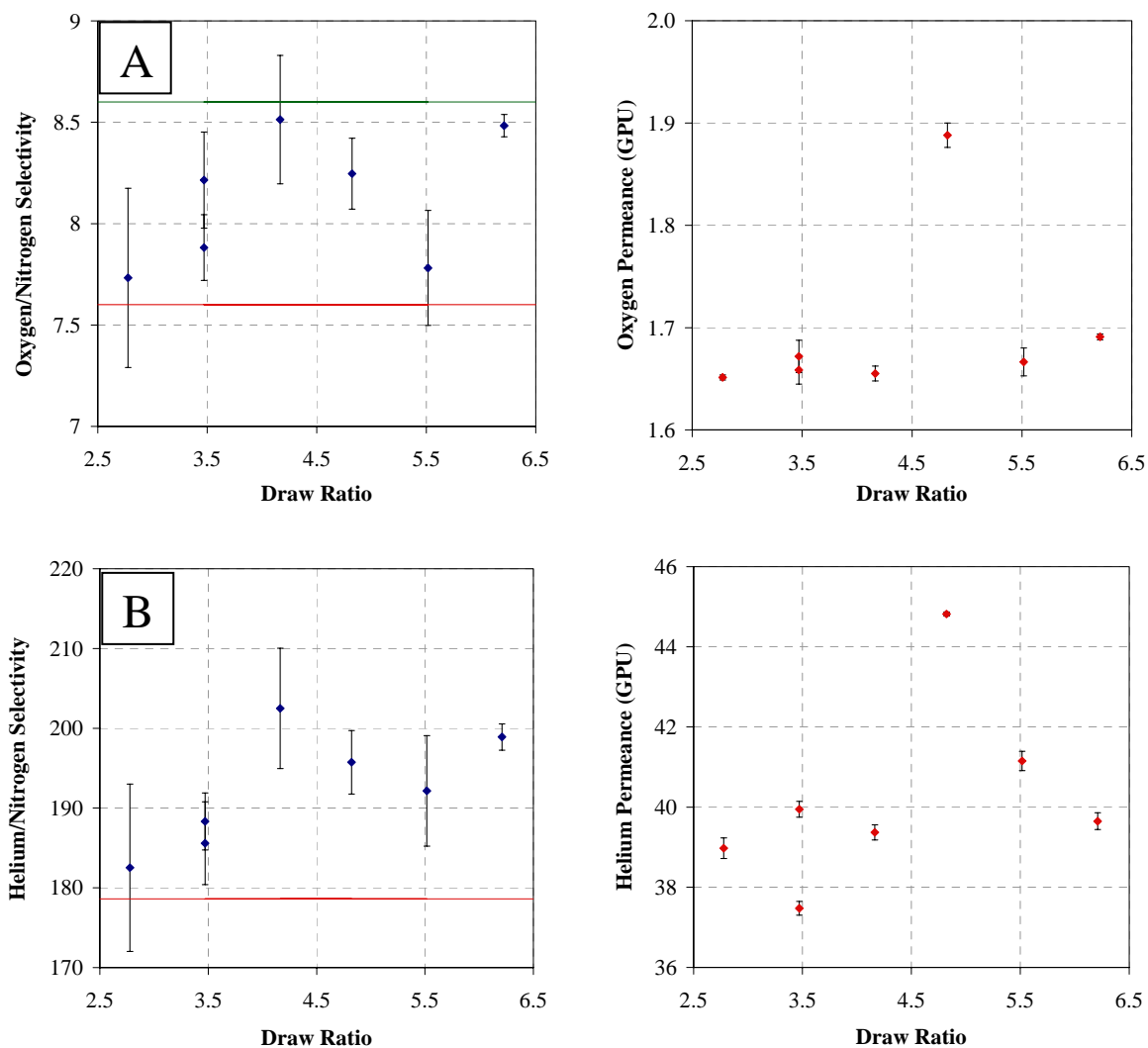
Figure 5.8: Selectivities and permeances for post-treated Ultem®-Ultem® dual layer mixed matrix hollow fibers incorporating Grignard treated zeolite 4A as a function of draw ratio. Fibers spun at constant extrusion rates and air gap (10 cm). (A) Oxygen/Nitrogen selectivity. The lower bound (red line) and upper bound (green line) represent Ultem® intrinsic and Maxwell model prediction selectivities, respectively; (B) Helium/Nitrogen selectivity. The solid red line represents Ultem® intrinsic selectivity. Measurements made at feed pressure 114.7 psia and 35 ºC. Error bars represents the standard deviation in the measurements.

It is interesting to note that a small increase in selectivity of the membranes is seen with increasing draw ratio for the He/N_2 gas pair. These results are difficult to decouple considering the combined effects of polymer chain orientation under increasing draw ratios and post-treatment layer variability, and thus require further study.

5.4.3. Dual Layer Ultem®-Matrimid® Mixed Matrix Hollow Fiber Membranes Incorporating GT Zeolite 4A

Earlier researchers have shown a strong dependence of polymer flexibility on polymer-sieve adhesion in mixed matrix membranes. This conclusion was drawn on the basis of successful results using rubbery polymers, followed by glassy polymers with low glass transition temperatures (T_g) to form mixed matrix membranes. Although higher T_g polymers, more relevant for commercial membranes, were attempted for use as the polymer matrix in mixed matrix membranes, limited success was achieved [20-22]. Of particular interest, Matrimid® polyimide has attractive permeabilities for oxygen and carbon dioxide which are 5 and 7 times higher than that for Ultem® and comparable selectivites for O_2/N_2 and CO_2/CH_4 gas pairs. It is therefore attractive to use such a higher permeability polymer as the matrix material.

Attempts to form dense film mixed matrix membranes with a high glass transition temperature (Tg) polymer, Matrimid®, were made by Mahajan [23]. He found that polymer-sieve adhesion could be improved by the addition of plasticizers, however, the plasticizers decreased the permeability of the matrix polymer. Although favorable selectivity results were obtained, long term stability testing of the membranes was not performed.

The following sections discuss the results of Matrimid® based mixed matrix asymmetric hollow fiber membranes incorporating Grignard treated zeolite 4A.

5.4.3.1. Hollow Fiber Morphology and Sieve-Polymer Adhesion

Using the procedures outlined in section 3.3.2., a mixed matrix dope using Matrimid® as the base polymer was prepared. A similar core dope composition used in earlier spins was used, however, a new formulation of the sheath dope was developed based on the principles outlined in Chapter 2. The mixed matrix dope in combination with an Ultem® based support was co-extruded through a dual layer spinneret. The core and sheath dope compositions are provided in Table 5.5.

Table 5.5: Core and sheath dope compositions for Ultem®-Matrimid® hollow fiber membranes containing Grignard treated zeolite 4A

Component	Core Dope (wt %)	Sheath Dope (wt %)
Ultem® 1000	32.0	-
Matrimid® 5218	-	19.2
N-methyl-2-pyrrolidione	57.4	57.7
Tetrahydrofuran	8.1	19.1
Lithium Nitrate	2.5	-
Grignard treated zeolite 4A – Batch 3 [†]	-	4.1

[†] See section 6.2.3.2. for characterization of zeolite batch

Circular and concentric dual layer hollow fiber membranes were obtained. Based on multiple SEM micrographs, some macrovoids were seen in the fibers all of which originate in the core region of the fiber rather than the important sheath zone. A representative SEM micrograph of a fiber cross-section with a single macrovoid is shown in Figure 5.9.
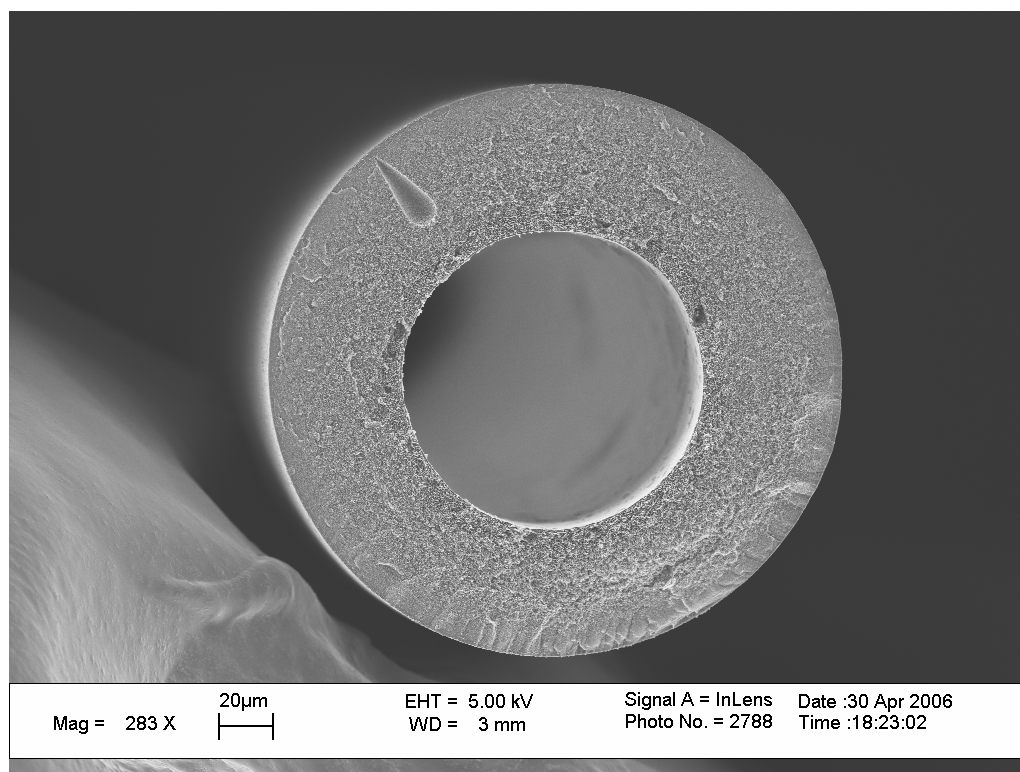
Figure 5.9: SEM image of an Ultem®- Matrimid® mixed matrix fiber based on 14.4 vol. % (17.6 wt %) Grignard treated zeolite 4A in Matrimid® sheath

An interface between the Ultem® core and the Matrimid based sheath layers is observed in the fibers observed at higher magnification. However, as can be seen from Figure 5.10, this interface does not show signs of delamination. It is believed that the interface, characterized by an abrupt change in the porosity of the membrane, represents the changing phase separation characteristics of the two different polymers used for the core (Ultem®) and sheath (Matrimid®) dopes. This interface could presumably be eliminated by dope optimization, but for the current study, it is not a crucial aspect.
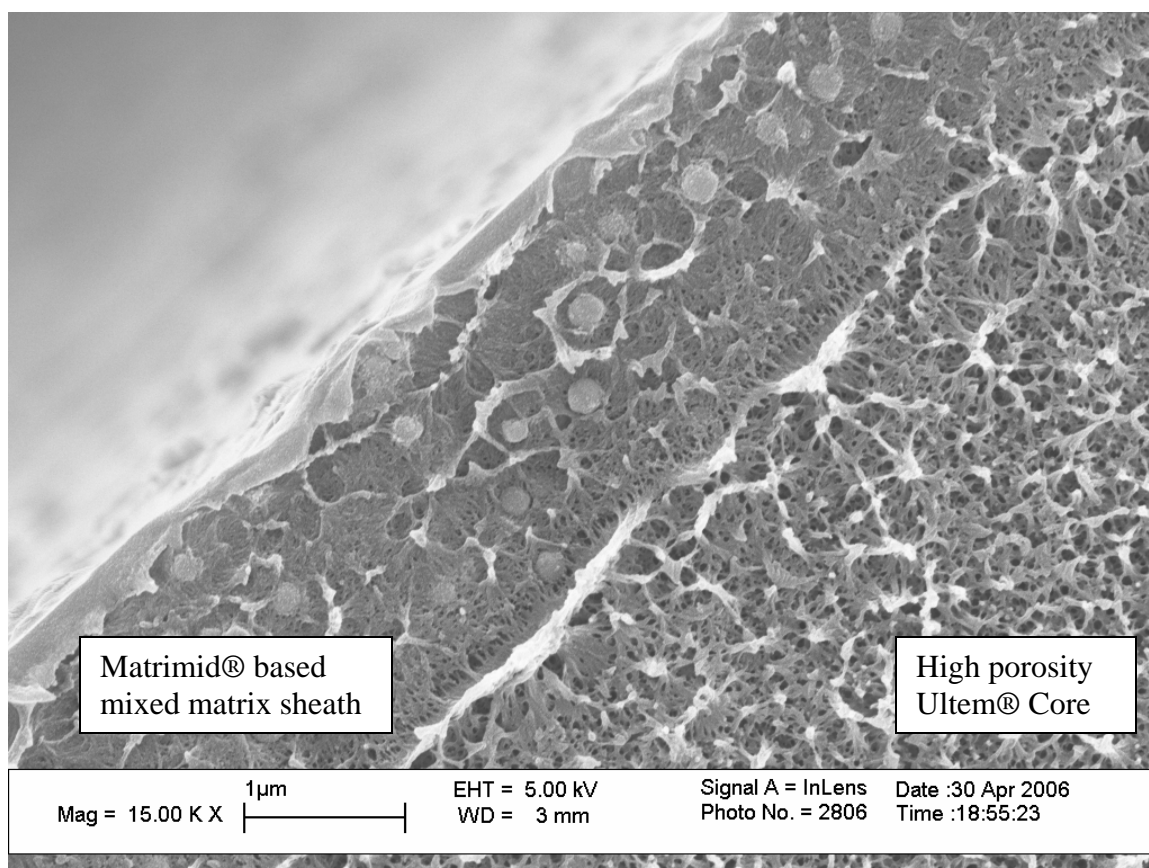
Figure 5.10: Well bonded interface between the sheath (Matrimid®) and core (Ultem®) layers.

Excellent sieve-polymer adhesion can be observed in Figure 5.11 representing a collection of micrographs of the sheath and skin region of the fibers.
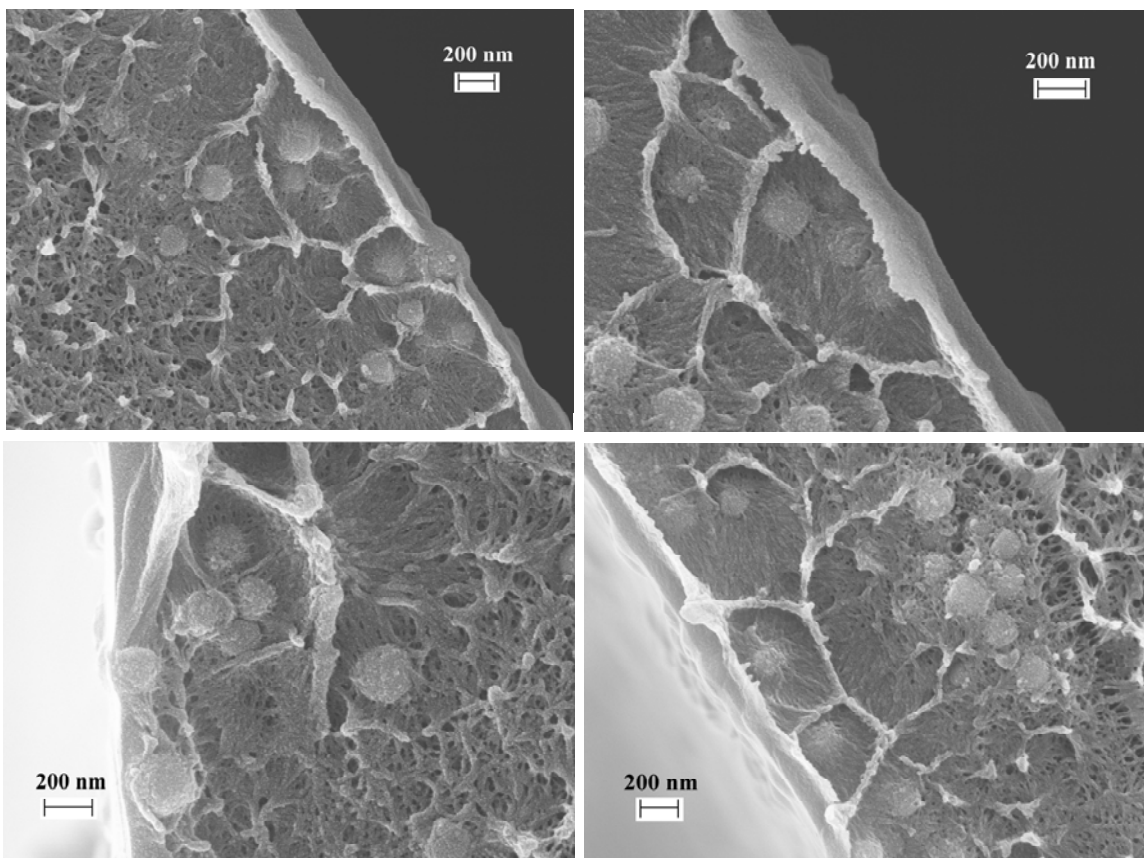
Figure 5.11: SEM images of the skin region of the fiber showing excellent adhesion between the zeolite (Grignard treated zeolite 4A) and polymer (Matrimid®) matrix

5.4.3.2. *Permeation Results*

The permeability data for the post-treated Ultem®-Matrimid® hollow fiber incorporating Grignard treated zeolite 4A display conflicting selectivity results for O_2/N_2 and He/N_2 gas pairs. While He/N_2 selectivity exceeds intrinsic Matrimid® values, O_2/N_2 selectivity is significantly less than the intrinsic value. The permeation data is shown in Figure 5.12. The results are not well understood at this juncture. One conjecture may be that the gas separation layer consists of a blend of the Ultem® based core layer with the Matrimid® layer, which forms at the interface, as the observed selectivities for both O_2/N_2 (6.3) and He/N_2 (125) in the above fibers are below those of intrinsic Ultem® (O_2/N_2 =7.6 and He/N_2 =178).
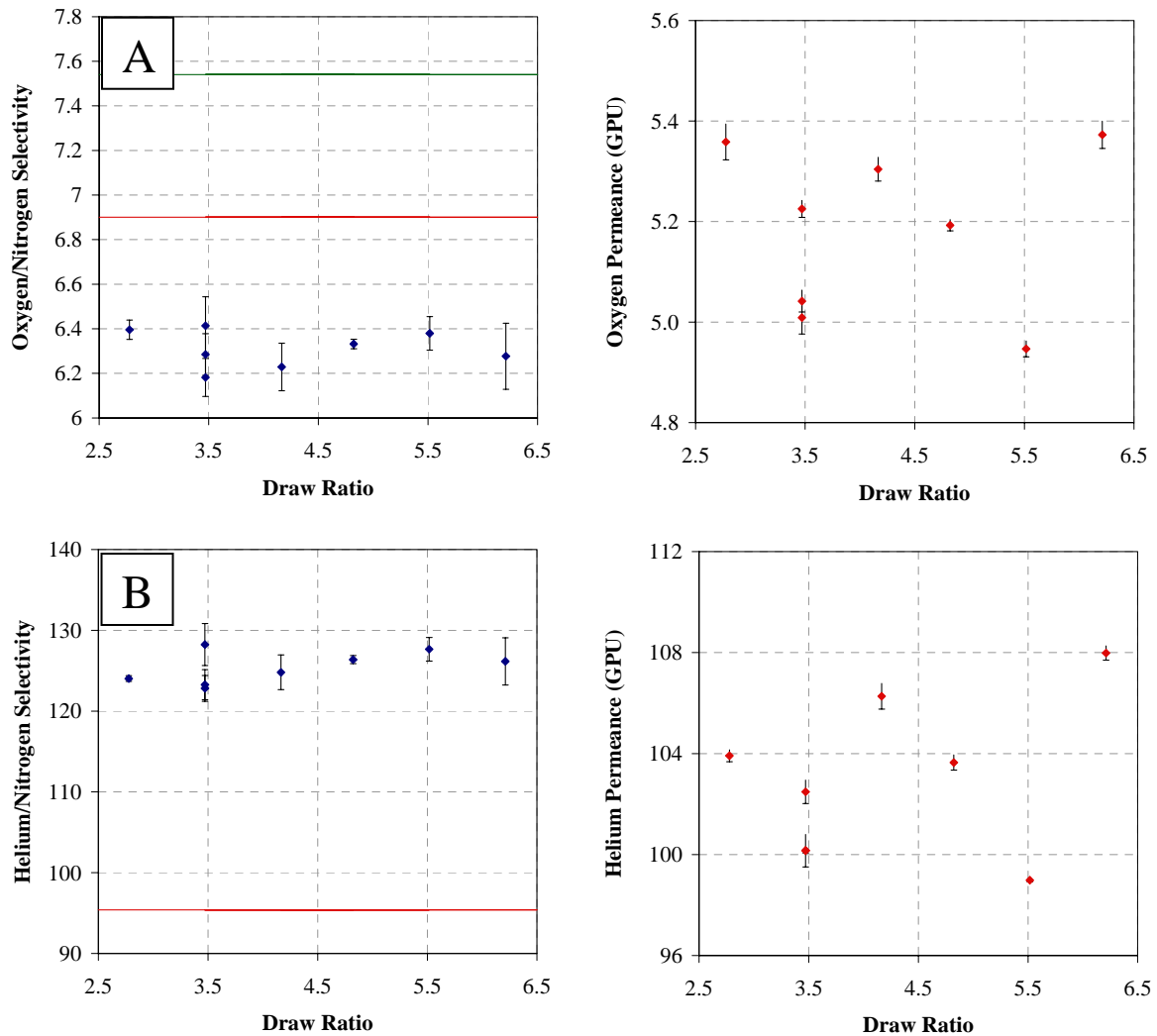
Figure 5.12: Selectivities and permeances for post-treated Ultem®-Matrimid® dual layer mixed matrix hollow fibers incorporating Grignard treated zeolite 4A as a function of draw ratio. Fibers spun at constant extrusion rates and air gap (10 cm). (A) Oxygen/Nitrogen selectivity and permeability. The lower bound (red line) and upper bound (green line) represent Matrimid® intrinsic and Maxwell model prediction seelctivities, respectively; (B) Helium/Nitrogen selectivity. The solid red line represents Matrimid® intrinsic selectivity. Measurements made at feed pressure 114.7 psia and 35 ºC. Error bars represents the standard deviation in the measurements.

Although enhancement in selectivity of Ultem®-Matrimid®- GT 4A fibers is not clearly

observed in the above fibers, based on selectivity enhancement seen with Matrimid®-GT

93

4A dense films (15 wt% zeolite loading) shown in Table 5.6, the potential for achieving mixed matrix effect in Matrimid®-GT 4A hybrid membranes exists [24]. However, it is not known what the added complexity of the phase separation process used to generate hollow fiber membranes can do in the Matrimid®-GT 4A hybrid system. Understanding the effect of the Grignard treatment on the zeolites and further spinning experiments using the Matrimid®-GT 4A hybrid system are required following better dope optimization.

Table 5.6: Comparison of dense film results for Matrimid®/GT-4A, Neat Matrimid® and Maxwell model predictions for zeolite loading of 14.3 wt %. Pure gas measurements made at 35 ºC and 65 psia [24].

Dense Film	O_2/N_2 Selectivity	O_2 Permeability (Barrer)	CO_2/CH_4 Selectivity	CO_2 Permeability (Barrer)
Matrimid/GT-4A	7.7	1.89	41.2	9.17
Neat Matrimid® Film	6.7	2.1	35	11.3
Maxwell Model	7.12	1.91	41.1	11.7

5.5. CONCLUSIONS

A novel zeolite surface modification technique was developed using a thionyl chloride and a Grignard reagent (methyl magnesium bromide). The treatment was pursued with the goal of reducing solvent-zeolite interaction and suppressing solvent and nonsolvent nucleation tendencies of the zeolite surface.

Grignard treated zeolites were found to have excellent polymer-zeolite adhesion for the Ultem®-Ultem®-GT SSZ-13, Ultem®-Ultem®-GT-4A and Ultem®-Matrimid®-GT-4A mixed matrix hollow fiber membranes. Permeation results display selectivity

enhancement for the Ultem®-GT zeolite (SSZ-13 and 4A) cases with O_2/N_2, He/N_2 and CO_2/CH_4 gas pairs.   Although positive mixed matrix results are not observed for the Ultem®-Matrimid®-GT 4A fibers, significant potential for the Matrimid®- GT 4A mixed matrix system exists based on dense mixed matrix film results.

The following chapter attempts to decipher the effect of the Grignard treatment on SSZ-13 and zeolite 4A and presents a coherent hypothesis of the affected changes supported by multiple characterization techniques.

5.6. REFERENCES

1.   Pesek, J.J., M.T. Matyska, R.R. Abuelafiya, and Editors, *Chemically Modified Surfaces: Recent Developments. (Proceedings of the 6th International Symposium on Chemically Modified Surfaces was held in San Jose, California, June 19-21, 1995.) [In: Spec. Publ. - R. Soc. Chem., 1996; 173]*. 1996. 146 pp.

2.   Plueddemann, E.P., *Silane Coupling Agents*. 1982, New York: Plenum Press. 235 pp.

3.   Ballard, C.C., E.C. Broge, R.K. Iler, D.S. St. John, and J.R. McWhorter, *Esterification of the surface of amorphous silica.* Journal of Physical Chemistry, 1961. **65**: p. 20-5.

4.   Lowen, W.K. and E.C. Broge, *Effects of dehydration and chemisorbed materials on the surface properties of amorphous silica.* Journal of Physical Chemistry, 1961. **65**: p. 16-19.

5.   Iler, R.K., *The Chemistry of Silica: Solubility, Polymerization, Colloid and Surface Properties and Biochemistry*. 1979, New York: John Wiley & Sons. 892 pp.

6.   Leboda, R., *Modification of surface properties of silica gels in aspects of their utility in chromatography. XIV. Modification of the texture and skeleton structure of silica gels with C1-10 aliphatic alcohols.* Chemia Analityczna (Warsaw, Poland), 1978. **23**(6): p. 935-43.

7.   Gaynor, J.F. and J. Huang, *Dispersions of silicalite and zeolite nanoparticles in nonpolar solvents*. 2003, (Novellus Systems, Inc., USA). Application: US. p. 10 pp.

8.   Vassylyev, O., J. Chen, G.S. Hall, and J.G. Khinast, *Efficient surface functionalization of zeolites via esterification.* Microporous and Mesoporous Materials, 2006. **92**(1-3): p. 101-108.

9.   Tertykh, V.A. and L.A. Belyakova, *Solid-phase hydrosilylation reactions with participation of modified silica surface.* Studies in Surface Science and Catalysis, 1996. **99**(Adsorption on New and Modified Inorganic Sorbents): p. 147-89.

10.   Ossenkamp, G.C., T. Kemmitt, and J.H. Johnston, *Toward Functionalized Surfaces through Surface Esterification of Silica.* Langmuir, 2002. **18**(15): p. 5749-5754.

11.   Pesek, J.J. and S.A. Swedberg, *Allyl-bonded stationary phase as possible intermediate in the synthesis of novel high-performance liquid chromatographic phases.* Journal of Chromatography, 1986. **361**: p. 83-92.

12. Tao, T. and G.E. Maciel, *Reactivities of Silicas with Organometallic Methylating Agents.* Journal of the American Chemical Society, 2000. **122**(13): p. 3118-3126.

13. Bansal, A., X. Li, I. Lauermann, N.S. Lewis, S.I. Yi, and W.H. Weinberg, *Alkylation of Si Surfaces Using a Two-Step Halogenation/Grignard Route.* Journal of the American Chemical Society, 1996. **118**(30): p. 7225-7226.

14. Bansal, A., X. Li, S.I. Yi, W.H. Weinberg, and N.S. Lewis, *Spectroscopic studies of the modification of crystalline Si(111) surfaces with covalently-attached alkyl chains using a chlorination/alkylation method.* Journal of Physical Chemistry B, 2001. **105**(42): p. 10266-10277.

15. Sunseri, J.D., T.E. Gedris, A.E. Stiegman, and J.G. Dorsey, *Complete Methylation of Silica Surfaces: Next Generation of Reversed-Phase Liquid Chromatography Stationary Phases.* Langmuir, 2003. **19**(20): p. 8608-8610.

16. Husain, S. and W.J. Koros. *Mixed Matrix Hollow Fibers for Gas Separation.* in *North American Membrane Society.* 2005. Providence, RI.

17. Henis, J.M.S. and M.K. Tripodi, *Composite hollow fiber membranes for gas separation: the resistance model approach.* J. Membr. Sci., 1981. **8**(3): p. 233-46.

18. Koros, W.J. and G.K. Fleming, *Membrane-based gas separation.* J. Membr. Sci., 1993. **83**(1): p. 1-80.

19. Chern, R.T., W.J. Koros, B. Yui, H.B. Hopfenberg, and V.T. Stannett, *Selective permeation of carbon dioxide and methane through Kapton polyimide: effects of penetrant competition and gas-phase nonideality.* Journal of Polymer Science, Polymer Physics Edition, 1984. **22**(6): p. 1061-84.

20. Duval, J.M., A.J.B. Kemperman, B. Folkers, M.H.V. Mulder, G. Desgrandchamps, and C.A. Smolders, *Preparation of zeolite filled glassy polymer membranes.* J. Appl. Polym. Sci., 1994. **54**(4): p. 409-18.

21. Mahajan, R. and W.J. Koros, *Mixed matrix membrane materials with glassy polymers. Part 2.* Polymer Engineering and Science, 2002. **42**(7): p. 1432-1441.

22. Pechar, T.W., M. Tsapatsis, E. Marand, and R. Davis, *Preparation and characterization of a glassy fluorinated polyimide zeolite-mixed matrix membrane.* Desalination, 2002. **146**(1-3): p. 3-9.

23. Mahajan, R., R. Burns, M. Schaeffer, and W.J. Koros, *Challenges in forming successful mixed matrix membranes with rigid polymeric materials.* J. Appl. Polym. Sci., 2002. **86**(4): p. 881-890.

24. Shu, S., S. Husain, and W.J. Koros. *Formation of Nano-scale Morphology on Zeolite Surfaces for Enhanced Interfacial Interaction in Mixed Matrix Membranes.* in *North American Membrane Society.* 2006. Chicago.

CHAPTER 6

EFFECT OF GRIGNARD TREATMENT ON ZEOLITE SURFACE

6.1. OVERVIEW

The preceding chapter presented the spinning and permeation results of Grignard treated SSZ-13 in Ultem®, Grignard treated zeolite 4A in Ultem® and Grignard treated zeolite 4A in Matrimid®. Apparently excellent polymer-zeolite adhesion was observed via microscopy. Selectivity increases above the intrinsic polymer were achieved with Ultem® based polymer matrix suggesting true compatibility was achieved at the sieve-matrix polymer interface.

The Grignard treatment as described in Section 5.3, is a two step process, where thionyl chloride is first reacted with the zeolites followed by the reaction of the zeolite with the Grignard reagent. To explore the effect of the Grignard treatment on the surface of the zeolite, XPS, microscopy, nitrogen adsorption and infra-red spectroscopy were carried out on the as-received, thionyl chloride only treated, and Grignard treated zeolites.

The results of the characterizations are then used to propose a picture of the chemical and structural changes on the surface of the Grignard treated zeolites. Based on the picture, an argument of the polymer-zeolite adhesion observed in Chapter 5 is presented, based on enthalpic and entropic considerations. The argument modifies the earlier hypothesis of nucleation suppressed/reduced by a hydrophobic (methyl capped) zeolite surface to that of nucleation suppressed/reduced by poor interaction between the basic solvent (NMP) and the Grignard treated zeolite surface.

6.2. CHARACTERIZATION OF THE GRIGNARD TREATED ZEOLITES

6.2.1. X-ray Photoelectron Spectroscopy (XPS)

6.2.1.1.   *Grignard Treated SSZ-13*

XPS was used in this work to identify and quantify the elemental composition of the zeolite surfaces. The surface elemental compositions of the as-received and modified SSZ-13 zeolites are provided in Table 6.1.

Table: 6.1: Surface elemental atomic percent for as received and modified SSZ-13 zeolite

Element	XPS Data (Atomic %)			Theoretical SSZ-13 (Atomic %) [†]
	SSZ-13	TC SSZ-13	GT SSZ-13	
Oxygen	65	64	60	66
Carbon	1.8	5.5	5.6	-
Silicon	31	29	21	32
Magnesium	N/A	-	14	-
Aluminum	1.6	1.1	-	1.3
Sodium	0.74	-	-	1.3 [‡]

GT = Grignard treated; TC = only thionyl chloride treated
[†] Based on a Si:Al ratio of 25:1 [1]
[‡] Assuming Na:Al ratio of 1

The XPS results for the known elemental composition of as-received SSZ-13 match quite well to the theoretical elemental composition based on a Si:Al ratio of 25. The SSZ-13 zeolite used in this work is ion-exchanged with ammonium to remove the sodium ion, followed by multiple water washings. The zeolite is then calcined at 450 ºC to decompose the ammonium to the proton form of the zeolite. Thus the sodium concentration in the as-received zeolite is expected to be lower than the calculated

theoretical atomic percent which is based on equivalent sodium and aluminum atoms in the unit structure.

Zeolite literature suggests that dealumination of the zeolite can be carried out by acidic reagents [2-4]. Dealumination of zeolites has been reported using acid halides at temperatures higher than 100 ºC and typically around 400 - 800 ºC [2]. It is reported that the degree of dealumination depends on the structure, the cationic type of zeolite, the type and concentration of the dealumination agent and the temperature of the reaction [2].

While reaction temperatures do not exceed 110 ºC in the experiments in this work, it is estimated that during sonication, local temperature caused by inter-particle collisions (for ~10 μm particles) could reach 2600 – 3400 ºC [5]. Thus it is possible that the dealumination reaction using thionyl chloride could take place at lower macroscopic temperatures because of the extremely high local temperatures generated during sonication.

Comparing the XPS data for the as-received SSZ-13 with TC SSZ-13, partial dealumination of the sample is observed with the silicon:aluminum (Si:Al) ratio increasing from 19.3 (as-received SSZ-13) to 26.3 (GT SSZ-13). A higher degree of dealumination is expected for zeolite 4A where the Si:Al ratio is expected to be closer to unity.

Surprisingly, the elemental analysis of the surface of the Grignard treated zeolites indicates the presence of magnesium on the surface. This discovery was first made by Dr. Alexis M.W. Hillock while pursuing her graduate studies at Georgia Tech [6]. The magnesium was then identified to be in the form of magnesium hydroxide using X-ray diffraction studies by a colleague, Shu Shu [7].

Although the original hypothesis was that the Grignard treatment would replace the surface hydroxyls with methyl groups, the presence and quantification of these groups has been difficult. No conclusion can be drawn about the presence of methyl groups bonded to silicon from the XPS data as extraneous carbon is difficult to remove within the XPS and a few atomic percent of carbon is always observed. As the last processing step for the as-received SSZ-13 is calcination at 450 ºC, the XPS detected amount of carbon on the as-received SSZ-13 can be viewed as the base carbon content from extraneous sources. Most likely, some IPA, used during the subsequent washings of the zeolites after the reactions remains adsorbed to the surface of the zeolite and can be attributed as the source of carbon detected in TC SSZ-13. If 5.5 atomic % of carbon in TC SSZ-13 can be considered to be from the extraneous source and IPA, the value can be used as the control for carbon content for comparison to Grignard treated samples. By this analysis, the 5.6 carbon % detected in Grignard treated SSZ-13 (GT SSZ-13) cannot be considered to be from any source other than the surroundings and IPA.

6.2.1.2.   *Grignard Treated Zeolite 4A*

The XPS elemental analysis of as-received and modified zeolite 4A, shown in Table 6.2, display considerable variation in magnesium and carbon content for the three batches of Grignard treatments. The difference was empirically observed to be linked with the purity of the Grignard reagent used. It was found that older Grignard reagent was less active in the reaction resulting in a less vigorous reaction during the quench step with IPA.

Comparing the surface data of as-received 4A and TC 4A, very little dealumination is seen in the zeolite after the thionyl chloride treatment. Although a higher degree of dealumination was expected, this result may be due to the unusually high Si:Al ratio of three detected at the surface for the as-received zeolite (bulk zeolite 4A Si:Al ratio is 0.7-1.2 [8]). It is quite possible that the bulk Si:Al ratio of the as-received zeolite used in this

work is closer to the typical value of unity and that the Si:Al ratio of three, detected by the surface technique of XPS, indicates the presence of excess silica on the surface of the zeolite. It may be conjectured that the Grignard treatment is removing the surface silica and "cleaning" up the zeolite. This could then account for the variability in Si:Al ratios (2.2 – 2.8) seen in the batch to batch (Batch 1 – Batch 3) results in Table 6.2 being a consequence of small differences between the reaction procedures and/or small variation in reactant purity.

Table 6.2: Surface elemental atomic percent for as-received and modified zeolite 4A

Element	XPS Data (Atomic %)					Theoretical Zeolite 4A (Atomic %) [†]
	As-received 4A	TC 4A	GT 4A Batch 1	GT 4A Batch 2	GT 4A Batch 3	
Oxygen	59	61	55	60	56	57
Carbon	1.6	3.5	10	8.2	4.9	-
Silicon	24	24	14	17	20	14
Magnesium	-	-	14	6.9	5.6	-
Aluminum	8.0	7.1	6.3	6.0	9.3	14
Sodium	7.8	4.2	1.7	2.6	3.9	14 [‡]

GT = Grignard treated; TC = only thionyl chloride treated
[†] Based on a dehydrated unit cell: $Na_{12}[(AlO_2)_{12}(SiO_2)_{12}]$ [8]
[‡] Assuming Na:Al ratio of 1;

Compared to the 3.5 % carbon seen in the TC 4A sample, the presence of 10 atomic % carbon in the GT 4A Batch 1 and similar result for Batch 2 (8.2%) could indicate the presence of methyl groups on the surface. To corroborate this result, Infra-red spectroscopy is used (section 6.2.4) to ascertain if any methyl groups are attached to the zeolite surface after the Grignard treatment.

The mechanism of the deposition of magnesium hydroxide and the absence of *detectable* methyl groups on the surface are not fully understood at this juncture. However, the analysis provided here and in the following sections attempts to build a coherent picture of the changes that could be taking place on the zeolite surface.

6.2.2. Microscopy

A possible mechanism of the dealumination reaction at the gas-solid interface is proposed by Fejes [2]. The mechanism, using carbonyl chloride (similar in reactivity to thionyl chloride) as the dealuminating agent, is as follows [2]:

$$\{AlO_2^-\}H^+ + COCl_2 \rightarrow \{AlO_2^-\}C^+Cl_2OH \xrightarrow{-HCL} \{AlO_2^-\}C^+OCl \tag{6.1}$$

The positively charged halo-acylium ($\{AlO_2^-\}C^+OCl$) ion is unstable and removes an O^{2-} ion from the framework, liberating carbon dioxide and leaving behind an aluminum vacancy and aluminum oxychloride;

$$\{AlO_2^-\}C^+OCl \rightarrow CO_2 \uparrow + AlOCl + \{\bullet\bullet\bullet\} \tag{6.2}$$

where $\{\bullet\bullet\bullet\}$ designates a "nest" left behind by the extraction of the aluminum. The final step is the reaction of the aluminum oxychloride with the carbonyl chloride;

$$AlOCl + COCl_2 \rightarrow AlCl_3 \uparrow + CO_2 \uparrow \tag{6.3}$$
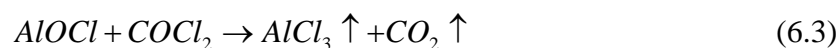
Based on Fejes' postulated reaction pathway, it can be conjectured that thionyl chloride primarily acts to remove aluminum from the zeolite framework leaving behind hydroxyl nests. Figure 6.1 shows a representation of the hydroxyl nest formed by the dealumination using an acid (hydrochloric acid).
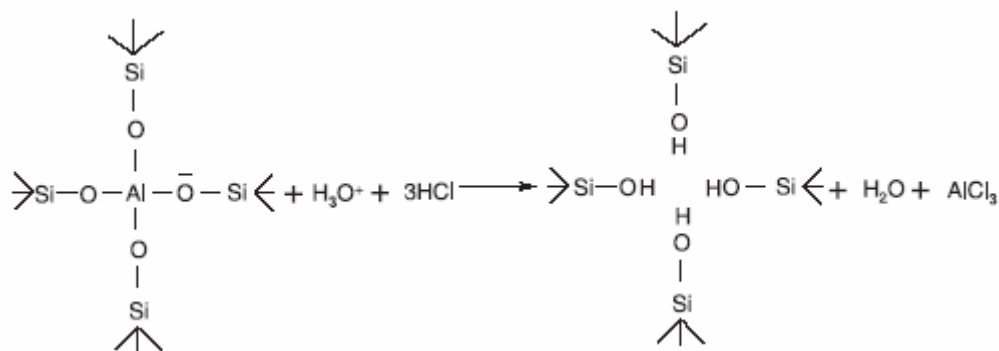
Figure 6.1: Representation of a hydroxyl nest formed using dealumination by an acid [9]

Additionally, the abstraction of aluminum under acidic conditions is also reported to result in a decrease in crystallinity of the sample [2]. The abstraction of aluminum leaves behind hydroxyl nests, which may then be covered with deposited magnesium hydroxide during the Grignard reaction. This could lead to an increase in the surface roughness of the zeolite. Observation of the zeolites using SEM microscopy reveals no change in the surface of SSZ-13 after the thionyl chloride treatment. However, increase in surface roughness is observed after the reaction with the Grignard reagent. It is believed that magnesium hydroxide is deposited on the surface, thereby increasing the surface roughness [10]. The SEM microphotographs of the as-received, thionyl chloride only treated and Grignard treated SSZ-13 zeolites are shown in Figure 6.2.
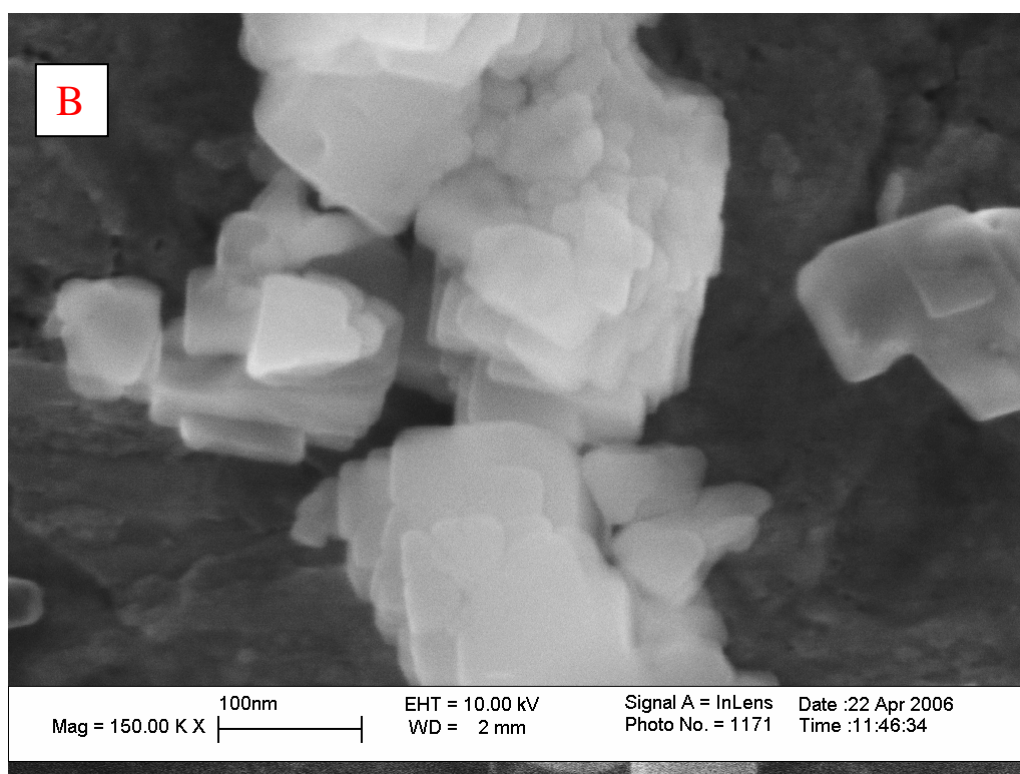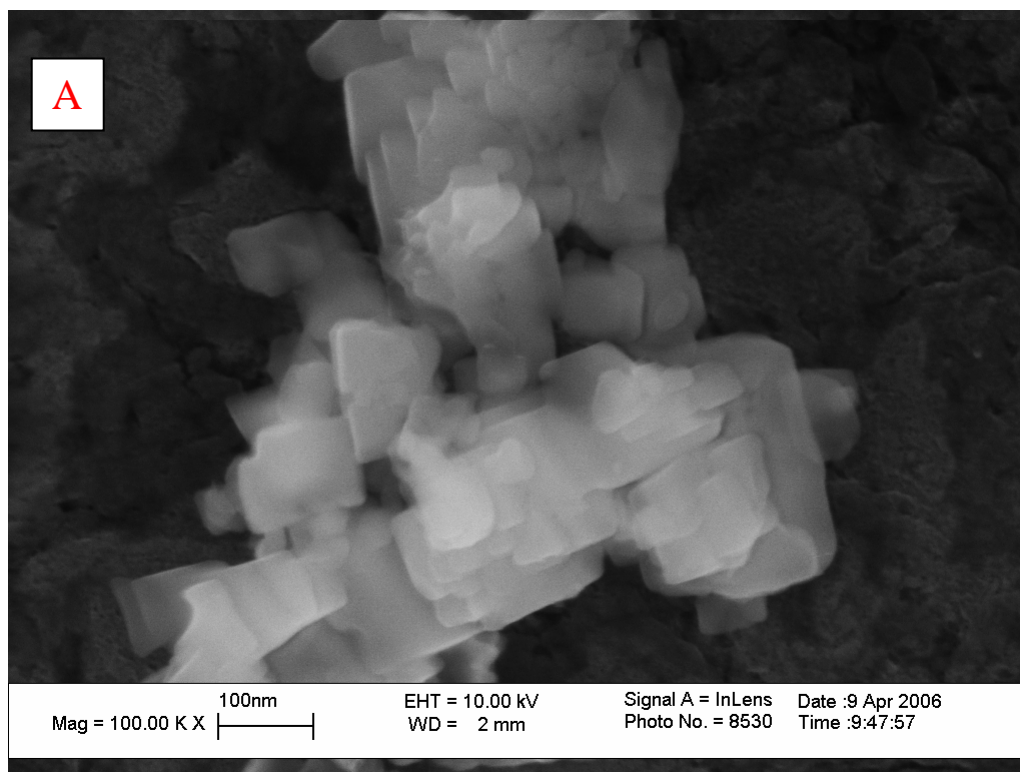
Figure 6.2: SEM microphotographs of, (A) As-received SSZ-13, (B) Thionyl chloride only treated SSZ-13 zeolite; (C) Grignard treated SSZ-13 zeolite

C

| 100nm | EHT = 10.00 kV | Signal A = InLens | Date :9 Apr 2006 |
| Mag = 100.00 K X ├──────┤ | WD = 3 mm | Photo No. = 8537 | Time :10:01:48 |
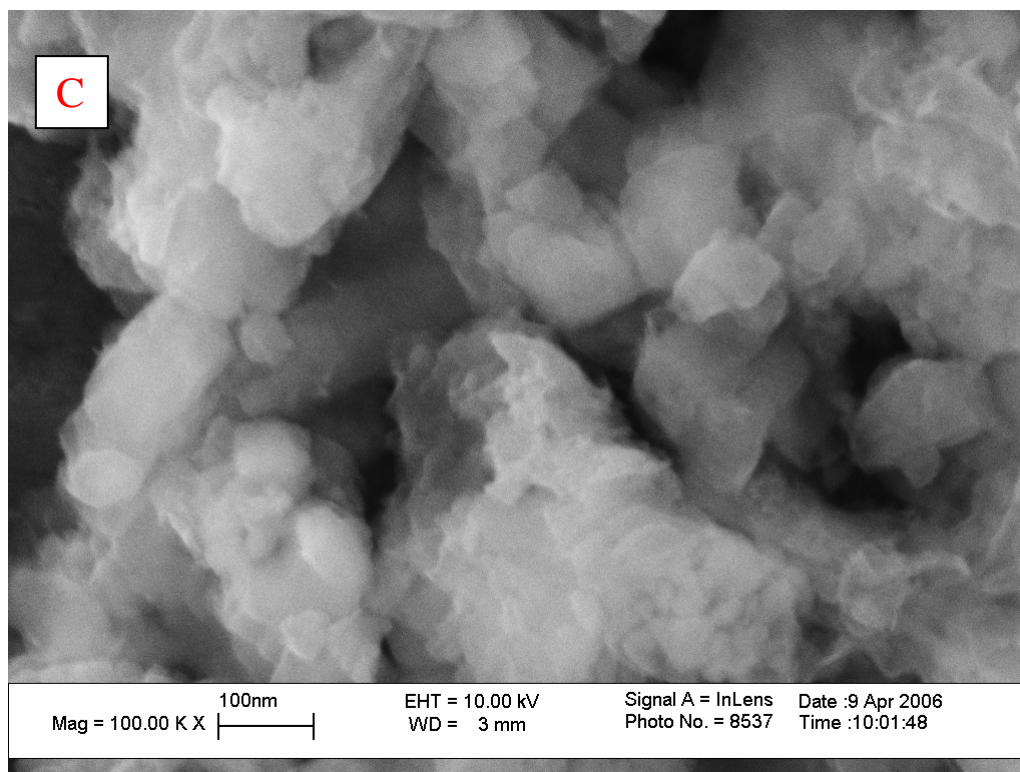
Figure 6.2: SEM microphotographs of, (A) As-received SSZ-13, (B) Thionyl chloride only treated SSZ-13 zeolite; (C) Grignard treated SSZ-13 zeolite

Zeolite 4A shows increased surface roughness after the Grignard treatment. Similar to the results of the SSZ-13, the surface of zeolite 4A shows no change after the only reacting with thionyl chloride. SEM microphotographs of as-received, thionyl chloride only treated and Grignard treated zeolite 4A are shown in Figure 6.3.
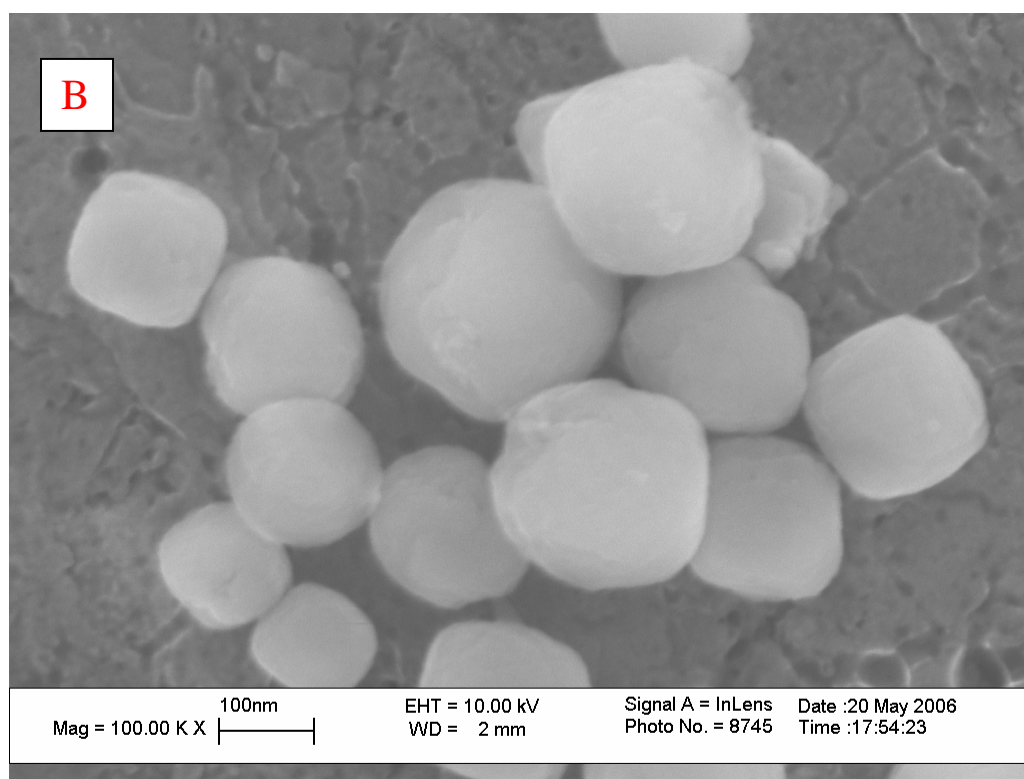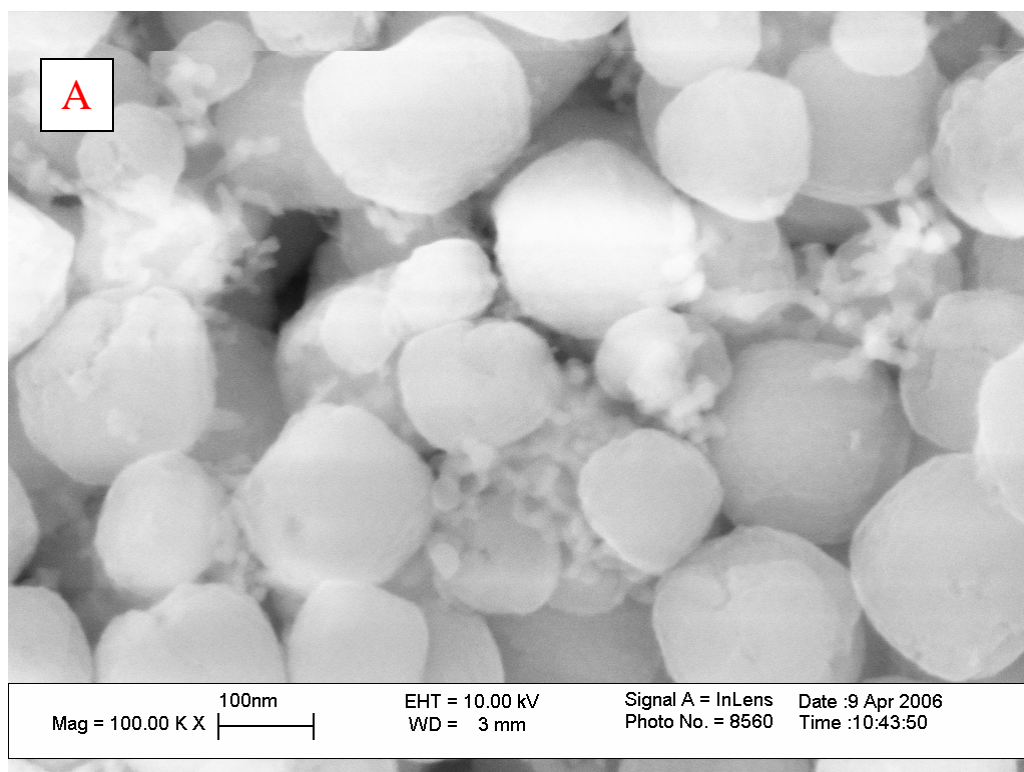
Figure 6.3: SEM micrographs of (A) as-received zeolite 4A, (B) Thionyl chloride only treated zeolite 4A, (C) Grignard treated zeolite 4A
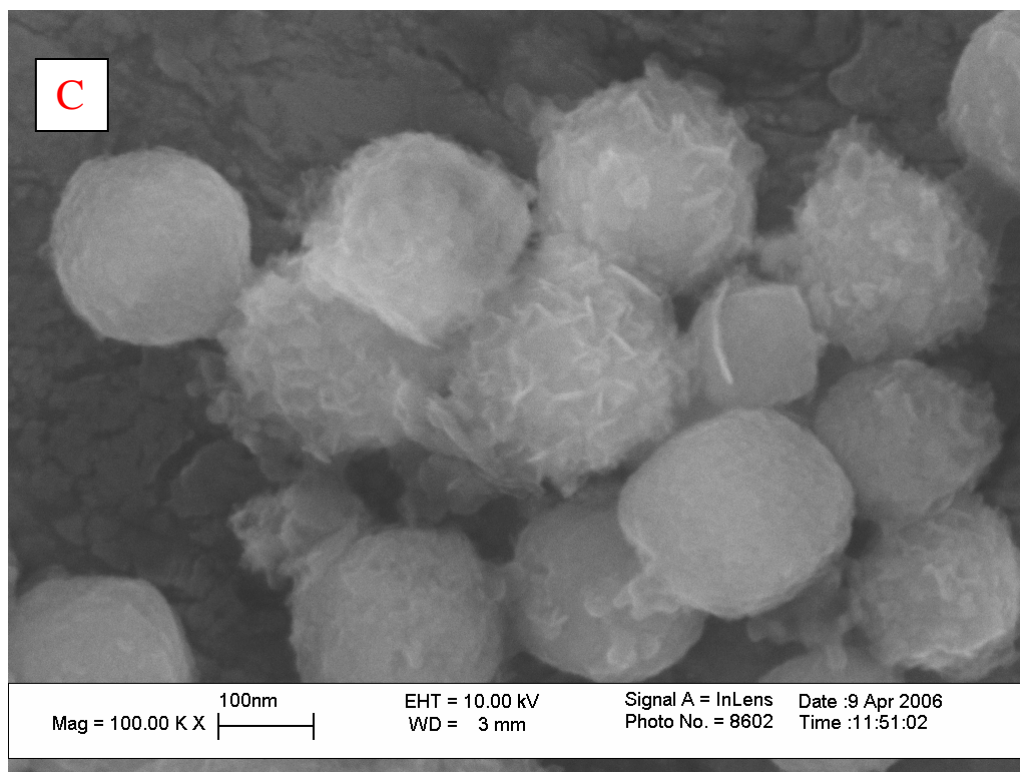
Figure 6.3: SEM micrographs of (A) as-received zeolite 4A, (B) Thionyl chloride only treated zeolite 4A, (C) Grignard treated zeolite 4A

Although, microscopy serves as an excellent tool to decipher the surface morphology of the modified zeolites, the effect of the Grignard treatment on the molecular sieving attribute of the zeolites can only be probed by sorption experiments. The following section uses nitrogen adsorption to determine surface areas and pore volumes of the zeolites to identify the effect of the modification.

6.2.3. Nitrogen Adsorption

Nitrogen adsorption serves as a basic tool to determine pore volumes and surface areas for microporous and mesoporous materials. The as-received, thionyl chloride treated and Grignard treated samples were analyzed by nitrogen adsorption to determine changes in pore volumes and surface area as a result of the chemical treatments. Prior to the analysis, the zeolites were dried at 300 ºC for 18 hrs under 2μm Hg vacuum.

6.2.3.1.   Analysis of As-received and Modified SSZ-13

Reduction in the surface areas and pore volume were seen after the reaction of SSZ-13 zeolite with thionyl chloride and Grignard reagent. The decrease in the surface area and volumes may indicate a small loss in crystallinity of the sample during the reactions, forming an amorphous phase. This conclusion appears valid, as most of the reduction in total surface area and volume occurs just after the thionyl chloride reaction, which is believed to act as a dealuminating agent. Alternatively, this decrease may also be from the deposition of the non-porous magnesium hydroxide on the zeolite surface. Table 6.3 lists the surface areas and pore volumes for as received and modified SSZ-13 zeolite samples.

Table 6.3: Nitrogen adsorption results for the as-received and modified SSZ-13 zeolite

Sample	BET Surface Area (m^2/g)	Pore Volume (cm^3/g) [†]	Pore Volume Fraction (cm^3/cm^3) [‡]	Normalized t-Plot External Surface Area
As-received SSZ-13	831.9	0.3678	0.555	1.00
Thionyl chloride treated SSZ-13	741.7	0.3299	0.498	0.93
Grignard treated SSZ-13	650.3	0.3147	0.475	1.90

[†] Determined using the Horvath-Kawazoe (H-K) method (cylindrical pore). Similar pore volume is obtained using Density Functional Theory (DFT) modeled with oxide surfaces and cylindrical pores
[‡] Calculated from pore volume based on zeolite density; 1.51 g/cm^3 (SSZ-13)

The normalized t-Plot external surface area for TC SSZ-13 remains fairly similar to the as-received sample supporting microscopy analysis indicating no surface roughening.

Based on the results of t-Plot external surface area calculations of non-porous silica and plugged TC zeolite 4A (see Table 6.4) the t-Plot calculations (in the absence of the user defined adjustable parameter) overestimates the external surface areas of microporous solids, however, the t-Plot external surface area is not expected to vary significantly for multiple batches of the same microporous material (see section 3.3.3). After the reaction with the Grignard reagent, the normalized t-Plot external surface area of the GT SSZ-13 zeolite increases to twice the original value (as-received SSZ-13), supporting microscopy observations of increased surface roughness.

6.2.3.2.   *Analysis of As-received and Modified Zeolite 4A*

Considerably different results are seen for Grignard treatment of submicron zeolite 4A compared to the TC SSZ-13 and GT SSZ-13 samples (see Table 6.4). The BET surface area of the zeolite 4A decreases by over 90%, from 396.4 m^2/g to 32.4 m^2/g, after the thionyl chloride reaction and the pore volume is almost completely lost. The results indicate complete plugging of the pores. However, when the thionyl chloride reaction is followed by the reaction with the Grignard reagent, the pores appear unplugged.

It is possible that the unusual surface Si:Al ratio of three identified for the zeolite 4A used in this work may be a source of silica that is dissolved by the thionyl chloride. This dissolved silica could be redeposited into the pores of the zeolite when the reactants are evaporated. This hypothesis could be tested by filtering the zeolites after the thionyl chloride reaction mixture instead of evaporating the mixture. Alternatively, the TC 4A sample could be reacted with the Grignard reagent to determine if the plugging of the pores is a sample specific error related to processing.

Table 6.4: Nitrogen adsorption results for as-received and modified zeolite 4A

Sample	BET Surface Area (m^2/g)	Pore Volume $(cm^3/g)^{\dagger}$	Pore Volume Fraction $(cm^3/cm^3)^{\ddagger}$	Normalized T-plot External Surface Area
As-received zeolite 4A	396.39	0.1863	0.283	1.00
Thionyl chloride treated 4A	32.43	0.0208	0.032	0.39 (actual value of 34.7 m^2/g)
Grignard treated 4A - Batch 1	511.05	0.2553	0.388	1.89
Grignard treated 4A - Batch 2	537.01	0.2581	0.392	1.70
Grignard treated 4A - Batch 3	412.08	0.1967	0.299	1.31

[†] Determined using the Horvath-Kawazoe (H-K) method (cylindrical pore). Similar pore volume is obtained using Density Functional Theory (DFT) modeled with oxide surfaces and cylindrical pores
[‡] Calculated from pore volume based on zeolite 4A density of 1.52 g/cm^3

The normalized t-Plot external surface area for TC 4A is also seen to decrease to a value of 0.39, however, based on the earlier discussion (Section 6.2.3.1), the t-Plot calculated external area of 34.7 m^2/g appears reasonable in light of particle diameters of 100 – 200 nm for the zeolites. This conclusion is backed by the BET surface area of 32.4 m^2/g and pore volume of 0.0208 cm^3/g for TC 4A.

The normalized external surface area of the GT 4A samples increases to almost twice the original value for two out of three batches (batch 1 and batch 2). Further, when the thionyl chloride reaction is followed by the reaction with the Grignard reagent, the pore volume *increases by 38 percent compared to the as-received 4A* for two out of the three batches. This observation is explained by the results of Rozwadowski et al. [11] for water sorption in ion-exchanged zeolite 4A as discussed below.

The pore volume fraction of 0.283 cm^3/cm^3 for the as-received zeolite 4A, as determined by nitrogen adsorption, matches the water sorption results (0.284 cm^3/cm^3) of Rozwadowski et al. [11] for sodium-4A (Na-4A). Similarly, the pore volume fraction of Grignard treated zeolite 4A for two out of the three batches match the water sorption capacity of 0.396 cm^3/cm^3 (22 moles water per kg of zeolite) observed by Rozwadowski et al. for magnesium exchanged zeolite 4A (62.5 exchange %). These results, supported by infra-red spectroscopy (section 6.2.4), suggest that zeolite 4A is being ion-exchanged by the Grignard treatment resulting in the formation of magnesium exchanged zeolite 4A (Mg-Na-4A). It is expected that the results may alter the gas transport properties of the 4A zeolites (Na-4A) and complicate the modeling results. At this point, such an extensive study should be done with dense films and is beyond the scope of the current work.

Finally, the batch to batch variation (see Table 6.4) of the Grignard treatment is believed to be the result of variation in the quality of the Grignard reagent used, with older (> 1 month) reagent providing poor results. The results for Batch 3 indicate minor increase in BET surface area and pore volume leading to the hypothesis that the proposed magnesium ion exchange may not have taken place in that specific batch.

6.2.4. Infra-red Spectroscopy

Several structural characteristics of zeolites can be effectively probed with infra-red spectroscopy. Three regions are of interest, (1) vibration of cations in the far-IR range (200 – 50 cm^{-1}), (2) vibrations of zeolite frameworks in the 1250 – 300 cm^{-1} range, and (3) hydroxyl groups in the 3500 – 3800 cm^{-1} range. Additionally, alkylation of the zeolite surface by organic molecules could potentially be identified by typical C-H vibrations in the 2800 – 3000 cm^{-1} range.

An attempt was made to identify the presence of methyl groups on the Grignard modified zeolite surfaces using Attenuated Total Reflectance Infra-red spectroscopy (ATR-IR). Scans for SSZ-13, TC-SSZ-13 and GT-SSZ-13 are shown in Figure 6.4. No visible presence of methyl C-H vibrations in 2950 cm^{-1} region can be seen in the GT-SSZ-13 sample. Although, the absence of C-H vibration indicates the absence of methyl groups, further study is warranted. It should be noted that even with 100 % surface coverage (4 methyl groups per nm^2) of a 200 nm zeolite, the concentration of methyl groups would be only 1.3 mmols per gram of zeolite. Thus it is very possible that the signal of the C-H vibrations is overwhelmed by the response of the bulk zeolite. Although, infra-red studies were unable to detect the presence of methyl groups on the surface of the zeolite, FT-Raman spectroscopy may be more helpful where the C-H vibrations have a strong Raman signal [12].
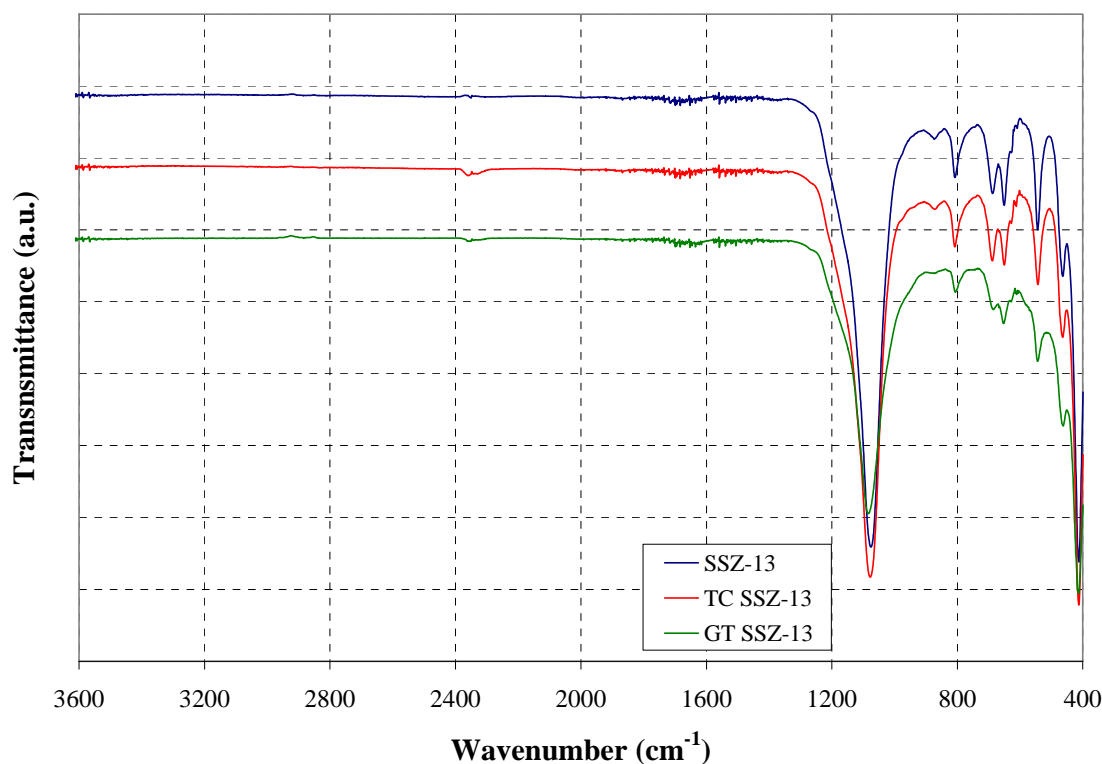
Figure 6.4: ATR-IR spectra of as-received SSZ-13, thionyl chloride only treated SSZ-13 and Grignard treated SSZ-13

Additionally, framework vibrations (T-O-T, T = Si or Al) have been used to identify structural changes in the zeolite including isomorphic substitution of framework silicon and aluminum [13]. The IR bands of typical zeolite framework vibrations are given in Table 6.5 [14].

Table 6.5. IR vibrational bands for typical zeolite frameworks [14]

Assignment	IR Band (cm^{-1})
Internal tetrahedra:	
Asymmetric stretch	1250 - 920
Symmetric stretch	720 - 650
T-O bend;	500 - 420
External linkages:	
Double ring vibrations	650 - 500
Pore opening vibrations	420 - 300
Asymmetric stretch	1150 - 1050
Symmetric stretch	820 - 750

When comparing the spectra for the Grignard and as-received zeolite 4A, a new peak is observed at 915 cm^{-1} in the Grignard treated sample (see Figure 6.5). This peak is absent from the infra-red scans of the as-received and thionyl chloride only treated zeolite 4A. Observations of new peaks in the asymmetric (1100 cm^{-1}) and symmetric (800 cm^{-1}) region have been attributed to perturbations in the zeolite framework vibrations arising from cation coordination changes in ion exchanged zeolites [15, 16]. The changes in cation coordination are believed to cause changes in the electron density around the AlO$_4$ tetrahedra, resulting in the weakening of the aluminum-oxygen bond [17]. Considered in conjunction with the nitrogen adsorption results, the peak at 915 cm^{-1} observed in Grignard treated 4A is evidence of magnesium exchange in the zeolite. Likewise, the

absence of this peak in the GT SSZ-13 sample can be explained by the much smaller ion-exchange capacity of the high Si:Al ratio in the SSZ-13 zeolite.
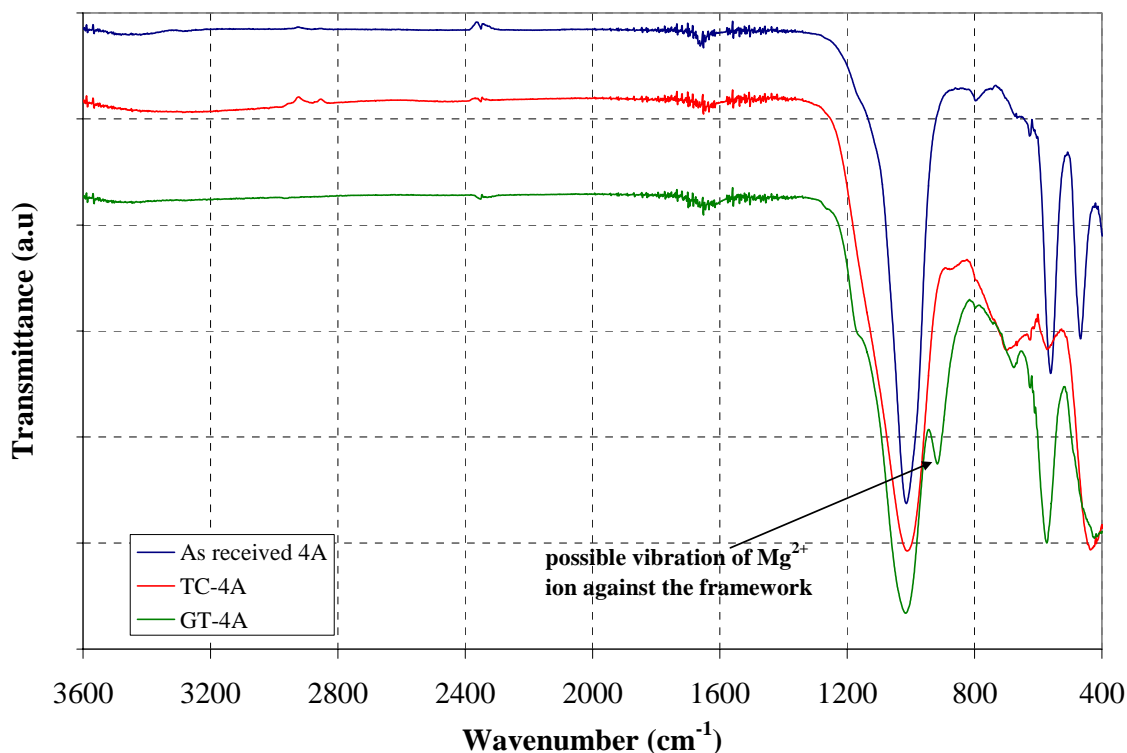
Figure 6.5: ATR-IR spectra of as-received, thionyl chloride only treated and Grignard treated zeolite 4A

Independent research concurrently being carried out on the alkylation of ZSM-5 zeolite surfaces using chlorination ($SiCl_4$) and Grignard reagent (C_4H_9MgCl) reports the presence of alkyl groups on the surface using Infra-red spectroscopy [18]. The authors also found high alkyl loading on zeolites with high Si:Al ratios (ZSM-5), while zeolites with low Si:Al ratios (zeolite Y) were prone to dealumination. Further, the authors also speculate that a magnesium ion exchange for zeolite Y may be the cause of the shift of the T-O-T vibration to lower wave numbers, similar to the observation made in Figure 6.5 above.

If true, the exchange of magnesium for sodium ions in zeolite 4A could cause deviation in the selectivities and permeability predicted by the Maxwell model (based on values for Na-4A) for the Grignard treated zeolite 4A mixed matrix membranes in Sections 5.4.2, and 5.4.3. Estimation of the actual permeabilities of the modified zeolites can be carried out by performing transient and equilibrium sorption measurements to obtain the diffusion and sorption coefficients as suggested by Moore [1] or by performing studies using polyvinyl acetate (PVAc) - GT 4A mixed matrix membranes and back-calculating the gas permeabilities for the modified zeolite using the Maxwell model.

6.2.5. Summary of Surface Modification Characterization

Based on the XPS, microscopy, nitrogen adsorption, infra-red spectroscopy and X-ray diffraction results, the following conclusions can be drawn about the surface modification of the zeolites used in this work:

Thionyl chloride primarily acts as a dealuminating agent in the reaction with the zeolites. The reaction, based on Feje's proposed pathway, results in the formation of hydroxyl nests on the surface of the zeolites and aluminum chloride as the side-product.

Under the reaction conditions used in this work, the Grignard reagent deposits magnesium hydroxide on the surface of the zeolites leading to a roughened surface. In the case of zeolite 4A, evidence suggests that the Grignard reagent ion exchanges the sodium ions with magnesium counter-ions via a yet to be proposed mechanism.

After the thionyl chloride step, aluminum chloride is believed to be deposited onto the surface of the zeolites in nano-crystalline form or as separate crystals dispersed with the zeolites. These crystals are difficult to image in the vacuum environment of the SEM, as the electron beam, over multiple scans, causes heating on the local scale resulting in the sublimation of the crystals (sublimation temperature 178 ºC). This fact can be used to

remove all aluminum chloride after the thionyl chloride reaction to test the effect of the aluminum chloride crystals on the nucleation of magnesium hydroxide.

Further, the presence of the magnesium hydroxide is hypothesized to play a primary role in the dispersion of the zeolite particles in the solvents used in fiber spinning. Before a discussion on the role of magnesium hydroxide in mixed matrix membrane formation is carried out, background on the stabilization of colloidal particles is provided. This background serves as framework within which the experimental observations of Grignard treated zeolites are rationalized.

6.3. STABILIZATION OF COLLOIDAL DISPERSIONS AND THE IMPORTANCE OF DISPERSION STABILITY IN HOLLOW FIBER SPINNING

6.3.1. Stabilization of Colloidal Dispersions

Aggregation of colloidal particles is driven by a group of attractive forces collectively listed as van der Waal forces. The forces are classified as dipole-dipole, dipole-induced dipole and dispersion (London) forces. These forces, being quantum mechanical in nature are ubiquitously present and generally prevalent over a range of 5-10 nm [19]. Therefore, any colloidal stabilization technique must be operative over this distance to be effective.

Two general stabilization techniques are available for colloidal dispersions; electrostatic and polymer stabilization. Electrostatic stabilization results from the formation of a charged double layer around a particle which provides columbic repulsion between the particles. The formation of such charged layers occur primarily through the adsorption of charged ions or the selective dissolution of ions from the particle surface. The thickness

117

of the double layer is a strong function of the ionic concentration of the dispersion and is described by the Debye length ($1/\kappa$). The Debye length is given by:

$$\frac{1}{\kappa} = \left[\frac{e^2}{\varepsilon_0 \varepsilon_r kT} \sum_i n_{0i} z_i^2 \right]^{-1/2}$$

(6.4)

where e is the charge on an electron, ε_0 is the permittivity in vacuum, ε_r is the relative permittivity (dielectric constant), k is the Boltzmann constant, n_{0i} is the ion concentration and z_i is the valency of the ion.

For nonaqueous systems of low dielectric constants, the concentration of ions within the dispersion is very low due to low solubility [20]. The low concentration of ions results in a very large diffused double layer that does not provide sufficient repulsion during particle collisions. Thus for the stability of the dispersion, the solvent must be sufficiently polar in nature to allow ionization of charged species to take place (some dissolution of ions) and for a double layer to form a steep potential decay around the particle. However, the concentration of ions within the dispersion should not be so high as to compress the double layer which could lead to the coagulation of the dispersion [20].

The second colloid stabilization method makes uses of polymers to maintain interparticular distances greater than 5 – 10 nm, over which the van der Waal forces are operative. Two types of polymeric stabilization of colloidal particles can be implemented. The first technique employing adsorbed or grafted polymer chains on the surface of the particle, relies on entropic constraints of overlapping polymer chains to

keep particles apart. Depletion stabilization, on the other hand, employs non-adsorbing polymer chains in solution which stabilize the dispersion via an excluded volume effect. Figure 6.6 shows schematic representations of steric and depletion stabilization. Details on colloidal stabilization techniques in aqueous and non-aqueous environments can be found in multiple sources [19, 21-24].

| Steric Stabilization | Depletion Stabilization |
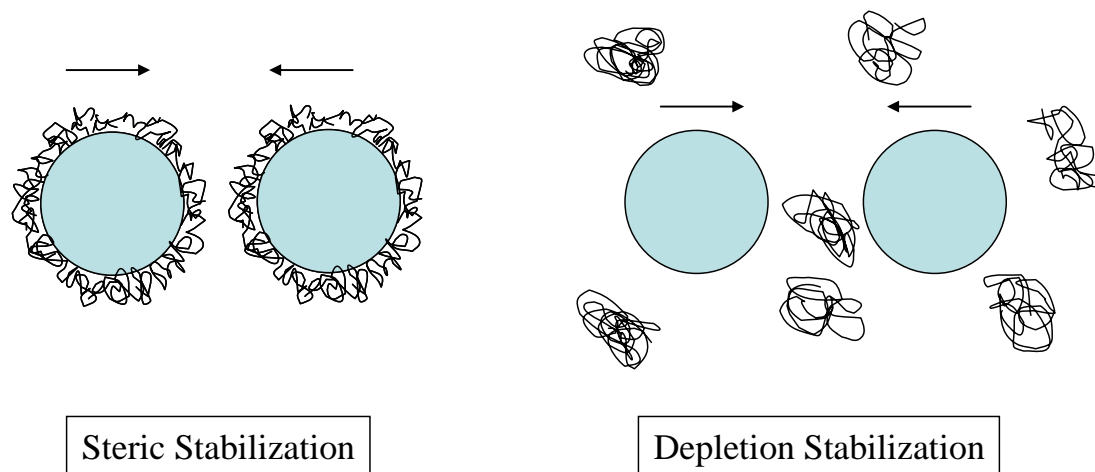
Figure 6.6: Schematic representation of steric and depletion stabilization using polymers [19]

The choice of the primary method for colloidal stabilization has up till recently been primarily dependent on the nature of the medium. Electrostatic stabilization has been almost exclusively used for aqueous systems, while polymeric stabilization has been employed in both aqueous and non-aqueous systems.

General perception that very low ionic concentrations exist in non-aqueous dispersion has restricted the use of electrostatic stabilization in such systems. That view is gradually changing, especially for dispersions of protic and aprotic organic solvents where charging of particles via an acid-base type interaction has been suggested [25, 26].

The charging mechanism for carbon particles in non-aqueous solvents has been proposed by Fowkes [27] to take place via three possible routes; (1) Adsorption of undissociated charged species, (2) dissociation of adsorbed molecules, and (3) desorption of anions into the solvent. Thus the possibility of electrostatically stabilized dispersion in non-aqueous, though highly polar solvents appears valid.

The following section provides a spinning process perspective on colloidal stability, which along with the background on colloidal stability is used to hypothesize the role of magnesium hydroxide deposited on the surface of the zeolites.

6.3.2. Dispersion Stability in Dope Processing

Formation of mixed matrix hollow fibers can be broadly segregated into three stages where the defects between the sieve/insert and polymer may be introduced in the upstream and propagated in downstream operations. Broadly, the steps in hollow fiber spinning can be divided into the dope preparation, fiber spinning and solvent exchange/post-treatment areas. The following section expands on the possible causes of sieve-polymer failure within each of the segments and hypothesizes the strongest contributing factors to poor mixed matrix performance.

6.3.2.1. Dope Preparation

As outlined in chapter 3, the dope preparation step provides the first indicator of molecular sieve/solvent/and polymer compatibility. It is essential that the sieve particles be well dispersed in the solvent before viscosity of the suspension is significantly increased by the addition of main portion of the polymer.

At higher particle loadings (greater than 10 - 15 volume %) the Grignard treated zeolite dispersions display gel-like behavior characteristic of electrostatically stabilized dispersions. This gel-like behavior is caused by the interaction between overlapping double layers around the particles [19]. As the diffuse layers are much larger in organic

solvents this implies that only a lower concentration of particles can be electrostatically stabilized within organic media compared to aqueous dispersions [28].

Aggregates that remain in the solvent-particle dispersion would then perpetuate though the remaining mixing and subsequent spinning process. This is especially true for submicron particles, where attractive interactions for non-stabilized particles exceed energy that is produced by stirring or thermal motion [29]. Table 6.6 list the energies in particulate systems based on particle size.

Table 6.6. Interaction energies of particles [29]

Interaction	Particle Size (micron)		
	0.1	1	10
van der Waals attraction	~ 10 kT	~ 10^2 kT	~ 10^3 kT
Electrostatic repulsion	0 - 10^2 kT	0 - 10^3 kT	0 - 10^4 kT
Thermal motion (Brownian)	1 kT	1 kT	1 kT
Kinetic energy:			
Sedimentation	10^{-13} kT	10^{-6} kT	10 kT
Stirring	~ 1 kT	~ 10^3 kT	~ 10^6 kT

k – Boltzmann Constant
T = temperature

Based on the values in Table 6.6, it is evident that submicron particles can not be separated by stirring. Sonication is very effective in dispersing the particles, however, a stabilization technique (electrostatic or polymeric) must be used to prevent agglomeration once sonication is stopped.

The presence of agglomerates can be extremely detrimental to the selectivity of the membrane. If an agglomerate traverses through the skin region of the fiber, the

agglomerate can provide percolation pathways for the gas molecules to move nonselectively through the membrane resulting in a loss of selectivity for the membrane. This defect is depicted in Figure 6.7.
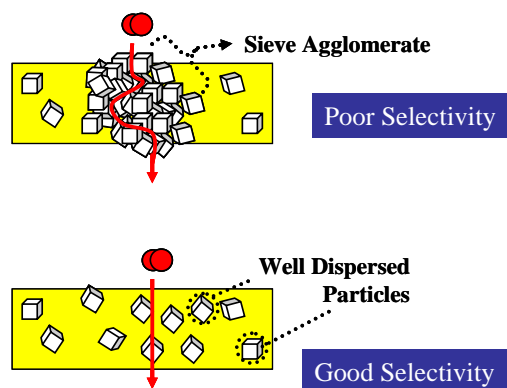
Figure 6.7: Effect of agglomerates on membrane selectivity [1]

Based on the interactions of the dope components it is believed that the mixed matrix dope can be probed rheologically to determine stability under shear and for the presence of particle aggregates [30]. Although, the rheology of the mixed matrix dope cannot be currently measured in situ, the analysis of the dope can be performed offline to determine the dope flow characteristics and effect of shear on particle aggregation and possible structure formation. This testing method was applied to multiple mixed matrix dopes to determine if final membrane performance could be predicted. The rheology of multiple dope samples was graciously tested by Ryan Collins in Dr. Breedveld's lab. The results are discussed in Appendix C.

6.3.2.2. Fiber Spinning

The spinning process subjects the mixed matrix dopes to high shear rates within the spinneret, elongational stresses in the air gap, and finally phase separation in the quench bath. Within the range of spinning parameters (spinning temperature, dope extrusion

rates, air gap and draw ratio), phase separation of the membrane is believed to be the strongest determinant of polymer-zeolite adhesion. As outlined earlier in chapter 4, attractive interactions between the zeolite and the solvents and nonsolvents within the dope and quench bath are found to be detrimental to good polymer-zeolite adhesion. Long term dope stability characterized by phase stability of the dope components is essential for good polymer-zeolite adhesion. This stability for a dope based on Grignard treated zeolites versus a dope based on Ultem® "sized" zeolites is shown is compared in Figure 6.8.

Dope based on Grignard treated SSZ-13

Dope based on Ultem® "sized" SSZ-13
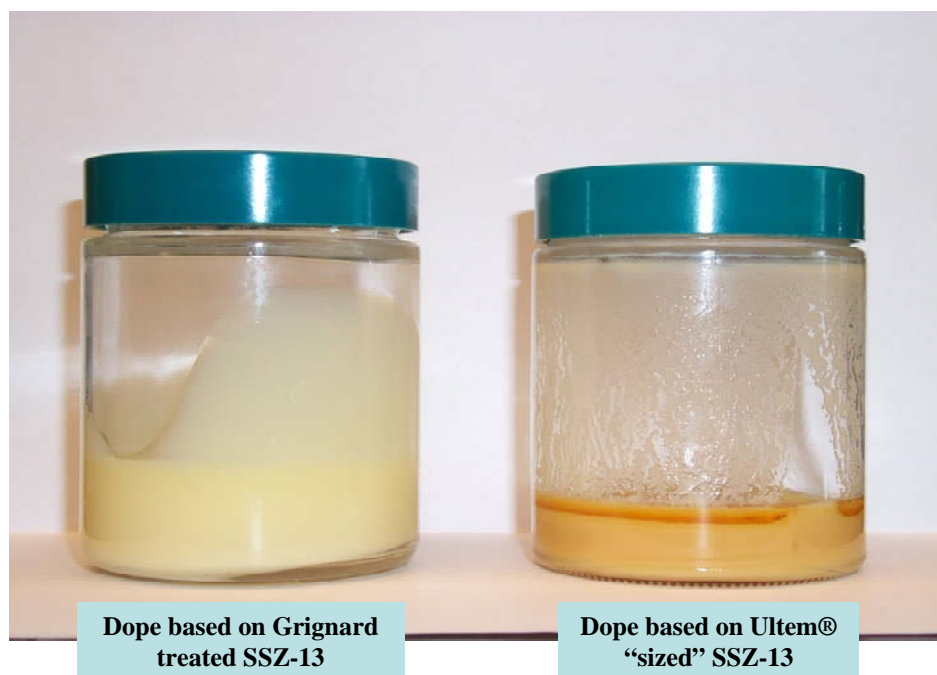
Figure 6.8: Comparison of long term dope stability of dope based on Grignard treated zeolites versus a dope based on Ultem® "sized" zeolites. Note the beading (phase separation) on the walls of the glass container for the dope based on Ultem® "sized" zeolites. The dopes are of comparable age and equivalent polymer (Ultem®) concentration.

6.3.2.3. *Solvent Exchange and Post-treatment*

The phase separation of the fiber "traps" the membrane morphology. Solvent exchange with strong polymer nonsolvents (methanol and hexane) is not believed to change the morphology or the polymer-zeolite interface. However, care must be taken not to dry the fibers at too high temperatures as defects in the delicate skin have been observed to form after heating at high temperatures [31].

With the framework of particle stability in dope processing in place, the following section addresses the role of magnesium hydroxide in the formation of excellent polymer-zeolite adhesion.

6.4. HYPOTHETICAL ROLE OF MAGNESIUM HYDROXIDE ON THE SURFACE OF THE ZEOLITE

Based on the earlier analysis of the structural and chemical changes on the zeolites surface, an asymmetric structure is envisioned for the Grignard treated zeolites. The large size of the reactant molecules (thionyl chloride and Grignard reagent) prevents the reaction from taking place in the bulk of the zeolite, however, exchange of sodium ions with magnesium ions in zeolite 4A appears to occur. Although the sorption capacity of the zeolite is changed after the ion-exchange, it is believed that the original zeolite porous structure is present under a layer of magnesium hydroxide crystals. This discussion is independent of the changes within the bulk of the zeolite and only concerns the surface characteristics. It is proposed that the presence of magnesium hydroxide overcomes two critical steps in the formation of mixed matrix membranes described in section 6.3.2.

The first step relates to particle stability in the dope solvent, N-methyl-2-pyrrolidione (NMP), where it is proposed that due to the presence of magnesium hydroxide on the particle surface, the dispersion is electrostatically stabilized. Magnesium hydroxide $(Mg(OH)_2)$is poorly soluble in water with a solubility of 1.2×10^{-4} mol/L at 25 ºC [32]. The low solubility of $Mg(OH)_2$ in water dispersions is believed to result in charging of

the zeolite particles and impart stability via electrostatic stabilization. Hunter [22] proposes the following equilibria at work at oxide surfaces leading to charging of the particles;

$$MO^- + H^+ \leftarrow M - OH \xrightarrow{\quad OH^- \quad} M - O^- + H_2O \qquad (6.5)$$
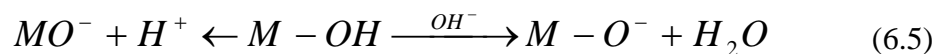
The solubility of salts in organic media is proposed to be a function of the dielectric constant, solvent size, viscosity and acid-base interactions [33, 34]. As the dielectric constant of NMP is 32.2 (dielectric constant of water = 78 at 25 ºC), reasonably high $Mg(OH)_2$ solubility, though less than that in water, is postulated. Additionally, during the dispersion process, water adsorption by NMP is expected to aid the dissolution of the salt. The presence of these ions could provide a similar, though more diffuse, double layer around the Grignard treated zeolites in NMP.

The charging of the particles and thus the stability of the dispersion can be measured by the Zeta potential of the system. The Zeta potential measures the electrostatic potential at or very near the start of the diffuse double layer [35]. The Zeta potential of the Grignard treated zeolites were measured by a colleague, Shu Shu, and found to have very high values indicating the formation of stable dispersions in NMP. These data are presented in Table 6.7.

In the second step, the presence of magnesium hydroxide on the zeolite surface is proposed as the cause for the excellent polymer-zeolite adhesion observed in Chapter 5. Two base hypotheses, one relating to enthalpy as an acid-base type interaction, and the other entropic based on the surface roughness, can be formulated.

Table 6.7: Zeta potential of unmodified and Grignard treated zeolite 4A in NMP. Measured at 25 ºC. [7]

Zeolite	Zeta Potential in N-methyl-2-pyrrolidione
Zeolite 4A	-30
Thionyl chloride only treated zeolite 4A	-17.5
Grignard treated (including thionyl chloride) zeolite 4A	127
Grignard treated (including thionyl chloride) zeolite 4A (calcined at 400 ºC in synthetic air)	134.5

6.4.1. Gibbs Free Energy

The combination of the enthalpic and entropic terms as described by the Gibb free energy form the basis of addressing dispersion behavior [10]. The Gibbs free energy is defined as:

$$\Delta G = \Delta H - T\Delta S \qquad (6.6)$$

Where ΔH is the enthalpic component based on the change in molecular interactions and ΔS comprises any entropic element which accounts for the change in number of possible configurations of the molecule from one state to another. When applied to the polymer/solvent/zeolite system, the enthalpic term is based on polymer-solvent, polymer-zeolite and solvent-zeolite interactions. The entropic term primarily captures the possible configurational states of the polymer molecule.

For adhesion between the polymer and particle, the change in free energy of the polymer-zeolite adhesion must be negative. As the adsorption of polymer on the zeolite surface reduces the number of possible configurations the polymer coil can have, the change in

entropy for the polymer chain is always somewhat negative. This value, however, is partially offset by the gain in entropy from the freeing solvent molecules [36]. Thus the change in enthalpy of polymer-particle adhesion (governed by the polymer-zeolite, zeolite-solvent, and polymer-solvent interactions) must therefore always be negative (exothermic) for adhesion to take place. The following section expands on enthalpic and entropic contributions for adhesion to take place between the polymer and particle.

6.4.2. Enthalpic Considerations in Adsorption of Polymer on the Zeolite Surface

The effect on adsorption of a basic polymer on acidic surfaces from acidic, neutral and basic solvents has been studied earlier by Fowkes [37]. Fowkes found that a basic polymer adsorbed most strongly on an acidic silica surface from a neutral solvent while acidic and basic solvents reduced polymer adsorption by their strong interactions with the polymer and silica surface, respectively. Base on this conclusion, Mahajan [38] and Moore [1] suggested that acid-base type interactions in the polymer/solvent/zeolite system may have a greater role in determining polymer adsorption on the zeolite surface in mixed matrix membrane formation than previously considered. Figure 6.9 shows a schematic of the variation in the quantity of polymer adsorbed on an acidic surface based as a function of the acidic/basiccharacter of the solvent.
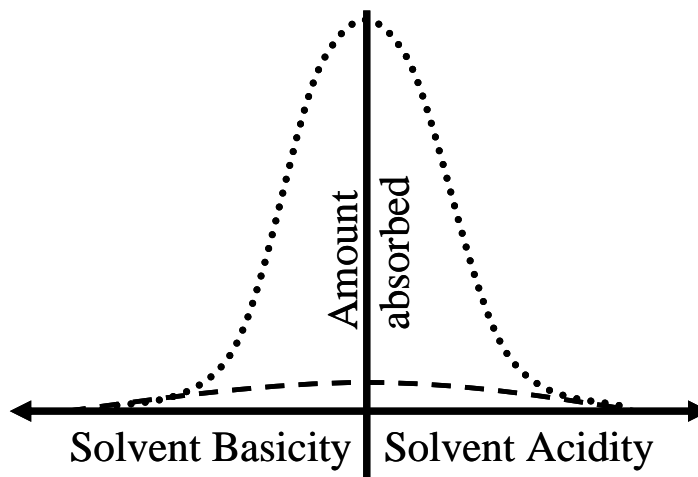
Figure 6.9: Amount of polymer adsorbed onto an acidic surface as a function of the solvent character: acidic polymer (---), basic polymer (...) [1]

6.4.3. Role of Zeolite Acidity in Mixed Matrix Membranes Formation

Evidence suggesting the effect of zeolite acidity (considering both number of acid sites and acid strength) on difficulty in forming good zeolite-Ultem® interfaces was observed in this work. It is hypothesized that a more acidic molecular sieve surface has more favorable interaction with the basic solvent (NMP). Polymer-zeolite adhesion is then hypothesized to be inversely proportional to the strength of the solvent-zeolite interactions, since these interactions must be overcome to achieve a well adsorbed polymer on the sieve surface.

The above hypothesis, developed by the author, rests on an earlier hypothesis developed by Mahajan [39]. Mahajan argued that better polymer-zeolite adhesion could be obtained by reducing the zeolites-solvent interaction strength. Attempts were made by both Mahajan and Moore [1] to increase polymer adsorption on the zeolites surface by decreasing the solvency power of the solvent in a polymer, solvent and zeolite dispersion. Unfortunately, these attempts resulted in particle agglomerates that were difficult to redisperse in solvent. In this work, it is believed that, the same goal has been

successfully achieved by an alternative route of modifying the surface of the zeolites to decrease interaction with the solvent and non-solvents (hereafter included with solvents) present in the dope.

Three zeolites are considered in this analysis.

- Zeolite 4A – High number of acid sites

- SSZ-13 – Intermediate number of acid sites

- SAPO-34 – Low number of acid sites

Earlier work was unsuccessful in incorporating native zeolite 4A and SSZ-13 in Ultem® matrices [40, 41]. Silanation and polymer sizing of the zeolite were attempted next with limited success [1]. In this work, the zeolite surface is modified using thionyl chloride followed by a Grignard reagent. This surface modification has produced excellent zeolite-polymer interfaces and the resultant mixed matrix effect in both asymmetric hollow fiber membranes and dense films.

The Grignard treatment process developed in this work is believed to decrease the acidity (acid strength) of the zeolite surface through the deposition of magnesium hydroxide. This conclusion is supported by the results of Hu et al. who concluded that a reduction in the surface acidity of HZSM-5 takes place after magnesium hydroxide deposition on the surface of the zeolite [42].

The number of acid sites of the zeolites can be characterized as zeolite 4A > SSZ-13 > SAPO-34, while the acid strength of SAPO-34 is reported to be less than that of SSZ-13 [43]. It is believed that internal acidic nature of the molecular sieve can be translated to surface acidity as well. Ultem®-Ultem® hollow fiber membranes incorporating unmodified SAPO-34 were spun to test the hypothesis of reduced zeolite-NMP

interactions via reduced acidity of the zeolite. A SEM microphotograph of SAPO-34 molecular sieves is shown in Figure 6.10.

| Mag = 15.00 K X | 1μm | EHT = 10.00 kV WD = 5 mm | Signal A = InLens Photo No. = 9381 | Date :25 May 2006 Time :1:06:20 |
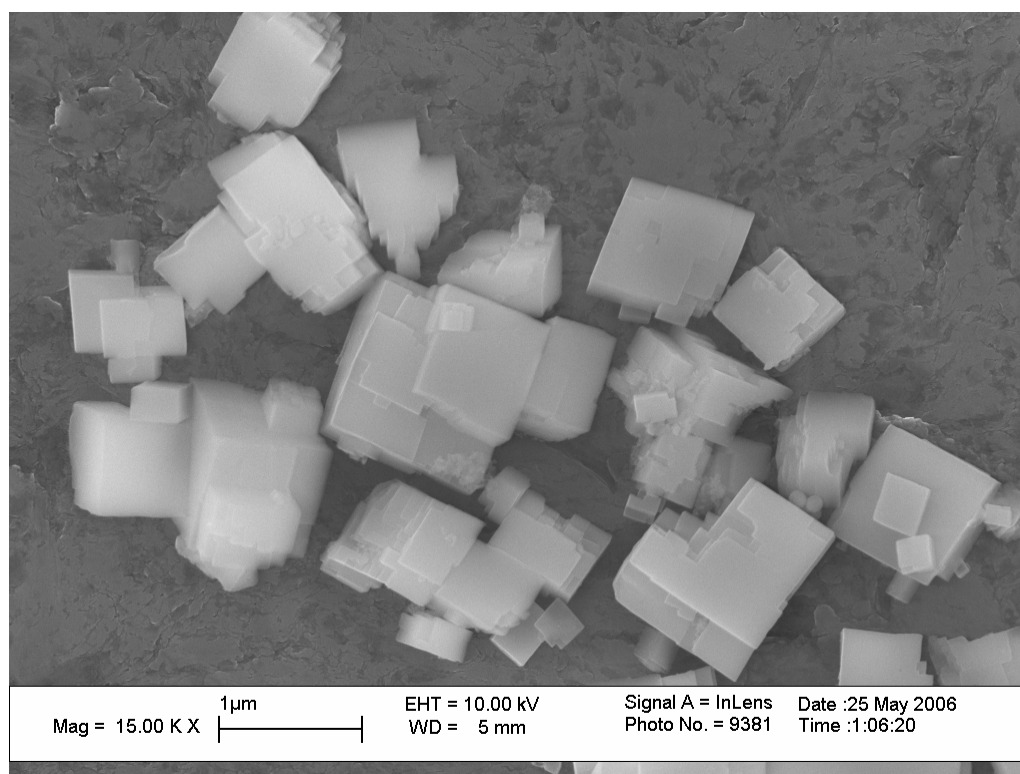
Figure 6.10: SEM microphotograph of SAPO-34 silicoaluminophosphate

The SAPO-34 sieves were spun in an Ultem®-Ultem® dual layer hollow fiber membrane. Preliminary results indicate excellent polymer-sieve adhesion as shown in SEM micrographs in Figure 6.11.
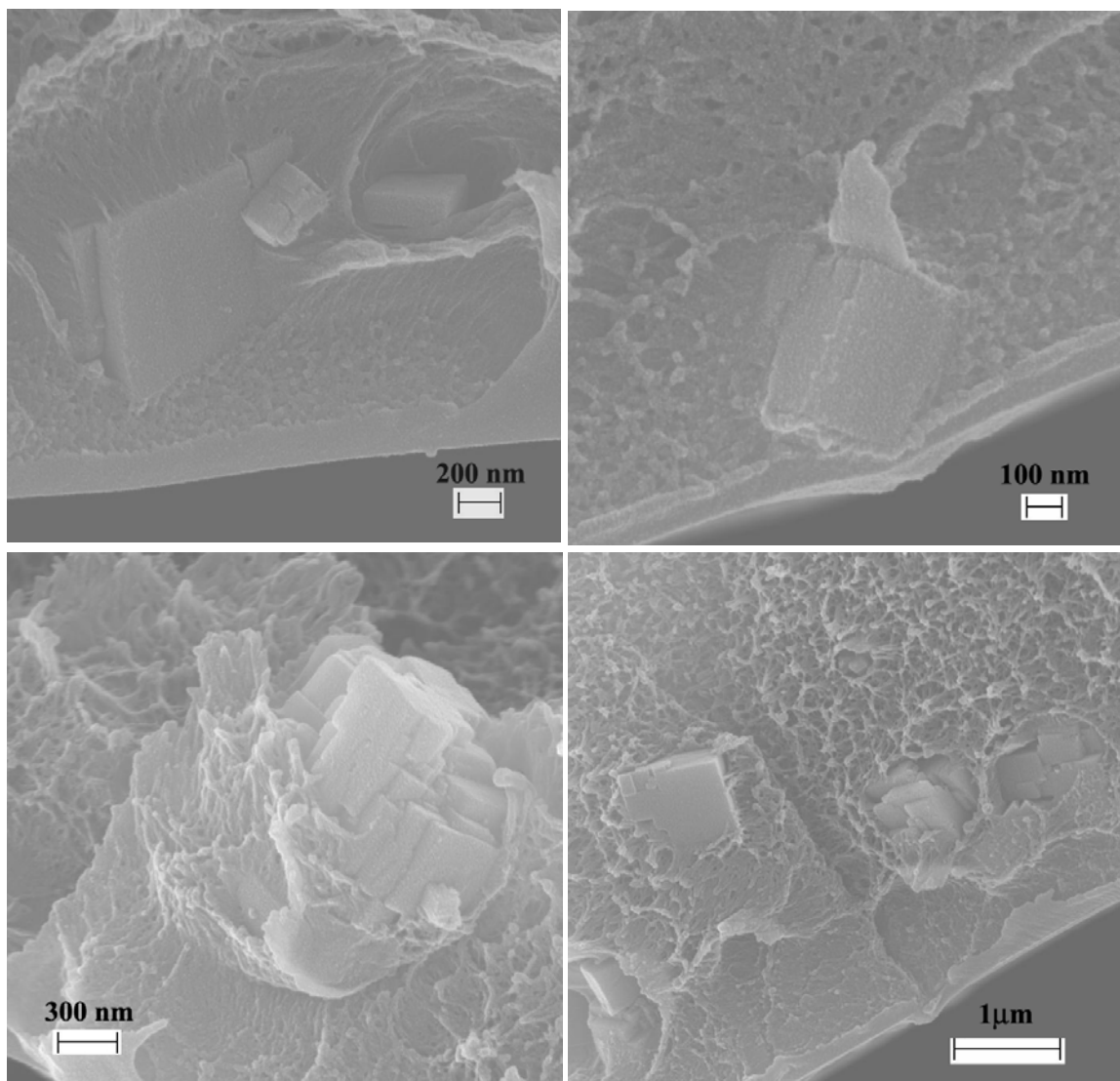
Figure 6.11: SEM microphotographs of Ultem®-Ultem® mixed matrix hollow fiber membranes incorporating SAPO-34 molecular sieve

As can be seen from the micrographs in Figure 6.11, excellent polymer zeolite adhesion is apparently observed at the smooth zeolite surfaces suggesting the importance enthalpic considerations in Ultem®/NMP based polymer/solvent system. However, it must be noted that the ultimate characterization of adhesion is via permeation characterization of the mixed matrix fibers. Due to the scarcity of the SAPO-34 sieve, further work could

not be pursued, however, based on above preliminary results, the sieve appears to be an excellent candidate as a mixed matrix material in Ultem® based polymer matrix.

6.4.4. Entropic Considerations in Adsorption of Polymer on the Zeolite Surface

A complementary hypothesis suggested by a colleague, Shu Shu [7], proposes that the polymer-zeolite adhesion observed in Grignard treated zeolite-polymer composites is encouraged by the entanglement of polymer chains with the surface roughened features of the zeolite. The claim is made that the roughened features, envisioned as "whiskers" allow polymer chains to coil on the surface in a lower entropic state as compared to loops and trains formed on a flat surface. The conclusion is provided that the lower change in entropy of the polymer adsorbed on the roughened surface (ΔS_1) versus the smooth surface (ΔS_2) results in an increase polymer-zeolite adhesion. Figure 6.12 depicts a schematic of the proposed hypothesis.

Random coil in solution or melt

Proposed magnesium
hydroxide "whiskers"

Polymer chain

$\Delta S_1 < 0$

$\Delta S_2 < 0$

Grignard treated zeolite surface

Flat native zeolite surface

$$|\Delta S_1| < |\Delta S_2|$$
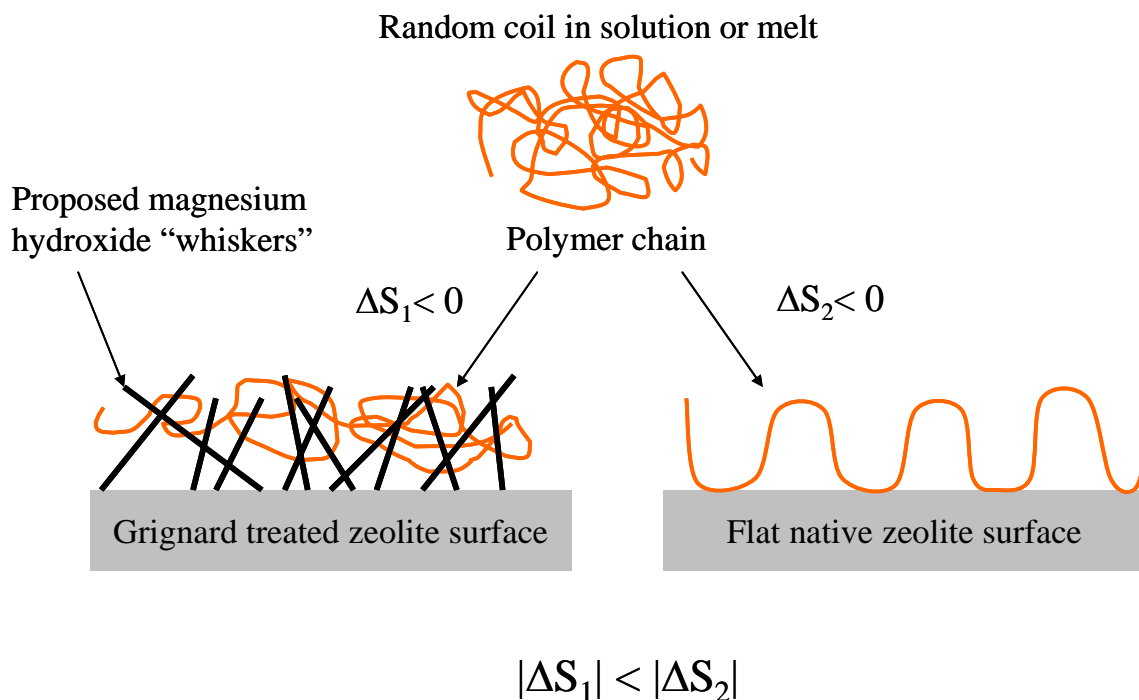
Figure 6.12: Proposed mechanism of enhanced polymer-zeolite adhesion based on entropic considerations [10]

In reality, beyond simple "entanglement" effects, other entropic issues may be a factor as well. For instance, displacement of adsorbed solvent molecules by adsorbed segments could affect the change in entropy and thus contribute to the adhesion of the polymer and insert.

Although the SAPO-34 results suggest the dominant role of enthalpic contributions in the Ultem/NMP/SAPO-34 system, both enthaplic and entropic contributions are likely to be of importance in determining adhesion between polymer and insert (zeolite, molecular sieve or silica).

6.5. CONCLUSIONS

The Grignard treated zeolites are characterized using XPS, SEM microscopy, nitrogen adsorption, and infra-red spectroscopy. An asymmetric zeolite consisting of the original zeolite core and deposits of magnesium hydroxide on the surface is believed to form. The Grignard treatment increases the external surface area of the zeolites corresponding to an increased roughness of the surface that is evident from microscopy and nitrogen adsorption experiments. Ion exchange of magnesium in zeolite 4A is speculated and an increase in pore volume of the zeolite is observed. This increase in pore volume may be beneficial in increasing the gas permeabilities of the zeolite, however, the resultant effect on selectivity needs to be explored.

Magnesium hydroxide is proposed to aid electrostatic stabilization of the particles in organic solvents via a dissolution based charging effect. The concept of using a low solubility salt to induce charging of the particle for better stability in aqueous and non-aqueous media appears to be another unique application of the Grignard treated zeolites developed in this work.

The two mechanisms for the increased enhancement between the polymer and modified zeolite are hypothesized to be of, (1) enthalpic, (2) entropic consideration. It is believed that a reduction in acidity of the zeolites occurs due to the surface deposition of magnesium hydroxide, resulting in reduced acid-base type interaction between the zeolite and solvent/nonsolvent. This observation suggests that enthalpic considerations are important in determining adhesion, a conclusion that is supported by the apparent excellent adhesion observed with unmodified SAPO-34 and Ultem®.

Further study is warranted with multiple polymer/solvent /insert systems to determine the subtleties of the adhesion mechanism and determine methods of weighting the effect of either of the two arguments in a particular system. Thus it may be possible to engineer systems where the correct choice of solvent may increase adhesion or a surface roughening of the insert may be required.

The results presented in this work suggest that the acidity of the zeolite is an important factor in determining polymer-zeolite adhesion in *basic organic solvent* (e.g. NMP) systems. As most engineering polymers used for membrane formation dissolve in few environmentally benign solvents, the choice of available solvents is severely restricted. Additionally, changing the solvent of a membrane system is not an easy task and would involve redesigning the process. This obstacle could then be pursued by modifying the insert surface to tailor enthalpic interations and by introducing surface roughness on the insert to improve adhesion via entropic effects. Thus both enthalpic and entropic effects could be used in conjunction to enhance polymer-insert adhesion.

6.6. ACKNOWLEDGEMENTS

6.7. REFERENCES

1.   Moore, T.T., *Effects of materials, processing, and operating conditions on the morphology and gas transport properties of mixed matrix membranes*. 2004. p. 311 pp.

2.   Fejes, P., I. Kiricsi, I. Hannus, A. Kiss, and G. Schobel, *A novel method for the dealumination of zeolites.* Reaction Kinetics and Catalysis Letters, 1980. **14**(4): p. 481-8.

3.   Young, D.A., *Treatment of aluminosilicate*. 1972: Application: US. p. 13 pp.

4.   Saxton, R.J., G.L. Crocco, and J.G. Zajacek. 1996: US Patent.

5.   Doktycz, S.J. and K.S. Suslick, *Interparticle collisions driven by ultrasound.* Science (Washington, DC, United States), 1990. **247**(4946): p. 1067-9.

6.   Hillock, A.W.M., *Personal Communication*. 2005.

7.   Shu, S., *Personal Communication*. 2006.

8.   Breck, D.W., *Zeolite Molecular Sieves: Structure, Chemistry, and Use*. 1974, Malabar, FL: Robert E. Krieger Publishing Co, Inc. 771.

9.   Sokol, A.A., C.R.A. Catlow, J.M. Garces, and A. Kuperman, *Transformation of hydroxyl nests in microporous aluminosilicates upon annealing.* Journal of Physics: Condensed Matter, 2004. **16**(27): p. S2781-S2794.

10.   Shu, S., S. Husain, and W.J. Koros. *Formation of Nano-scale Morphology on Zeolite Surfaces for Enhanced Interfacial Interaction in Mixed Matrix Membranes*. in *North American Membrane Society*. 2006. Chicago.

11.   Rozwadowski, M., R. Wojsz, K.E. Wisniewski, and J. Kornatowski, *Description of adsorption equilibrium on type A zeolites with use of the Polanyi-Dubinin potential theory.* Zeolites, 1989. **9**(6): p. 503-508.

12.   McKittrick, M.W. and C.W. Jones, *Toward Single-Site Functional Materials-Preparation of Amine-Functionalized Surfaces Exhibiting Site-Isolated Behavior.* Chemistry of Materials, 2003. **15**(5): p. 1132-1139.

13.   Perego, G., G. Bellussi, C. Corno, M. Taramasso, F. Buonomo, and A. Esposito, *Titanium-silicalite: a novel derivative in the pentasil family.* Studies in Surface Science and Catalysis, 1986. **28**(New Dev. Zeolite Sci. Technol.): p. 129-36.

14.   Karge, H.G., *Characterization by IR Spectroscopy*, in *Verified Syntheses of Zeolite Materials*, H. Robson, Editor. 2001, Elsevier Science B.V.: Amsterdam.

15.	Sarkany, J. and W.M.H. Sachtler, *Redox chemistry of Cu/NaZSM-5: Detection of cuprous ions by FTIR.* Zeolites, 1994. **14**(1): p. 7-11.

16.	Sponer, J.E., Z. Sobalik, J. Leszczynski, and B. Wichterlova, *Effect of Metal Coordination on the Charge Distribution over the Cation Binding Sites of Zeolites. A Combined Experimental and Theoretical Study.* Journal of Physical Chemistry B, 2001. **105**(35): p. 8285-8290.

17.	Koningsberger, D.C. and J.T. Miller, *Withdrawal of electron density by cations from framework aluminum in Y zeolite determined by Al XAFS spectroscopy.* Studies in Surface Science and Catalysis, 1995. **97**(Zeolites: A Refined Tool for Designing Catalytic Sites): p. 125-31.

18.	Vassylyev, O., G.S. Hall, and J.G. Khinast, *Modification of zeolite surfaces by Grignard reagent.* Journal of Porous Materials, 2006. **13**(1): p. 5-11.

19.	Napper, D.H., *Polymeric Stabilization of Colloidal Dispersions.* 1983. 428 pp.

20.	Raj, P.M. and W.R. Cannon, *Electrosteric stabilization mechanisms in nonaqueous high solids loading dispersions.* Surfactant Science Series, 2002. **104**(Polymers in Particulate Systems): p. 27-61.

21.	Overbeek, J.T.G., *Recent developments in the understanding of colloid stability.* Journal of Colloid and Interface Science, 1977. **58**(2): p. 408-422.

22.	Hunter, R.J., *Foundations of Colloid Science, Vol. 1.* 1986. 600 pp.

23.	Piirma, I., *Polymeric Surfactants.* Surfactant Science Series. Vol. 42. 1992, New York, NY: Marcel Dekker, Inc. 289 pp.

24.	Hackley, V.A., P. Somasundaran, J.A. Lewis, and Editors, *Polymers in Particulate Systems: Properties and Applications. [In: Surfactant Sci. Ser., 2002; 104].* 2002. 367 pp.

25.	Labib, M.E., *The origin of the surface charge on particles suspended in organic liquids.* Colloids and Surfaces, 1988. **29**(3): p. 293-304.

26.	Lyklema, J., *Principles of the stability of lyophobic colloidal dispersions in nonaqueous media.* Advances in Colloid and Interface Science, 1968. **2**(2): p. 65-114.

27.	Pugh, R.J., T. Matsunaga, and F.M. Fowkes, *The dispersibility and stability of carbon black in media of low dielectric constant. 1. Electrostatic and steric contributions to colloidal stability.* Colloids and Surfaces, 1983. **7**(3): p. 183-207.

28.	Albers, W. and J.T.G. Overbeek, *Stability of emulsions of water in oil. II. Charge as a factor of stabilization against flocculation.* Journal of Colloid Science, 1959. **14**: p. 510-18.

29. Somasundaran, P. and Editor, *Fine Particles Processing, Vol. 2. [Proceedings of an International Symposium, Las Vegas, Nevada, February 24-28, 1980]*. 1980. 921 pp.

30. Bicerano, J., J.F. Douglas, and D.A. Brune, *Model for the viscosity of particle dispersions.* Journal of Macromolecular Science, Reviews in Macromolecular Chemistry and Physics, 1999. **C39**(4): p. 561-642.

31. Wallace, D.W., *Crosslinked hollow fiber membranes for natural gas purification and their manufacture from novel polymers*, in *Chemical Engineering*. 2004, University of Texas--Austin. p. 221 pp.

32. Skoog, D.A., D.M. West, and F.J. Holler, *Fundamentals of Analytical Chemistry. 7th Ed*. 1996. 870 pp.

33. Takei, T., *Properties of non-aqueous solvents: solubility and conductivity of solutions.* Surface and Coatings Technology, 1988. **35**(1-2): p. 57-67.

34. Kim, S.-J., O.D. Bonner, and D.-S. Shin, *Solvent-solute interactions in dimethyl sulfoxide.* Journal of Chemical Thermodynamics, 1971. **3**(4): p. 411-17.

35. Hunter, R.J. and Editor, *Colloid Science: Zeta Potential in Colloid Science: Principles and Applications*. 1981. 386 pp.

36. Myers, D., *Surfaces, Interfaces, and Colloids: Principles and Applications*. 1991. 433 pp.

37. Fowkes, F.M. and M.A. Mostafa, *Acid-base interactions in polymer adsorption.* Ind. Eng. Chem. Prod. Res. Dev., 1978. **17**(1): p. 3-7.

38. Mahajan, R., *Formation, characterization and modeling of mixed matrix membrane materials*, in *Department of Chemical Engineering*. 2000, University of Texas at Austin: Austin, TX. p. 230.

39. Mahajan, R. and W.J. Koros, *Factors Controlling Successful Formation of Mixed-Matrix Gas Separation Materials.* Ind. Eng. Chem. Res., 2000. **39**(8): p. 2692-2696.

40. Duval, J.M., A.J.B. Kemperman, B. Folkers, M.H.V. Mulder, G. Desgrandchamps, and C.A. Smolders, *Preparation of zeolite filled glassy polymer membranes.* Journal of Applied Polymer Science, 1994. **54**(4): p. 409-18.

41. Moore, T.T., *Personal Communication*. 2001.

42. Hu, Z., W. Lihui, S. Chen, J. Dong, and S. Peng, *External modification of zeolite by metal surfactant for methanol amination.* Microporous and Mesoporous Materials, 1998. **21**(1-3): p. 7-12.

43.   Bordiga, S., L. Regli, D. Cocina, C. Lamberti, M. Bjorgen, and K.P. Lillerud, *Assessing the Acidity of High Silica Chabazite H-SSZ-13 by FTIR Using CO as Molecular Probe: Comparison with H-SAPO-34.* Journal of Physical Chemistry B, 2005. **109**(7): p. 2779-2784.

CHAPTER 7

MACROVOIDS IN MIXED MATRIX HOLLOW FIBER MEMBRANES

7.1. OVERVIEW

Large, characteristically tear or finger shaped voids found in polymer hollow fiber membranes, termed macrovoids, have been known since the early development of asymmetric membranes. These voids are undesirable as they decrease the mechanical integrity of the hollow fiber membrane, restricting membrane usage with high pressure feeds. With current membrane technology moving towards a mixed matrix format with inorganic and carbon molecular sieves embedded in a polymer matrix, the presence of macrovoids must be viewed in light of additional complications caused by the spinning of the mixed matrix dopes. While numerous hypotheses have been suggested regarding the formation of macrovoids formed in polymer-only membranes [1-5], no mention so far has been made of such macrovoids initiated in hollow fiber membranes by particles embedded in the polymer matrix. This chapter provides evidence for the presence of such macrovoids and presents a hypothesis for their formation in terms of a similar basic mechanism for macrovoid formation in mixed matrix membranes as that for conventional polymer-only asymmetric membranes. Additional suggestions on macrovoids formation caused by the presence of the particles are discussed. Consistent with observations for fiber spinning in the absence of particles, macrovoids are found to be suppressed by increasing fiber draw ratio. Moreover, decreasing the sieve particle size tends to suppress macrovoid formation tendency for a fixed particle size range.

7.2.   THEORETICAL BACKGROUND

Asymmetric membranes made via a phase separation process often suffer from long tear or finger shaped voids, termed macrovoids across the thickness of the membrane. These voids decrease the mechanical strength of the membrane and make the membrane susceptible to failure at high pressures differentials. As pressure differential or the chemical potential difference across the membrane is the driving force for gas separation, great incentive exists to design membranes to withstand high transmembrane pressure differentials.

Asymmetric membranes formed using phase separation in a single step process result in a gradient in porosity of the membrane characterizing its asymmetric nature. Although composite membranes using multilayer stacking of different porosity membranes have been used, the simplicity of the phase separation process and especially the applicability of the process to the formation of hollow fibers has led to its general acceptance. Yet the phase separation process and the subsequently formed membrane morphology are dependent on a wide number and range of factors, most of which have having strong interdependencies, leading to seemingly conflicting results being reported for multiple polymer/solvent/coagulant systems in the open literature. An example is the opposite effects of the air gap on macrovoid formation in polyethersulfone reported by Chung [6] and that reported by Ekiner [7] for polyaramide based dope. Chung found that macrovoids were suppressed at higher air gaps while Ekiner reported the suppression of macrovoids at lower air gaps.

The conflicting results are not unique to the effect of air gaps on macrovoid formation. Examples of seemingly contradictory results can be found, especially on the formation mechanisms and suppression of macrovoids in multiple polymer/solvent/coagulant systems [4, 5]. As of yet, no unified theory of macrovoid formation exists, however, some mechanisms are more suited to the particular membrane formation process.

The diverse solutions suggested for macrovoid suppression have met with considerable success in their respective systems, however, they also indicate that the macrovoid suppression methods suggested can be specific to a polymer/solvent/nonsolvent system [8]. Until a general model on macrovoid formation and suppression can be established, the collective knowledge on macrovoid formation and suppression can be used by trial and error to optimize the morphology of a new polymer/solvent/nonsolvent system.

7.2.1. Macrovoid Formation

The macrovoids have been shown to relate to the phase separation kinetics of the nascent membrane [9], so the many factors that determine the kinetics of phase separation also affect macrovoids formation. Significant work has been performed by Frommer [10], Strathmann [9], Kesting [3, 11] and Smolders [4] in trying to understand the formation of macrovoids in asymmetric hollow fiber membranes made via the wet and dry/wet spinning processes. Earlier work by Frommer suggested that the driving force for the solvent/coagulant mixing was osmotic pressure and control of membrane porosity could be achieved by changing rate of phase separation within the coagulating membrane. This control was demonstrated by reducing the osmotic pressure driving force by Frommer [12] using an aqueous salt quench bath with reduced water activity. Strathmann [9] using the same principles, showed a suppression in macrovoid formation by incorporating increasing concentrations of solvent within the coagulation bath. Kesting [3] suggested that macrovoid suppression was a function of the polymer solution's nonsolvent tolerance, with dope compositions close to the binodal resulting in less dense macrovoid free membrane morphologies.

These observations linking phase separation kinetics to membrane morphology invigorated research in determining a mass transfer model for the formation of asymmetric membranes. Cohen [13] and later Reuvers [14] were among the first to present a mass transfer model for the formation of asymmetric membranes which laid the

foundation for Smolders to propose that macrovoids were formed from the ingress of solvent and non-solvent into a nucleus of polymer lean phase driven by osmotic pressure. The osmotic force was believed to draw solvent (from the bulk dope) and non-solvent (from the coagulation bath) into a nucleus causing the nucleus to expand as long as the walls did not vitrify. Mckelvey [15] used this analysis as a basis to explain the tear shaped structure of macrovoids as being a result of non-uniform plasticity of the expanding nucleus driven by osmotic pressure forces as high as 750 bar for a polyethersulfone/ N-methyl-2-pyrrolidione/water system.

7.2.2. Macrovoid Suppression

7.2.2.1. Macrovoid Suppression Through Dope Additives

Kesting [3] showed macrovoids in polysulfone hollow fibers could be suppressed by the use of additives that formed a Lewis acid: Lewis base complex with the solvent. He argued that the complex formation allowed additional nonsolvent to be incorporated into the dope mixture which was "released" when the coagulant entered the membrane. This action promoted rapid phase separation in the quench bath. Earlier work by Cabasso [2], later followed by Boom [16], with water soluble polymeric additives forming miscible mixtures with polysulfone showed a similar suppression of macrovoids and a highly porous membrane structure. Likewise, Bloch [17] was able to suppress macrovoids in cellulose acetate by using a solvent with reduced miscibility with the coagulating nonsolvent.

A number of varied methods have been proposed to suppress macrovoids by addressing multiple factors believed to lead to the formation of macrovoids. These factors include the use of additive water-soluble polymer, polyvinylpyrrolidine, and increase in evaporation prior to immersion in the coagulation bath. In general, macrovoid formation occurs when rapid ingress of nonsolvent, driven by high osmotic pressure, occurs within the membrane coupled with low viscosity of the dope at one of the boundaries of the

phase separated nucleus. Fortunately the predominant factor/s in the formation of macrovoids for a particular polymer/solvent/additive system can be identified and suppressed using one or a combination of methods described in the literature.

The addition of nonsolvents to the dope mixture brings the dope composition closer to the binodal and phase separation is initiated rapidly upon immersion of the membrane in the coagulation bath. The objective is to drive phase separation of the membrane into the spinodal region and to form a bi-continuous structure; so nuclei do not have the opportunity to grow once initiated. The typical compositional changes of nascent fiber are plotted schematically in a ternary phase diagram of polymer/solvent/nonsolvent system shown in Figure 7.1. Starting from a dope composition at point 1 in the diagram, skin formation is believed to take place without phase separation in the air gap through the evaporation of volatiles at an arbitrary composition point 2 closer to the vitrified zone of the phase diagram. The interior layers, beneath this skin, retain the original composition of the initial dope, which via a rapid quench, is driven preferably into the spinodal region with the objective of forming a porous, bicontinuous support layer.
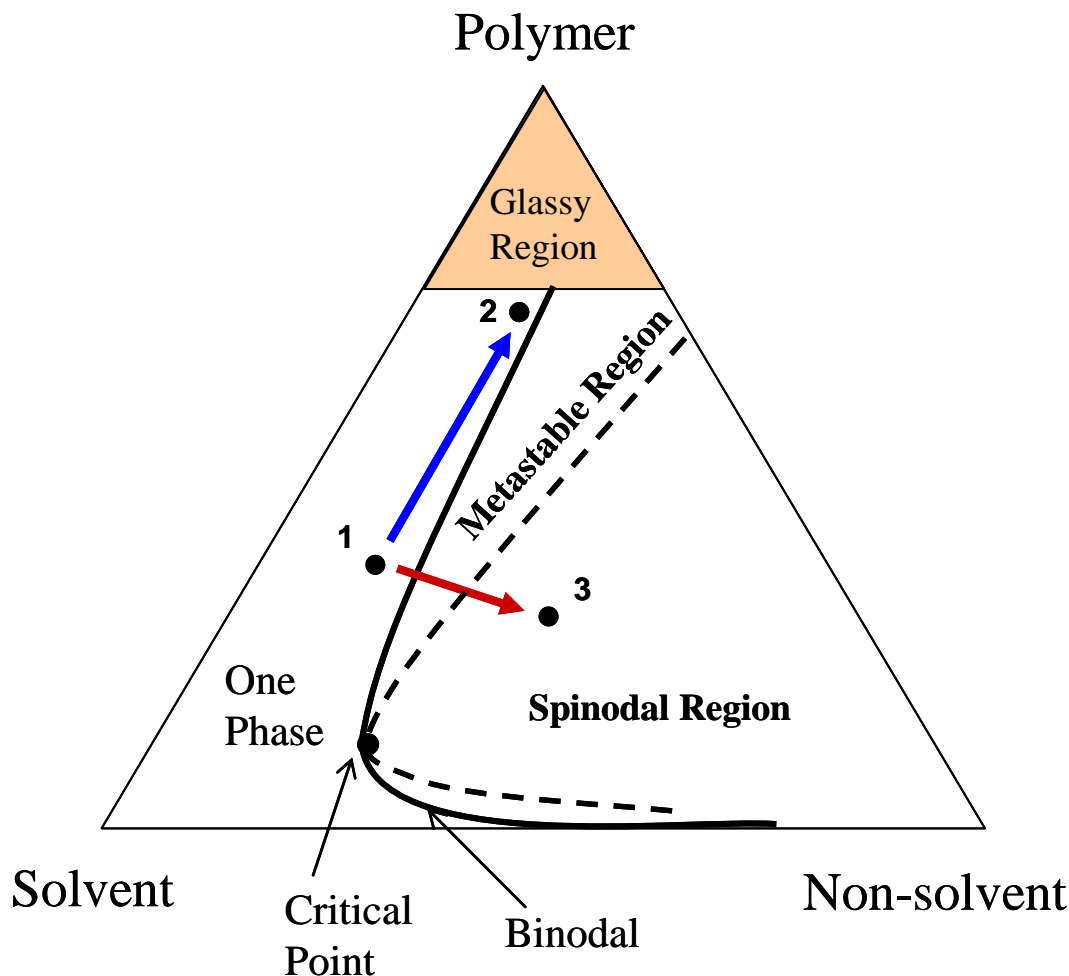
Figure 7.1: Hypothesized compositional changes in the nascent hollow fiber during membrane formation. Compositional change from point 1 to 2 is hypothesized for the skin and from point 1 to an arbitrary position 3 (in the spinodal region) for the support layer of the membrane

The use of solvents with lower affinity for the coagulating media reduces the osmotic pressure driving force for coagulant entry into the nucleus. Examples of such techniques can be seen in multiple polymer systems where surfactants and solvents with lower solvent-coagulant miscibility have been successfully used to suppress macrovoid formation [18, 19]. Decreased solvent entry into the nucleus can also be achieved by forming complexes with the solvent molecule to reduce its diffusivity within the polymer solution. If the complexing agent is a nonsolvent for the membrane forming polymer,

then its presence also helps to vitrify the nucleus rapidly [3]. Furthermore, enhanced viscosity imparted by anti-lyotropic (complexing with the solvent) salts can also work to reduce solvent diffusivity within the dope mixture. Based on the above framework, other researchers have adopted solvent replacement from the dope and/or the use of additives, both either complexing with the primary solvent or acting as nonsolvents to the spinning dope, as the primary mechanisms for the suppression of macrovoids.

The use of anti-lyotropic or lyotropic salts, can respectively, increase or decrease dope viscosity. Although an increase in dope viscosity has led macrovoids suppression [20], the mechanism of this suppression remains open to speculation. Specifically, high osmotic pressures generated within the phase separating membrane are believed to be adequate to overcome obstructions to the expansion of nuclei via enhanced viscosity of the dope. It is possible that the reduction in macrovoid intensity in higher viscosity dopes is due to the decrease in the diffusion of solvent and nonsolvent within the dope mixture. Examples of macrovoid-free membranes formed from polymer systems that increase in viscosity (viscosity harden) with increased extensional stress, such as polyaramides, provide some proof of the effect of increasing viscosity on macrovoid suppression [7].

7.2.2.2. *Macrovoid Suppression Through Spinning Process*

Aside from dope compositional changes, macrovoids have been also suppressed by using high draw ratios [7, 21]. These authors hypothesize that enhanced extensional stress within the nascent fiber increases the propensity for phase separation. Wolf [22] has described the effects of shear on the phase behavior of polymer solutions leading to either increase or decease in the homogeneous envelope based on energy contribution from flow to the Gibbs free energy of the polymer solution.

It can also be envisioned that shear induced instability allows nuclei to form rapidly in front of growing nuclei and thus restrict the growth of macrovoids. This enhanced

instability could also be promoted by high shear and extensional stresses in the spinneret resulting from increased dope extrusion rates. Likewise, uniformity of phase separation generally resulting from thinner membrane film or fiber wall thicknesses was observed to suppress the formation of macrovoids [20, 23, 24]. As decrease in fiber wall thickness is usually found with enhanced draw ratio, the individual effects of both factors are difficult to study as multiple spinneret dimensions would be required. A preliminary study on the effect of increasing extrusion shear rate concludes a suppression of macrovoid takes place at high shear rates in spite of increasing fiber wall thickness [25]. As of yet, a study decoupling the effects of higher draw ratio from decreased wall thickness and enhanced shear stress in the spinneret has not been performed. However, experimentally, it remains proved that higher draw ratios suppress the formation of macrovoids, though the mechanism of the suppression has not been conclusively identified.

In this chapter, Smolders hypothesis of an enlarging nucleus of polymer lean phase driven by ingressing solvent and nonsolvent is used as the foundation of macrovoid growth across all polymeric systems undergoing wet quench observed so far. The suppression of macrovoids can be concluded to depend either on instantaneous phase separation, that is, spinodal decomposition throughout the membrane or on the rapid phase separation/vitrification of the initiated nucleus.

The following conclusions appear relevant in the suppression of macrovoids:

- Increased instability of the dope mixture brought about by, (1) close proximity to the binodal, and (2) stresses subjected on the nascent membrane prior to immersion in the coagulation bath

- *Reduced* flow of solvent into an initiated nucleus

- *Enhanced* flow of nonsolvent into an initiated nucleus

It is the objective of this chapter to describe the applicability of Smolders' macrovoid formation model to macrovoids seen in wet quenched composite organic-inorganic hollow fiber membranes initiated by large particles and provide initial observations on macrovoid formation in the spinning of mixed matrix hollow fiber membranes.

7.3. MACROVOIDS IN ULTEM® BASED HOLLOW FIBER MEMBRANES

Suppression of macrovoids in mixed matrix membranes requires a two pronged approach. Firstly, macrovoids must be suppressed in the conventional (without particles) dope composition. Secondly, any macrovoids generated by the presence of particles must be suppressed in mixed matrix membranes. However, care must be taken to make certain that additives and changes in dope composition affected to suppress macrovoid formation do not interfere with the intended enhancement in selectivity brought about by the addition of molecular sieves to the polymer dope.

The selection of polymer, Ultem® 1000 polyetherimide (hereafter referred to as Ultem®) and zeolite, SSZ-13, for fiber spinning in this report was based on earlier dense film research work [26, 27]. The Ultem® only based spinning dope using N-methyl-2-pyrrolidone (NMP) as solvent and water as the coagulant suffer from a high number of macrovoids. A dual layer hollow fiber was spun using separate Ultem® based compositions, hereafter referred to as the core and sheath formulations.

Considering Smolders' hypothesis, the presence of the voids indicates high solvent mobilities and delayed demixing within the membrane. Lithium nitrate added to the dope decreases the formation of the voids and at high enough concentrations suppresses their formation completely. Kurdi et al [28] have suggested that the lithium ion complexes with two molecules of the solvent (N-methyl-2-pyrrolidone) leading us to conclude that the macrovoid suppression in Ultem® fibers results from the lowered solvent diffusivity within the coagulating membrane as suggested by Cohen-Addad [29]. Further, as per

148

Kesting's hypothesis, lithium nitrate can also act as a nonsolvent, thus it is also feasible that the complex formation allows the incorporation of "additional" quantity of nonsolvent into the nascent membrane which aids rapid phase separation.

Additionally, evaporating solvent in the air gap can lead to phase separation in the skin region of the membrane which is undesirable at this stage as it leads to a highly porous and defective skin in the final membrane. This issue was resolved using tetrahydrofuran (THF) as the volatile component of the dope in concentrations up to 20 wt % of the dope. THF is a weak swelling agent for polyetherimide, and although, the solubility of Ultem® in THF is poor, significantly high concentration of THF can be incorporated in an Ultem®/NMP/THF dope. The binodal for Ultem/NMP/THF system for the polymer concentration of interest (26 – 35 wt %) is shown in Figure 7.2.
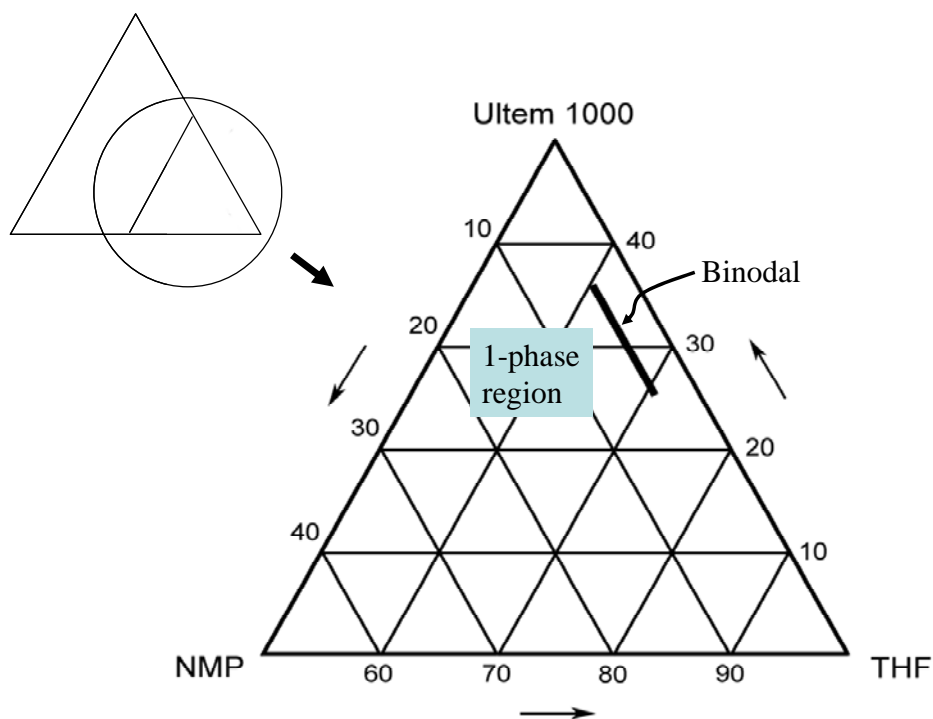
Figure 7.2: Binodal for the Ultem®/NMP/THF system. Thick solid line represents the binodal line separating the 1 phase and 2 phase region

149

7.4. MACROVOIDS IN MIXED MATRIX MEMBRANES

In light of Smolder's macrovoid formation hypothesis [4], the nuclei formation picture is further complicated in the spinning of a suspension as is the case in the spinning of an inorganic molecular sieve – polymer composite, namely, a mixed matrix dope. Here, with respect to nuclei forming potential, the stability of the interface between the dispersed and continuous phase must also be taken into account. The stability of the interphase is determined by the surface energetics of the dispersed phase (inorganic sieve) and its interaction with the components of the continuous phase (polymer, solvents and nonsolvents). A typical spinning solution consists of at least two and most likely three to five components. Particle-solvent, particle-polymer, solvent-polymer and solvent-nonsolvent interactions must be taken into account to describe the free energy of the system. Generally, zeolites with hydroxyl groups on the surface are hydrophilic and interact strongly with polar and hydrophilic solvents in the dope mixture. This leads to a tendency of the zeolite to act a nucleating agent towards the dope components.

Such a nucleating effect is undesirable from the point of view of successful mixed matrix membranes as discussed in Chapter 4, however, it can be beneficial in the suppression of macrovoids. Even though the nucleating tendency can easily be pictured to increase the formation of nuclei which could evolve into macrovoids, it is also expected that at a critical concentration of particles, the formation of multiple nuclei would suppress the formation of macrovoids by allowing additional nuclei to form rapidly in front of prior formed nuclei, thereby preventing existing nuclei from expanding into macrovoids [4] . Wara [30] observed such a suppression of macrovoids at particle loadings exceeding 77 wt% submicron alumina with respect to polymer and concluded that the particles lowered the interdiffusion rate of the polymer lean phase (PLP). However, the nucleating effect of molecular sieves may be lower for mixed matrix membranes where particle loading in the range of 10-40 wt% with respect to polymer is envisioned.

In situations where it is believed that the nucleating tendency is suppressed, that is, with the use of Grignard treated zeolites, the low water permeability (the primarily used coagulant) of zeolites along with a large particle size provides conditions for the opposite effect, that is, for the formation and growth of macrovoids. In experiments performed with the spinning of dual layer Ultem® based hollow fiber consisting of a polydispersed sample of Grignard treated zeolites of 0.2 – 3 micron size particles in the sheath dope quenched in a water bath, macrovoids initiated by the larger 2 – 3 micron zeolite particles were observed. A collection of such particle initiated macrovoids is shown in Figure 7.3.

The mechanism of the formation of such macrovoids can be explained by understanding the mass transfer of solvents and nonsolvents during phase separation process of asymmetric mixed matrix membranes. As the membrane is immersed in the quench bath, water (the nonsolvent coagulant), driven by osmotic forces [15], penetrates the membrane while solvent from the nascent membrane enters the coagulation bath. The external phase separation, that is, the formation of the outer dense layer also "freezes" the volume of the membrane and phase separation of the interior of the membrane takes place at a separate rate with a high degree of porosity [31]. This porosity develops because only 20 – 40 wt% of the composition of a spinning dope is made up of polymer/solids, the remaining being composed of solvents and nonsolvents which are removed from the final membrane. If the kinetics of phase separation in the interior of the membrane are slow, the growth of a few large voids is favored over the formation of many microvoids due to the inter diffusion of the polymer lean phase driven by a lowering of the interfacial free energy. However, rapid local phase separation and subsequently formed polymer structure of sufficient strength can oppose the coalescing tendencies of the microvoids. The formation of small (micro) versus large (macro) voids thus should depend on the local rate (kinetics) of phase separation of the membrane [4].
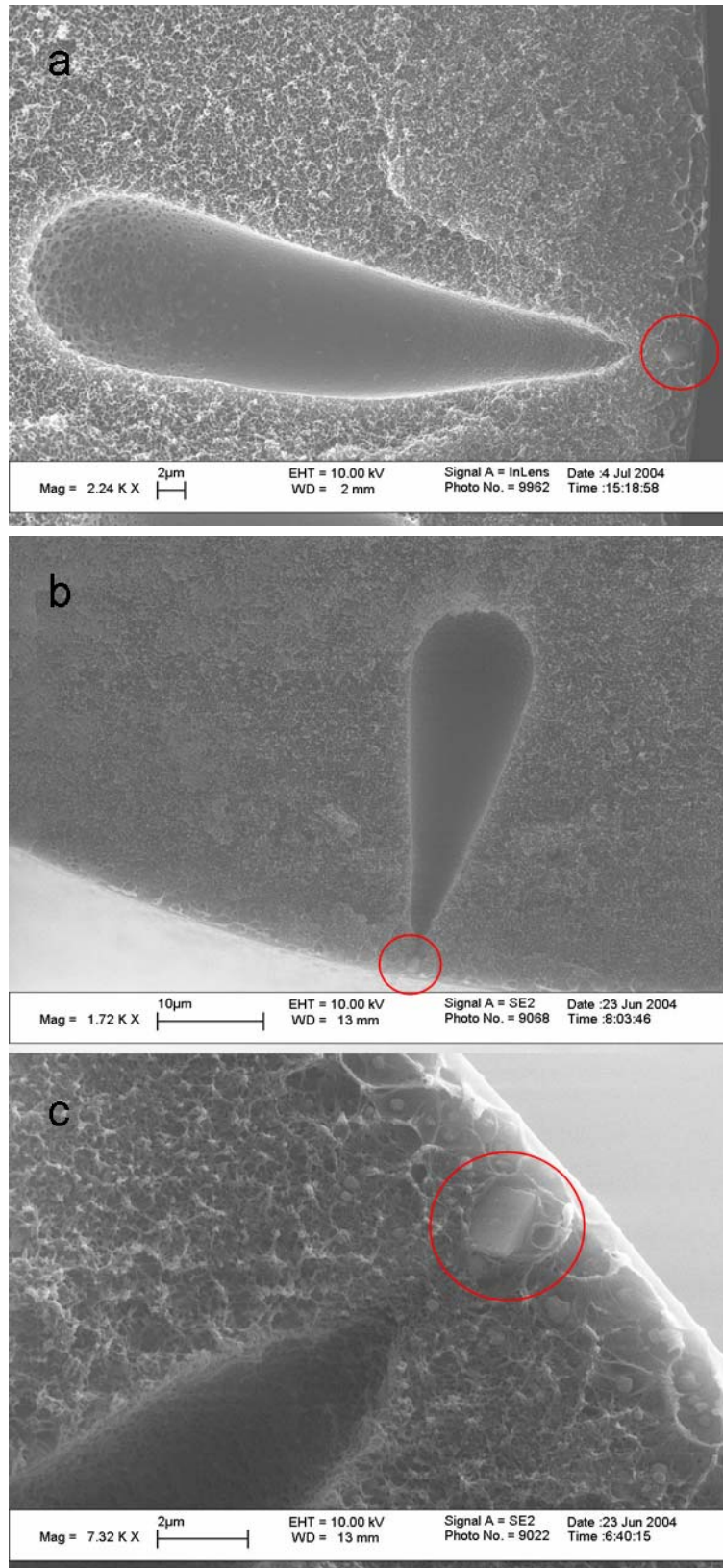
Figure 7.3: Macrovoids initiated by large sieve particles in Ultem® polymer matrix.

As the difference between the eventual formation of a small pore versus a macrovoid is the local rate of demixing, any non-uniformity of phase separation of the membrane could result in a site for macrovoid formation [20]. Generally as noted earlier, this non-uniformity in phase separation is caused by a plastic nucleus containing a sufficient quantity of solvent to prevent its vitrification. Alternatively, the non-uniformity can also be represented by a plastic nucleus in which a lowered inflow of nonsolvent takes place, preventing phase separation of the polymer around the nucleus. In the case of a mixed matrix membrane, it is hypothesized that nonuniformity of phase separation can be provided by the large sieve particles within the coagulating membrane. The particles, due to their large size and low water permeability, can act as an obstruction to the ingressing nonsolvent molecules leading to a deficit of the nonsolvent in the region immediately behind the particles as shown at stage 1 in Figure 7.4. The phase separating front thus moves nonuniformly through the membrane in the region on either side of the particle. As the area surrounding the particle phase separates, the polymer lean phase is driven into the viscous but still fluid region behind the particle as seen in stage 2. The large particle acts as a barrier to the ingressing coagulant and allows the void to grow plastically with sufficient inflow of solvent (from the bulk) to prevent phase separation of the walls of the growing void. By stage 3 the characteristic shape of the macrovoid is seen to develop with the fluid contents of the void consisting of solvent and nonsolvent causing the phase separation of the void walls. This hypothesis is ably supported by SEM micrographs of particle initiated macrovoids shown in Figure 7.3. Figure 7.5 shows a close-up of a sieve particle initiating a macrovoid with excellent bonding of the polymer around it, thus negating the counter hypothesis that the macrovoid can be formed by the rapid ingress of coagulant from the coagulation bath through defects at the polymer-sieve interface.

Stage 1   Stage 2   Stage 3

Phase separated region

Viscous dope region

Fluid solvent/nonsolvent region

Coagulant

Solvent/polymer lean phase
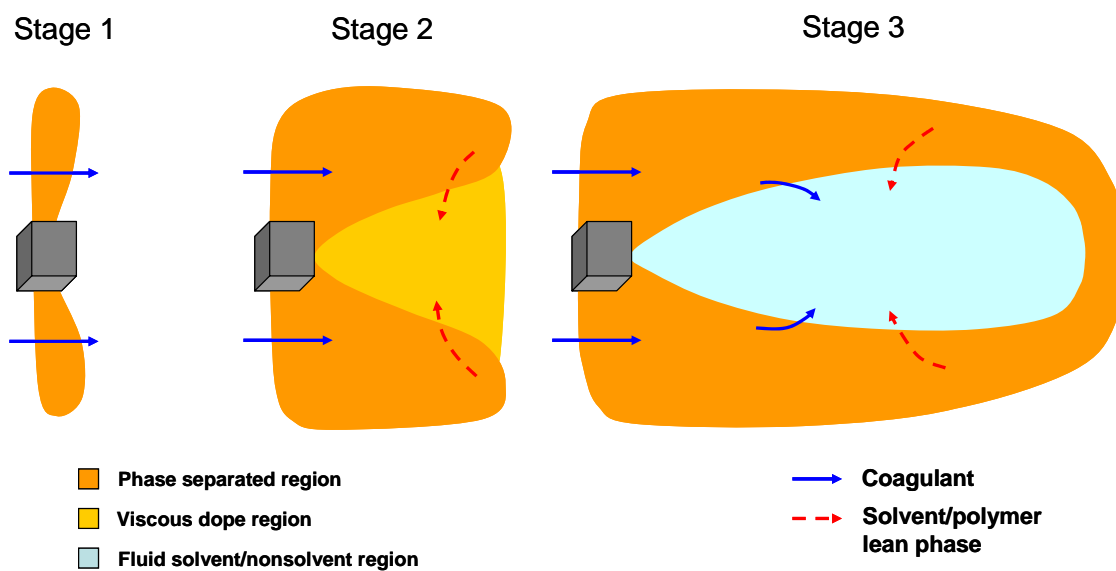
Figure 7.4: Cartoon showing the proposed evolution of a particle initiated macrovoid
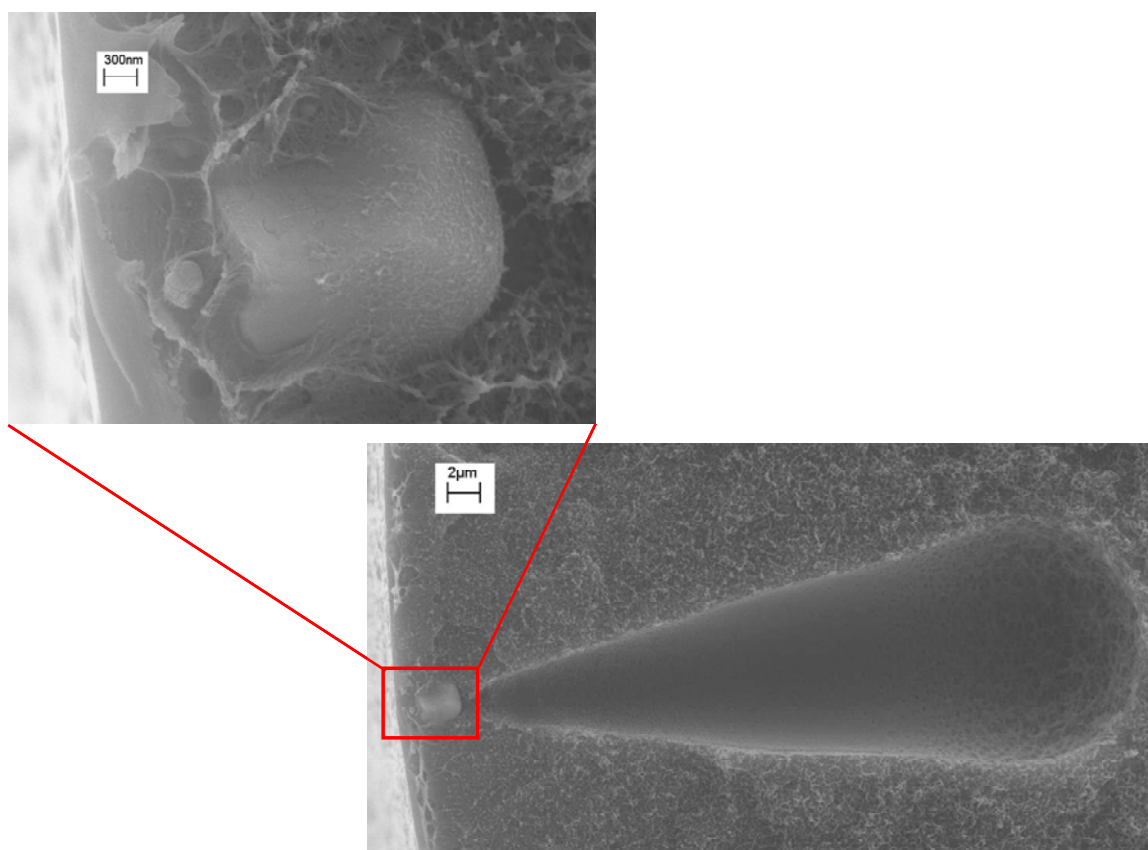
Figure 7.5: SEM microphotograph of macrovoid initiated by a large zeolite particle

The above hypothesis is analogous to the macrovoid forming potential of rapidly phase separating membranes when a larger air gap is used to form a thicker skin. The increased air gap allows the formation of the skin via the evaporation of volatile solvent or nonsolvent leading to an increased polymer concentration in the outer region of the fiber. If the skin thickness is non uniform across the circumference of the fiber, conditions for non-uniform phase separation are formed. Any non-uniformity in phase separation can then become the site for the accumulation and expansion of the polymer lean phase leading to the eventual development of a macrovoid. The presence of non-uniformly distributed macrovoids in polymer-only hollow fibers was also noted by Mckelvey, who attributed chaotic air flows in the hood as the cause [32].

If the hypothesis of the large particle acting as a coagulant barrier is true, then the size of the particle necessary to cause macrovoids must therefore be related to the velocity at which the nonsolvent front moves through the membrane. The rate of the front's movement through the membrane is moderated first by the membrane skin which acts as the primary resistance, and then on the diffusivities of the solvent and nonsolvent within the coagulating membrane. Since the rate of coagulation is dependent on the dope composition, temperature and quench bath composition, holding these conditions constant is necessary to clarify the effect of particles. In this case only particles larger than a certain critical size would be able to impede non-solvent entry sufficiently to allow macrovoids to form in the region behind. For the case of poor sieve-polymer adhesion, if the particle is hydrophilic, the presence of the particle can lead to heterogeneous nucleation of the polymer lean phase and the formation of a nucleus (as described in Chapter 4), which may grow into a macrovoid. Figure 7.6 shows a schematic of the possible routes of macrovoid formation.
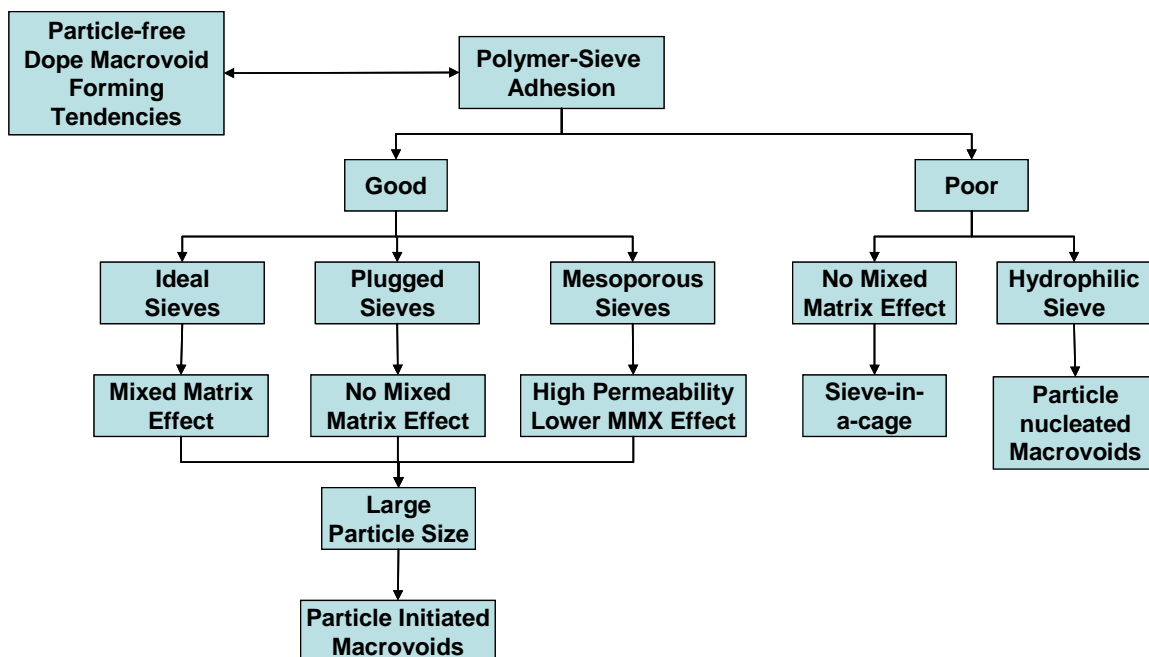
Figure 7.6: Schematic outlining possible routes to macrovoid formation

This previously unknown role of particles in the formation of macrovoids restricts the maximum size of the molecular sieve particles that can be used in wet quenched asymmetric mixed matrix membranes. Incorporating smaller particle sizes in the dope mixture is complicated since the smaller particles tend to agglomerate and are difficult to disperse homogeneously in dopes. Thus the optimization of the particle size must be performed for ideal mixed matrix hollow fiber production to account for processing membrane morphology challenges.

To test the above hypothesis, a dope mixture with small zeolite particles is spun to prove or disprove the hypothesis of the formation of a blockage region necessary to allow the growth of macrovoids.

7.5. MIXED MATRIX MEMBRANES INCORPORATING SUBMICRON ZEOLITE 4A

Very few macrovoids were observed in dual layer Ultem®-Ultem® and Ultem®-Matrimid fibers incorporating 8.6 and 14.4 volume percent Grignard treated submicron zeolite 4A, respectively. The particle size of the zeolites varied between 100 – 250 nm, with an average size of 200 nm, as observed by microscopy. All the macrovoids observed, based on 36 fibers imaged for each spin above, were found in the core regions of the fiber and were not initiated by particles. Additionally, it was observed that the presence of macrovoids in the core region of the fiber decreased in frequency as the draw ratio was increased. Figure 7.7 shows a SEM micrograph of one such macrovoid seen in the fibers. The suppression of these macrovoids in the core region of the fiber is discussed in the following section.
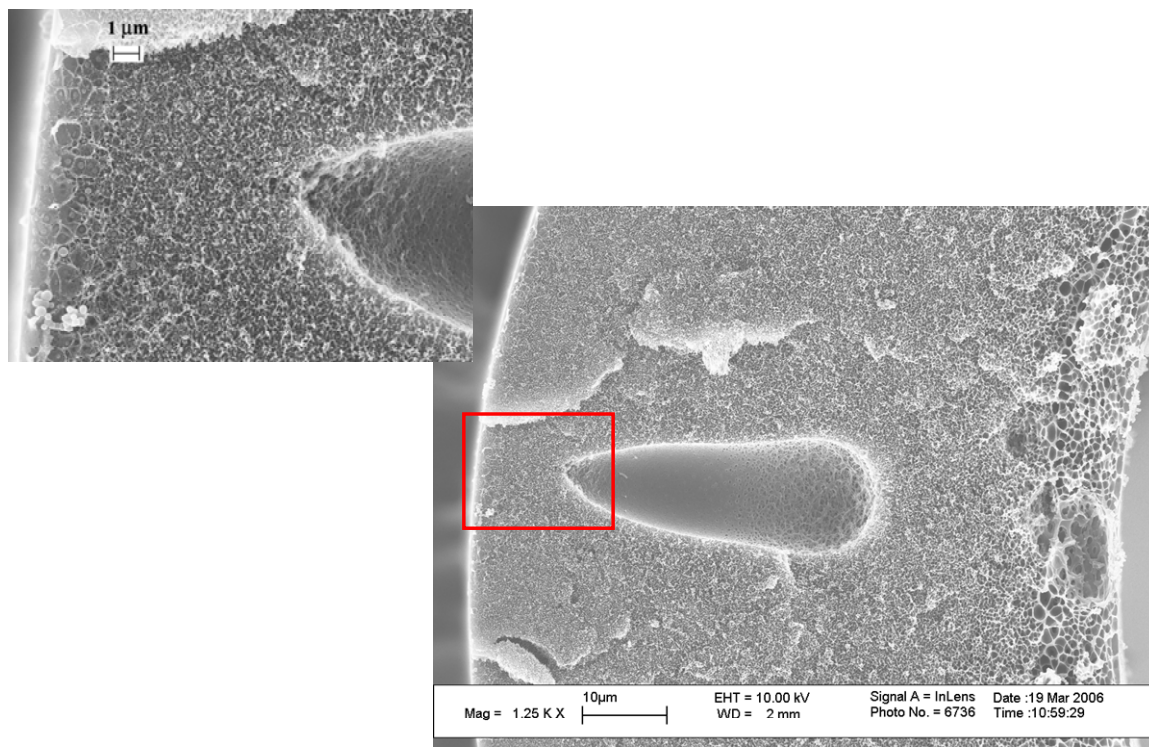
Figure 7.7: Macrovoid initiated in the core of Ultem®-Ultem® fibers incorporating Grignard treated submicron zeolite 4A. Inset: Zeolite particles (100 – 250 nm) are present only in the sheath region approximately 3 microns thick from fiber edge

157

7.5.1. Effect of Draw Ratio on Macrovoid Suppression

While particle size seems to be the dominant factor in the initiation of macrovoids in mixed matrix fibers, effects of shear and extensional stresses on fiber spinning can be considerable as mentioned earlier on the topic of macrovoid formation in polymer-only fibers. While no particle initiated macrovoids were observed in fibers incorporating 200 nm (average particle size) Grignard treated zeolite 4A, some macrovoids in the core region of the fibers were observed. These core region macrovoids could potentially be suppressed at higher draw ratios, however, the corresponding effect of high draw ratio on polymer-zeolite adhesion in the sheath region of the fiber are unknown.

The presence of such defects would result in the loss of the mixed matrix effect as the gas molecules could bypass the zeolite. Based on the selectivity results presented in section 5.4.2., it is not believed that the draw ratios, used in this work, "pull" the polymer away from the zeolite even at the highest draw ratios tested (up to a draw ratio of 6.2).

However, the effect of higher draw ratios is apparent on the suppression of macrovoids in the core region of the fibers from the Ultem®-Matrimid®- Grignard treated zeolite 4A spin (section 5.4.3). Figure 7.8 shows the decrease in the number of macrovoids observed with increasing draw ratios for fibers spun with a constant extrusion rate (shear stress in the spinneret) and air gap. Based on the fibers imaged per draw ratio (minimum of 3 fibers), the number of macrovoids decreases from an average of 18 at a draw ratio of 2.8 to an average of less than 1 at a draw ratio of 6.2. Representative SEM images of these fibers at different draw ratios are shown in Figure 7.9. As the core region of the hollow fibers does not contain particles, the suppression of macrovoids at higher draw ratios observed here, is similar to the observations made by Ekiner and Vassilatos [7] and Wang et al. [21] on the suppression of macrovoids in polymer-only membranes.

To add complexity to the picture of macrovoid formation presented above, draw ratio cannot be considered the only variable leading to the suppression of macrovoids. Macrovoid formation may also be suppressed by a decreasing fiber wall thickness (FWT), corresponding to the results of Paulsen et al., who saw a decrease in the number of macrovoids with decreasing film thickness [23]. As the fibers, shown in Figure 7.9, were spun from the same spinneret and constant extrusion rate, the wall thickness of the fibers is observed to decrease with increasing draw ratio. Further experiments decoupling the role of draw ratio from FWT and shear stress in the spinneret on the formation of macrovoids are required with multiple dimension spinnerets to ascertain their individual effects on macrovoids suppression.
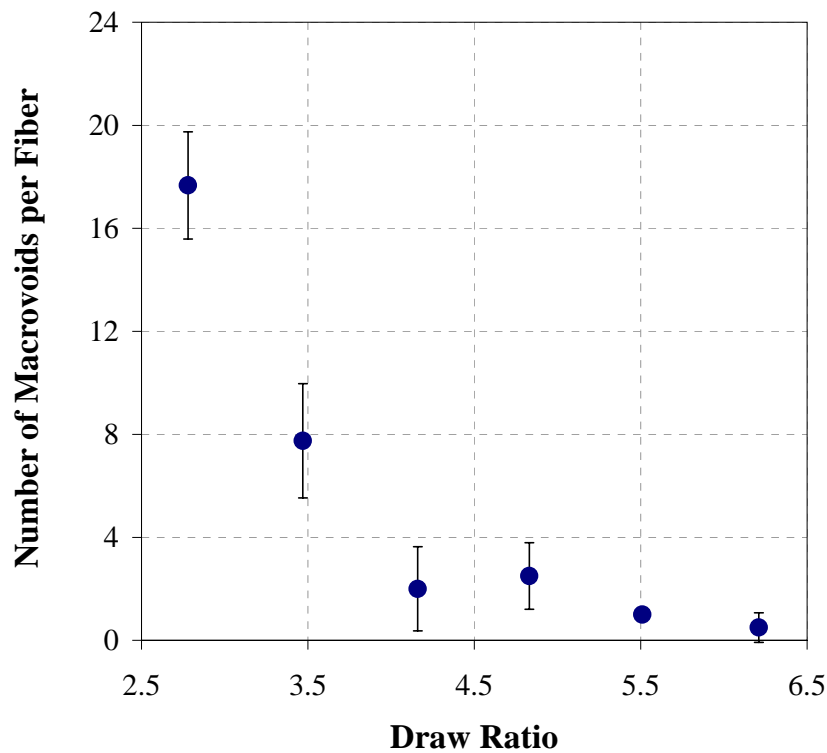
Figure 7.8: Macrovoid frequency dependence on draw ratio for an air gap of 10 cm and constant extrusion rate in Ultem®-Matrimid® mixed matrix fibers incorporating Grignard treated submicron zeolite 4A. A minimum of 3 fibers were imaged at each draw ratio to determine macrovoid frequency
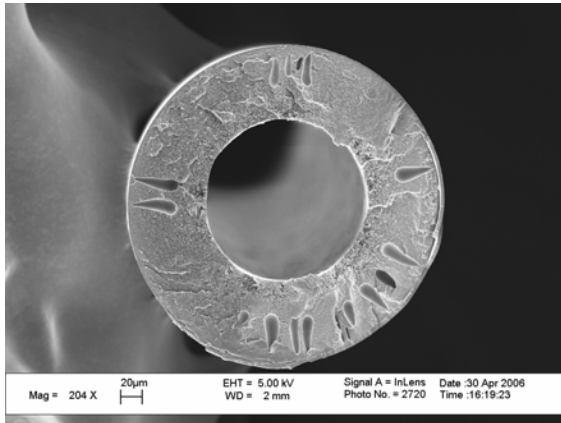
DR = 2.8, FWT = 75 μm
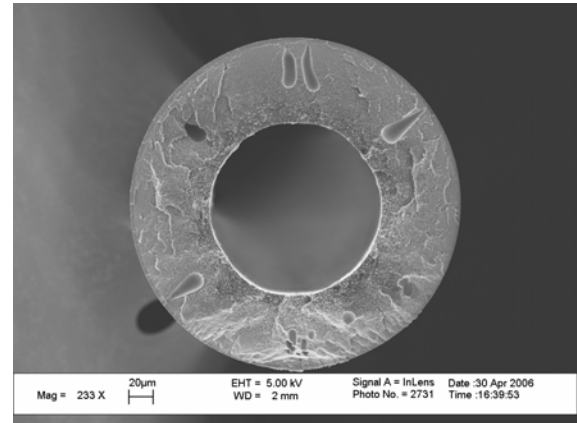
DR = 3.5, FWT = 67 μm
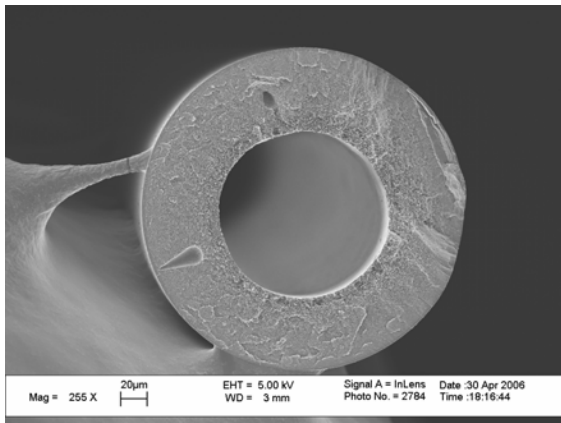
DR = 4.2, FWT = 61 μm
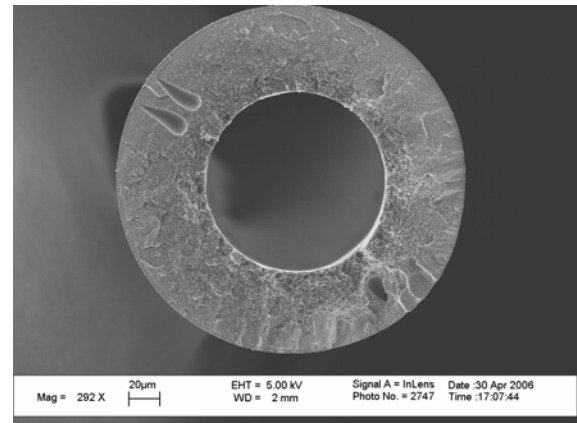
DR = 4.8, FWT = 57 μm
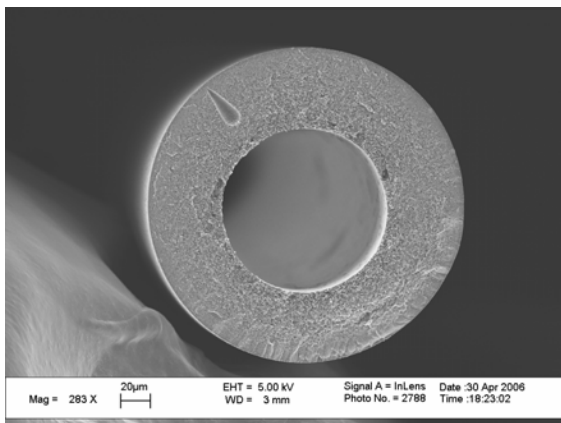
DR = 5.5, FWT = 50 μm
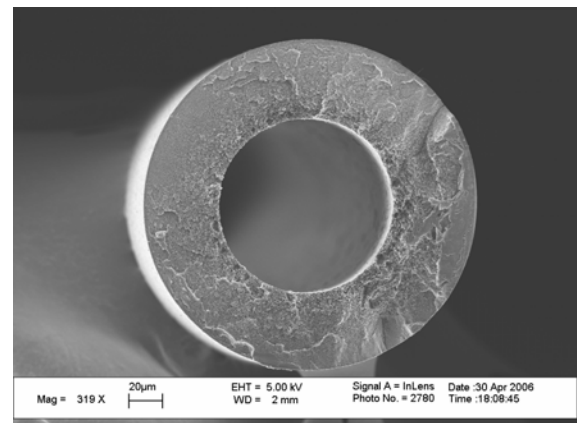
DR = 6.2, FWT = 46 μm

Figure 7.9: Effect of draw ratio on macrovoid suppression in Ultem®-Matrimid® mixed matrix fibers incorporating Grignard treated submicron zeolite 4A; DR – Draw Ratio, FWT- Fiber Wall Thickness.

160

7.6. SUMMARY AND CONCLUSIONS

Aside from the presence of macrovoids seen in wet quenched polymer-only membranes, macrovoids are also observed to be initiated by large zeolite particles in mixed matrix hollow fibers. The large particles are hypothesized to provide resistance to the entry of coagulant from the quench bath, and thus promote nonuniform phase separation within the mixed matrix membrane. The nonuniformity of the phase separation is in turn believed to lead to the formation of macrovoids as hypothesized by Smolders.

These particle initiated macrovoids were eliminated by the use of 200 nm sized zeolite particles. These results indicate a dependence of particle initiated macrovoid formation on the size of the particle.

It was also preliminarily found that macrovoids in the core region of dual layer mixed matrix membranes could be suppressed at higher draw ratios. These higher draw ratios were obtained in combination with decreasing fiber wall thickness, which may also be a factor in the suppression of macrovoids. These preliminary results may be confirmed by the use of multiple spinneret pore sizes, which would allow fibers of different draw ratios to be spun with constant extrusion rates and fiber wall thickness.

7.7. REFERENCES

1.   Frommer, M.A., R. Matz, and U. Rosenthal, *Mechanism of formation of reverse osmosis membranes. Precipitation of cellulose acetate membranes in aqueous solutions.* Industrial & Engineering Chemistry Product Research and Development, 1971. **10**(2): p. 193-6.

2.   Cabasso, I., E. Klein, and J.K. Smith, *Polysulfone hollow fibers. II. Morphology.* Journal of Applied Polymer Science, 1977. **21**(1): p. 165-80.

3.   Kesting, R.E., A.K. Fritzsche, C.A. Cruse, and M.D. Moore, *The second-generation polysulfone gas-separation membrane. II. The relationship between sol properties, gel macrovoids, and fiber selectivity.* Journal of Applied Polymer Science, 1990. **40**(9-10): p. 1575-82.

4.   Smolders, C.A., A.J. Reuvers, R.M. Boom, and I.M. Wienk, *Microstructures in phase-inversion membranes. Part 1. Formation of macrovoids.* Journal of Membrane Science, 1992. **73**(2-3): p. 259-75.

5.   Shojaie, S.S., W.B. Krantz, and A.R. Greenberg, *Dense polymer film and membrane formation via the dry-cast process. Part II. Model validation and morphological studies.* Journal of Membrane Science, 1994. **94**(1-3): p. 281-98.

6.   Chung, T.-S. and X. Hu, *Effect of air-gap distance on the morphology and thermal properties of polyethersulfone hollow fibers.* Journal of Applied Polymer Science, 1997. **66**(6): p. 1067-1077.

7.   Ekiner, O.M. and G. Vassilatos, *Polyaramide hollow fibers for H2/CH4 separation II. Spinning and properties.* Journal of Membrane Science, 2001. **186**(1): p. 71-84.

8.   McKelvey, S.A., D.T. Clausi, and W.J. Koros, *A guide to establishing hollow fiber macroscopic properties for membrane applications.* Journal of Membrane Science, 1997. **124**(2): p. 223-232.

9.   Strathmann, H., K. Kock, P. Amar, and R.W. Baker, *The formation mechanism of asymmetric membranes.* Desalination, 1975. **16**(2): p. 179-203.

10.   Frommer, M.A. and R.M. Messalem, *Mechanism of Membrane Formation. VI. Convective Flows and Large Void Formation during Membrane Precipitation.* Ind. Eng. Chem. Prod. Res. Develop., 1973. **12**(4): p. 328-333.

11.   Kesting, R.E., A.K. Fritzsche, M.K. Murphy, C.A. Cruse, A.C. Handermann, R.F. Malon, and M.D. Moore, *The second-generation polysulfone gas-separation membrane. I. The use of Lewis acid:base complexes as transient templates to increase free volume.* Journal of Applied Polymer Science, 1990. **40**(9-10): p. 1557-74.

12.   Frommer, M.A., R. Matz, and U. Rosenthal, *Mechanism of formation of reverse osmosis membranes.* 1971. **10**(2): p. 193-6.

13.   Cohen, C., G.B. Tanny, and S. Prager, *Diffusion-controlled formation of porous structures in ternary polymer systems.* Journal of Polymer Science, Polymer Physics Edition, 1979. **17**(3): p. 477-89.

14.   Reuvers, A.J., J.W.A. Van den Berg, and C.A. Smolders, *Formation of membranes by means of immersion precipitation. Part I. A model to describe mass transfer during immersion precipitation.* Journal of Membrane Science, 1987. **34**(1): p. 45-65.

15.   McKelvey, S.A. and W.J. Koros, *Phase separation, vitrification, and the manifestation of macrovoids in polymeric asymmetric membranes.* Journal of Membrane Science, 1996. **112**(1): p. 29-39.

16.   Boom, R.M., *Membrane formation by immersion precipitation: the role of the polymeric additive.* 1992, University of Twente, The Netherland.

17.   Bloch, R. and M.A. Frommer, *The mechanism for formation of "skinned" membranes I. Structure and properties of membranes cast from binary solutions.* Desalination, 1970. **7**(2): p. 259-264.

18.   Wang, D.-M., F.-C. Lin, T.-T. Wu, and J.-Y. Lai, *Formation mechanism of the macrovoids induced by surfactant additives.* Journal of Membrane Science, 1998. **142**(2): p. 191-204.

19.   Albrecht, W., T. Weigel, M. Schossig-Tiedemann, K. Kneifel, K.V. Peinemann, and D. Paul, *Formation of hollow fiber membranes from poly(ether imide) at wet phase inversion using binary mixtures of solvents for the preparation of the dope.* Journal of Membrane Science, 2001. **192**(1-2): p. 217-230.

20.   McKelvey, S.A., *Formation and characterization of hollow fiber membranes for gas separation (fiber breaks, macrovoids)*, in *Department of Chemical Engineering*. 1997, Univ. of Texas, Austin, TX, USA. p. 227 pp.

21.   Wang, K.Y., D.F. Li, T.-S. Chung, and S.B. Chen, *The observation of elongation dependent macrovoid evolution in single- and dual-layer asymmetric hollow fiber membranes.* Chemical Engineering Science, 2004. **59**(21): p. 4657-4660.

22.   Wolf, B.A., *Thermodynamic theory of flowing polymer solutions and its application to phase separation.* Macromolecules, 1984. **17**(4): p. 615-18.

23.   Paulsen, F.G., S.S. Shojaie, and W.B. Krantz, *Effect of evaporation step on macrovoid formation in wet-cast polymeric membranes.* Journal of Membrane Science, 1994. **91**(3): p. 265-82.

24.	Vogrin, N., C. Stropnik, V. Musil, and M. Brumen, *The wet phase separation: the effect of cast solution thickness on the appearance of macrovoids in the membrane forming ternary cellulose acetate/acetone/water system.* Journal of Membrane Science, 2002. **207**(1): p. 139-141.

25.	Wang, K.Y., T. Matsuura, T.-S. Chung, and W.F. Guo, *The effects of flow angle and shear rate within the spinneret on the separation performance of poly(ethersulfone) (PES) ultrafiltration hollow fiber membranes.* Journal of Membrane Science, 2004. **240**(1-2): p. 67-79.

26.	Mahajan, R. and W.J. Koros, *Mixed matrix membrane materials with glassy polymers. Part 2.* Polymer Engineering and Science, 2002. **42**(7): p. 1432-1441.

27.	Moore, T.T., *Effects of materials, processing, and operating conditions on the morphology and gas transport properties of mixed matrix membranes*, in *Department of Chemical Engineering*. 2004, Univ. of Texas, Austin, TX, USA. p. 312.

28.	Kurdi, J. and A.Y. Tremblay, *The influence of casting solution structure on the microporosity of polyetherimide gas separation membranes prepared by the coagulation post-leaching method.* Journal of Membrane Science, 2001. **184**(2): p. 175-186.

29.	Cohen Addad, J.P. and P. Panine, *Pore generation in asymmetric polymeric membranes. Correlation with solvent mobilities.* Polymer Bulletin (Berlin), 1999. **42**(3): p. 345-352.

30.	Wara, N.M., L.F. Francis, and B.V. Velamakanni, *Addition of alumina to cellulose acetate membranes.* J. Membr. Sci., 1995. **104**(1-2): p. 43-9.

31.	Sarbolouki, M.N., *Properties of Asymmetric Polyimide Ultrafiltration Membranes. I. Pore Size and Morphology Characterization.* Journal of Applied Polymer Science, 1984. **29**: p. 743-753.

32.	McKelvey, S.A., *Formation and characterization of hollow fiber membranes for gas separation (fiber breaks, macrovoids).* 1997. p. 227 pp.

CHAPTER 8

CONCLUSIONS AND RECOMMENDATIONS

8.1. SUMMARY AND CONCLUSIONS

This work represents the successful culmination of the objectives outlined in Chapter 1. The research set out to accomplish the following objectives;

1. To identify challenges in mixed matrix hollow fiber spinning

Most of the parameters for the formulation, dispersion and processing of asymmetric mixed matrix membranes were developed in this work in the absence of significant prior art. Initial guidelines for the formulation, dispersion and processing of mixed matrix dopes on 5 – 10 ml level (used for dense film preparation), were scaled to the 100 – 500 ml level required for spinning of mixed matrix hollow fibers. Significant challenges that were addressed in this work are:

   a) Development of a polymer/solvent/nonsolvent/zeolite/additive formulation that was considerably more complex than that polymer/solvent/zeolite system used in dense film formulations. The formulations were developed to attain specific membrane morphologies (support porosity, zeolite-solvent interaction, skin thicknesses) and specifically avoid others such as macrovoids.

   b) Understanding the effects of membrane phase separation on the polymer-zeolite interface including nucleation tendencies of the zeolite surface. Based on the nucleation hypothesis, a zeolite surface modification technique modification technique was developed.

c) Address the highly stringent zeolite dispersion requirements for mixed matrix spinning. Dense films with thicknesses of 25 – 50 microns are more forgiving in the casting and testing to the presence of multi-micron sized agglomerates that are completely enclosed by the surrounding polymer. Additionally, only a small portion of a film is visually selected for permeation testing. For mixed matrix spinning, the suspension is filtered to prevent plugging of the spinneret. Further, the presence of agglomerates can cause excessive pressure drops across the filter. Even agglomerates a few microns in size can completely destroy the selectivity of fibers with ideal skin thicknesses of 100 nm.

2. Explain defective morphologies in mixed matrix hollow fiber membranes that decrease their gas separation potential

Two major defective morphologies are found identified during the research. Hypotheses for the defects identified in the work are developed and tested. The defects identified in this work are:

a) Sieve-in-a-cage morphologies; hypothesized to form due to the nucleating tendencies of the solvents and nonsolvents on the surface of the zeolite

b) Macrovoids initiated by large zeolite particles as a consequence of non-uniform phase separation

3. Define a framework to practically form mixed matrix membranes with different combinations of inorganic molecular sieve and polymers

A new surface modification technique was developed which uses a two step reaction to first, dealuminate the zeolite surface, followed by a reaction with a Grignard reagent. The treatment resulted in magnesium hydroxide being deposited on the surface of the zeolite.

The surface deposition of magnesium hydroxide is proposed to serve two functions leading to the formation of good polymer-sieve adhesion and subsequent mixed matrix effect. In its first role, the hydroxide is believed to dissociate in the solvent leading to the formation of charged zeolite particles that are electrostatically stabilized. Secondly, the hydroxide is proposed to, (1) reduce the acidity of the zeolite surface, thereby, reducing solvent-zeolite interaction and allowing the basic solvent to be displaced from the surface by the polymer; (2) increase polymer/insert adhesion via entropic effects. The modified zeolites were successfully incorporated into two different polymer matrices and formed into asymmetric hollow fiber membranes. These mixed matrix hollow fiber membranes had increased selectivities for O_2/N_2, He/N_2 and CO_2/CH_4 gas pairs that approached or exceeded model predictions for mixed matrix materials.

8.2. RECOMMENDATIONS FOR FUTURE WORK

While the objective of any research work is to answer questions, a more considerable challenge is to raise key questions that remain unanswered, and develop strategies to test those questions in a scientific manner. This work has resulted in the generation of a considerable number of hypotheses that were impossible to test rigorously given even the long time of 5 years. The focus of this work as defined by objective 1, was to test the limits in the area of mixed matrix hollow fiber spinning and explore the area to establish the most productive topics for more in-depth study. Thus the ideas and hypotheses developed in this work serve as an excellent platform to drive mixed matrix research in multiple directions. The following sections expand on the possible areas of research that should be addressed.

8.2.1. Exploring Enthalpic versus Entropic Control

As outlined in Chapter 6, it is proposed that increased polymer-zeolite adhesion observed for polymers (Ultem® and Matrimid®) and Grignard treated zeolites (SSZ-13 and 4A) can be explained from both enthalpic and entropic considerations. However, it is

expected that based on a particular polymer/solvent/sieve system, either enthalpic or entropic effect may be dominant.

Based on this analysis, various polymer/solvent/insert systems can be probed to conclude if the above assessment is generally applicable and whether a unified approach to mixed matrix membrane formation can be developed. The polymer/solvent/insert system used in this work, defined in the acid-base framework of Fowkes [1], is neutral polymer/basic solvent/acidic zeolite where acidic zeolite refers to the unmodified versions of zeolite 4A and SSZ-13. Additional combinations of polymer/solvent/zeolite of interest could be:

a) Acidic polymer/Grignard treated insert/neutral solvent.

b) Basic polymer/acidic insert/neutral solvent

8.2.2. Alternative Magnesium Hydroxide Deposition Techniques

It was hypothesized that Magnesium hydroxide plays a critical role in the dispersion and subsequent modification of the acidity of the zeolite surface. While the Grignard treatment remains a treatment that has been "tried and tested", alternative methods of less complexity should be explored for magnesium hydroxide deposition on the acidic zeolite surfaces. The technique suggested by Hu et al. [2] using magnesium valerate appears attractive, along with other techniques using magnesium nitrate [3] and magnesium acetate [4].

8.2.3. Magnesium Exchange in zeolite 4A

The nitrogen adsorption data and infra-red spectroscopy of the Grignard treated zeolite 4A presented in Chapter 6 suggests the exchange of sodium with magnesium ions in the zeolite as a consequence of the Grignard treatment. This proposal needs to be tested by X-ray diffraction studies to determine any change in lattice parameters. Additionally the

transport properties of these modified zeolites needs to be determined to allow better matching of transport between polymer and zeolite.

8.2.4. High Loading Mixed Matrix Membranes

This work has successfully developed processes, chemical modifications and strategies to form mixed matrix membranes with maximum particle loadings of around 15 volume %. The next stage in mixed matrix membranes is the transition into higher zeolite/molecular sieve loadings of 30 volume % and above. The main challenges are expected to be in the areas of particle dispersion and dope flow characteristics of the concentrated suspension under shear during the spinning process. Several strategies for the formation of high solids asymmetric membrane can be pursued, namely;

1) combining electrostatic and polymeric stabilization to increase zeolite dispersibility in solvent – this would primarily be achieved with the introduction of a suitable surfactant (amphipathic block copolymers, silanes, carboxylic acids and others) during the dispersion phase to prevent coagulation

2) using surfactants and surface modification agents that reduce interaction of the zeolite surface with the solvent and nonsolvents of the system.

8.2.5. Determination of Zeolite Acidity

Based on the polymer/solvent/zeolite system used in this work, it was found that poorly acidic or neutral zeolites had better interface properties with Ultem® and Matrimid® than their acidic counterparts. Unfortunately, a study on the acidic properties of as-received and surface modified zeolites was not performed. It is however, conjectured that an ideal level of interaction of the zeolite surface with the solvent is required for good polymer-zeolite bonding. This solvent-zeolite interaction must be of sufficient strength for the zeolite to form stable dispersions in the solvent, however, the polymer

should be able to displace the solvent from the zeolite surface and adsorb on the zeolite surface in order to form a good interface.

Determination of zeolite surface acidity can be performed with the sorption of amine molecules that are too large to penetrate the pores of the zeolite. One candidate for sorption studies is pyridine.

8.2.6. Explore Alternative Surfactants for Steric Stabilization

Steric stabilization of zeolite particles was initially pursued in this work with the use of Ultem® "sized" and silanated SSZ-13 in Ultem® matrix as discussed in chapter 4. Although it was found that the particles were highly stable in the solvent at high loadings ~ 15 – 20 volume %), the particles have significant attraction for the solvent molecules. This attraction was hypothesized to result in polymer being excluded from the surface of the zeolite and the zeolite acting as a nucleating agent for the polymer lean phase. Although the sterically stabilized particles used earlier in this work provided poor mixed matrix performance, the technique has several very desirable attributes. Steric stabilization can be used at high particle loadings, have reversibility of flocculation, are relatively insensitive to ionic concentrations and are well suited to non-aqueous environments [5]. An even more effective strategy would be the use of both steric and electrostatic stabilization in combination (electrosteric) as suggested by Napper [5].

8.3. REFERENCES

1. Fowkes, F.M. and M.A. Mostafa, *Acid-base interactions in polymer adsorption.* Ind. Eng. Chem. Prod. Res. Dev., 1978. **17**(1): p. 3-7.

2. Hu, Z., W. Lihui, S. Chen, J. Dong, and S. Peng, *External modification of zeolite by metal surfactant for methanol amination.* Microporous and Mesoporous Materials, 1998. **21**(1-3): p. 7-12.

3. Miller, S., *Personal Communication; Chevron Research and Technology Company.* 2005.

4. David, E., V. Stanciu, D. Stefanescu, and A.C. Nicolae, *Microstructure and properties of the sintered composites from zeolite 4A and magnesium oxide.* Journal of Materials Processing Technology, 2001. **119**(1-3): p. 288-292.

5. Napper, D.H., *Polymeric Stabilization of Colloidal Dispersions.* 1983. 428 pp.

APPENDIX A

MAKING OF HOLLOW FIBER MODULES

In order to test the gas permeation properties of hollow fiber membranes, a module analogous to a shell and tube exchanger is used. The module serves as the interface between the permeation system (gas cylinder, tubing, valves, etc.) and the polymeric membrane. The parts, procedure and notes for constructing a double-ended hollow-fiber module for laboratory-scale experiments provided below. This design has been used in a number of prior studies [1-3].

A.1. PARTS

The parts required to make hollow fiber modules are listed in Table A.1 below.

Table A.1: Hollow fiber module components

Name	Manufacturer	Notes
Ferrules	Swagelok	Brass or Stainless Steel
Nut	Swagelok	Brass or Stainless Steel
Female Adapter	Swagelok	Brass or Stainless Steel
Male Adapter	Swagelok	Brass or Stainless Steel
Tee	Swagelok	Brass or Stainless Steel
Metal Tubing	Swagelok	Brass or Stainless Steel
Cap	Swagelok	Brass or Stainless Steel
Plug	Swagelok	Brass or Stainless Steel
ID Tag		
Tygon® Tubing	Fisher	
Stycast 2651-40 Epoxy	Emerson & Cuming	This epoxy breaks cleaner
DP-100 ("5 min") Epoxy	3M	

A.2. PROCEDURE

Summary: Combining a number of Swagelok® parts depicted in Figure A.1, a "Blank" module without fibers is constructed.   Then, fibers are inserted into the module the ends are sealed Teflon tape and epoxy. Finally, the permeation testing is performed
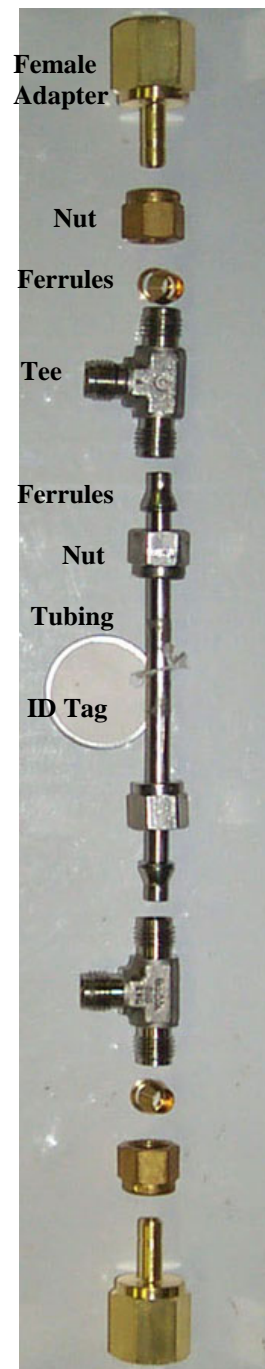
Figure A.1: Parts for a "Blank" Module

1. **The "Blank" Module**

    a. Stainless Steel (S.S.) Parts.

        i. An 11.5 – 15 cm piece of ¼" S.S. tubing is cut.

        ii. The sharp edges of the tubing are de-burred.

        iii. The ends of the tube are tested for burrs with a cotton Q-tip. This is an important step as any remaining burrs may ruin the delicate skin of the fibers as they are pulled through the module.

        iv. A S.S. nut, ferrule and tee are added to each end. Brass tees are acceptable, but the nut and ferrules should be S.S.

    b. Brass Parts

        i. A Brass nut and ferrule are attached to a Brass female ¼" NPT adapter.

        ii. The S.S. tee from step 1a(iv) is attached to the Brass nut on the female adapter.

        iii. Steps (i) and (ii) are repeated for the other end of the module. Both ends should be identical.

    c. An ID tag is attached to the S.S. tubing.

2. **Adding the Hollow Fibers.**

    a. Nominally 25 1-meter long hollow fibers are separated out from the main hank of fibers.

    b. The fibers are recounted as a check.

    c. A thin nylon fishing thread is looped around the middle of the 25 fibers. A 2ft piece of string is tied to the nylon loop.

    d. The string is slid through the Blank Module, gently pulling the fibers through as well. (NOTE: Be careful and slow while pulling the fibers through - they break easily.)

e. The fibers are arranged so that equal length sections extend from each end of the module. The ends of the fibers are taped together with Scotch tape so that they can easily be threaded through ¼" tubing.

3. **Sealing the Module.**

    a. A Teflon tape "worm" is packed into one of the Female Adapters and around the fibers. Care must be taken not to crush the fibers, yet still assure a good seal between the fibers and the brass wall of the female adapter. (A "worm" is a 5-cm long roll made up of ~16-20 layers of Teflon tape. It looks like a small joint.)

    b. A 2-cm piece of Tygon® Tubing (ID: 3/16") is placed onto a Brass Male ¼" NPT Adapter.

    c. A 1:1 ratio of the 3M DP-100 epoxy Hardener and Resin is added into the Brass Female Adapter using a mixing nozzle, filling the adapter slightly beyond the top. (Stycast brand epoxy may be used as well, see footnote.)

    d. The fibers are slid the Brass Male Adapter and Tygon® tubing piece. The Male Adapter is screwed into the Female Adapter until the epoxy fills the Tygon® tubing piece.

    e. After a 10 minute wait for the epoxy to harden, the module is flipped over and the steps 3a - 3d repeated for the other end of the module.

4. **Final Steps before Permeation Testing**

    a. Once the epoxy has fully cured (~30 minutes after mixing for the GC Electronics '5 minute' epoxy.), the Tygon® tubing piece is broken by tapping it on the countertop. The fibers should be all open, with an encapsulating seal of epoxy around them. Note that a longer wait of 8-24

hrs is preferred before breaking the Tygon® piece as the epoxy hardens further and a cleaner break (more open bores) is achieved.

b. A Brass nut and ferrule are placed on the Male Adapter on each end of the module.

c. A Plug is placed into one end of the module, a Cap on the nearest Tee fitting, and a Port connecter on the furthest Tee fitting.

A.3. NOTES

Type of Epoxy: The GC Electronics **'5 minute' epoxy** may be used for general purpose modules. It is easy to use, inexpensive and cures quickly (within 30 minutes). For a more durable seal, you may use **Stycast®** 2651 from Emerson & Cuming, Billerica, MA. Stycast has excellent adhesion to a wide range of substrates, lower viscosity to fully encapsulate the fibers, high tensile strength (> 6500 psi) after curing for high-pressure applications and a high upper temperature tolerance (130°C). However, Stycast requires 24 hrs to cure at room temperature, is somewhat more difficult to use/mix, and is slightly more expensive.

A.4. REFERENCES

1.   Djoekita, G., D.Q. Vu, and W.J. Koros, *Pervaporative introduction of organic vapors into high-pressure gas feeds.* Journal of Applied Polymer Science, 2001. **80**(2): p. 311-315.

2.   Carruthers, S.B., *Integral-skin formation in hollow fiber membranes for gas separations*. 2001. p. 233 pp.

3.   Wallace, D.W., *Crosslinked hollow fiber membranes for natural gas purification and their manufacture from novel polymers*. 2004. p. 221 pp.

APPENDIX B

PERMEATION TESTING OF HOLLOW FIBER MODULES

This appendix includes the procedures used in this work for pure and mixed gas testing. All tests are run in a temperature-controlled 'black-box'.

B.1. PURE GAS PERMEATION TESTING – BUBBLE FLOW METER [1, 2]

B.1.1. Setup

The shell and tube configuration of the testing module allows feed gas to be applied either at the bore side or the shell side. The selection of bore versus shell side feed depends on the requirements of the experiment. Hollow fibers are typically able to withstand up to two to four times the shell side pressure than bode side pressure before failure. However, feed bypass can occur in shell side flows and can result in dubious results in mixed gas testing. Additionally, for high flux gases, pressure drop within the bore must be taken into account for shell-side feeds.

Swagelok fittings (Union Crosses and Female-Female Unions) are used to attach the feed inlet of the modules to the feed gas port in the permeation system. A pressure transducer is attached inline to read pressure of the feed gas.

B.1.2. System Purge

1. The pressure transducer is zeroed.
2. The Retentate outlet on all the modules is opened. (Only *Slightly* open if Shell Feeding)

3. The gas cylinder is opened and the entire system is pressurized slowly pressurized. Care must be taken not to "shock" the membranes with a high pressure feed.

    a. Gas should be flowing through the entire system and exiting through the retentate of each module.

    b. The gas is allowed to flow for at least 5 seconds to purge the system.

4. The regulator valve is dialed down.

    a. The pressure should slowly drop in the system.

5. The regulator valve is gradually opened

6. Steps 4 and 5 are repeated <u>three more times</u>.

    a. The entire system has been purged, or 'rinsed', a total of four times with 'clean gas'.

7. The retentate of each module is closed.

8. The feed pressure is adjusted as desired, and the permeation system allowed to equilibrate to testing temperature.

9. After 15 minutes or more, the permeation flow rates and inner box temperature should equilibrate. However, data collection is usually begun 45 minutes after the start of permeation.

B.1.3. Testing

1. *(0-45 minutes)* During the 45 min. equilibration, the following steps are performed:

    a. The active length and number of fibers in each module is recorded

    b. Wet the bubble flowmeter.

2. *(> 45 minutes)* Each module's permeate flowrate is measured using a bubble flowmeter.

   a. The bubble is allowed to travel for at least 15 seconds, and preferably an easily measured distance.

      i. GOOD--10.00 mL in 17.67 seconds

      ii. GOOD--200 mL in 31.27 sec

      iii. BAD--10.00 mL in 11.21 seconds (too short, too much error).

   b. Smallest measurable flowrate is ~ 0.5 mL / minute.

   c. Electronic Flowmeters do NOT seem to be as accurate or precise at low flowrates (< 100 ml/min). A Bubble Flowmeter should be used.

   d. Record the Feed Pressure for each flowrate measurement.

3. *(> 45 minutes)* Test the modules *again* 45 min after equilibration (1 hr after pressurization).

   a. If there's greater than a **5%** difference between the '45 minute measurement' and the '15 min measurement', wait another 45 minutes and measure a 3rd time.

   b. Keep testing until there is less than a **5%** change over 45 minutes. Only 2 measurements are generally necessary if the system was purged well.

4. Permeances and selectivities for the membranes are calculated. The modules are retested as desired.

5. All cylinder valves are closed, and the pressure transducer turned off.

B.1.4. Analysis

1. Permeance

   a. The equation shown here results in units of GPU. Constants in the equation convert common measurement units to those required for GPU.

   b. $P_A = 10^{-6} \dfrac{(\text{Permeate flow}) \cdot 273.15}{T \cdot A \cdot \Delta p \cdot 5.17}$

      i. Permeate flow is in mL/sec.

      ii. T is the testing temperature in Kelvin.

      iii. A is the area available for permeation in cm^2.

      iv. Δp is the pressure drop between upstream and downstream sides of the membrane in psi.

2. Ideal selectivity

   a. $\alpha_{A/B} = \dfrac{P_A}{P_B}$

B.2. PURE GAS TESTING - ISOCHORIC (CONSTANT-VOLUME, VARIABLE PRESSURE) TECHNIQUE [3]

The permeance of a given gas and the selectivities for gas pairs are determined using the standard isochoric (constant-volume, variable pressure) technique [4-6]. In this technique the steady-state increase in the permeate pressure is directly proportional to the permeance:

$$ P_A/L = 193375 \frac{dp/dt \, V_D}{TAP_{up}}, \tag{B.1} $$

where

$$\frac{dp}{dt} = \text{permeate pressure rise} \left[=\right] \text{torr/sec}$$

$$V_D = \text{downstream volume} \left[=\right] \text{cm}^3$$

$$T = \text{temperature} \left[=\right] \text{K}$$

$$A = \text{membrane surface area} \left[=\right] \text{cm}^2$$

$$P_{up} = \text{upstream pressure} \left[=\right] \text{psia}$$

.

Prior to permeation testing, the asymmetric hollow fibers must be potted into a testable module. The details of the module making process are standardized and are described in Appendix A. The completed membrane module is loaded into the permeation apparatus diagrammed schematically in Figure B.1. A measurement is taken by first evacuating the upstream and downstream faces of the membrane overnight to remove any sorbed gases from the membrane. After evacuation, the upstream pressure may be increased to the desired pressure with the gas of interest. A period of 30 minutes is given to allow for permeation through the membrane to reach steady state. Due to the thin skin thickness of asymmetric hollow fibers, the diffusive time lag to reach steady state is less than 5 minutes. After steady state is reached, the downstream vacuum valve is closed and the pressure rise in the downstream volume is monitored with a MKS pressure transducer.
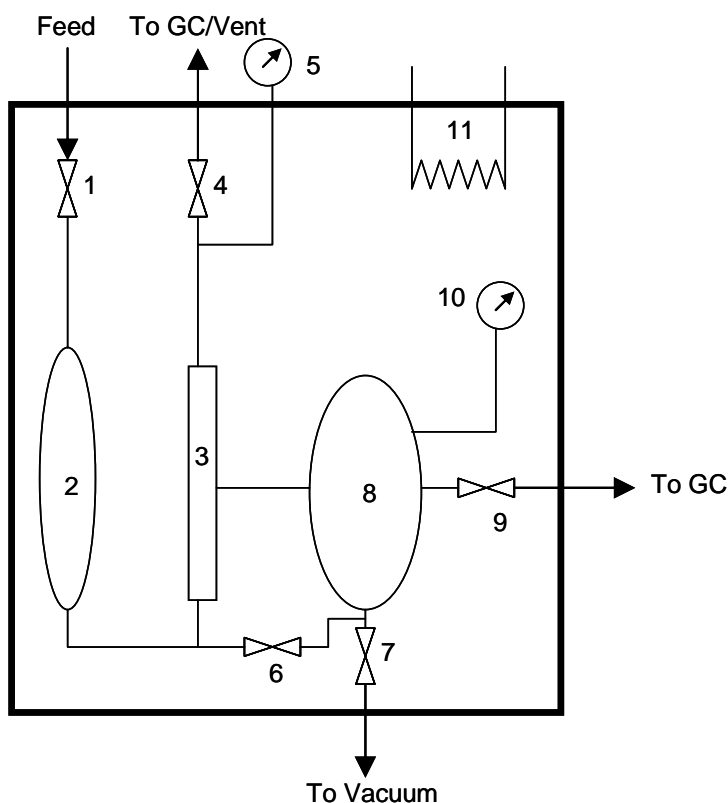
Figure B.1: Schematic of pressure-rise permeation apparatus. 1. Feed Shutoff Valve, 2. Upstream Ballast, 3. Membrane Module, 4. Retentate Metering Valve, 5. Upstream Pressure Transducer, 6. Bypass Valve, 7. Vacuum Valve, 8. Downstream Volume, 9. GC Valve, 10. Downstream Pressure Transducer, 11. Thermostated Heat Tape

The upstream pressure is monitored using a 1000 psia Sensotec SC Series pressure transducer. The pressure in the downstream volume is measured using a 1000 torr MKS Baratron® (Type 127) pressure transducer. The output from the downstream pressure transducer is interfaced with a personal computer using LabView® data acquisition software to allow for real-time data recording. The entire permeation system is maintained to within ± 0.1 °C using a proportional controller (Cole Parmer Catalog No. BA-2155-54).

B.3.   MIXED GAS PERMEATION TESTING [2]

B.3.1.   Gas Chromatograph Set-up

1. The helium gas is turned on and the regulator set to 50 psi

2. Using knobs on the gas chromatograph (GC), flowrate is adjusted from both columns to equal 30 mL/min

3. The GC is switched on and column temperature set to 65 ºC. (WARNING: DO NOT turn on the GC without helium running through the columns. The columns may not survive.)

4. The Bridge Setting knob is set to "Thermistor", the Output knob to "1024", and the Readout knob to "Left Column"

5. The integrator is turned on, and date and time entered at prompts.

6. After a few minutes, the "level" button on the integrator is pushed. The level should be 1000 after the system has had time to warm up. The coarse and fine adjustment knobs are used to set the level to 1000. The "level" button is pressed after each adjustment to see the effect. If no number prints, the GC needs some more time to warm up. The system will likely take 1-3 hours to stabilize enough to take a reading.

B.3.2. Module Set-up

Note: This set-up assumes only one module is being tested.

1. Modules can be set up in either bore or shell fed configurations. It is checked that the modules are operating in counter-current flow (retentate and permeate taken from different ends of the module).

2. The feed line is attached to the module.

3. At the retentate exit, fine control needle valve is attached

4. The permeate side closest to the retentate exit is caped.

5. A T-valve is attached to the permeate side closest to the feed. One exit from the valve leads to the GC, the other to a flowmeter.

6. The module is purged in the same way as in pure gas testing (this is made easier by the existence of the retentate valve).

7. The retentate valve is set to the desired flowrate (higher retentate flowrates = lower stage cuts = higher selectivity).

8. The permeate is directed to the GC and the GC sampling valve is placed in the "Load" position.

B.3.3. Testing

1. After at least 45 minutes of equilibration after the GC has completely warmed up and the gas has been flowing, data can be collected.

2. The level on the integrator is pressed and adjusted to 1000.

3. The GC sample valve is set to "Inject" and "Inj A" pressed on the integrator. These are done simultaneously.

4. The GC is now independent of the module. The permeate T-valve is turned to the flowmeters.

5. The following are measured and recorded

    a. Module ID

    b. Feed composition

    c. Feed pressure

    d. Retentate flow

    e. Retentate pressure (normally atmospheric)

    f. Permeate flow

g. Permeate pressure (normally atmospheric)

h. Module temperature

6. When all peaks have eluted, "Inj A" is pressed on the integrator again to stop the run.

7. The sample valve is turned back to "Load" position and the permeate T-valve back to the GC.

8. After 45 minutes and steps 2-7 are repeated. The measurements are repeated three to five times for reproducibility.

B.3.4. Calibration

1. Calibration is done external to the gas chromatograph (GC)

2. The calibration tests are run in the same way as shown above, eliminating the module. Calibration gases are directly piped to the GC, and after equilibration, sample is taken (steps 3 and 6 from "Testing Procedure")

3. At least three injections of each calibration gas are performed to certify reproducibility.

4. The correct retention time for each gas is obtained. This can be checked by injecting pure gas samples.

5. Once 3-5 calibration gases have been run, the data is used to construct a calibration curve, composition on one axis and GC area percentage on the other.

B.3.5. Analysis

1. The area percentages from the GC are used to determine mixture composition using the calibration curve.

2. Permeance

a. The permeance equation given here is in units of GPU. The constants in the equation are used to convert commonly measured units to those required for GPU.

b. $P_A = 10^{-6} \dfrac{(\text{Permeate flow}) \cdot Y_A \cdot 273.15}{T \cdot A \cdot (p_X \cdot X_A - p_Y \cdot Y_A) \cdot 5.17}$

    i. Permeate flow is in mL/sec.

    ii. Y_A is the permeate mole fraction.

    iii. X_A is the upstream mole fraction. With a small stage cut (large retentate flow), X_A is essentially equal to the feed composition.

    iv. T is the measurement temperature in Kelvin.

    v. A is the area available for permeation in cm^2.

    vi. p_X and p_Y are the upstream and downstream total pressures, respectively (psi).

3. Separation Factor

a. $SF_{A/B} = \dfrac{Y_A}{Y_B} \cdot \dfrac{X_B}{X_A}$

    i. Y_A and Y_B are the permeate mole fractions

    ii. X_A and X_B are the upstream mole fractions. With a small stage cut (large retentate flow), X_A and X_B are essentially equal to the feed mole fractions.

4. Intrinsic Selectivity

a. Fugacity coefficients can be obtained from the literature. They are often 1 or nearly so, in which case they can be dropped from the calculation.

b. $\alpha_{A/B} = \dfrac{Y_A}{Y_B} \cdot \left[\dfrac{p_X X_B - p_Y Y_B}{p_X X_A - p_Y Y_A} \right] \cdot \left(\dfrac{\phi_{YB}}{\phi_{YA}} \cdot \dfrac{\phi_{XA}}{\phi_{XB}} \right)$

i. Y_A and Y_B are the permeate mole fractions

ii. X_A and X_B are the upstream mole fractions. With a small stage cut (large retentate flow), X_A and X_B are essentially equal to the feed mole fractions.

iii. p_X and p_Y are the upstream and downstream pressures, respectively.

iv. ϕ is the fugacity coefficient. Subscripts represent upstream (X) or downstream (Y) and component (A or B).

B.4. REFERENCES

1.   Carruthers, S.B., *Integral Skin Formation in Hollow Fiber Membranes for Gas Separations*, in *Chemical Engineering*. 2001, University of Texas--Austin: Austin, TX. p. 233.

2.   Wallace, D.W., *Crosslinked hollow fiber membranes for natural gas purification and their manufacture from novel polymers*, in *Chemical Engineering*. 2004, University of Texas--Austin. p. 221 pp.

3.   Madden, W.C., *The Performance of Hollow Fiber Gas Separation Membranes in the Presence of an Aggressive Feed Stream*, in *Chemical Engineering*. 2005, Georgia Institute of Technology: Atlanta. p. 219.

4.   O'Brien, K.C., W.J. Koros, T.A. Barbari, and E.S. Sanders, *A new technique for the measurement of multicomponent gas transport through polymeric films.* J. Membr. Sci., 1986. **29**(3): p. 229-38.

5.   Pye, D.G., H.H. Hoehn, and M. Panar, *Measurement of gas permeability of polymers. I. Permeabilities in constant volume/variable pressure apparatus.* J. Appl. Polym. Sci., 1976. **20**(7): p. 1921-31.

6.   Moore, T.T., S. Damle, P.J. Williams, and W.J. Koros, *Characterization of low permeability gas separation membranes and barrier materials; design and operation considerations.* Journal of Membrane Science, 2004. **245**(1-2): p. 227-231.

APPENDIX C

RHEOLOGICAL TESTING OF MIXED MATRIX DOPES

C.1. INTRODUCTION

Stringent dispersion stability and homogeneity is required for hollow fiber spinning. The presence of any agglomerates or flocs (loose aggregates of particles) within the dope mixture would result in extremely high pressure drops in the filter before the spinneret and in the spinneret itself. Additionally, the dopes are sheared considerably within the spinneret (~1000 – 3000 s^{-1}) and formation of particle aggregates under shear is also a possibility [1].

Rheology can be used to probe the effect of particles on mixed matrix dope flow behavior. The rheological performance of four dope solutions is discussed as follows:

1) Ultem®-Ultem® with Grignard treated (GT) SSZ-13 – MMX1

2) Ultem®-Ultem® with Ultem® sized SSZ-13– MMX2

3) Ultem®-Ultem® with Thionyl Chloride (TC) only SSZ-13 – MMX3

4) Ultem®-Ultem® with Grignard treated (GT) zeolite 4A – MMX4

As a baseline, equivalent polymer-only compositions (designated MMX1-PO, MMX2-PO…) to the above mixed matrix dopes (MMX1-MMX4) were also tested. The polymer and solvency power (ratio of solvents and nonsolvents) were kept constant between the mixed matrix and its equivalent polymer-only dopes. The compositions and characterization of the polymer-zeolite adhesion as viewed by scanning electron microscopy (SEM) for the mixed matrix dopes is provided in Table C.1.

Table C.1: Composition and polymer-zeolite bonding characterization for mixed matrix dopes tested by rheology

	MMX-1	MMX-2	MMX-3	MMX-4
Ultem	28.2	28.3	27.3	29.0
N-methyl-2-pyrrolidione	49.9	49.5	48.3	48.9
Tetrahydrofuran	17.1	17.1	18.7	17.9
Lithium Nitrate	1.00	0.99	1.03	1.03
Zeolite (wt % w.r.t total dope)	3.80	4.19	4.64	3.15
Zeolite (vol % w.r.t total dope)	2.67%	2.95%	3.26%	2.22%
Zeolite (vol % w.r.t. polymer)	10.3	10.5	11.8	8.4
Sieve/insert	GT SSZ-13	Ultem "sized" SSZ-13	TC SSZ-13	GT 4A
SEM - polymer-insert bonding	Good	Poor	Poor	Good

GT = Grignard treated; TC = only thionyl chloride treated

C.2. TESTING PROCEDURE

The rheological testing was carried out by Ryan Collins in Dr. Breedveld's laboratory. Not all the data from the tests are discussed here, however, the entire testing procedure is provided to show sample history.

1. Warm up period – This three minute interval ensures that the sample is at temperature (20°C) and measurement can begin

2. Viscosity meas. – Rotational measurement. Sample is sheared at a rate from 0.1 s^{-1} to 100 s^{1}, and viscosity is measured. The lower bound is set by the

192

sensitivity of the instrument, and the upper bound is set by the maximum torque the instrument can provide.

3. Viscosity meas. – Same as above, except interval is from 100 s^{-1} to 0.1 s^{-1}.

4. Heating period – During this 7.5 minute interval, the sample is heated to 50 ^{o}C.

5. Strain Sweep – Sample is strained from a value of 1E^{-3} to a value of 10 at a constant frequency of 1 Hz. This range starts near the sensitivity limit of the instrument and goes through the range of all interesting effects. A frequency of 1 Hz allows for good resolution of data, and any higher would start to introduce inertial effects.

6. Viscosity meas. – Same as (2) except the experiment is being run at 50 ^{o}C.

7. Viscosity meas. – Same as (3) except the experiment is being run at 50 ^{o}C.

8. High shearing – During this 30 minute interval, the sample is sheared at a constant rate of 100 s^{-1}.

9. Strain Sweep – The strain sweep in step (5) is repeated. Data obtained from interval (5) vs. interval (9) give information about how the structure has changed after the viscosity measurements, and the 30 minute shear interval.

10. Freq. Sweep – Sample was strained at a constant value of 0.03, with frequencies ranging from 0.1 Hz to 100 Hz. The lower bound is set by instrument sensitivity and the range cover all useful results.

C.3. VISCOSITY AS A FUNCTION OF SHEAR RATE

The change in viscosity of the mixed matrix dopes with shear rate is shown in Figure C.1.

As can be seen from the data, there is significant shear thinning (decrease in viscosity with increasing shear rate) for MMX3 (TC SSZ-13) and MMX1 (Ultem "sized" zeolites) dopes in the low shear rate (0.1-10 1/s) range at 20 ℃. The dopes containing Grignard treated zeolites, MMX2 and MMX4 show a constant viscosity with shear rate in the same range.
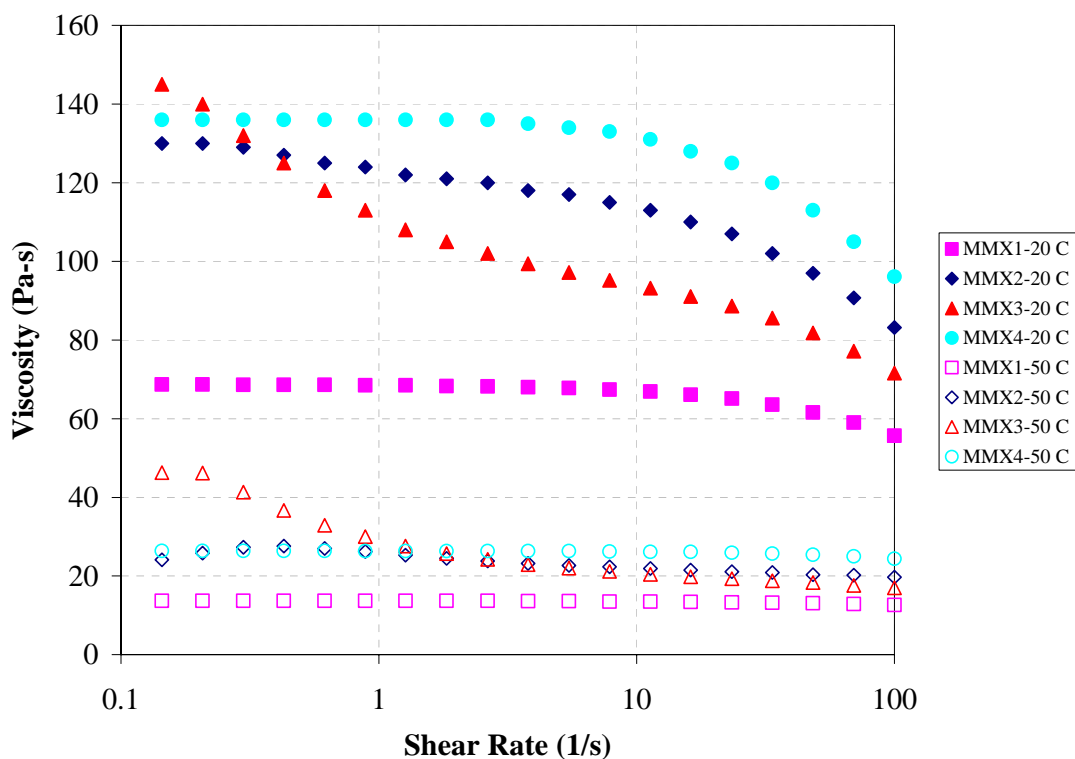

Figure C.1: Viscosity of mixed matrix dopes as a function of shear rate at 20 ℃ and 50 ℃. MMX1 - Ultem®-Ultem® with Grignard treated (GT) SSZ-13, MMX2 - Ultem®-Ultem® with Ultem® sized SSZ-13, MMX3 - Ultem®-Ultem® with Thionyl Chloride (TC) only SSZ-13, MMX4 - Ultem®-Ultem® with Grignard treated (GT) zeolite 4A

C.4. RELATIVE VISCOSITIES

The relative viscosity is the ratio of the mixed matrix dope viscosity to the polymer-only dope equivalent. This ratio provides information of the effect of the particle addition on the dope viscosity. As can be seen from the results shown in Figure C.2, the results deviate significantly from Einstein's prediction for the effective viscosity of a suspension of non-interacting particles [2], given below;

$$\eta = \mu(1 + \frac{5}{2}\varphi) \tag{C.1}$$

where μ is the viscosity of the medium and φ is the particle volume fraction. For volume percent of the particles, varying from 2.2 – 3.3 vol % (Table C.1), Einstein's equation predicts viscosity increase of only 5.5 – 8 % for the suspension versus the original medium. Considerably different results are seen for the mixed matrix dopes, with viscosity increasing by a *minimum of 200 %* for the 4 mixed matrix dopes tested.

The primary mechanism for such increase in viscosity is believed to be due to the formation of particle flocs/aggregates, with highly aggregated mixed matrix dopes displaying greater relative viscosity and higher shear thinning. These dopes when spun as asymmetric hollow fiber membranes, show differences in polymer-sieve adhesion as viewed by SEM microscopy. Sample SEM micrographs of the polymer-sieve adhesion in the skin region (300 – 500 nm) of hollow fibers incorporating MMX1 – MMX4 sheath dopes are shown in Figure C3. Poor polymer-sieve bonding is observed for the MMX2 (B in Figure C.3) and MMX3 (C in Figure C.3).

Correspondingly, a lower relative viscosity is found to correlate to an apparent good polymer-zeolite interface. This observation would permit rheological testing to be used to screen mixed matrix dopes before the actual spinning process to estimate the homogeneity of the dispersion and predict aggregation levels in the mixed matrix dopes.
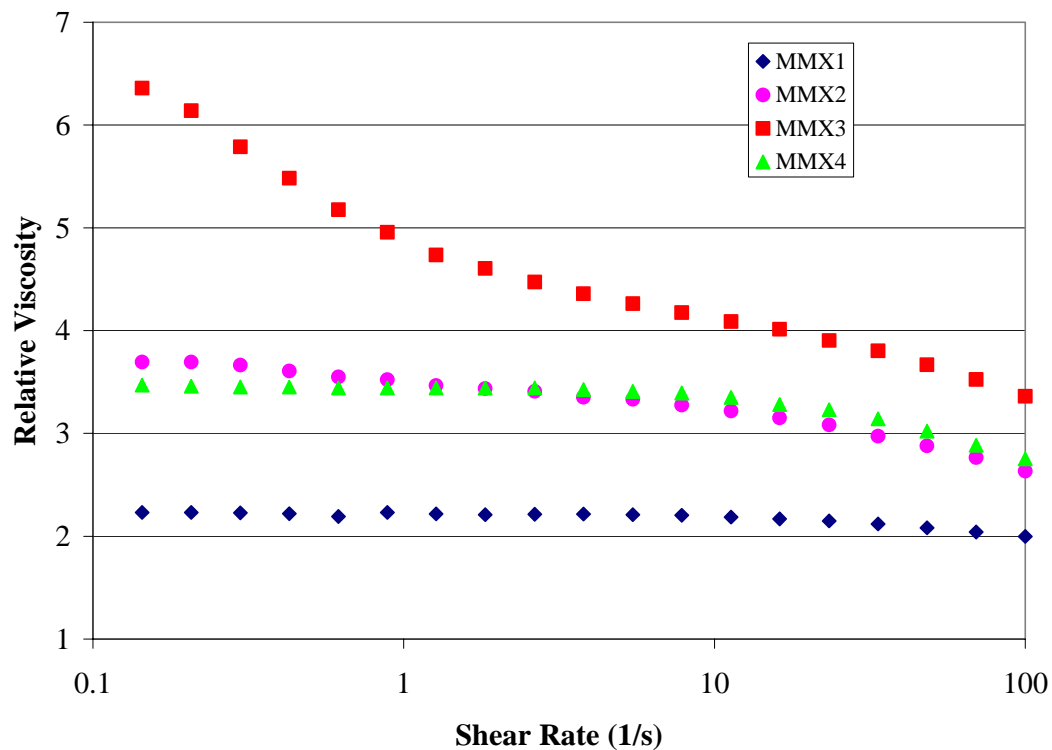
Figure C.2: Relative viscosities of mixed matrix dopes with respect to their polymer-only equivalents. MMX1 - Ultem®-Ultem® with Grignard treated (GT) SSZ-13, MMX2 - Ultem®-Ultem® with Ultem® sized SSZ-13, MMX3 - Ultem®-Ultem® with Thionyl Chloride (TC) only SSZ-13, MMX4 - Ultem®-Ultem® with Grignard treated (GT) zeolite 4A
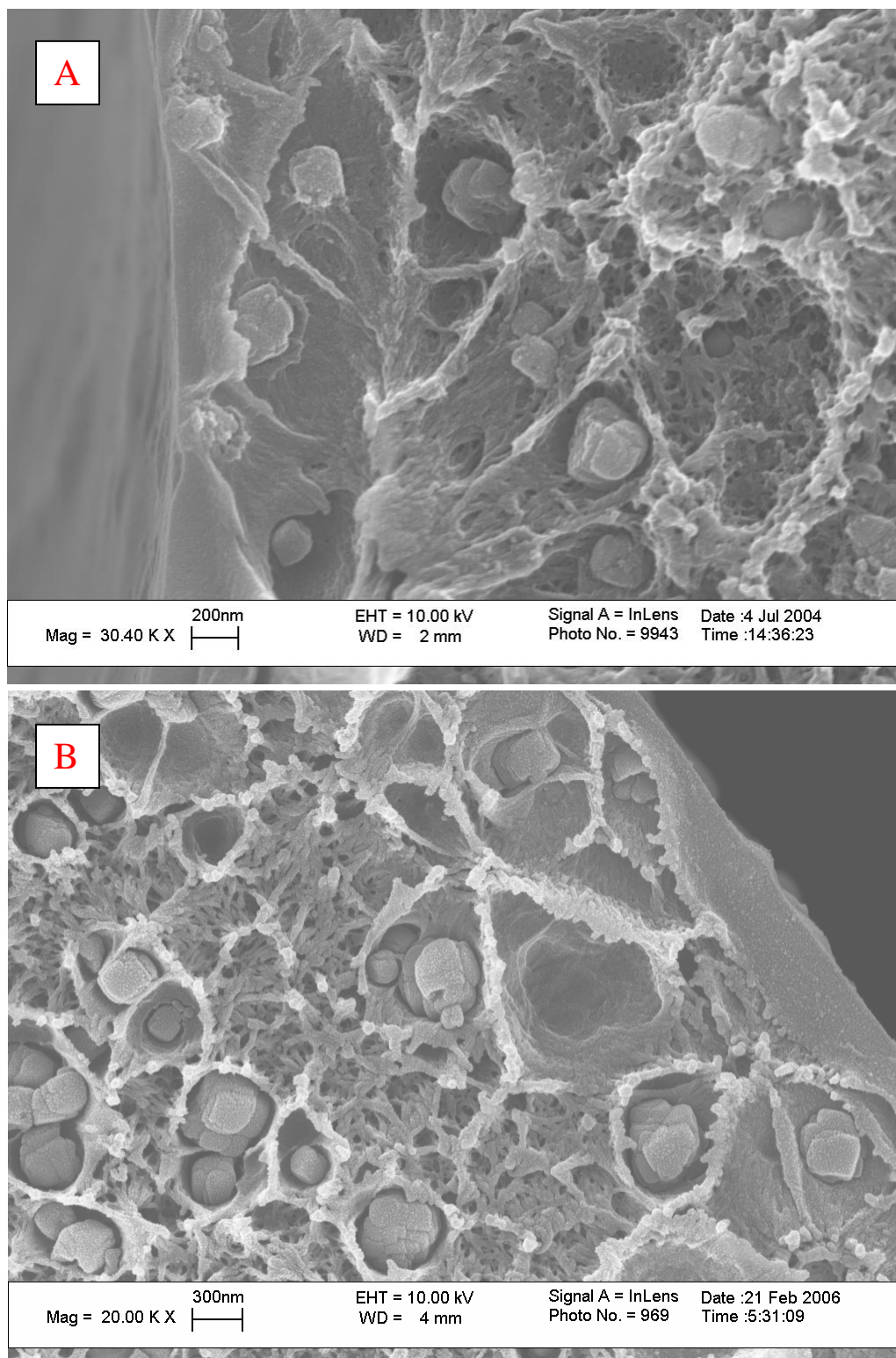
Figure C.3: SEM micrographs of the skin region of the mixed matrix Ultem®-Ultem® hollow fiber membranes incorporating, (A) Grignard treated (GT) SSZ-13 (MMX1), (B) Ultem® sized SSZ-13 (MMX2), (C) Thionyl Chloride (TC) only SSZ-13 (MMX3), (D) Grignard treated (GT) zeolite 4A (MMX4)
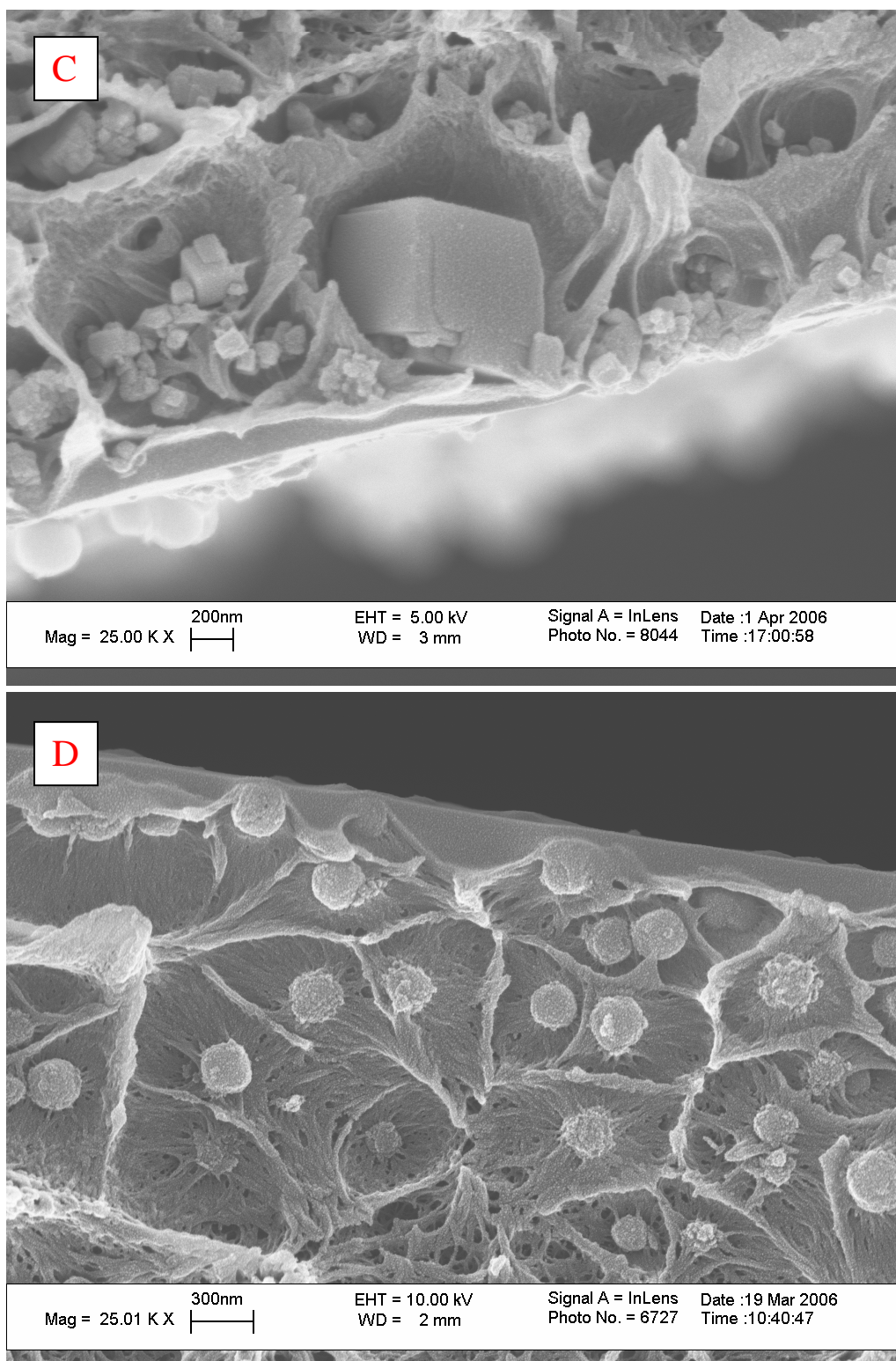
Figure C.3: SEM micrographs of the skin region of the mixed matrix Ultem®-Ultem® hollow fiber membranes incorporating, (A) Grignard treated (GT) SSZ-13 (MMX1), (B) Ultem® sized SSZ-13 (MMX2), (C) Thionyl Chloride (TC) only SSZ-13 (MMX3), (D) Grignard treated (GT) zeolite 4A (MMX4)

C.5. REFERENCES

1.   Kulkarni, S.S., *Personal Communication, Medal L.P / Air Liquide*. 2003.

2.   Einstein, A., *Eine neue Bestimmumng der Molekudimensionen.* Annalen der Physik (Weinheim, Germany), 1906. **19**: p. 289-306.

BIBLIOGRAPHY

(1997). Ultem Product Data Sheet. Pittsfield, MA, GE Plastics.

(2000). Matrimid Product Data Sheet. Brewster, NY, Vantico, Inc.

Albers, W. and J. T. G. Overbeek (1959). "Stability of emulsions of water in oil. II. Charge as a factor of stabilization against flocculation." Journal of Colloid Science **14**: 510-18.

Albrecht, W., T. Weigel, et al. (2001). "Formation of hollow fiber membranes from poly(ether imide) at wet phase inversion using binary mixtures of solvents for the preparation of the dope." Journal of Membrane Science **192**(1-2): 217-230.

Altena, F. W. and C. A. Smolders (1982). "Calculation of liquid-liquid phase separation in a ternary system of a polymer in a mixture of a solvent and a nonsolvent." Macromolecules **15**(6): 1491-7.

Baker, R. "Future directions of membrane gas-separation technology." Membrane Technology(138): 5-10.

Baker, R. W. (2002). "Future Directions of Membrane Gas Separation Technology." Industrial & Engineering Chemistry Research **41**(6): 1393-1411.

Baker, R. W. (2004). Membrane Technology and Applications, John Wiley & Sons, Ltd.

Ballard, C. C., E. C. Broge, et al. (1961). "Esterification of the surface of amorphous silica." Journal of Physical Chemistry **65**: 20-5.

Bansal, A., X. Li, et al. (1996). "Alkylation of Si Surfaces Using a Two-Step Halogenation/Grignard Route." Journal of the American Chemical Society **118**(30): 7225-7226.

Bansal, A., X. Li, et al. (2001). "Spectroscopic studies of the modification of crystalline Si(111) surfaces with covalently-attached alkyl chains using a chlorination/alkylation method." Journal of Physical Chemistry B **105**(42): 10266-10277.

Barbari, T. A., W. J. Koros, et al. (1989). "Polymeric membranes based on bisphenol A for gas separations." Journal of Membrane Science **42**(1-2): 69-86.

Barrer, R. M. (1968). Diffusion and permeation in heterogeneous media. Diffusion in polymers. J. Crank and G. S. Park. New York, Academic Press**:** 165-217.

Barton, A. F. M. (1983). <u>CRC Handbook of Solubility Parameters and Other Cohesion Parameters</u>. Boca Raton, FL, CRC Press Inc.

Bicerano, J., J. F. Douglas, et al. (1999). "Model for the viscosity of particle dispersions." <u>Journal of Macromolecular Science, Reviews in Macromolecular Chemistry and Physics</u> **C39**(4): 561-642.

Bloch, R. and M. A. Frommer (1970). "The mechanism for formation of "skinned" membranes I. Structure and properties of membranes cast from binary solutions." <u>Desalination</u> **7**(2): 259-264.

Boom, R. M. (1992). Membrane formation by immersion precipitation: the role of the polymeric additive, University of Twente, The Netherland.

Boom, R. M., I. M. Wienk, et al. (1992). "Microstructures in phase inversion membranes. Part 2. The role of a polymeric additive." <u>Journal of Membrane Science</u> **73**(2-3): 277-92.

Bordiga, S., L. Regli, et al. (2005). "Assessing the Acidity of High Silica Chabazite H-SSZ-13 by FTIR Using CO as Molecular Probe: Comparison with H-SAPO-34." <u>Journal of Physical Chemistry B</u> **109**(7): 2779-2784.

Breck, D. W. (1974). <u>Zeolite Molecular Sieves: Structure, Chemistry, and Use</u>. Malabar, FL, Robert E. Krieger Publishing Co, Inc.

Bruggemann, D. A. G. (1935). "Berechnung verschiedener physikalischer Konstanten von heterogenen Substanzen. I. Dielektrizitatskonstanten und Leitfahigkeiten der Mischkorper aus isotropen Substanzen (The calculation of various physical constants of hetereogeneous substances. I. The dielectric constants and conductivities of mixtures composed of isotropic substances." <u>Annalen der Physik V</u> **24**: 636.

Cabasso, I., E. Klein, et al. (1976). "Polysulfone hollow fibers. I. Spinning and properties." <u>Journal of Applied Polymer Science</u> **20**(9): 2377-94.

Cabasso, I., E. Klein, et al. (1977). "Polysulfone hollow fibers. II. Morphology." <u>Journal of Applied Polymer Science</u> **21**(1): 165-80.

Callister, W. D. (1996). <u>Materials Science and Engineering: An Introduction,</u>, John Wiley & Sons.

Carruthers, S. B. (2001). Integral Skin Formation in Hollow Fiber Membranes for Gas Separations. <u>Chemical Engineering</u>. Austin, TX, University of Texas--Austin**:** 233.

Carruthers, S. B. (2001). Integral-skin formation in hollow fiber membranes for gas separations**:** 233 pp.

Carruthers, S. B., G. L. Ramos, et al. (2003). "Morphology of integral-skin layers in hollow-fiber gas-separation membranes." Journal of Applied Polymer Science **90**(2): 399-411.

Carter, W. B. (2006). Personal Communication, Department of Material Science and Engineering, Georgia Institute of Technology.

Chern, R. T., W. J. Koros, et al. (1984). "Selective permeation of carbon dioxide and methane through Kapton polyimide: effects of penetrant competition and gas-phase nonideality." Journal of Polymer Science, Polymer Physics Edition **22**(6): 1061-84.

Chinn, D. (2004). Personal communication. Chevron Corp.

Chung, T.-S. and X. Hu (1997). "Effect of air-gap distance on the morphology and thermal properties of polyethersulfone hollow fibers." Journal of Applied Polymer Science **66**(6): 1067-1077.

Clausi, D. T., S. A. McKelvey, et al. (1999). "Characterization of substructure resistance in asymmetric gas separation membranes." Journal of Membrane Science **160**(1): 51-64.

Cohen Addad, J. P. and P. Panine (1999). "Pore generation in asymmetric polymeric membranes. Correlation with solvent mobilities." Polymer Bulletin (Berlin) **42**(3): 345-352.

Cohen, C., G. B. Tanny, et al. (1979). "Diffusion-controlled formation of porous structures in ternary polymer systems." Journal of Polymer Science, Polymer Physics Edition **17**(3): 477-89.

Cornelius, C., C. Hibshman, et al. (2001). "Hybrid organic-inorganic membranes." Separation and Purification Technology **25**(1-3): 181-193.

David, E., V. Stanciu, et al. (2001). "Microstructure and properties of the sintered composites from zeolite 4A and magnesium oxide." Journal of Materials Processing Technology **119**(1-3): 288-292.

Djoekita, G., D. Q. Vu, et al. (2001). "Pervaporative introduction of organic vapors into high-pressure gas feeds." Journal of Applied Polymer Science **80**(2): 311-315.

Doktycz, S. J. and K. S. Suslick (1990). "Interparticle collisions driven by ultrasound." Science (Washington, DC, United States) **247**(4946): 1067-9.

Dunning, W. J. (1955). Theory of crystal nucleation from vapor, liquid, and solid systems. Chemistry of the Solid State. W. E. Garner. London, Butterworths Publication Ltd**:** 159-83.

Duval, J. M., A. J. B. Kemperman, et al. (1994). "Preparation of zeolite filled glassy polymer membranes." Journal of Applied Polymer Science **54**(4): 409-18.

Einstein, A. (1906). "Eine neue Bestimmumng der Molekudimensionen." Annalen der Physik (Weinheim, Germany) **19**: 289-306.

Ekiner, O. M., R. A. Hayes, et al. (1989). Reactive posttreatment for gas separation membranes. Application: US, (du Pont de Nemours, E. I., and Co., USA). 7 pp.

Ekiner, O. M. and S. S. Kulkarni (2003). Process for making hollow fiber mixed matrix membranes. United States, L' Air Liquide Societe Anonyme a Directoire et Conseil de Surveillance pour l'Etude et l'Exploitation des Procedes Georges Claude.

Ekiner, O. M. and S. S. Kulkarni (2003). Process for making mixed matrix hollow fiber membranes for gas separation. US 6,663,805, (L'Air Liquide Societe Anonyme A Directoire Et Conseil De Surveillance Pour L'etude Et L'exploitation Des Procedes Georges Claude, Fr.).

Ekiner, O. M. and G. Vassilatos (1990). "Polyaramide hollow fibers for hydrogen/methane separation - spinning and properties." J. Membr. Sci. **53**(3): 259-73.

Ekiner, O. M. and G. Vassilatos (2001). "Polyaramide hollow fibers for H2/CH4 separation II. Spinning and properties." Journal of Membrane Science **186**(1): 71-84.

Ekiner, O. M. and G. Vassilatos (2002). "Polyaramide hollow fiber membranes for gas separation-spinning and properties." Polymeric Materials Science and Engineering **86**: 120.

Ershova, G. F., Z. M. Zorin, et al. (1975). "Temperature dependence of the thickness of polymolecular adsorption films of water on quartz surfaces." Kolloidnyi Zhurnal **37**(1): 208-10.

Fejes, P., I. Kiricsi, et al. (1980). "A novel method for the dealumination of zeolites." Reaction Kinetics and Catalysis Letters **14**(4): 481-8.

Fowkes, F. M. and M. A. Mostafa (1978). "Acid-base interactions in polymer adsorption." Ind. Eng. Chem. Prod. Res. Dev. **17**(1): 3-7.

Fritzsche, A. K., C. A. Cruse, et al. (1990). "Polysulfone hollow-fiber membranes spun from Lewis acid:base complexes. II. The effect of Lewis acid-to-base ratio on membrane structure." Journal of Applied Polymer Science **39**(9): 1949-56.

Frommer, M. A., I. Feiner, et al. (1970). "The mechanism for formation of "skinned" membranes : II. Equilibrium properties and osmotic flows determining membrane structure." Desalination **7**(3): 393-402.

Frommer, M. A., R. Matz, et al. (1971). "Mechanism of formation of reverse osmosis membranes." **10**(2): 193-6.

Frommer, M. A., R. Matz, et al. (1971). "Mechanism of formation of reverse osmosis membranes. Precipitation of cellulose acetate membranes in aqueous solutions." Industrial & Engineering Chemistry Product Research and Development **10**(2): 193-6.

Frommer, M. A. and R. M. Messalem (1973). "Mechanism of Membrane Formation. VI. Convective Flows and Large Void Formation during Membrane Precipitation." Ind. Eng. Chem. Prod. Res. Develop. **12**(4): 328-333.

Gauthier, F., H. L. Goldsmith, et al. (1971). "Particle Motions in Non-Newtonian Media. II. Poiseuille Flow." Trans. Soc. Rheology **15**(2): 297-330.

Gaynor, J. F. and J. Huang (2003). Dispersions of silicalite and zeolite nanoparticles in nonpolar solvents. Application: US, (Novellus Systems, Inc., USA). 10 pp.

Gerner, F., B. Svensson, et al. (2004). Gas Flaring and Venting: A Regulatory Framework and Incentives for Gas Utilization. Public Policy Journal Note No. 279. Washington, D.C, World Bank.

Hackley, V. A., P. Somasundaran, et al. (2002). Polymers in Particulate Systems: Properties and Applications. [In: Surfactant Sci. Ser., 2002; 104].

He, T., M. H. V. Mulder, et al. (2002). "Preparation of composite hollow fiber membranes: co-extrusion of hydrophilic coatings onto porous hydrophobic support structures." Journal of Membrane Science **207**(2): 143-156.

Henis, J. M. S. and M. K. Tripodi (1981). "Composite hollow fiber membranes for gas separation: the resistance model approach." J. Membr. Sci. **8**(3): 233-46.

Higuchi, W. I. (1958). "A new relation for the dielectric properties of two-phase mixtures." J. Phys. Chem. **62**: 649-53.

Higuchi, W. I. and T. Higuchi (1960). "Theoretical analysis of diffusional movement through heterogeneous barriers." J. Am. Pharm. Assoc., Sci. Ed. **49**: 598-606.

Hillock, A. W. M. (2005). Personal Communication.

http://www.energy.gov/energysources/naturalgas.htm, Date accessed, May 9, 2006.

Hu, Z., W. Lihui, et al. (1998). "External modification of zeolite by metal surfactant for methanol amination." Microporous and Mesoporous Materials **21**(1-3): 7-12.

Hunter, R. J. (1986). Foundations of Colloid Science, Vol. 1.

Hunter, R. J. and Editor (1981). <u>Colloid Science: Zeta Potential in Colloid Science: Principles and Applications</u>.

Husain, S. and W. J. Koros (2005). <u>Mixed matrix hollow fibers for gas separation</u>. North American Membrane Society, Providence, RI.

Iler, R. K. (1979). <u>The Chemistry of Silica: Solubility, Polymerization, Colloid and Surface Properties and Biochemistry</u>. New York, John Wiley & Sons.

Jiang, L. Y., T. S. Chung, et al. (2005). "Fundamental understanding of nano-sized zeolite distribution in the formation of the mixed matrix single- and dual-layer asymmetric hollow fiber membranes." <u>Journal of Membrane Science</u> **252**(1-2): 89-100.

Karge, H. G. (2001). Characterization by IR Spectroscopy. <u>Verified Syntheses of Zeolite Materials</u>. H. Robson. Amsterdam, Elsevier Science B.V.

Karnis, A. and S. G. Mason (1966). "Particle motions in sheared suspensions. XIX. Viscoelastics media." <u>Transactions of the Society of Rheology</u> **10**(2): 571-92.

Kesting, R. and A. Fritzsche (1993). <u>Polymeric Gas Separation Membranes</u>. New York, John Wiley & Sons.

Kesting, R. E., A. K. Fritzsche, et al. (1990). "The second-generation polysulfone gas-separation membrane. II. The relationship between sol properties, gel macrovoids, and fiber selectivity." <u>Journal of Applied Polymer Science</u> **40**(9-10): 1575-82.

Kesting, R. E., A. K. Fritzsche, et al. (1990). "The second-generation polysulfone gas-separation membrane. I. The use of Lewis acid:base complexes as transient templates to increase free volume." <u>Journal of Applied Polymer Science</u> **40**(9-10): 1557-74.

Kim, S.-J., O. D. Bonner, et al. (1971). "Solvent-solute interactions in dimethyl sulfoxide." <u>Journal of Chemical Thermodynamics</u> **3**(4): 411-17.

Kiyono, R., G. H. Koops, et al. (2004). "Mixed matrix microporous hollow fibers with ion-exchange functionality." <u>Journal of Membrane Science</u> **231**(1-2): 109-115.

Knudsen, M. (1909). "The Law of the Molecular Flow and Viscosity of Gases Moving through Tubes." <u>Annalen der Physik (Weinheim, Germany)</u> **28**: 75-130.

Koningsberger, D. C. and J. T. Miller (1995). "Withdrawal of electron density by cations from framework aluminum in Y zeolite determined by Al XAFS spectroscopy." <u>Studies in Surface Science and Catalysis</u> **97**(Zeolites: A Refined Tool for Designing Catalytic Sites): 125-31.

Koros, W. J. (2004). "Evolving beyond the thermal age of separation processes: Membranes can lead the way." <u>AIChE Journal</u> **50**(10): 2326-2334.

Koros, W. J. and G. K. Fleming (1993). "Membrane-based gas separation." J. Membr. Sci. **83**(1): 1-80.

Koros, W. J. and R. Mahajan (2000). "Pushing the limits on possibilities for large scale gas separation: which strategies?" J. Membr. Sci. **175**(2): 181-196.

Kulkarni, S. S. (2003). Personal Communication, Medal L.P / Air Liquide.

Kulkarni, S. S. and D. J. Hasse (2005). Molecular sieve-containing polyimide mixed matrix membranes. Application: US, (USA). 13 pp.

Kulkarni, S. S., D. J. Hasse, et al. (2003). Gas separation membrane with organosilicon-treated molecular sieve. Application: US, (L'Air Liquide - Societe Anonyme a Directoire et Conseil de Surveillance pour l'Etude et l'Exploitation des Procedes Georges Claude, Fr.). 12 pp.

Kulprathipanja, S., R. W. Neuzil, et al. (1988). Separation of fluids by means of mixed matrix membranes. U.S., (Allied-Signal, Inc., USA)**:** 7 pp.

Kurdi, J. and A. Y. Tremblay (2001). "The influence of casting solution structure on the microporosity of polyetherimide gas separation membranes prepared by the coagulation post-leaching method." Journal of Membrane Science **184**(2): 175-186.

Labib, M. E. (1988). "The origin of the surface charge on particles suspended in organic liquids." Colloids and Surfaces **29**(3): 293-304.

Landauer, R. (1952). "The electrical resistance of binary metallic mixtures." J. Appl. Phys. **23**: 779-84.

Leboda, R. (1978). "Modification of surface properties of silica gels in aspects of their utility in chromatography. XIV. Modification of the texture and skeleton structure of silica gels with C1-10 aliphatic alcohols." Chemia Analityczna (Warsaw, Poland) **23**(6): 935-43.

Leighton, D. and A. Acrivos (1987). "The shear-induced migration of particles in concentrated suspensions." Journal of Fluid Mechanics **181**: 415-39.

Li, D. F., T.-S. Chung, et al. (2002). "Fabrication of fluoropolyimide/polyethersulfone (PES) dual-layer asymmetric hollow fiber membranes for gas separation." Journal of Membrane Science **198**(2): 211-223.

Li, S. G., G. H. Koops, et al. (1994). "Wet spinning of integrally skinned hollow fiber membranes by a modified dual-bath coagulation method using a triple orifice spinneret." Journal of Membrane Science **94**(1-3): 329-40.

Liu, Y., T.-S. Chung, et al. (2003). "Chemical Cross-Linking Modification of Polyimide/Poly(ether sulfone) Dual-Layer Hollow-Fiber Membranes for Gas Separation." Industrial & Engineering Chemistry Research **42**(6): 1190-1195.

Loeb, S. and S. Sourirajan (1963). "Sea water demineralization by means of an osmotic membrane." Advances in Chemistry Series **38**: 117-32.

Lowen, W. K. and E. C. Broge (1961). "Effects of dehydration and chemisorbed materials on the surface properties of amorphous silica." Journal of Physical Chemistry **65**: 16-19.

Lyklema, J. (1968). "Principles of the stability of lyophobic colloidal dispersions in nonaqueous media." Advances in Colloid and Interface Science **2**(2): 65-114.

Madden, W. C. (2005). The Performance of Hollow Fiber Gas Separation Membranes in the Presence of an Aggressive Feed Stream. Chemical Engineering. Atlanta, Georgia Institute of Technology**:** 219.

Mahajan, R. (2000). Formation, characterization and modeling of mixed matrix membrane materials. Department of Chemical Engineering. Austin, TX, University of Texas at Austin**:** 230.

Mahajan, R., R. Burns, et al. (2002). "Challenges in forming successful mixed matrix membranes with rigid polymeric materials." Journal of Applied Polymer Science **86**: 881-90.

Mahajan, R., R. Burns, et al. (2002). "Challenges in forming successful mixed matrix membranes with rigid polymeric materials." J. Appl. Polym. Sci. **86**(4): 881-890.

Mahajan, R. and W. J. Koros (2000). "Factors Controlling Successful Formation of Mixed-Matrix Gas Separation Materials." Ind. Eng. Chem. Res. **39**(8): 2692-2696.

Mahajan, R. and W. J. Koros (2002). "Mixed matrix membrane materials with glassy polymers. Part 1." Polymer Engineering and Science **42**(7): 1420-1431.

Mahajan, R. and W. J. Koros (2002). "Mixed matrix membrane materials with glassy polymers. Part 2." Polymer Engineering and Science **42**(7): 1432-1441.

Maxwell, J. C. (1873). A treatise on electricity and magnetism. Oxford, Clarendon press.

McKelvey, S. A. (1997). Formation and characterization of hollow fiber membranes for gas separation (fiber breaks, macrovoids)**:** 227 pp.

McKelvey, S. A., D. T. Clausi, et al. (1997). "A guide to establishing hollow fiber macroscopic properties for membrane applications." Journal of Membrane Science **124**(2): 223-232.

McKelvey, S. A. and W. J. Koros (1996). "Phase separation, vitrification, and the manifestation of macrovoids in polymeric asymmetric membranes." Journal of Membrane Science **112**(1): 29-39.

McKittrick, M. W. and C. W. Jones (2003). "Toward Single-Site Functional Materials-Preparation of Amine-Functionalized Surfaces Exhibiting Site-Isolated Behavior." Chemistry of Materials **15**(5): 1132-1139.

Meyer, H. S. and D. Leppin "Research targets lower gas-processing operating costs." Oil & Gas Journal **95**(52): 83.

Miller, S. (2005). Personal Communication; Chevron Research and Technology Company.

Moore, S., E. (1994). Apparatus for spining of multicomponent hollow fibers. US 5,320,512, E.I. du Pont de Nemours and Company.

Moore, T. T. (2001). Personal Communication.

Moore, T. T. (2004). Effects of materials, processing, and operating conditions on the morphology and gas transport properties of mixed matrix membranes**:** 311 pp.

Moore, T. T. (2004). Personal communication.

Moore, T. T., S. Damle, et al. (2004). "Characterization of low permeability gas separation membranes and barrier materials; design and operation considerations." Journal of Membrane Science **245**(1-2): 227-231.

Moore, T. T. and W. J. Koros (2005). "Non-ideal effects in organic-inorganic materials for gas separation membranes." Journal of Molecular Structure **739**(1-3): 87-98.

Moore, T. T., R. Mahajan, et al. (2004). "Hybrid membrane materials comprising organic polymers with rigid dispersed phases." AIChE Journal **50**(2): 311-321.

Mulder, M. and Editor (1996). Basic Principles of Membrane Technology, Second Edition.

Myers, D. (1991). Surfaces, Interfaces, and Colloids: Principles and Applications**:** 433 pp.

Myers, D. (1991). Surfaces, Interfaces, and Colloids: Principles and Applications.

Napper, D. H. (1983). Polymeric Stabilization of Colloidal Dispersions.

Nutting, P. G. (1927). "The adsorptive force of silica for water." Journal of Physical Chemistry **31**: 531-4.

O'Brien, K. C., W. J. Koros, et al. (1986). "A new technique for the measurement of multicomponent gas transport through polymeric films." J. Membr. Sci. **29**(3): 229-38.

Ossenkamp, G. C., T. Kemmitt, et al. (2002). "Toward Functionalized Surfaces through Surface Esterification of Silica." Langmuir **18**(15): 5749-5754.

Overbeek, J. T. G. (1977). "Recent developments in the understanding of colloid stability." Journal of Colloid and Interface Science **58**(2): 408-422.

Paulsen, F. G., S. S. Shojaie, et al. (1994). "Effect of evaporation step on macrovoid formation in wet-cast polymeric membranes." Journal of Membrane Science **91**(3): 265-82.

Pechar, T. W., M. Tsapatsis, et al. (2002). "Preparation and characterization of a glassy fluorinated polyimide zeolite-mixed matrix membrane." Desalination **146**(1-3): 3-9.

Perego, G., G. Bellussi, et al. (1986). "Titanium-silicalite: a novel derivative in the pentasil family." Studies in Surface Science and Catalysis **28**(New Dev. Zeolite Sci. Technol.): 129-36.

Pereira, C. C., R. Nobrega, et al. (2003). "Hollow fiber membranes obtained by simultaneous spinning of two polymer solutions: a morphological study." Journal of Membrane Science **226**(1-2): 35-50.

Pesek, J. J., M. T. Matyska, et al. (1996). Chemically Modified Surfaces: Recent Developments. (Proceedings of the 6th International Symposium on Chemically Modified Surfaces was held in San Jose, California, June 19-21, 1995.) [In: Spec. Publ. - R. Soc. Chem., 1996; 173].

Pesek, J. J. and S. A. Swedberg (1986). "Allyl-bonded stationary phase as possible intermediate in the synthesis of novel high-performance liquid chromatographic phases." Journal of Chromatography **361**: 83-92.

Pesek, S. C. (1993). Aqueous quenched asymmetric polysulfone flat sheet and hollow fiber membranes prepared by dry/wet phase separation. Department of Chemical Engineering, Univ. Texas, Austin, TX, USA.**:** 260 pp.

Pesek, S. C. (2003). Personal Communication.

Pesek, S. C. and W. J. Koros (1993). "Aqueous quenched asymmetric polysulfone membranes prepared by dry/wet phase separation." Journal of Membrane Science **81**(1/2): 71-88.

Pesek, S. C. and W. J. Koros (1994). "Aqueous quenched asymmetric polysulfone hollow fibers prepared by dry/wet phase separation." Journal of Membrane Science **88**(1): 1-19.

Petropoulos, J. H. (1985). "A comparative study of approaches applied to the permeability of binary composite polymeric materials." J. Polym. Sci., Polym. Phys. Ed. **23**(7): 1309-24.

Piirma, I. (1992). Polymeric Surfactants. New York, NY, Marcel Dekker, Inc.

Pinnau, I. (1991). Skin Formation of Integral-Asymmetric Gas Separation Membranes Made By Dry/Wet Phase Inversion (Gas Separation). Department of Chemical Engineering, Univ. of Texas, Austin, TX, USA.**:** 342.

Pinnau, I. and W. J. Koros (1991). "Relationship between substructure resistance and gas separation properties of defect-free integrally skinned asymmetric membranes." Industrial & Engineering Chemistry Research **30**(8): 1837-40.

Pinnau, I. and W. J. Koros (1991). "Structures and gas separation properties of asymmetric polysulfone membranes made by dry, wet, and dry/wet phase inversion." Journal of Applied Polymer Science **43**(8): 1491-1502.

Plueddemann, E. P. (1982). Silane Coupling Agents. New York, Plenum Press.

Polotskaya, G., Y. Biryulin, et al. (2004). "Asymmetric Membranes Based on Fullerene-Containing Polyphenylene Oxide." Fullerenes, Nanotubes, and Carbon Nanostructures **12**(1 & 2): 371-376.

Pugh, R. J., T. Matsunaga, et al. (1983). "The dispersibility and stability of carbon black in media of low dielectric constant. 1. Electrostatic and steric contributions to colloidal stability." Colloids and Surfaces **7**(3): 183-207.

Pye, D. G., H. H. Hoehn, et al. (1976). "Measurement of gas permeability of polymers. I. Permeabilities in constant volume/variable pressure apparatus." J. Appl. Polym. Sci. **20**(7): 1921-31.

Raj, P. M. and W. R. Cannon (2002). "Electrosteric stabilization mechanisms in nonaqueous high solids loading dispersions." Surfactant Science Series **104**(Polymers in Particulate Systems): 27-61.

Rao, M. B. and S. Sircar (1993). "Nanoporous carbon membranes for separation of gas mixtures by selective surface flow." J. Membr. Sci. **85**(3): 253-64.

Reuvers, A. J., J. W. A. Van den Berg, et al. (1987). "Formation of membranes by means of immersion precipitation. Part I. A model to describe mass transfer during immersion precipitation." Journal of Membrane Science **34**(1): 45-65.

Robeson, L. M. (1991). "Correlation of separation factor versus permeability for polymeric membranes." J. Membr. Sci. **62**(2): 165-85.

Robeson, L. M., A. Noshay, et al. (1973). "Physical property characteristics of polysulfone/poly(dimethylsiloxane)block copolymers." Angew. Makromol. Chem. **29-30**: 47-62.

Rojey, A., A. Deschamps, et al. (1990). Process for separation of the constituents of a mixture in the gas phase using a composite membrane. US, (Institut Francais Du Petrole)**:** 10 pp.

Rozwadowski, M., R. Wojsz, et al. (1989). "Description of adsorption equilibrium on type A zeolites with use of the Polanyi-Dubinin potential theory." Zeolites **9**(6): 503-508.

Sarbolouki, M. N. (1984). "Properties of Asymmetric Polyimide Ultrafiltration Membranes. I. Pore Size and Morphology Characterization." Journal of Applied Polymer Science **29**: 743-753.

Sarkany, J. and W. M. H. Sachtler (1994). "Redox chemistry of Cu/NaZSM-5: Detection of cuprous ions by FTIR." Zeolites **14**(1): 7-11.

Saxton, R. J., G. L. Crocco, et al. (1996). US Patent.

Shieh, J. J., T. S. Chung, et al. (2001). "Gas separation performance of poly(4-vinylpyridine)/polyetherimide composite hollow fibers." Journal of Membrane Science **182**(1-2): 111-123.

Shojaie, S. S., W. B. Krantz, et al. (1994). "Dense polymer film and membrane formation via the dry-cast process. Part II. Model validation and morphological studies." Journal of Membrane Science **94**(1-3): 281-98.

Shu, S. (2006). Personal Communication.

Shu, S., S. Husain, et al. (2006). Formation of Nano-scale Morphology on Zeolite Surfaces for Enhanced Interfacial Interaction in Mixed Matrix Membranes. North American Membrane Society, Chicago.

Skoog, D. A., D. M. West, et al. (1996). Fundamentals of Analytical Chemistry. 7th Ed.

Smolders, C. A., A. J. Reuvers, et al. (1992). "Microstructures in phase-inversion membranes. Part 1. Formation of macrovoids." Journal of Membrane Science **73**(2-3): 259-75.

Sokol, A. A., C. R. A. Catlow, et al. (2004). "Transformation of hydroxyl nests in microporous aluminosilicates upon annealing." Journal of Physics: Condensed Matter **16**(27): S2781-S2794.

Somasundaran, P. and Editor (1980). Fine Particles Processing, Vol. 2. [Proceedings of an International Symposium, Las Vegas, Nevada, February 24-28, 1980].

Spillman, R. W. (1989). "Economics of gas separation membranes." Chem. Eng. Prog. **85**(1): 41-62.

Sponer, J. E., Z. Sobalik, et al. (2001). "Effect of Metal Coordination on the Charge Distribution over the Cation Binding Sites of Zeolites. A Combined Experimental and Theoretical Study." Journal of Physical Chemistry B **105**(35): 8285-8290.

Strathmann, H. (2001). "Membrane separation processes: current relevance and future opportunities." AIChE Journal **47**(5): 1077-1087.

Strathmann, H., K. Kock, et al. (1975). "The formation mechanism of asymmetric membranes." Desalination **16**(2): 179-203.

Sunseri, J. D., T. E. Gedris, et al. (2003). "Complete Methylation of Silica Surfaces: Next Generation of Reversed-Phase Liquid Chromatography Stationary Phases." Langmuir **19**(20): 8608-8610.

Takei, T. (1988). "Properties of non-aqueous solvents: solubility and conductivity of solutions." Surface and Coatings Technology **35**(1-2): 57-67.

Tao, T. and G. E. Maciel (2000). "Reactivities of Silicas with Organometallic Methylating Agents." Journal of the American Chemical Society **122**(13): 3118-3126.

Tehrani, M. A. (1996). "An experimental study of particle migration in pipe flow of viscoelastic fluids." Journal of Rheology (New York) **40**(6): 1057-1077.

Tertykh, V. A. and L. A. Belyakova (1996). "Solid-phase hydrosilylation reactions with participation of modified silica surface." Studies in Surface Science and Catalysis **99**(Adsorption on New and Modified Inorganic Sorbents): 147-89.

Vankelecom, I. F. J., S. Van den Broeck, et al. (1996). "Silylation To Improve Incorporation of Zeolites in Polyimide Films." J. Phys. Chem. **100**(9): 3753-8.

Vassylyev, O., J. Chen, et al. (2006). "Efficient surface functionalization of zeolites via esterification." Microporous and Mesoporous Materials **92**(1-3): 101-108.

Vassylyev, O., G. S. Hall, et al. (2006). "Modification of zeolite surfaces by Grignard reagent." Journal of Porous Materials **13**(1): 5-11.

Vogrin, N., C. Stropnik, et al. (2002). "The wet phase separation: the effect of cast solution thickness on the appearance of macrovoids in the membrane forming ternary cellulose acetate/acetone/water system." Journal of Membrane Science **207**(1): 139-141.

Volmer, M. (1939). Kinetik der Phasenbildung, Steinkopff, Dresden and Leipzig.

Vu, D. Q. (2001). Formation and characterization of asymmetric carbon molecular sieve and mixed matrix membranes for natural gas purification. Department of Chemical Engineering, Univ. of Texas, Austin, TX, USA.

Vu, D. Q., W. J. Koros, et al. (2003). "Mixed matrix membranes using carbon molecular sieves. I. Preparation and experimental results." Journal of Membrane Science 211(2): 311-334.

Wachtman, J. B. and Z. H. Kalman (2003). Characterization of Materials. Boston, Butterworth-Heinemann.

Wallace, D. W. (2004). Crosslinked hollow fiber membranes for natural gas purification and their manufacture from novel polymers. Chemical Engineering, University of Texas--Austin: 221 pp.

Wang, D.-M., F.-C. Lin, et al. (1998). "Formation mechanism of the macrovoids induced by surfactant additives." Journal of Membrane Science 142(2): 191-204.

Wang, K. Y., D. F. Li, et al. (2004). "The observation of elongation dependent macrovoid evolution in single- and dual-layer asymmetric hollow fiber membranes." Chemical Engineering Science 59(21): 4657-4660.

Wang, K. Y., T. Matsuura, et al. (2004). "The effects of flow angle and shear rate within the spinneret on the separation performance of poly(ethersulfone) (PES) ultrafiltration hollow fiber membranes." Journal of Membrane Science 240(1-2): 67-79.

Wara, N. M., L. F. Francis, et al. (1995). "Addition of alumina to cellulose acetate membranes." J. Membr. Sci. 104(1-2): 43-9.

Wolf, B. A. (1984). "Thermodynamic theory of flowing polymer solutions and its application to phase separation." Macromolecules 17(4): 615-18.

Yong, H. H., H. C. Park, et al. (2001). "Zeolite-filled polyimide membrane containing 2,4,6-triaminopyrimidine." Journal of Membrane Science 188(2): 151-163.

Young, D. A. (1972). Treatment of aluminosilicate. Application: US: 13 pp.

Ziabicki, A. (1976). Fundamentals of fibre formation. London, John Wiley & Sons.

Zimmerman, C. M., R. Mahajan, et al. (1997). "Fundamental and practical aspects of mixed matrix gas separation membranes." Polymer Material Science and Engineering 77: 328-329.

Zimmerman, C. M., A. Singh, et al. (1997). "Tailoring mixed matrix composite membranes for gas separations." <u>Journal of Membrane Science</u> **137**(1-2): 145-154.